THE CREATION OF A VIABLE POROUS SILICON GAS SENSOR

A Thesis
Presented to
The Academic Faculty

by

Stephen Lewis

In Partial Fulfillment
Of the Requirements for the Degree
Doctor of Philosophy in the
School of Physics

Georgia Institute of Technology
May 2006

THE CREATION OF A VIABLE POROUS SILICON GAS SENSOR

Approved by:

James Gole, Advisor
School of Physics
Georgia Institute of Technology

Andrei Fedorov
School of Mechanical Engineering
Georgia Institute of Technology

Ahmet Erbil
School of Physics
Georgia Institute of Technology

Alexei Marchenkov
School of Physics
Georgia Institute of Technology

Date Approved: April 3, 2006

ACKNOWLEDGEMENTS

There are many people I wish to thank who have helped me during my time at Georgia Tech. Foremost among them is my advisor, James Gole; without whom I would not be here now. I have also been guided by many other friends, co-workers, and professors while pursuing my research. Peter Hesketh and John DeBoer were of great importance to the completion of my degree. Matt Bennett, Gary Gray, Angela Tse, Jimmy Corno, Se-il Lee, Edwin Greco, Lenward Seals, have all given me great advice and assistance on many, many occasions, and hopefully will continue to do so in the years to come. The people whom I have worked with over the years are in fact too numerous to list here, and I feel my dissertation is long enough already, so to all of you, thanks a shit-load. I would finally like to thank Catherine Fraas for reading and editing this dissertation, my thesis committee for reading this dissertation, as well as Andy Zangwill and Mei-Yin Chou for helping me to complete my final degree here at Georgia Tech.

TABLE OF CONTENTS

LIST OF TABLES

LIST OF FIGURES

LIST OF SYMBOLS AND ABBREVIATIONS

C_σ	Coefficient of Variance
CHEMFET	Chemical FET
DI	De-ionized water
EDS	Energy Dispersive Spectrometer
FET	Field Effect Transistor
ISFET	Ion Selective FET
LEL	Lower Exposure Limit
LOD	Lower Onset of Detection
MeCN	Methyl Cyanide or Acetonitrile
MFC	Mass Flow Controller
MOSFET	Metal Oxide Semiconductor FET
ODE	Ordinary Differential Equation
Ω	Resistance of a Sensor
Ω_0	Baseline Resistance
ppb	Parts per Billion
ppht	Parts per Hundred Thousand
ppm	Parts per Million
ppt	Parts per Trillion
PR	Photoresist
PS	Porous Silicon
PSGS	Porous Silicon Gas Sensor
PECVD	Plasma Enhanced Chemical Vapor Deposition

RIE	Reactive Ion Etch
S	Sensitivity of a Device
SAFET	Surface Accessible FET
SCCM	Standard Cubic Centimeter per Minute
SGFET	Suspended Gate FET
SLA	Stereo-Lithographic Assembly
TBAP	Tetra-butyl-ammonium-perchlorate
t_R	Response Time of a Device
v_i	Flow rate of Gas Species ‘i’
x_i	Concentration of Gas Species ‘i’

SUMMARY

This dissertation describes the fabrication and operation of porous silicon gas sensors. The first chapter describes the motivation behind gas sensor research and provides the reader with background knowledge of gas sensors including the terminology and a review of various gas sensors. The following two chapters describe both how the porous silicon gas sensors are created and how they have been tested in the laboratory. Chapter 4 describes the steps required to create arrays of gas sensors to provide for a selective device through the application of patented selective coatings. Chapter 5 proposes a physical model that leads to a numerical solution for predicting the operation of the gas sensor. The next chapter builds from this model to analyze and optimize the experimental methods that are used to test both this and other gas sensors. The final chapter of this dissertation describes the prototype gas sensor system that has most recently been created, the company that was formed to further the development of that system, and the future applications of the porous silicon gas sensor.

CHAPTER 1

BACKGROUND OF GAS SENSOR TECHNOLOGY

This chapter is intended to provide background knowledge helpful for understanding the porous silicon gas sensor. Some terminology is presented first to provide a common basis for understanding gas sensors. The need for gas detection in both industrial and personal environments, leading to a rapid increase in the role for gas sensors is then considered. Several modern gas sensing systems are also discussed to provide a means for comparing both the performance and the physical sensing mechanisms of the sensors which we have developed. An overview of these topics also explains the motivation for conducting this research on gas sensors. Finally, the existing uses of porous silicon in various sensing applications will be presented to familiarize the reader with the material before it is discussed in more depth in Chapter 2.

Overview of Terminology

A gas sensor is defined as any device that assesses one or more characteristics of a sample of gas. Several phrases and acronyms are used to describe the performance of gas sensors. They include ways to accurately describe concentration levels, response, sensitivity, selectivity, signal to noise, interference, and additional characteristics that are described here to familiarize the reader with the terminology.

The gases that a gas sensor detects are called analytes, and are typically measured in parts per million (ppm) concentrations. Parts per billion (ppb), parts per trillion (ppt), percent, or parts per hundred thousand (ppht) are also commonly used to express gas

concentration. All of these values represent the molar concentrations of the analyte within the sample of gas being tested.

A sensor's response is measured from a baseline, which is the signal of the device before exposure to an analyte. The time between exposure and the observation of a response is called the response time of the device. Response time is defined here as the time taken to reach 90% of the steady state response. After exposure, a response is observed if the device is sensitive to the analyte. The analyte may then be removed, which will cause the sensor to return to the baseline condition (if the device is reversible) over some recovery time. Recovery time, the time taken for the sensor to return to the baseline condition, is typically dependant on both the concentration of the analyte within the sample of gas and the duration of the exposure. An example of this terminology is given in Figure 1-1.

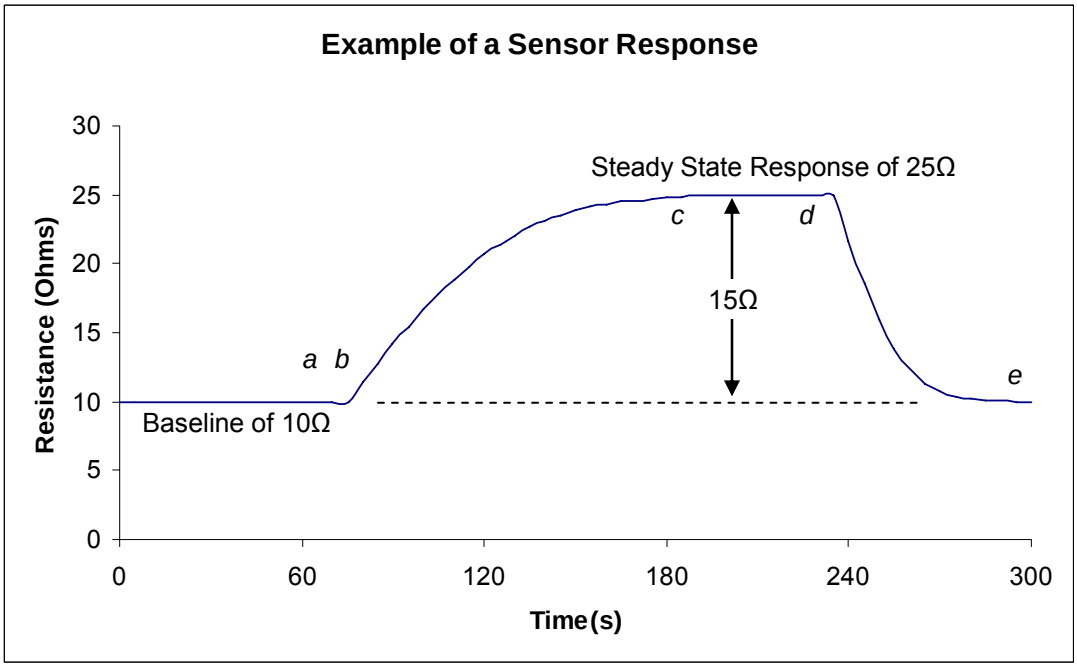

a) Analyte delivered at 60s
b) Sensor starts to respond at 75s
c) 90% of steady state response at 180s
d) Analyte removed from the sensor at 220s
e) Device recovers at 300s

Figure 1-1: An example of a possible sensor response is given.

Sensitivity characterizes the magnitude of a response to a particular analyte. The sensitivity can be recorded as a ratio between some measure of the response and the concentration of analyte being delivered. Current per ppm, voltage per ppm, and resistance per ppm, for example, are all common measures of sensitivity for "linearly responding" gas sensors. To determine the sensitivity, a device's response must be determined to several different levels of analyte. An example of this data is shown in Table 1-1.

Table 1-1: Sample data relating the response of the example device to several different concentrations of analyte.

Conc. Of Analyte (ppm)	Response (Ohms)
5	15.21183
3	10.01665
1	3.487914
7	22.78638
9	30.05098

Continuing with this example, Figure 1-2 shows how the sensitivity would be calculated for such a device.

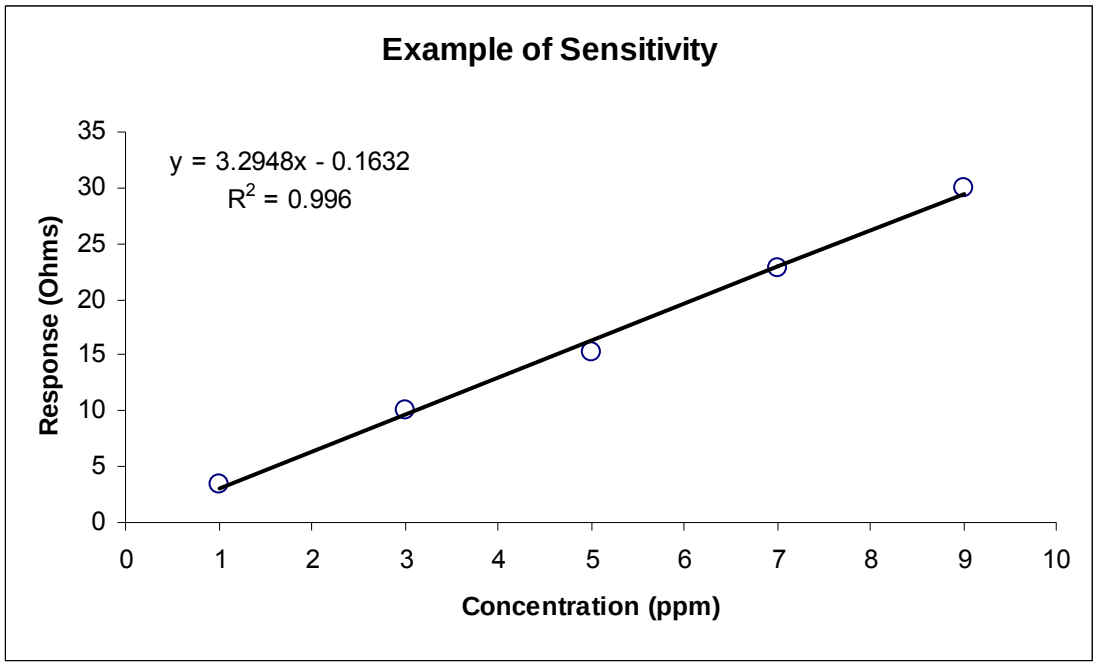

Figure 1-2: The sensitivity of an example device is shown to be around 3.3 Ohms per ppm by plotting the response to several concentrations of gas.

The lowest concentration of analyte that can be reliably detected is called the lower onset of detection (LOD). The LOD is calculated as shown in Equation 1-1 from the difference between the average response: S_i and the measured response: $S(x_i)$. N is the number of samples measured.

$$\sigma^2 = \sum_{i=1}^{N} \left(S(x_i) - S_i\right)^2 / N$$

Equation 1-1: The standard deviation of a sensor's response to a particular gas is found from the difference between the measured and average value of the response.

Twice the standard deviation of the response is used to calculate the LOD; this provides a 95% certainty that the response of the device is genuine down to that concentration. We arrive at the LOD by inserting this value (twice the deviation of the response) into the fit of the response shown in Figure 1-2.

For our example, the deviation is found to be near 0.61Ω, which leaves a LOD of 0.42 ppm. This signifies that with 95% confidence, the sensor used in the example can respond to 420 ppb of analyte. And there is an unacceptably large possibility that responses observed below this concentration are due to other factors.

The performance of a sensor is adversely affected by both noise and drift. Noise refers to short time scale (<5 second) changes in sensor response which can result from many factors. Noise can be caused by the nature of the sensor transduction mechanism, which we consider in a later section, by measurement electronics, or by external sources. The drift of a device refers to its longer time scale response. Drift is usually attributed to slowly fluctuating external factors such as temperature, pressure, or humidity. The ideal gas sensor technology has identifiable sources of noise and drift and is able to minimize their deleterious impact on performance.

Interference can also enhance the difficulty of operating a gas sensor. An interference gas is one which responds similarly to the desired analyte being measured. Interference can also cause an increased or decreased response to the analyte, or it can poison the sensor, rendering it inoperable. Some methods of removing the impact of interference include the arraying of gas sensors with different relative sensitivities to gases, as well as the use of filters which remove certain components of the sample before it is introduced to the sensor.

Motivation

The roles of gas sensors are ever increasing in society today, with a particular emphasis in the areas of health, law enforcement, and medical diagnostics. A study done

in 2002 by the Freedonia Group, Inc. indicates that the 2.3 billion dollar chemical sensors industry will grow roughly 8.6% per year until 2006[1].

Health Applications

The motivation for sensing ammonia (NH_3), carbon monoxide (CO), and nitrogen oxide (NO) is driven primarily their negative impact on personal health in both household and industrial environments.

Ammonia results primarily from agricultural sources, whereas, in urban areas, automotive emissions contribute to the majority of health issues related to this gas. A major concern regarding ammonia emissions is that they are not addressed in the Clean Air Act. Therefore, the levels of ammonia emissions are not usually considered when designing new technologies[2].

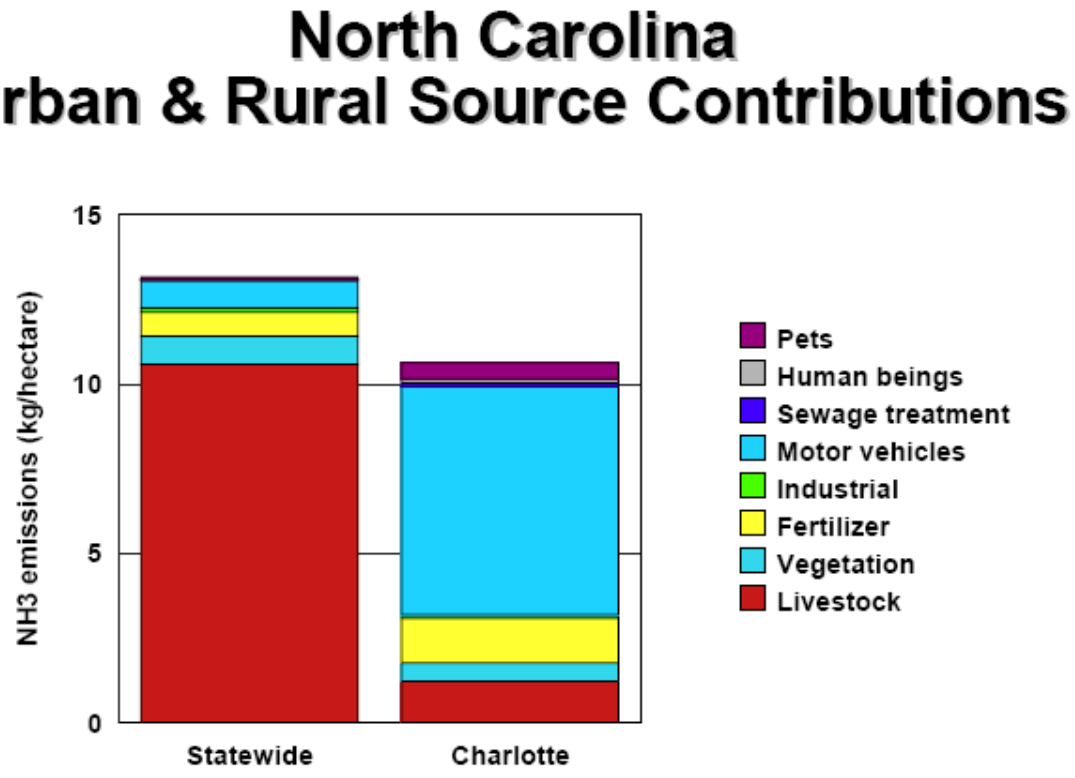

Figure 1-3: Ammonia emissions throughout North Carolina and specific to Charlotte, NC.

Exposure to ammonia at 50 parts per million (ppm) can cause severe burns to the skin, eyes, throat, and lungs[3]. Exposure to 5,000 ppm ammonia can lead to blindness, lung damage, and even death. Even at concentrations below 50 ppm, ammonia can cause coughing and irritation, with asthmatics being particularly susceptible[4]. Long term exposure to concentrations of 25 ppm can cause damage to the eyes, liver, kidneys, and lungs[5].

The effects of exposure to carbon monoxide (CO) are potentially much more harmful. CO, which is produced by virtually all combustion reactions, is found primarily in urban and household environments[6]. Any person in the average city is regularly exposed to 5 ppm CO (Figure 1-4), largely coming from vehicular exhaust. Up to 95% of the monitored CO exposure is from automotive emissions in dense urban areas. The recent decrease in CO associated with vehicular emissions is primarily responsible for recent improvements in air quality.

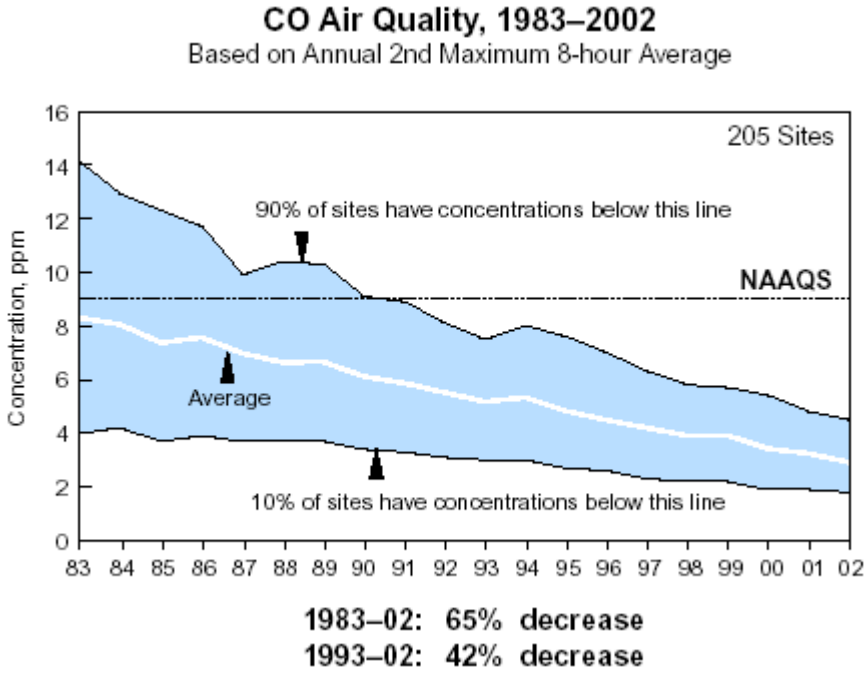

Figure 1-4: CO concentrations are steadily decreasing, but still represent a significant hazard for personal health.

Exposure to 30 ppm CO, or 10 ppm for individuals with preexisting heart conditions, can result in the weakening of the heart, reduction in the ability to perform manual tasks, and drowsiness[7]. At concentrations above 35 ppm for extended durations (>24 hrs), carbon monoxide exposure can result in headaches, irritability, blurred vision, lack of coordination, nausea, dizziness, and death. According to United States government regulations, the threshold exposure level for CO is 50 ppm for an eight hour period[8].

Nitrogen oxide (NO) is an unstable molecule that will slowly degrade into many other oxides of nitrogen such as NO_2. NO and the molecules it degrades to are referred to as NO_x. NO_x is produced in large quantities by vehicular emissions, and produces the dark brown smog over major cities such as Los Angeles. In rural settings, NO_x concentrations can become elevated due to fertilizers or an excessive density of livestock byproducts[9]. While levels are decreasing, NO_x levels are of more concern in recent years due to their contributions to ozone pollution.

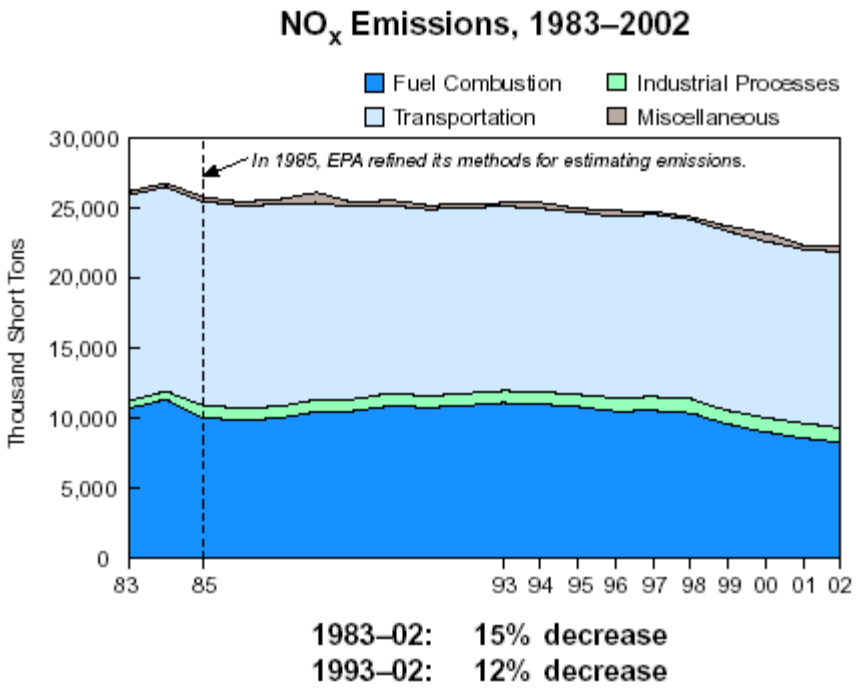

Figure 1-5: NO_x levels result almost entirely from fuel burning associated with power stations or automotive emissions.

Nitrogen oxide gas, at 1-5 ppm, is an irritant of the respiratory system as well as the eyes. Exposure over time results in fluid build-up in the lungs, nausea, and fatigue. Higher concentration exposures cause swelling of the throat, reduced oxygenation of the blood, and in severe cases, death[10]. Additionally, NO_x reacts to form ground level ozone, which, as a highly reactive and thus harmful gas, contributes to some asthmas[11].

Based upon the deleterious nature of these gases, considerable attention has been given to the monitoring of airborne pollutants. Automotive congestion elevates the presence of these gases in urban locations, causing poor air quality, asthma, and other pulmonary diseases. The development of gas sensors for both personal air quality monitoring and for emission source control is therefore an area of rapidly growing interest.

Industrial Applications

The need for industrial gas sensors is wide ranging and growing at an accelerated rate. The applications include monitoring of industrial pollution of the environment as well as quality control. In one example, Church and Dwight Co., Inc., who manufactures Arm and Hammer© baking soda, requires that the purity of CO_2 received from Exxon pipelines be 99.9% pure, with a maximum of 5 ppm SO_2, 2.5 ppm NO_x, and 1 ppm H_2S[12]. Sulfurous gases are typical of industrial contamination as they are primarily created from energy production through the burning of fossil fuels. Church and Dwight Co., Inc. requires the purity of the CO_2 to be within these specifications so that the carbonates which they market do not poison the consumers of their products.

Sulfur dioxide (SO_2) is a major pollutant that affects both the environment and personal health. SO_2 occurs primarily as the result of burning fossil fuels, causing an ambient SO_2 concentration of around 10 ppb[13]. SO_2, along with NO_x, contributes to acid rain formation which is associated with the acidification of small waterways and with accelerated corrosion. The exposure to 6 ppm SO_2 will cause instant irritation of the lungs and continual exposure will impair the immune system[14]. Additionally, SO_2 contributes to many pulmonary disorders.

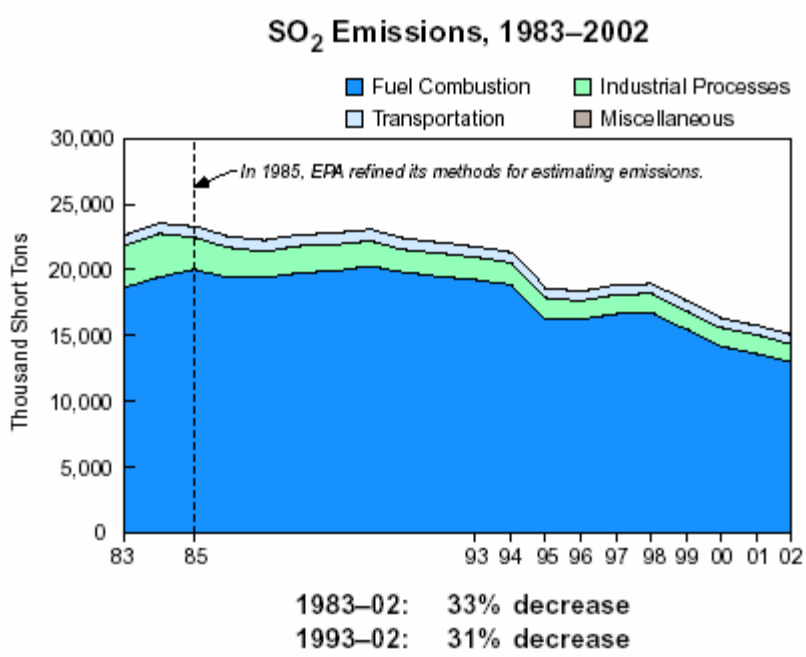

Figure 1-6: Sulfur dioxide emissions occur primarily from combustion of fuel at power stations.

Hydrogen disulfide (H_2S) is characterized upon initial exposure by a "rotten egg" odor, however, continual exposure, especially at high concentrations, can overcome a person's sense of smell. H_2S, formed primarily by the decomposition of organic materials, is found in natural gas, oil, mines, fertilizers, and sewers[15]. It is also a by-product of rayon, synthetic rubber, and dye production as well as the tanning of leather. Chronic exposure to over 20 ppm can result in headaches, eye disorders, bronchitis, or death. 50 ppm is the maximum safe dosage for a 10 minute exposure. H_2S must necessarily be monitored as there are no conclusive medical tests available to verify that the symptoms of H_2S poisoning were caused by H_2S exposure.

Other Applications

Hydrogen chloride (HCl) is not a major atmospheric pollutant (although it is produced by power plants) as the vast majority of HCl is produced by the oceans.

Though high doses of the vapor are harmful, this rarely occurs. HCl was of initial interest because it has a unique (ionic) chemical bonding structure relative to the other gases being tested. However, its detection does have some applications in the area of fire prevention (as burning PVC emits HCl) and medical diagnostic breath analysis.

Gas Sensor Transduction Methods

Many gas sensors can be grouped by the method which they use to transduce the concentration of a particular analyte. Within this framework, a basis for understanding the porous silicon gas sensor will be provided.

Thin Film Conductometric Sensors

A metal oxide, thin film sensor represents the simplest type of gas sensor. It operates with a thin sheet of material that is chemically reactive to a particular gas. The gas adsorbs into the material, changing its conductive properties and its resistance. The sensitive film is necessarily thin, as the adsorption only occurs at the interface between the metal oxide layer and the gas of interest. This form of sensor represents the first commercially available gas sensor. Iron oxide and tin oxide sensors, produced in Japan, can be used to detect hydrocarbons and combustible gases[16]. Though other materials can be used to form conductometric sensors, metal oxides are the most widely available due to their chemical stability, their ease of manufacture, and their low-cost of operation.

MOSFETs.

Integrating a sensitive materials with a field effect transistor (FET) provides for a several kinds of chemical sensors (see Figure 1-7)[17]. Many of these devices modify the metal-oxide-semiconductor FET (MOSFET) to construct a sensor. The simplest form is

the ISFET (Figure 1-7a), which uses the FET to amplify the effect of a sensitive layer, which is located between the source and drain of the FET. As charge accumulates through this layer, the conduction pathway between the source and drain is increased or decreased depending on the reaction. A similar device, the CHEMFET, uses a sensitive material in place of the gate in a standard MOSFET configuration (Figure 1-7b). Other MOSFETs include the Surface Accessible FET (SAFET), which has a standard gate both in contact with and suspended over an ISFET design (Figure 1-7c), and the more complex Suspended Gate FET (SGFET), which has a sensitive suspended mesh over a SGFET design (Figure 1-7d). Of all these devices, the CHEMFET is the only one able to operate practically (for long durations) due to poisoning of the chemically sensitive insulator in the other devices[16].

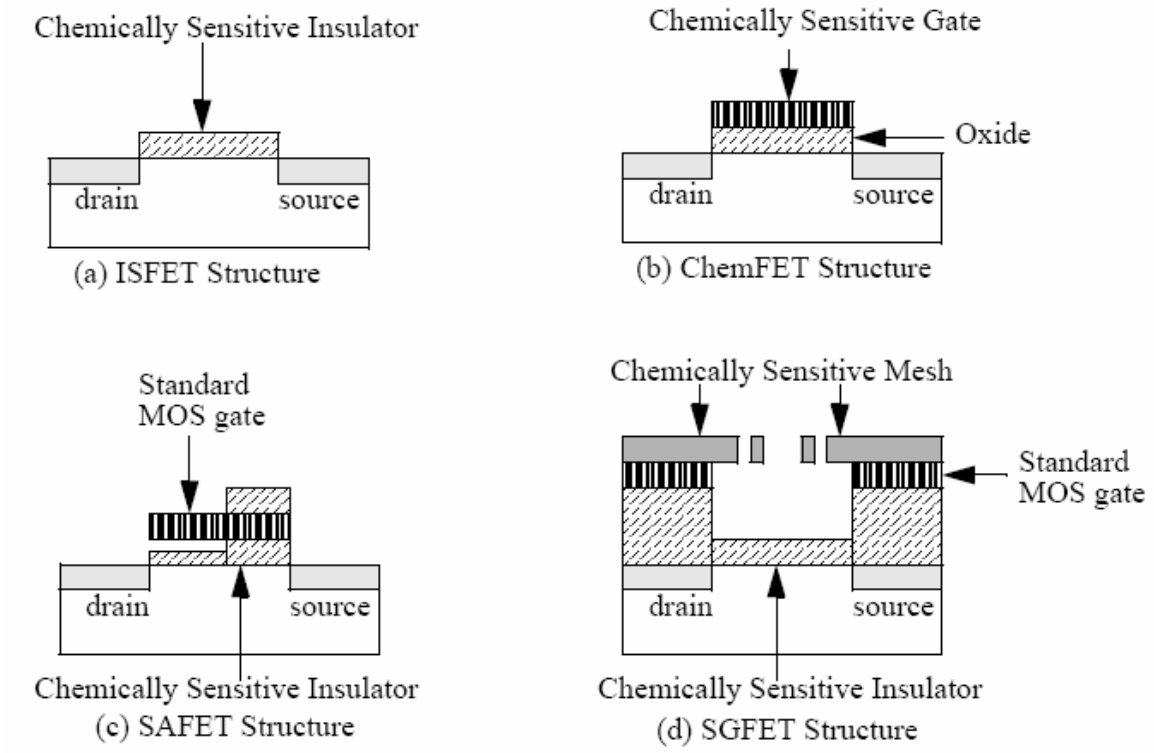

Figure 1-7: Shown above are the basic (a) ISFET (ion selective FET), (b) CHEMFET, (c) SAFET (surface accessible FET), and (d) SGFET (suspended gate FET).

Schottky Barrier

A Schottky barrier exists when the Fermi energy of electrons is different at the contacting materials through which current passes. A Schottky diode results when this interface is created[18]. The size of the barrier as measured is related to the difference in Fermi energy, and this barrier height translates directly to the impedance of current flow through the created diode which can easily be measured. A Schottky barrier sensor operates through the chemical modification of this barrier height via chemical adsorption at the triple-point contact of the metal, semiconductor, and modified gas. Thus, to produce a more effective Schottky barrier sensor, a porous material, or other high surface area thin film must be used for either the metal or semiconductor to maximize the region of contact that is able to adsorb the analyte.

In the example of the Pt/GaAs ammonia sensor, Pt is sputtered on an n-type GaAs wafer to produce a porous platinum film. Concentrations of ammonia are delivered to the wafer, and the resulting change in impedance is measured through ohmic contacts on the top and bottom of the wafer. The capacitance of the diode is measured in this device using impedance spectroscopy at zero bias voltage, which shows a response to 10 ppm of ammonia[19].

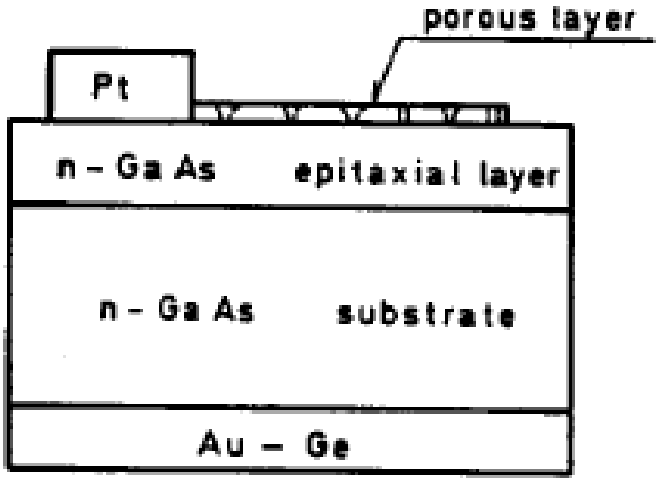

Figure 1-8: A schematic of the Pt/n-GaAs ammonia sensor. The Schottky barrier between the porous Pt and the n-GaAs transduces the ammonia concentration.

Other Transduction Mechanisms

Various more complicated kinds of gas sensors also exist[20]. Both the surface acoustic wave (SAW) sensors and optical gas sensors depicted in Figure 1-9 have become more prevalent in research. The SAW sensor is a gravimetric sensor. A highly absorptive film collects the chemical species of interest. This film is designed so as to adsorb the highest amount of material relative to its own weight. The film's weight is then measured after absorption (using surface acoustic waves) and compared to the weight before absorption to determine the amount of analyte adsorbed. Optical gas sensors are also complex devices, which operate using chemically absorbent materials to change the reflectivity or index of refraction of some material. Lasers are typically used to measure this change with a combination of a micro-mirror array and photo detectors.

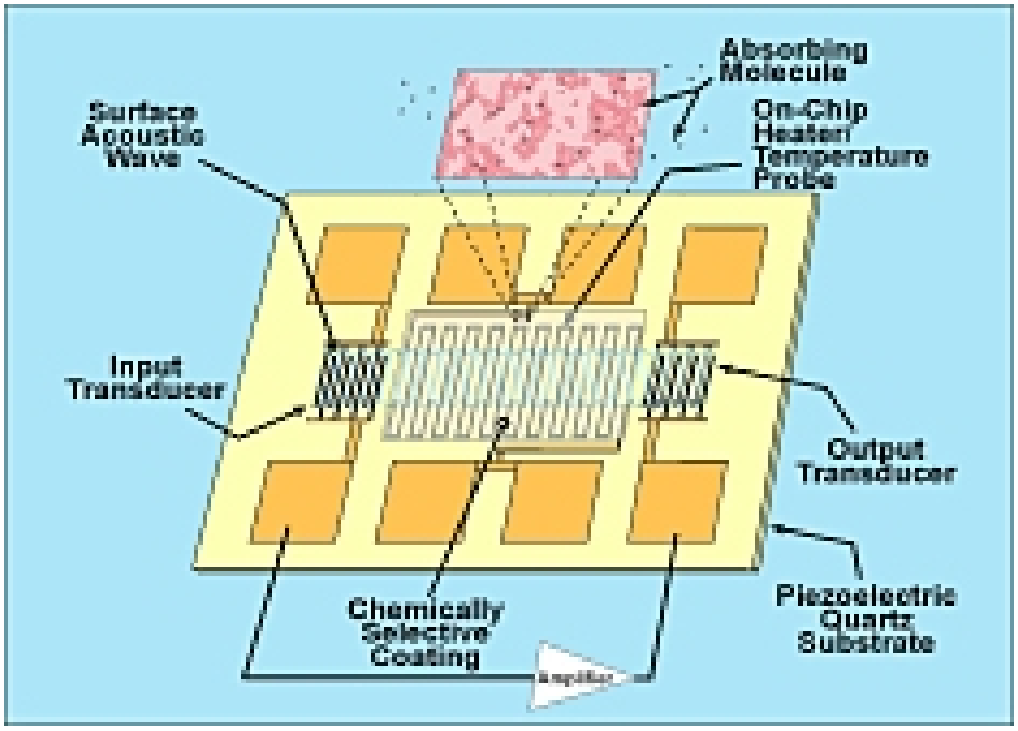

Figure 1-9: Schematics of examples of the SAW sensor (top) and the optical sensor (bottom) demonstrate the operation of such devices. These sensors are highly sensitive, but prohibitively expensive due to their complexity.

Porous Silicon Sensors

Porous Silicon (PS) covers a broad range of chemically etched, electrochemically etched, or micro-machined materials. All of these materials are made on a silicon wafer for the specific purpose of creating a region with a large surface to volume ratio. For this reason, Porous Silicon has been utilized many times as a sensitive layer to fabricate several kinds of sensors. Although only one type of PS was used in the fabrication of the Porous Silicon Gas Sensor discussed in this thesis, an overview of several PS devices will allow the reader a basis for comparison. These sensors include, but are not limited to, humidity transducers, liquid phase ion detectors, and gas sensors.

Many kinds of sensors can be realized with porous silicon materials. It has already been mentioned that porous silicon is a viable sensor material because it provides a very high surface area in comparison to bulk silicon. This being said, there are many ways that the material can be manipulated to transduce a desired property or response.

Both the time of transduction and the recovery time are of paramount importance in most sensor applications, and both are limited by the diffusion equation (Equation 1-2) in porous silicon sensors. If the material is nanoporous, the diffusion coefficient is typically determined on the basis of Knudsen or zeolite diffusion, and not by the notably faster Fickian diffusion, which is characteristic of open-air systems. When constructing a sensor system, the depth and width of nanoporous silicon must be analyzed to ensure rapid transduction and recovery.

$$\frac{dC(x,t)}{dt} = D_{ps}\frac{d^2C(x,t)}{dx^2}$$

Equation 1-2: The diffusion equation

In some instances, the sensing rate of porous silicon is determined by factors other than diffusion. These alternate effects are promoted when an analyte is drawn to surface sites, either chemically or electrochemically. In the case of the humidity sensor, water vapor condenses from the atmosphere onto the surface of the sensor. In the case of the sodium ion sensor, an electrochemical cell collects sodium ions on the surface. In either case, the Nernstian behavior of the configuration has a dramatic impact on the sensing behavior.

The Nernst equation (Equation 1-3) describes the potential at which electrochemical equilibrium is achieved for a concentration of a substance 'X'. The substance exists both above and within the surface of the sensor at some concentration. Since the surface of the sensor is of significantly smaller size than the region containing the substance in gas phase, adsorption into the surface does not change the substance's concentration above the sensor. The voltage represented by the Nernst equation is the voltage difference between the phases at the point of chemical equilibrium.

$$E = E^0 + \frac{RT}{F}\ln([X])$$

Equation 1-3: The Nernst equation

A brief overview of several kinds of PS sensors, each with different applications, construction, and benefits will provide the reader with a general understanding of the scope of these devices. While advances are being made through the integration of

CMOS, MEMS, and NEMS with existing sensors of all types, porous silicon sensors of several types are now being developed as platforms for ever-increasing applications.

Porous Silicon Humidity Sensors

Porous Silicon is a common material in humidity sensors because of several enabling properties. In general, these sensors use the inherent high surface area of porous silicon, in combination with a modified porous silicon surface, to serve as the medium for transduction due to humidity. Water, present in the air, collects onto the hydrophilic surface of the pores, changing the electrical properties of the bulk porous silicon framework. The amount of water condensed is related to the concentration of water in the air by the Nernst equation. Other factors, such as temperature and pressure, can also affect the pore conductivity. Methods for measuring the electrical modification of the porous silicon, in addition to producing and treating the porous silicon surface, account for most of the variations in the development of different porous silicon humidity sensors.

The most studied humidity sensors represent variations on a similar theme. The sensors use a porous silicon layer (2 to 15 nm diameter pore) to measure the relative humidity (RH) of air. The adsorbed moisture affects the capacitance of the pores, which is typically measured with two gold electrodes either on the surface of the porous silicon or on the top and bottom of a treated wafer. A number of variations are possible with these common devices enabling the realization of a variety of improvements in sensor performance.

A unique variation of the humidity sensor (Figure 1-10), constructed by P. Fürjes et. al., is fabricated with the PS etch as the final step[21]. An n^- layer is used to produce a Shottkey barrier restricting regions of current flow and thus defining the location of the

growth of a PS film. Metal contacts are then deposited to produce interdigitated electrodes and a resistive heating structure. Finally, a PS etch is done, producing a nanoporous structure between the electrodes (see Figure 1-10). Capacitance is measured from this device to transduce the humidity. However, the internal heating element allows slightly response times to be improved to approximately one minute by providing a driving force to speed the desorption of the water (see Figure 1-11). Performance of the device is improved through the elimination of a hysteretic behavior that is caused by cycling the sensor between high and low humidity.

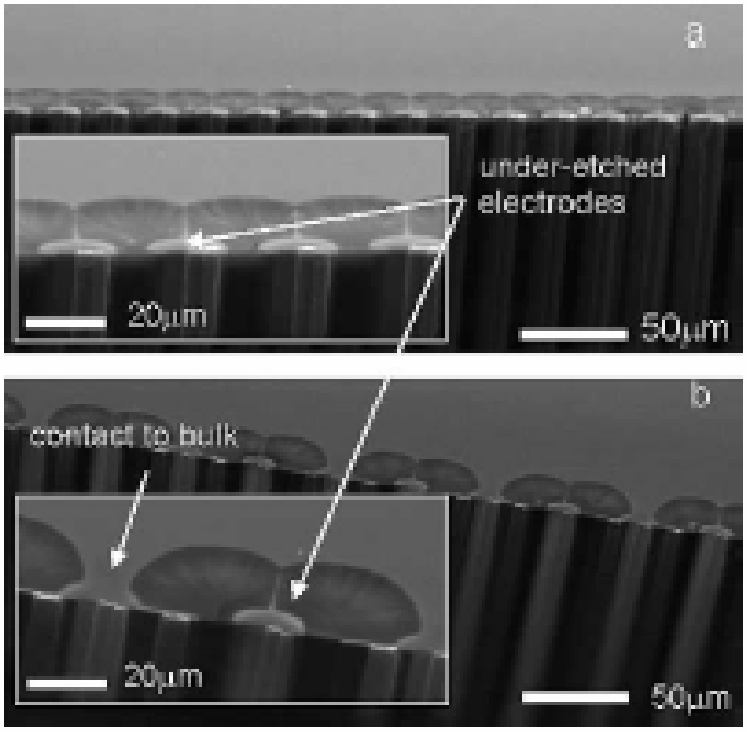

Figure 1-10: SEM cross-sections of a cleaved humidity sensor. Both electrodes (a), or one of the electrodes (b) is under-etched[21].

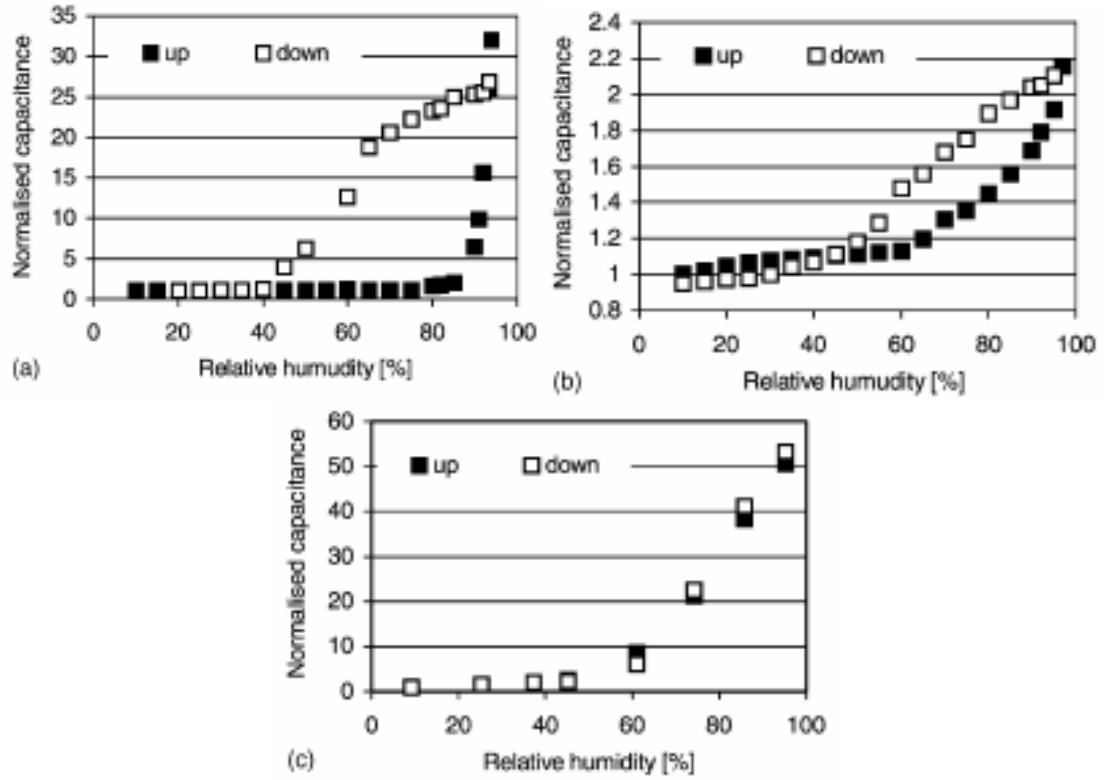

Figure 1-11: Influence of heating conditions on sensor operation: without heating (a); with continuously self-heating at a power of 30mW (b); and with refreshing before each measurement (20 s, 120mW) (c) [21].

Another variation of the PS sensor, developed by Foucaran et. al., couples a Peltier cooling device with the sensor[22]. This device uses gold contacts on the top and bottom of the sensor to measure the changing capacitance of a nanoporous film. The sensor is then affixed with a conductive epoxy to a thermoelectric cooler (TEC). The facility for cooling the sensor allows one the ability to force condensation to occur rapidly on the PS layer. This humidity sensor has extremely fast response and recovery times that are on the order of seconds (see Figure 1-12).

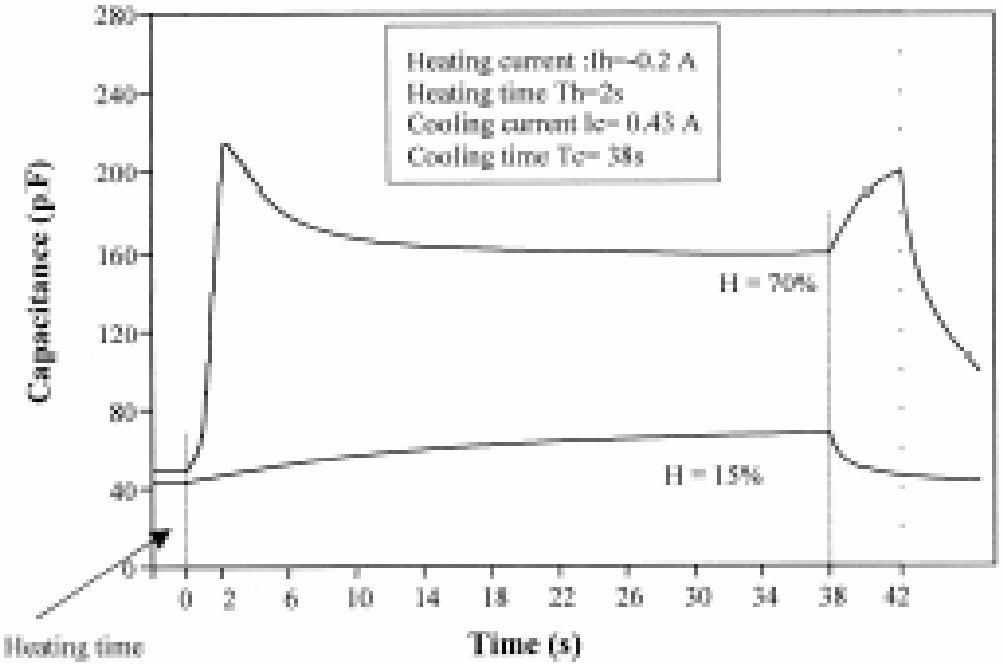

Figure 1-12: Typical curves of the TEC integrated humidity sensor showing the capacitance variations vs. time for a pulse current TEC[22].

An example of a PS humidity sensor using a modified coating is the Thermally Carbonized Porous Silicon (TC-PS) Humidity Sensor, created by M. Björkqvist et. al.[23,24]. The fabrication of this sensor (Figure 1-13) consists of the etching of p-type silicon with an HF-ethanol mixture to produce a 2.8 μm layer of pores which are an average of 6.1 nm in diameter. This film is then carbonized at 520 °C in a mixture of acetylene and nitrogen, producing a surface consisting of Si-C, Si-H, and C-H groups. 20 nm thick gold electrodes are sputtered in the form of two rectangles 0.5 mm apart to produce electrical contact to the TC-PS surface. A schematic of the finished sensor is shown in Figure 1-13. Humidity measurements are done at room temperature with impedance analysis at 100mV and frequencies ranging from 35 to 100 Hz. Figure 1-14 demonstrates the sensitivity and speed of the measurements. Capacitance is more sensitive at high humidity, while resistance is more sensitive at low humidity.

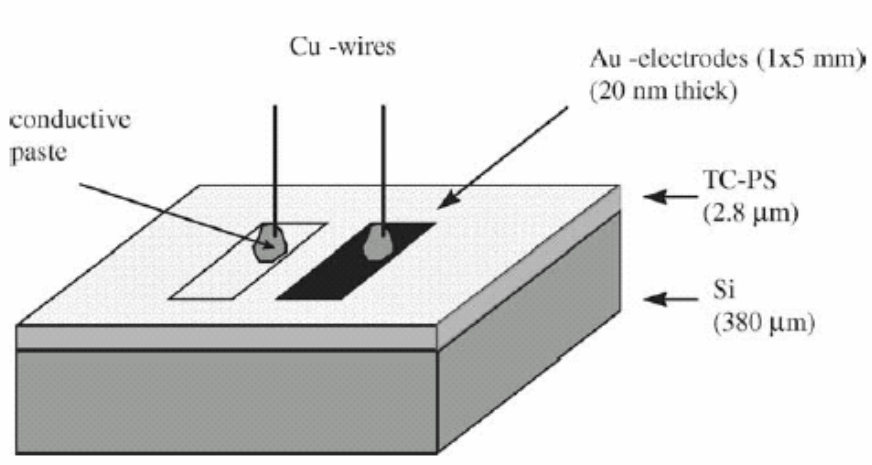

Figure 1-13: Schematic representation of a TC-PS humidity sensor[24].

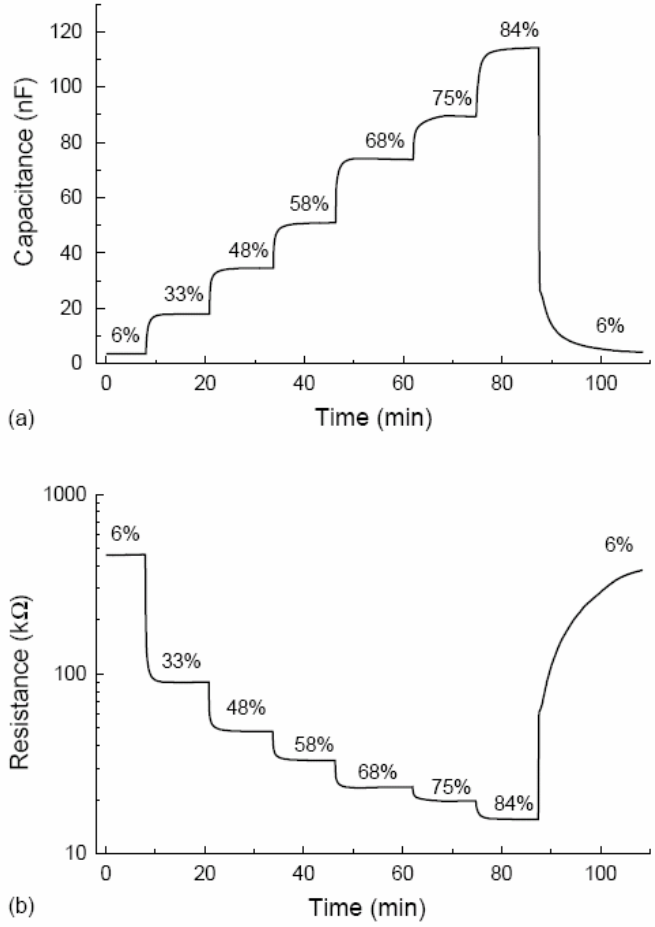

Figure 1-14: Dynamic response of (a) the capacitance and (b) the resistance of a TC-PS humidity sensor. Corresponding relative humidity values are shown in the figures. Electrical parameters were measured at a frequency of 85 Hz[24].

Additional unique humidity sensors have also been fabricated by several groups. The humidity sensor fabricated by D. G. Yarkin[25] is produced on an n-type silicon wafer, through the thermal oxidation of a PS film. The capacitance of the system is modulated following the diffusion of water into the porous layer, and measured between electrical contacts placed on the front and back sides of the wafer. A series of humidity sensors using porous polysilicon, and porous silicon carbide were fabricated by Connolly et. al. to produce devices for varying applications[26]. The porous polysilicon devices could be doped to eliminate temperature fluctuations in the capacitance of the sensor. This porous silicon carbide sensor can operate in high temperature environments where normal PS humidity sensors would be nonfunctional.

Porous Silicon Chemical Sensors

Porous silicon sensors for chemical detection can utilize the optical or photoluminescent properties of PS for transduction[27] or, more simply, they can use the PS layer as a framework and electrode for detection. For example, the PS layer could have a reactive or selective layer deposited on it, and the entire framework would be used as the counter electrode in an electrochemical cell. Bio-chemical sensors cover sensors produced to allow the detection of urea[28], glucose[29], and other biological molecules[30]. Chemical sensors which detect concentrations of either ionic solutions, or non-biological solutions constitute a second distinct group.

In the porous silicon chemical ion sensor, developed by M. Ben Ali et. al., porous silicon is used as a working electrode in an electrochemical cell[31]. P-type silicon, etched with an HF-ethanol solution, was subsequently oxidized to form a porous Si-O_x structure. This highly oxidized PS surface was used as a framework for the deposition of

calix(4)arene, a sensitive material for sodium ion detection. A sensitivity of 240 mV/decade (see Figure 1-15) to the concentration of sodium ions has been demonstrated with this device. The analysis of wafer resistivity and of the depth of the PS film was used to demonstrate the effect each has on the sensitivity of the device. Further analysis of this sensor explains the Nernstian mechanism of the response in detail[32,33].

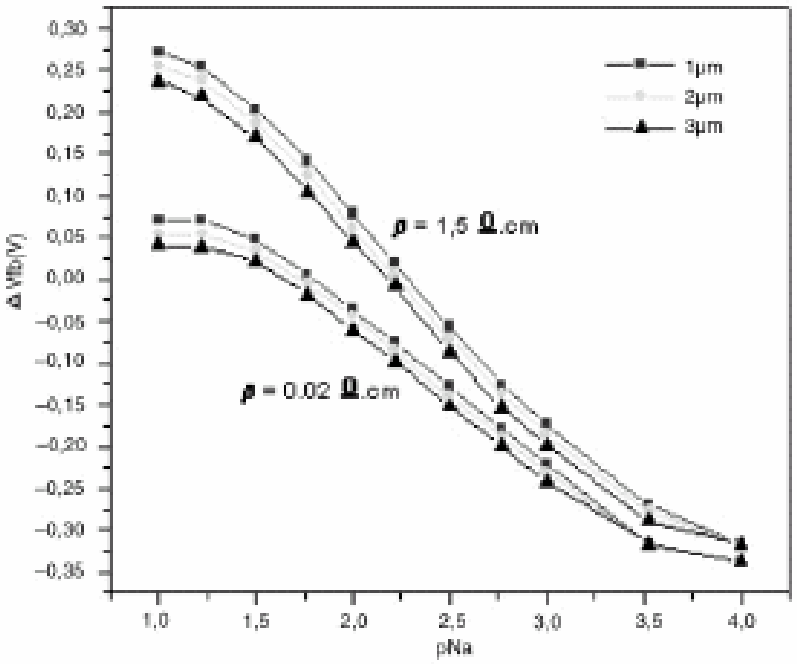

Figure 1-15: Calibration graph of functionalized PS samples for different PS layer thicknesses[31].

Porous Silicon NO_2 sensors

NO_2 sensors, which are important for air quality and emission testing, are being developed by two groups, each taking different approaches. Baratto et. al. have fabricated a device by first producing 15 µm thick and 1-2 µm wide pores using an etch solution of 50% isopropanol/50% hydrofluoric acid[34]. These pores were then detached with an electro-polishing voltage and transferred to an alumina substrate. The conductivity of the membrane was measured across pre-deposited platinum interdigitated contact (IDC) electrodes with a Solartron 1260 impedance analyzer. This system realized

a sensitivity to 100 ppb of NO_2 with a response time of around 10 minutes (see Figure 1-16).

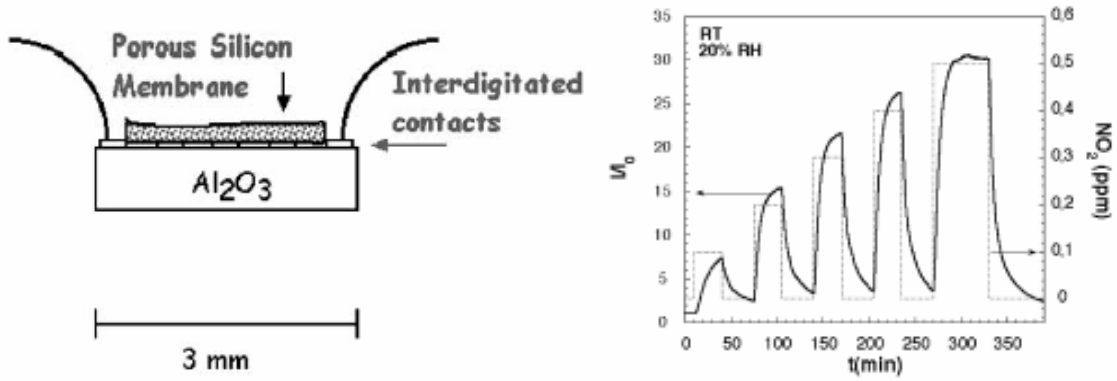

Figure 1-16: (left) Sketch of the NO_2 sensor of Baratto et. al. (lateral view). The porous silicon membrane is deposited on an alumina substrate. Sticking occurs with the IDC providing the electrical contacts. (right) Dynamic response of the sensor to sub-ppm concentrations of NO_2 and 20% relative humidity at room temperature. The continuous line represents the normalized current against time. The dotted line is the NO_2 concentration as a function of time[34].

Chakane et. al. are also investigating an NO_2 porous silicon sensor. This sensor is made through the deposition of Metallophthalocyanines (MPCs) on a nanoporous substrate 8-10 μm thick[35]. Metals tested for use with the MPCs consist of Cd, Al, and Co. These sensors produce a 70 to 100% resistance change (measured with a Keithley-2000 electrometer) when exposed to 100ppm of NO_2 with a response time of 4-5 minutes and a recovery time of 6-9 minutes (see Figure 1-17).

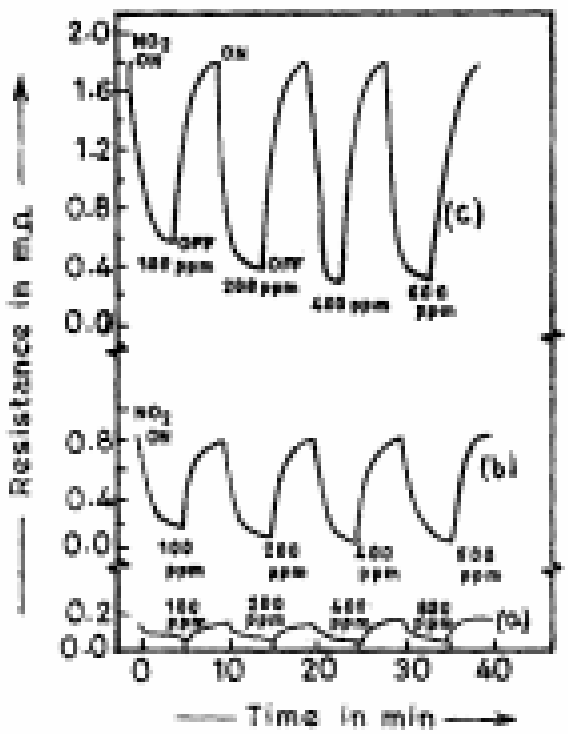

Figure 1-17: Dynamic response of (a) Al-PC, (b) Cd-PC, (c) Co-PC coated PS towards different ppm concentrations of NO_2[35].

Hydrocarbon sensors

Porous silicon hydrocarbon gas sensors represent an additional subset of those devices being investigated. Angelucci et. al. have constructed a sensor using integrated heating structures on a porous silicon membrane[36]. A microporous structure was fabricated through backside illumination and electrochemical etching. This structure was then oxidized and coated with SnO_2 to form a sensitive layer (see Figure 1-18). The sensor was evaluated by measuring the current across the layer as a one volt bias was applied to two sputtered Pt electrodes. This system senses sub-ppm C_6H_6 and CO with a response time of near one minute (see Figure 1-18).

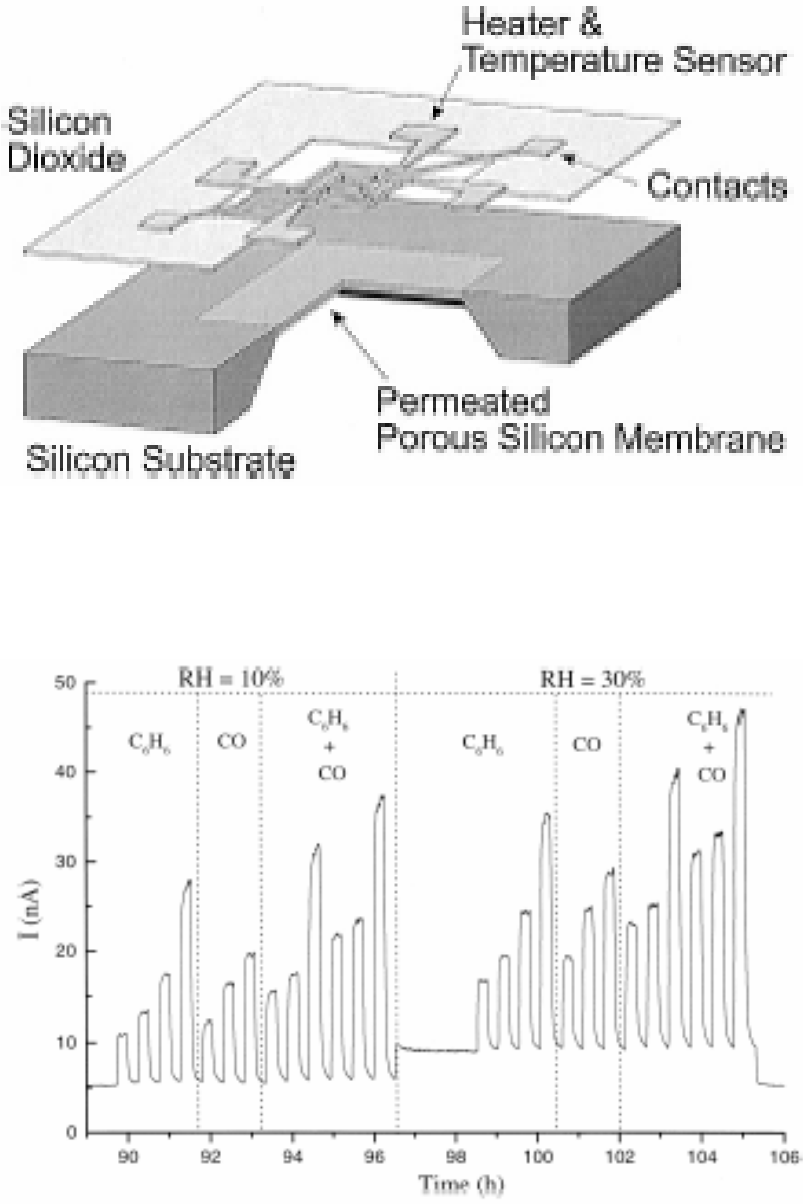

Figure 1-18: (top) Draft of a hydrocarbon sensor microstructure based on a suspended porous silicon membrane. (bottom) Electrical response of the permeated suspended porous silicon membrane sensor exposed to C_6H_6, CO, and a C_6H_6-CO mixture of differing composition, at 10% and 30% relative humidity.T=370°C, V bias= one Volt[36].

A second hydrocarbon gas sensor has been investigated by R. Liu and M. Sailor et. al. using polarization interferometry to detect the concentration of ethanol and heptane vapors[37]. The unique optical transduction mechanism that has been applied demonstrates optical sensitivity to ranges from 1 to 20 ppth of heptane, ethanol, and mixtures of the two. A response time of under one minute is also seen for 2% heptane vapors. A similar sensor has also been developed by M. Rocchia and M. Sailor et. al. which shows a reversible CO_2 sensitivity with the modification of a nanoporous surface with 3-amino-1-propanol[38]. This device is sensitive to 5 ppth of CO_2.

References

1 Sensors Online – Industry Market Studies (March 2002) http://www.sensorsmag.com/resources/research/index.htm.

2 Bayette, William, "Air Emissions of Ammonia: Sources, Estimation Methods, and Uncertainties" (December 2005) http://www.chesapeakebay.net/temporary/asc/pres/Battye.PDF

3 Toxicology Facts for Ammonia, Agency for Toxic Substances and Disease Control, (September 2002) http://www.atsdr.cdc.gov/tfacts126.html

4 Toxic Air Contaminant Identification List Summaries: Ammonia, California Air Research Board (September 1997) http://www.arb.ca.gov/toxics/tac/factshts/ammonia.pdf.

5 Chemical Profile: Ammonia, Children's Health Environmental Coalition (June 2001) http://www.checnet.org/healthehouse/chemicals/.

6 EPA Air Trends Carbon Monoxide (June 2005) http://www.epa.gov/airtrends/carbon.html

7 Health Facts: Carbon Monoxide, Wisconsin Department of Natural Resources, (March 2003) http://www.dnr.state.wi.us/org/aw/air/HEALTH/carbon.htm.

8 J Watson and G. Davies, A low level carbon Monoxide monitor, Sensors and Actuators B 2 (1990) 219-222.

9 R. Venterea, D. Rolston, Nitric and nitrous oxide eimission following fertilizer application to agricultural soil, biotic and abiotic mechanisms and kinetics, Journal of Geophysical Research, 105, (2000) 15117-15129.

[10] J. B. McCammon, W. D. Wagner, D. Groth, G. Hatfield, and L. Reed, Current Intelligence Bulletin 50: Carcinogenic Effects of Exposure to Diesel Exhaust, CDC Publication, (August 1988) http://www.cdc.gov/.

[11] EPA Air Trends Nitrogen Dioxide, (June 2005), http://www.epa.gov/airtrends/nitrogen.html.

[12] Correspondence between Alfred Hollman and Stephen Lewis, 3-22-2004.

[13] EPA Air Trends Sulfur Dioxide, (June 2005), http://www.epa.gov/airtrends/sulfur.html.

[14] Wisconsin Department of Natural Resources – Sulfur Dioxide sources and health effects, (September 2003) http://www.dnr.state.wi.us/org/aw/air/health/sulfurdiox.htm.

[15] "Hydrogen Sulfide Gas", Published by the Oil, Chemical, and Atomic Workers International Union (December 2005) http://www.webshells.com/ocaw/txts/doc999903.htm.

[16] D.M. Wilson, "Analog VLSI Architectures for Chemical Sensing Microsystems," Ph.D. Dissertation, Georgia Institute of Technology, Nov. 1995.

[17] D. M. Wilson, S. Hoyt, J. Janata, K. Booksh, and L. Obando, "Chemical Sensors for Portable, Handheld Field Instruments," IEEE Sensors Journal, 1, 4, Dec. 2001.

[18] Schottky Diodes (November 2002) "http://www.mtmi.vu.lt/pfk/funkc_dariniai/diod/schottky.htm".

[19] Lechuga, L.M., Calle, A.; Golmayo, D., Briones, F., de Abajo, J., de la Campa, J.G., "Ammonia sensitivity of Pt/GaAs Schottky barrier diodes. Improvement of the sensor with an organic layer.", Sensors and Actuators B, v B8, n 3, p 249-52, June 1992.

[20] Microsensors Technical Information – Chemical Microsensors (June 2005) "http://www.sandia.gov/mstc/technologies/microsensors/chem_list.html#IMS".

[21] P. Fürjes, A. Kovács, Cs. Dücső, M. Ádáma, B. Müller, U. Mescheder, "Porous silicon-based humidity sensor with interdigital electrodes and internal heaters", Sensors and Actuators B, 95, pp.140–144 (2003).

[22] A. Foucaran, B. Sorli, M. Garcia, F. Pascal-Delannoy, A. Giani, A. Boyer. "Porous silicon layer coupled with thermoelectric cooler: a humidity sensor", Sensors and Actuators A, 79 (2000) 189-193.

[23] M. Björkqvist, J. Salonen, and E. Laine, "Humidity behavior of thermally carbonized porous silicon", Applied Surface Science, 222, pp. 269–274 (2004).

[24] M. Björkqvist, J. Salonen, J. Paski, E. Laine, "Characterization of thermally carbonized porous silicon humidity sensor", Sensors and Actuators A, 112, pp. 244–247 (2004).

[25] D.G. Yarkin, "Impedance of humidity sensitive metal/porous silicon/n-Si structures", Sensors and Actuators A, 107, pp. 1–6 (2003).

[26] E. J. Connolly, P. J. French ,H. T. M. Pham, P. M. Sarro, "Relative Humidity Sensors Based on Porous Polysilicon and Porous Silicon Carbide", Proceedings of IEEE Sensors 2002, 2002, pt. 1, pp. 499-502 vol.1.

[27] M. Stewart and J. Buriak, "Chemical and Biological Applications of Porous Silicon Technology", Adv. Mater. 2000, 12, No. 12. pp. 859-869.

[28] J. H. Jin, N. K. Min, C. G. Kang, S. H. Park and S. I. Hong, "Characteristics of urea sensor based on platinum deposited porous silicon", Journal of the Korean Physical Society, v 39, suppl. pt. 1, Dec. 2001, p S67-9.

[29] S. Libertino and G. D'Arrigo, "Porous Si based bioreactors for glucose monitoring", Proceedings of the SPIE, v 5119, 2003, pp 149-155.

[30] L. DeStefano, I. Rendina, L. Moretti, A. Lamberti, O. Longo, and P. Arcari, "Porous silicon optical sensors for vapors, liquids, and biological molecules", Proceedings of the SPIE, v 5118, 2003, pp. 305-309.

[31] M. Ben Ali, R. Mlika, H. Ben Ouada, R. M'ghaïeth, H. Maâref, "Porous silicon as substrate for ion sensors", Sensors and Actuators, 74, pp. 123–125 (1999).

[32] S. Zairi, C. Martelet, N. Jaffrezic-Renault, F. Vocanson, R. Lamartine, R.M'gaïeth, H. Maâref, M. Gamoudi, "*p*-type porous-silicon transducer for cation detection: effect of the porosity, poremorphology, temperature and ion valency on the sensor response and generalisation of the Nernst equation", Appl. Phys. A, 73, pp. 585–593 (2001).

[33] S. Zairi, C. Martelet, N. Jaffrezic-Renault, R. M'gaïeth, H. Maâref, R. Lamartine, "Porous silicon a transducer material for a high-sensitive (bio) chemical sensor: effect of a porosity, pores morphologies and a large surface area on a sensitivity", Thin Solid Films 383, pp. 325–327 (2001).

[34] C. Baratto, G. Faglia, E. Comini, G. Sberveglieri, A. Taroni, V. La Ferrara, L. Quercia, D. Di Francia, "A novel porous silicon sensor for detection of sub-ppm NO_2 concentrations", Sensors and Actuations B 77 (2001) 62-66.

[35] S. Chakane, A. Gokarna, S. V. Bhoraskar, "Metallophthalocyanine coated porous silicon gas sensor selective to NO_2", Sensors and Actuators B, 91 (2003) 1-5.

[36] R. Angelucci, A. Poggi, L. Dori, G. C. Cardinali, A. Parisini, A. Tagliani, M. Mariasaldi, F. Cavani, "Permieated porous silicon for hydrocarbon sensor fabrication", Sensors and Actuators A, 74 (1999) 95-99.

[37] R. Liu, T. A. Schmedake, Y.Y. Li, M. J. Sailor, Y. Fainman, "Novel porous silicon vapor sensor based on polarization interferometry", Sensors and Actuators B, 87 (2002) 58-62.

[38] M. Rocchia, E. Garrone1, F. Geobaldo, L. Boarino, and M. J. Sailor, "Sensing CO_2 in a chemically modified porous silicon film", phys. stat. sol. (a) 197, No. 2, 365– 369 (2003).

CHAPTER 2

FABRICATION

The creation of the first rapidly responding porous silicon gas sensor (PSGS) occurred in 1999. Prior to this, the best response times of porous silicon gas sensors were on the order of 30 minutes[1]. The rapidly responding PSGS was constructed in a preliminary investigation whose goal was to determine if porous silicon could be used as a sensitive material in a gas sensor by Seals, Tse, Hesketh, and Gole[2,3]. This device was conceived as a means to detect gas based upon the extremely high surface area of porous silicon combined with the ability to produce low resistance contacts made possible through a photoluminescence-induced electroless metallization technique uniquely combined in a hybrid micro/nanoporous porous silicon framework (Figure 2-1). The potential for low cost fabrication and operation coupled with the preliminary measurements of sensitivity provided the motivation for additional investigations into these devices.

These initial sensors were fabricated as simple conductometric resistors. These resistors consisted of two low-resistance gold contacts deposited on a region of porous silicon defined by a silicon nitride dielectric masking layer. The response of the devices was measured as the change in impedance by an impedance spectroscopy device, the Solartron 1260. These devices were able to reversibly respond to premixed concentrations of ranging from 10-1000 ppm Hydrogen Chloride, Ammonia, and Nitric Oxide in an Argon background.

It is from this initial research effort that an approach to develop these gas sensors into a viable technology began. The first steps of this process involved an attempt to

characterize and establish the porous silicon etch process so as to produce the most advantageous structure to optimize the porous silicon layer of the gas sensors. Additional efforts to optimize other aspects of the fabrication process then followed based upon steps carried out which successfully attained improved sensors. The most significant improvements resulted from the use of silicon carbide rather than silicon nitride as the masking layer and the implementation of an anhydrous method for contact deposition to the sensors.

Hybrid Porous Silicon Etch

The most critical component of the PSGS is the sensitive porous silicon layer. This layer provides the framework by which the transduction mechanism that is used to detect trace levels of analyte gas is operative. While a variety of porous silicon pore structures can be generated, a hybrid micro/nanoporous PS layer was chosen to construct the gas sensors that have been investigated in this study[4]. Figure 2-1 depicts two SEM images of this pore structure. Within the walls of the micropores, there exists a continuous nanoporous coating, thus creating an extremely large surface area per given volume of PS. It is because of the high surface area of the hybrid micro-nanoporous surface that this PS morphology was chosen to create low gas concentration sensors.

The porous silicon we use in the formation of sensors is created with an electrochemical etch on the polished surface of a p-type (100) silicon wafer of 7-9 Ω-cm resistivity. The etch solution consists of a 1M H_2O, 1M HF, 0.1 M tetra-butyl-ammonium-perchlorate (TBAP) solution in acetonitrile (MeCN). The power that drives each etch process is monitored and recorded by computer (a detailed description of this program follows) so that the quality of the sample produced can be controlled. An etch

typically takes place at a constant current density, which can be selected from 0.2-50 mA/cm^2, and produces a porous structure with pores 1μm wide and from 1 to 20 μm deep. The best performing devices, those devices with both the lowest noise levels and the lowest detection limits, have a porous structure of shallow (1 to 2 μm deep) pores.

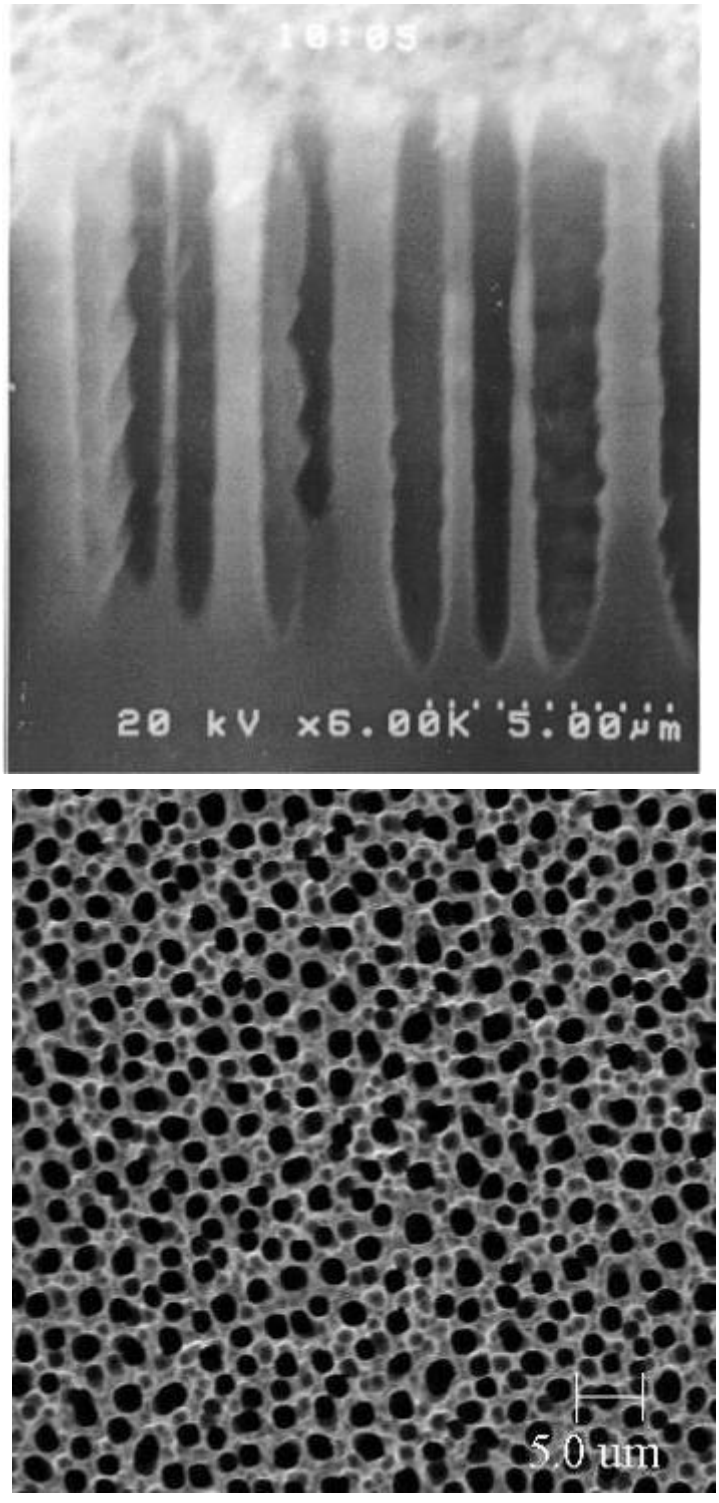

Figure 2-1: Images taken of a porous silicon structure illustrate micron-wide pores of varying depths close to 10µm etched in a p-type silicon wafer.

Experimental Design of Etch Equipment

The etching of porous silicon requires that several pieces of equipment and materials be brought together in a combination to generate the desired morphology. Of significant importance is a fume hood, which serves two purposes. First, the hood keeps the experimenter safe from the toxic chemicals and fumes present in the etch solution. Second, the hood greatly decreases the possibility of contamination that would exist if the etch were done in an open-air environment. A power supply is also needed to perform the electrochemical etch. This power supply must be capable of producing the etch current at a high enough voltage to etch the porous silicon surface. A supply capable of producing 1 Amp at 100 Volts was chosen so that large areas of the porous silicon could be etched into the silicon wafer.

An etch cell which houses the contact electrodes, wafer, and etch solution is the final component needed to etch the wafer. A schematic of a generalized etch cell is shown in Figure 2-2. There can be much variation in the size and shape of the cells, but virtually all are made from chemically-inert high density polyethylene. At the beginning of this project, a cell capable of etching one square centimeter of silicon was used. Due to this limitation, a cell was constructed that etches five square centimeters. With this cell, an area sufficient to produce 12 sensors was created. This cell was the most frequently used. Additionally, this cell was designed so that a stirring bar could be used with the etch solution. This improved the uniformity of the etch process by ensuring that the etch solution remains well mixed at the surface of the silicon wafer and that the products of the etching reaction are carried away. The silicon wafer is the anode in the etch process. A small platinum sheet acts as the cathode; this material is chosen due to its

chemical resistance to the etch solution. A metal plate wrapped in aluminum foil is used to provide support to the back of the wafer to avoid the wafer cracking under the stress of clamping. This metal plate also provides electrical contact to the backside of the wafer. A gasket cut from a sheet of Viton® is used as a seal between the wafer and the polyethylene etch cell.

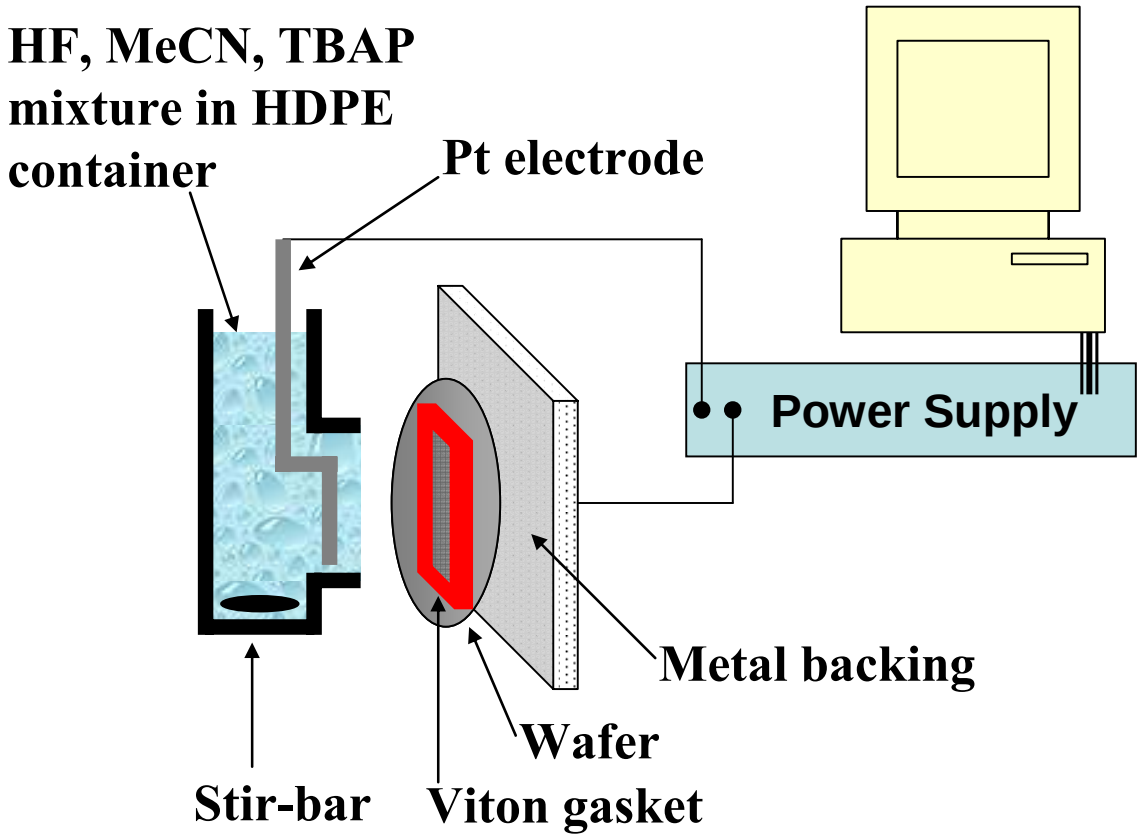

Figure 2-2: A schematic of the etch cell (separated components) indicating where the silicon wafer is clamped between the container for the etch solution and a metal plate for electrical contact to perform an electrochemical etch.

Procedure

To assemble the etch cell, the wafer is first aligned with the Viton® gasket and the metal backing. Next, the cell is placed in contact with the gasket, and the assembly is clamped with a C-clamp. To ensure a tight seal, methanol is poured into the cell. If

evidence for leaking is observed, the cell must be re-assembled or clamped tighter. If the gasket is sealed, the methanol is removed, and the etch solution is mixed and poured into the etch cell. Next, the stir bar is added and the solution is placed on a magnetic stirring device to mix the solution during the etching of the wafer. Finally, the etch cell is connected to the power supply. The porous silicon etch is now ready to commence.

To characterize the porous silicon etching process, the power supply (HP6634B) was interfaced with a computer using the LabView programming language. Two programs were created to control the etching of porous silicon. The first of these programs was designed to characterize the etch cell, but it serves an additional function by cleaning the surface of the wafer. The second program (which is used after the first) produces the pores in an established constant-current mode of operation. Three etch runs were conducted to evaluate the performance of this system, using the standard mixture of reactants in the 5 cm^2 etch cell.

The first program was created to characterize the cell before each run as some variation can occur during the assembly of the component parts of the etch cell. This program initiates a linear voltage sweep of the cell through the power supply. The voltage supplied and the current that is drawn through the cell are both recorded by the program. From this data, the resistance of the cell is plotted versus the voltage across it, which results in plots similar to those in Figure 2-3. Each plot is characterized by a maximum in the resistance at the point where the bias voltage is sufficient to begin the electrochemical etching of silicon, and lower resistances on either side. To the left (lower potential) of the peak, the reaction rate is limited by the voltage supplied by the power supply. To the right of the peak, the diffusion limited reaction rate is slowed by the

depleted concentration of reactants at the surface of the porous silicon. While differences in the precise nature of the assembly of the etch cell, particularly the contact resistance of the wafer to the metal backing material, cause some variation, this initial program allows the cell to be characterized before the etch occurs and thus establishes the detailed experimental conditions under which the etch is occurring. In addition, the voltage sweep acts as cleaning step to remove surface contaminants from the wafer by electropolishing. The electropolishing corresponds to the electrochemical dissolution of the entire surface (no pore formation) of the wafer.

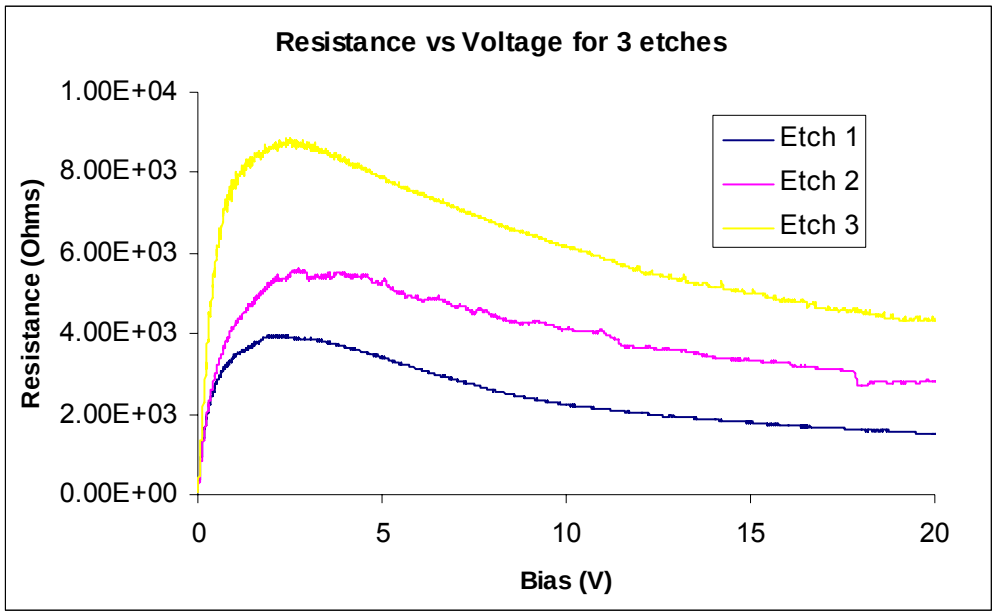

Figure 2-3: Three plots of resistance versus bias voltage for three "identically" assembled etch cells.

After the initial preparation and characterization of the silicon wafer, a second program performs the electrochemical etching to produce porous silicon. Etches were typically performed at a constant current so as to remove silicon at a constant rate. As such, the only parameters are the etch time and the etch current. At very high currents, the etch process occurs across the entire face of the silicon wafer, and results in electro-

polishing of the surface; at low currents, little or no reaction occurs. The etch time is chosen to range between 5 and 60 minutes, and the etch current density is chosen to range between 0.2 and 50 mA/cm^2. Typically, an etch process is performed for approximately 10 minutes at approximately 4 mA/cm^2. The depth of the porous silicon is proportional to the etch time, provided that electro-polishing does not occur. The question of establishing an optimal pore depth will be considered later in this dissertation (Chapter 6). During the etching of a wafer, the cell resistance is recorded and displayed. Figure 2-4 displays the results from three etches of porous silicon for various currents. The gentle increase in resistance over time is an indication that pores are being etched into the silicon, as the porous region has a higher resistance than the silicon which is, in part, due to the diffusion of reactants to the bottom of the pores. The pore walls limit the mixing of reactants inside the porous framework, where little or no flow can occur. This limitation increases the resistance as the lack of reactants increases the potential at which the electrochemical reaction occurs[5]. The sharp drops in resistance are synonymous with the dissolution of the higher resistance porous regions. This allows the establishment of a lower resistance pathway through the solution into an effectively thinner silicon wafer.

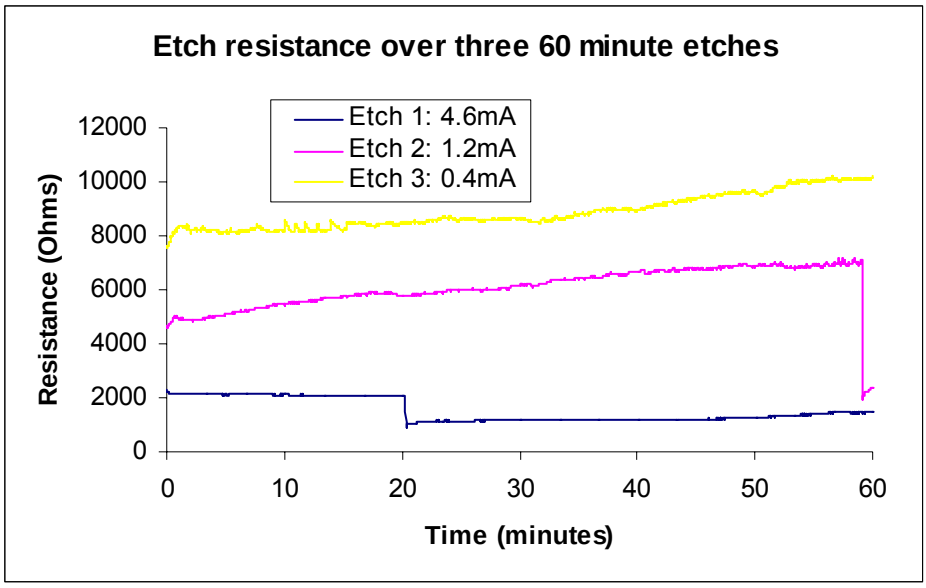

Figure 2-4: A plot of 60 minute etches using the 5cm^2 cells shown in Figure 2-3 under different currents demonstrates the pore breaking phenomenon.

As the breaking of the pores demonstrated in Figure 2-4 is obviously detrimental to the etch process and to the formation of porous silicon, a new mode of performing etches is being considered to replace the constant-current method previously discussed. The pores are broken as the voltage required to maintain a steady etch current increases over time with the increase in resistance. At some point, surface electropolishing begins, and the pores are removed by dissolution from the surface of the wafer. The modified etching mode would operate the etch cell only initially in a constant-current mode. After pore nucleation has occurred and a gentle increase in resistance is observed, the etch process can be switched to a constant voltage mode so as to slow the reaction rate and greatly decrease the possibility of electropolishing. In the constant-voltage mode, we expect the etch resistance to increase in time, as an increasing resistance within the pores is still characteristic of this system. However, this increasing resistance would not occur as quickly as is characteristic of the faster, constant-current mode. Further testing of these modes of operation in a controlled environment would yield the most effective

means to create the most sensitive porous silicon films for use in gas sensing applications.

Cleaning

A series of experiments[6,7,8] conducted in Prof. Gole's laboratory have focused on the characterization of the photoluminescence (PL) from porous silicon. PS absorbs ultraviolet radiation and emits photons in the green to orange-red region of the spectrum. The studies have resulted in the stabilization and optimization of the PL emission using primarily an HCl cleaning process[9,10]. Further, this stabilized PL was used to develop a method of contact formation[11,12], resulting in contact resistances as low as 20Ω to the porous structure. These highly improved contacts are created using the PL induced deposition of a gold layer from a basic (9-11 pH) electroless solution. The gold is deposited uniformly at the sites of the PL, at the nanoporous surface of the micropores. Contacts for bonding can be quickly deposited, through E-beam evaporation, into and onto the surface of the pores. While the contacts formed from electroless metallization are not currently used for fabrication of sensors with a current focus on the anhydrous fabrication of contacts, sensors are still cleaned with the HCl cleaning process as it consistently provides devices with higher sensitivity and lower noise during operation.

Sensor Fabrication Processes

Fabrication of the Porous Silicon Gas Sensor (PSGS) requires several different facilities at the Georgia Institute of Technology. While most of the fabrication occurs in the Georgia Tech Microelectronics Research Center (MiRC) cleanroom[13], the porous silicon etch is conducted in the School of Physics. Additionally, the HCl cleaning

process and the deposition of selective coatings (see Chapter 4) are chemical processes that have been carried out in both the School of Physics and in the MRDC-2 Mechanical Engineering building at Georgia Tech. This section describes, in detail, the steps required to produce a standard gas sensor. As will be indicated, the standard steps have been varied during the course of this study. However, the recipes represented in the development of this section are the established standard for the porous silicon gas sensor fabrication. In this section, the current standard fabrication process and several potential variations to it are discussed.

The most general fabrication process, shown in Figure 2-5, is first discussed. This process is the basis upon which all variations occur.

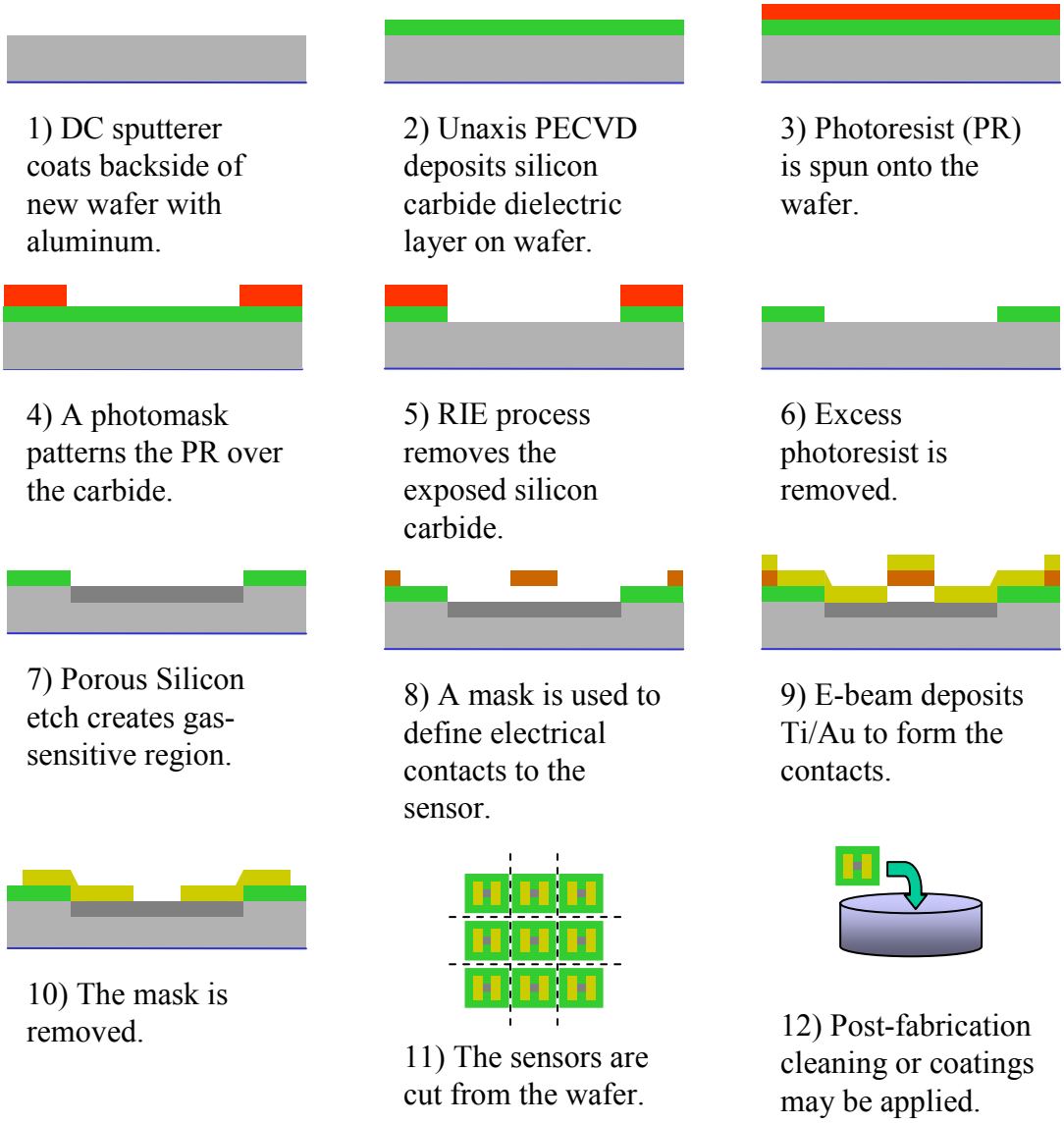

Figure 2-5: An overview of the most general fabrication process to produce porous silicon gas sensors is shown. Variation in this process occurs with changes in the sensor design. Additionally, two different methods for masking can be used in step 8.

DC Sputterer

The DC Sputterer system is used to deposit layers of metal across the surface of several wafers. The metals that were deposited using this device include aluminum, titanium and gold. Many other metals can also be sputtered with the sputterer including platinum, copper, iron, nickel, and most others. The sputterer has the capacity to deposit metal on over 24 2" wafers or 6 4" wafers at one time.

To deposit a layer of metal onto a wafer or set of wafers, they are inserted into the sputterer and the desired metal source is installed. Each metal is deposited at a different rate, so this information has to be considered based on the online manual.

For current PSGS devices, only aluminum is deposited using the sputterer for step 1 of the fabrication. It was abandoned as a deposition system for the titanium/gold contacts in step 9 due to the improved anisotropy of the E-beam evaporation. The aluminum is deposited on the backside of each wafer to obtain a better electrical contact. This contact improves the quality and continuity of the porous silicon etching by producing a constant potential source on the backside of the wafer. This limits charge build up inside the device and improves the stability of the signal.

Silicon Carbide Deposition

In step 2 of the fabrication process, a Unaxis Plasma Enhanced Chemical Vapor Deposition (PECVD) system was used to deposit a silicon carbide layer atop the silicon wafer. The silicon carbide was chosen for this layer, as it is not reactive with the component materials used to carry out a porous silicon etch and thus gives a measure of

control over where the etch takes place. Later fabrication steps allow the selective removal of the silicon carbide layer in regions where the etching process was required to produce the sensing layer.

Silicon carbide (SiC) was produced using a recipe labeled "SiC25_8.prc" on the Unaxis PECVD. The number 25 indicates that the process occurs at 250ºC and the 8 indicates the wattage used to power the layer deposition. This particular combination was chosen because it produces a more chemically resistant and uniform layer of silicon carbide. Research by Arnab Choudhury, under the supervision of Dr. Peter Hesketh, produced the formulation of this recipe[14]. The time of the active deposition determines the thickness of the layer of carbide deposited. The deposition rate is approximately 80-85 Å /min.

Prior to running a deposition on the Unaxis PECVD, a thorough cleaning of the system must be performed. The program Clean250.prc on the Unaxis PECVD will adequately clean the system if run for an hour before each deposition. This process is a high temperature removal of any contaminants in the chamber via a plasma etch of the entire chamber.

The carbide layer must be thin enough to allow electrical continuity of the gold across the carbide-sensor threshold, but thick enough to ensure electrical and chemical insulation. Efforts to minimize the layer thickness with respect to the first criteria required that the silicon carbide thickness to be set below 0.2 microns. A carbide deposition time of 10 minutes yields a layer 800Å thick, which provides the appropriate electrochemical insulation facilitating also the formation of selected regions for the PS etch. The section Silicon Carbide Reactive Ion Etching discusses the appropriate recipe

for selective removal of the carbide mask so as to expose the desired wafer regions for etching.

Photolithography

Photolithography represents a significant process in our efforts to create a PS sensor because it is the only means of transferring patterns on the MEMS scale to a wafer. The photolithographic process deposits a layer of photoresist (PR) polymer across the surface of a wafer in a selective manner. This polymer is resistive to many substances including HF and some RIE processes. However, solvents, including acetone and methanol, easily dissolve the photoresist.

Figure 2-6 below demonstrates the general process flow of photolithography for the positive photoresists used in creation of the PSGS. Details for the two photolithographic process recipes used for creating PS sensors are given in Table 2-1. The photolithographic process begins with the spinning of photoresist onto the surface of a wafer. This spinning ensures the resist is equally thick across the wafer. The wafer is then placed in an oven (typically 95°C) for a soft-bake process. The soft-bake hardens the resist slightly in preparation for the next steps. Next, the wafer is aligned under a mask aligner and then exposed to UV light. The mask blocks the light in some regions while allowing the light pass through in others. This selectively cures the photoresist and transfers the pattern on the mask to the wafer. Finally, the wafer is soaked in developer to develop the cured PR, further hardening it, while removing the uncured resist. The developer and remaining uncured resist is then rinsed from the wafer with DI water. The wafer is then dried and placed in an oven for a final bake (typically 120°C). This removes excess moisture from the wafer and PR, which hardens the PR completely.

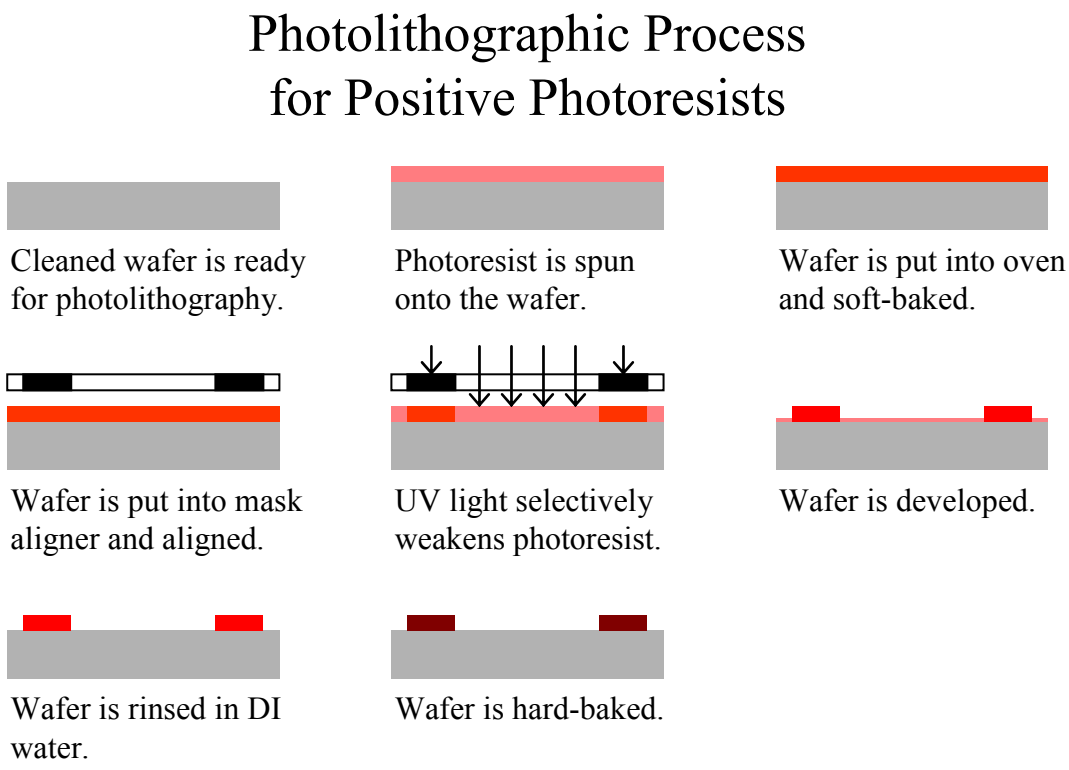

Figure 2-6: An example of a photolithographic process using positive photoresist. A process using negative photoresist would differ in that UV light strengthens the photoresist, rather than weakening it, and require that a "negative" photolithography mask be used. All photoresists used in fabrication of the PSGS were positive.

The photolithographic process was initially used in two stages (step 4 and step 8 in Figure 2-5) of fabrication. Step 4, which is presently used in the fabrication of sensors, uses photolithography to mask the silicon carbide layer so that it can be selectively removed from the wafer in regions where the porous silicon is to be etched for sensor fabrication. This photoresist layer, made from Shipley 1827 photoresist, is impervious to the plasma etch process used to remove silicon carbide. It is important to limit the growth of the sensitive PS layer to just the region of the sensor because the packaging of the sensor requires that a hard insulating surface (not porous silicon) be located beneath the metal contact electrodes.

The second photolithography masking step, step 8 in the fabrication process, shielded the porous silicon as gold electrodes were deposited over regions of the sensor. The photoresist layer used here consisted of Shipley 1813 resist. This resist was chosen because, if the hard bake step is skipped, it can be removed from the sensor with a simple 30 minute immersion in methanol. The methanol dissolution process was employed after it was found that the acetone, which was used to remove the cured Shipley 1813 photoresist, irreversibly destroys the sensitivity of the PS sensor. This second masking step was eventually replaced with an anhydrous method of depositing metal contacts to the sensor (discussion following) when it was discerned that both prolonged exposure to water and to temperatures in excess of 80°C damage the sensor performance[15,16].

Standard recipes (shown in Table 2-1) were used to produce each of the two photoresist layers. For the second masking layer, using the Shipley 1813 resist, the final hard bake step was not needed; the hardening of the photoresist provided no advantage to the resist acting as a masking layer for the gold deposition process and made the eventual removal of the resist more difficult.

Table 2-1: Standard recipes used to deposit photoresist during the fabrication of porous silicon gas sensors.

	Shipley 1827	Shipley 1813
Spin resist	3500rpm-30s	3500rpm-30s
Soft Bake	5 min @ 95°C	5 min @ 95°C
Aligner	MJB3-right[17]	MJB3-right
Align	Mask 1	Mask 2
Expose	180mJ	180mJ
Develop	MF319-60s	MF319-60s
Rinse	30s, then dry	30s, then dry
Hard Bake	15m @ 120°C	none

The removal of the S1827 photoresist can be accomplished using an acetone immersion, resulting in the dissolution of the resist into a liquid-slurry that can be rinsed

away in DI water. Acetone was used for the removal of the S1827 resist after the RIE of the silicon carbide layer to clean the surface for the PS etching process. Physical cleaning of a wafer with an ultrasonic agitator is also commonly used to speed up the dissolution of photoresist, but it was not needed.

Silicon Carbide Reactive Ion Etching

A Plasma Therm RIE (fabrication step 5) was used to remove the silicon carbide deposited by the Unaxis PECVD system. The silicon carbide is removed by an energetic plasma consisting of SF_6 gas. Either four 4" wafers or eight 2" wafers can be processed in a given production run using this system. Because this plasma does not penetrate or remove S1827 photoresist, this PR material was chosen for the masking layer.

In addition to removing the silicon carbide in the region not masked by the photoresist, the RIE also cleans the recently exposed silicon of any oxides, polymers, or other undesirable materials that have been deposited to the surface. These contaminants can arrive to the surface of the wafer during the time the wafer is placed in storage waiting to be processed. Their removal is vital to achieve a consistent and reliable porous silicon etch. Upon removal from the RIE, the photoresist, which masked the silicon carbide, can be removed with a rinse in a solvent such as acetone or methanol.

The plasma etch process "SiC_SF6.prc" was used to remove the silicon carbide resulting in windows to the silicon wafer. This removes carbide at a rate of 800Å per minute, so the RIE time is roughly 10% of the carbide deposition time. This process does not remove S1827 photoresist, but will penetrate weaker resists, such as S1813. The process also removes silicon from the bulk of the wafer, therefore, it was necessary to determine the exact time needed to remove the carbide, without removing too much of

the silicon beneath. Testing on several wafers showed that for a 10 minute carbide deposition process, a minimal RIE time of 45 seconds was needed to remove the carbide. After the process is completed, however, a visual inspection of the wafer is necessary to verify that the carbide layer is completely removed.

Porous Silicon Etch

The porous silicon etch which we use to produce sensors is identical to the hybrid porous silicon etch detailed earlier in this chapter. A variety of device tests over the course of the work presented in this dissertation has indicated that an etch is likely to yield the most sensitive, rapidly responding device if shallow, 1 to 2 micron, hybrid pores are produced as depicted in Figure 2-7.

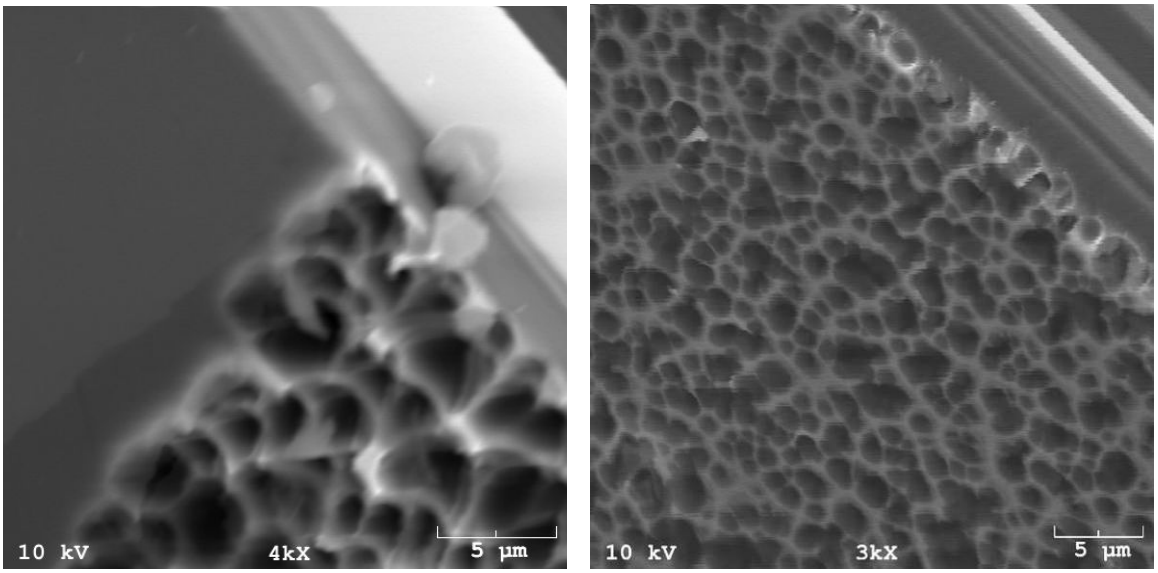

Figure 2-7: The shallow pores shown in device 5.2.2-9 (left, SEM taken at PS-carbide boundary) and 5.2.3-2 (right) are 1 to 2 microns deep. Devices from these wafer runs demonstrated the highest sensitivity and lowest noise levels.

To produce these sensitive layers, a current density close to 4 mA/cm^2 was used for 10 minutes. The R-V profiles (see Figure 2-8) and etch profiles (see Figure 2-9) of several sensor fabrication runs were collected, so as to provide a means of quality control.

All of the I-V sweeps were performed at a rate of 250mV/s, and all of etches (of the 1.2 cm^2 of open silicon provided by the mask in Figure 2-19) were done at a constant 3.3mA etch current. Important characteristics of both the R-V curve and the PS etch correlate, as indicated in the figures, to the performance of the sensors which were fabricated. While nearly 100% of the devices from batches 5.2.2 and 5.2.3 were able to detect low-ppm levels of NH_3, only some of the devices from batches 5.2.4, and no devices from batch 5.2.6 showed sensitivity. This sensitivity correlates directly with increased resistance as demonstrated in Figure 2-7.

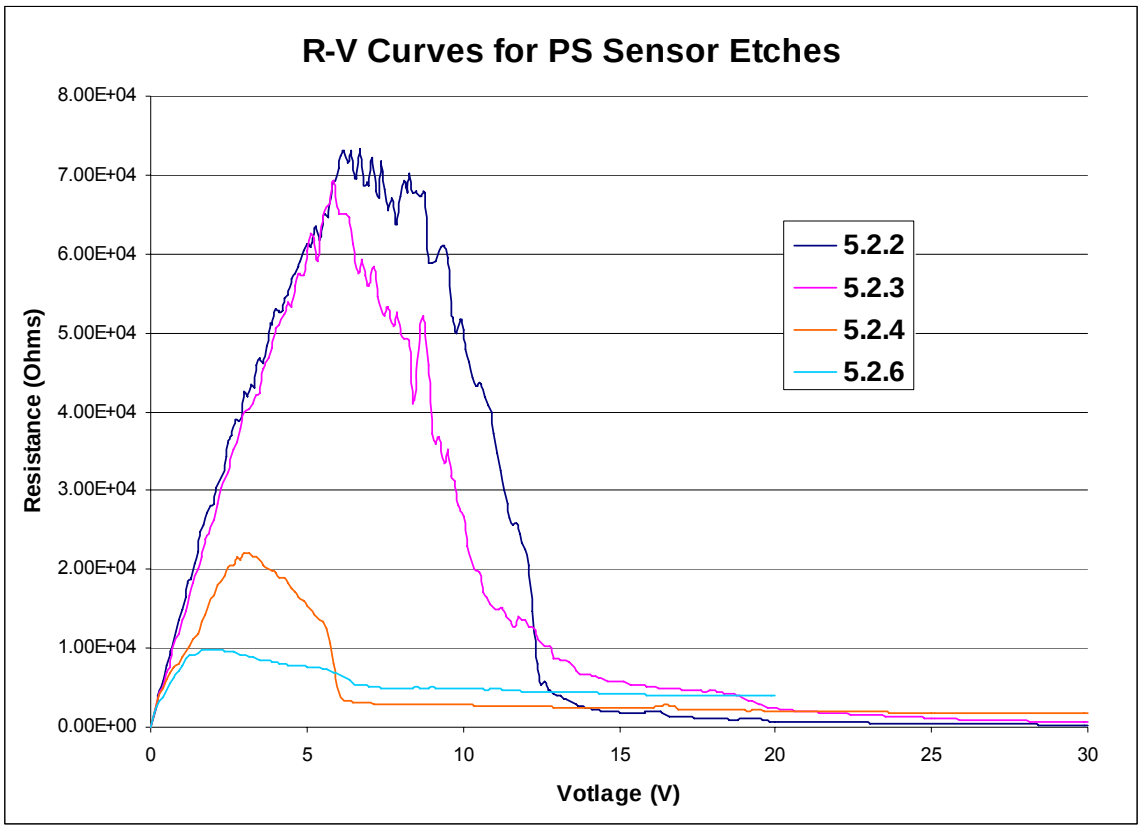

Figure 2-8: I-V sweeps were performed prior to etching several batches to produce the R-V curves above. The higher resistance batches provided much more sensitive sensors.

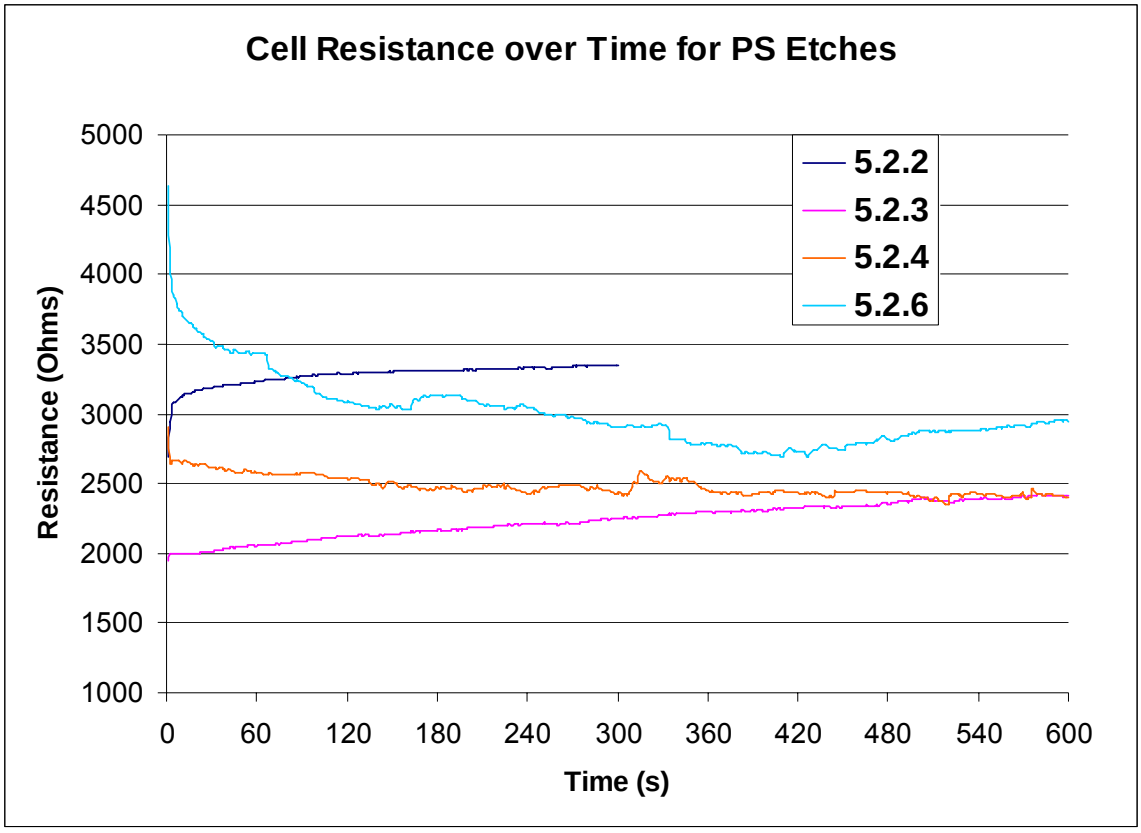

Figure 2-9: The resistance of the etch cell over time is depicted for the PS-etch step for several batches of sensors. The steady increase in resistance over time (5.2.3 and 5.2.4) is found to correlate to the formation of a sensitive PS layer.

The use of the R-V etch curve and the resistance profile of the etch itself provide a necessary quality control mechanism for the fabrication of the sensors. The structure of the porous silicon region of a non-functioning sensor from batch 5.2.4 is depicted in the SEM image of Figure 2-10. This porous structure is distinctly different from the functioning devices shown in Figure 2-7. This difference is likely caused when the platinum electrode of the etch cell (see Figure 2-2) is non-parallel to the surface of the wafer during the etch process. This is suggested since some devices from this etched wafer (5.2.4-1 for example) did show sensitivity. However, the non-functional behavior is predicted by the data presented in Figure 2-8 and Figure 2-9.

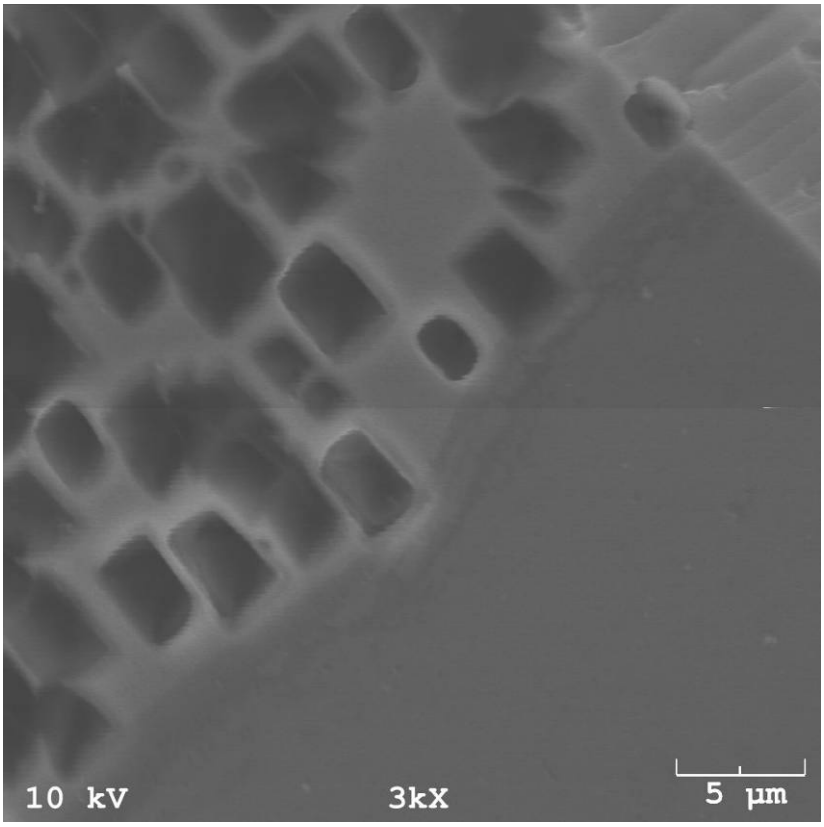

Figure 2-10: The different porous silicon structure of this non-functioning device from wafer 5.2.4 is shown.

Photolithographic Definition of Electrodes

As previously discussed, step 8 of the fabrication process can use one of two different methods for contact deposition. The initial method defined these contacts with a photolithography mask and the recipe for S1813 photoresist previously outlined in Table 2-1. There are both drawbacks and advantages provided by this method.

During the testing of gas sensors it was noted that both the presence of water and operative processes at temperatures exceeding 80°C degrade sensor performance. This effect was initially observed when, some of the devices which performed well, became irreversibly damaged due to operation under these conditions. The "breaking" of a device, commensurate with an increase in noise, rendered the device nonfunctional as the signal became immeasurably small compared to the noise. This occurred for tests where

temperatures reached or exceeded approximately 80°C and during cleaning steps which involved immersion of the sensors in DI water and subsequent drying which was not followed by immersion in methanol to leech the residual water from the pores. An example of the irreversibility of devices when heated is shown in Figure 2-11.

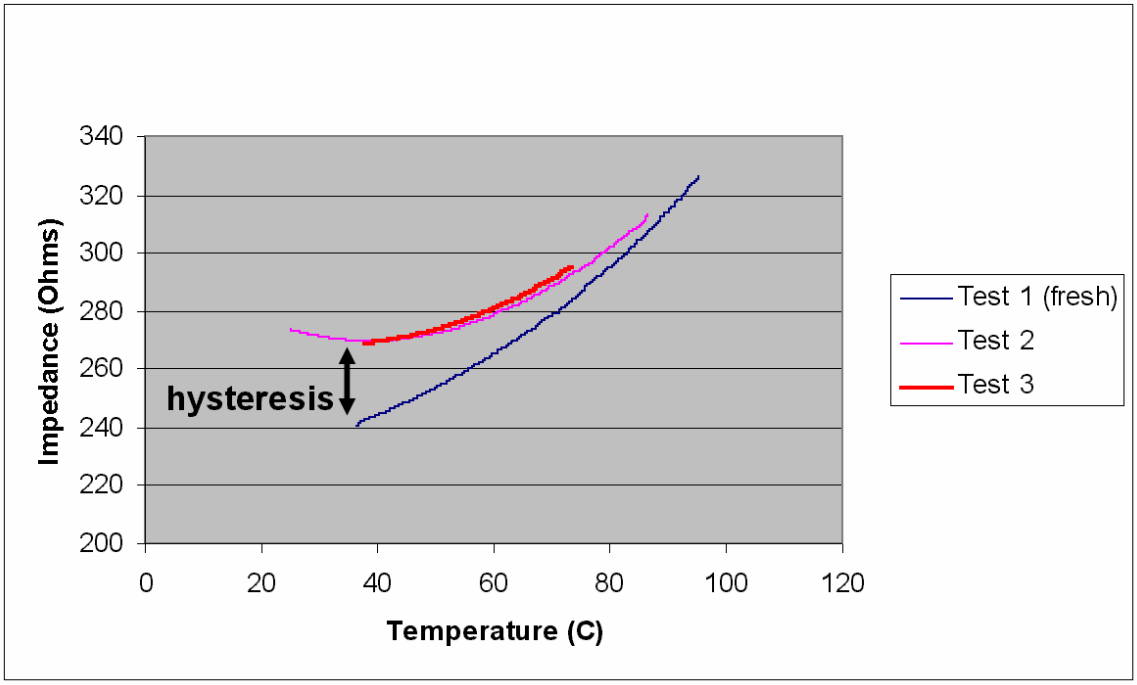

Figure 2-11: Example of the introduction of irreversibility and nonlinearity in the temperature sensitivity of a gas sensor.

It was surmised from these observations that an oxidation process was responsible for the damage to the sensors. Based on this observation, the fabrication process was assessed. All contact with water and exposure to temperatures in excess of 80°C were avoided after the formation of the porous silicon layer. Both of these conditions are unavoidable in a photolithography step, such as that which we have previously outlined, to define the contacts for step 8 (see Figure 2-5) of the fabrication procedure. The soft bake step of the photolithography heats the wafer to 95°C and the rinse after the developing step leaves residual water on the surface of the porous silicon. It was then

decided to replace the second masking step in the sensor fabrication process with shadowmasking in contrast to photolithography.

The advantage provided by the photolithographic definition of electrodes is the ability to deposit low resistance electrical contacts to the gas sensor[12]. The increased noise characteristic to the photolithographic process outweighs the advantage of lower resistance devices through electroless metallization. The second masking step was replaced by a low-temperature, anhydrous shadowmasking procedure to define the electrical contact to the sensor. While it has been investigated as to whether the photolithographic process could be modified to remove all contact with water and high temperatures, thus far no possibilities have been found.

Shadowmasking

Shadowmasking physically defines the metal contacts with a thin metal mask. The mask has holes in the regions where contacts are to be made. The holes allow the metal being deposited to pass through, while the mask stops the metal in all other regions. A shadowmask which was used in fabrication of gas sensors is shown in Figure 2-21.

Shadowmasking is typically deemed less desirable than photolithography because it is much less defined. While the feature sizes obtained with photolithography correspond to the smallest, sub-micron dimensions for the features which are used in current microchips, shadowmasking has inherently much less precision. This primarily results because the mask is not in direct contact with the wafer, which results in additional error in alignment for contact deposition.

We use the shadowmask, however, because it involves a simple, physical mask which avoids the need for exposure of the sensitive porous silicon layer to water and

excessive temperatures. An initial shadowmask made from copper foil (by hand) produced nine resistive devices and three four-point devices. The mask is discussed in more detail in following sections of this chapter and is shown in detail in Figure 2-21.

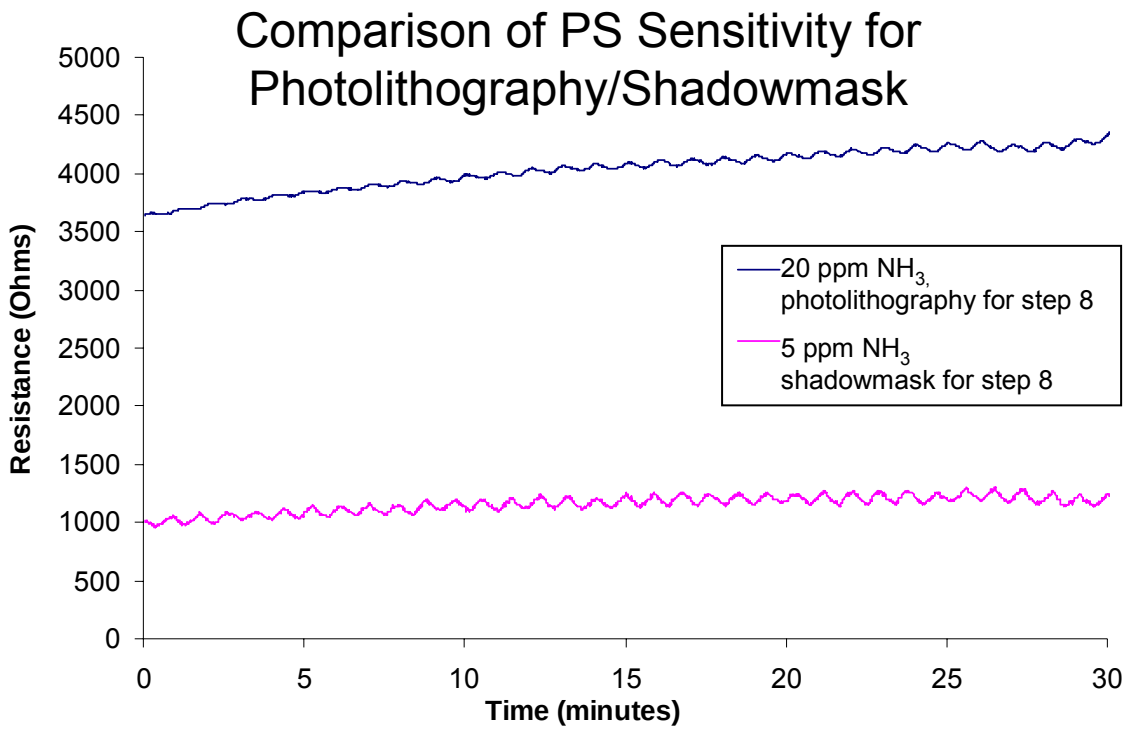

Figure 2-12: The shadowmask fabrication method dramatically improves the sensitivity of PS gas sensors versus previous designs. The response of the shadowmasked device (bottom) is enhanced relative to the photomasked device (top).

Electron-Beam Metal Evaporation of Contacts

A CVC E-beam evaporator was used to deposit the metal used for contact electrodes to the sensor formed in step 9 of the fabrication process. The E-beam system deposits metal in a more an-isotropic manner than the DC Sputterer, making it a better method for depositing contacts on the sensor. The metal is deposited onto the wafer by traveling perpendicular to the surface of the wafer, rather than through an isotropic "random walk" process as occurs with the DC sputterer. The E-beam is advantageous because as more gold enters the pores during deposition, the overall contact area between

the gold and the porous silicon is increased. This increased contact area reduces the resistance of the device and improves signal strength. Either one 4" wafer or seven 2" wafers can be processed in the E-beam at one time.

The E-beam evaporator system was used to deposit both titanium and gold to develop efficient contacts on the sensor. A thin 100Å layer of titanium is first deposited to improve adhesion between gold and the material beneath. Without this layer, bonding to the contacts is more difficult as the gold easily lifts off. After the titanium layer cools in the evaporator, a 3μm gold layer is deposited on top of the titanium. This gold is the electrical contact pad used for operating the sensor.

In lifting off the second Shipley 1813 photoresist mask after contact deposition, when photolithography was used for step 8 of the fabrication process, the wafer was immersed in Methanol for several hours until the excess gold could be removed. Some gentle hand-agitation was also used to remove the excess gold after the photoresist had been dissolved. The removal of the excess gold when using the shadowmask for step 8 of the fabrication process requires only the removal of the shadowmask from the wafer.

Packaging

Following the creation of gas sensors on a wafer, the wafer is diced so that individual devices can be tested. Two methods for the dicing of wafers exist. The most common method, the dicing saw, uses a high velocity stream of water to cut the wafer. The dicing saw was abandoned when the deleterious effect of water on the performance of the gas sensors was evaluated. A second mode of dicing the wafers is by hand, with a diamond scribe, was adopted. This method usually results in damage to one or more of the devices as a result of its lack of precision.

The placing of devices into a package which provides a more standardized means of electrical contact than a probe station has been investigated. Initially, this was investigated using TO-8 headers shown in Figure 2-13 which are packages capable of holding a chip for testing. This package was chosen because it is both compatible with the size of the sensors and is designed to facilitate installation in a virtually air-tight chamber which aids the testing of devices in a controlled environment. The flow chamber initially used for this testing is shown in Figure 2-13. This chamber was designed to have as small a dead volume as possible so that the response measured would be as accurately correlated as possible to the gas being delivered to the sensor. However, the use of these headers required the wirebonding of devices to the package. This wirebonding proved difficult as a result of several factors, the most important of which being that, during the coating and handling of devices, the bonds would break, losing contact to the wafer. Wirebonding was eventually abandoned to obtain a more viable method of contact.

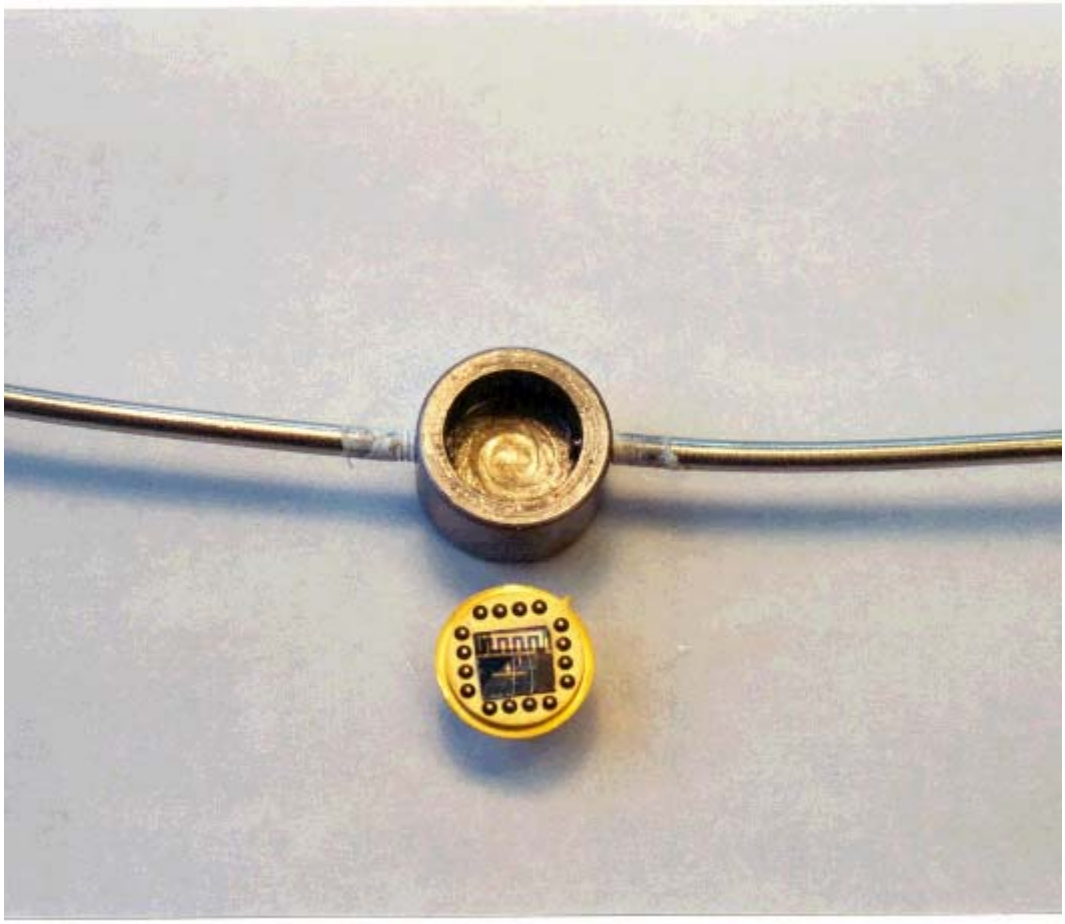

Figure 2-13: A picture of the TO-8 header with a sensor mounted on it beneath a custom-built flow chamber for the testing of sensors.

After device wirebonding was abandoned, an alternative, more viable, method was developed. This method involves making electrical contact to devices using probe stations, or other temporary physical-electrical connections based upon metal electrodes held in direct physical contact with the device. This method proved more effective and efficient than did the wirebonding of devices. Although it replaced the packaging of devices, it is technically an aspect of the sensor testing procedure, and will be discussed in Chapter 3. A second alternative mode of packaging was later established for contact to multiple sensors in an arrayed configuration. This mode of forming contacts to the sensor will be discussed in Chapter 7.

Variations to the Fabrication Process

Several aspects of the sensor fabrication are still being investigated and optimized to produce improved sensors. With these modifications, we expect to achieve a significant improvement in performance from the sensors that are discussed in this dissertation.

Contact Deposition Methods

While the use of the shadowmask rather than photolithography for contact definition clearly produces better sensors, it is still desirable to be able to combine the advantages of the anhydrous and low temperature shadowmask method with the ability to create low resistance electrolessly-formed contacts which we have previously generated[11]. At the present time, clear possibilities to deposit low resistance contacts from electroless gold while avoiding the aforementioned constraints of temperature and water are difficult to envision. In order to deposit the electroless gold in solution over

selective regions of porous silicon, we require a mask in physical contact with the wafer. As the shadowmask is merely held closely above the surface of the wafer, it will not suffice as a means to confine the electroless solution to the desired regions. The photoresist mask did provide this seal, but it requires that water to be applied to the surface of the wafer and that the temperature of the wafer be increased to 95°C. Again, it has been shown that water can be leached from the porous silicon before damage occurs, but this can only be done with solvents such as methanol that also dissolve the photoresist mask in the process.

An additional problem encountered with contact deposition via photolithography onto the porous silicon was the formation of gold-bands at the PS-carbide interface thus rendering the sensors inoperable. This band, as depicted in Figure 2-14, shorts together the contacts of the sensor. This band is thin, so it seems as though a ~100Ω sensor was produced, but the device has no response to test gas samples. This banding phenomenon must be taken into consideration if one attempts to produce photolithography based electrical contacts.

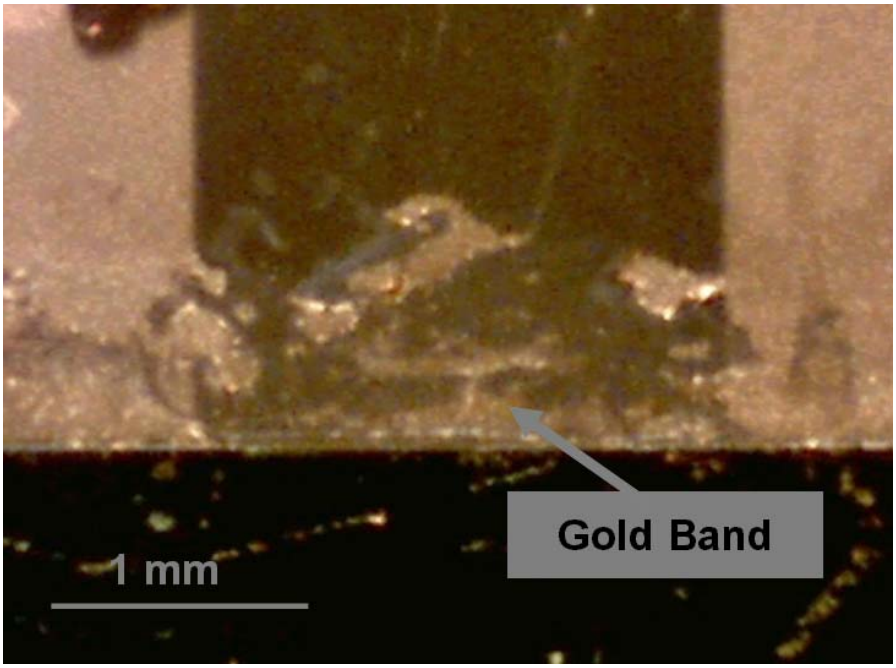

Figure 2-14: The gold band across the edge of a sensor renders it inoperable by shorting the device contacts together. The device behaves as a ~100Ω sensor, but with no gas response.

Trenching

An undesirable side-effect occurs when a highly chemically and electrically insulating material (silicon carbide) acts as the masking material for the porous silicon electrochemical etch. A trench is formed between the regions of the wafer during the etch process. Trenching results from an increased current density over the unmasked area of the etch at the border with the silicon carbide. The increased current results as the Pt electrode (see Figure 2-2) is present over the surface of the entire wafer, rather than just the unmasked regions. The current passing through the cell is blocked by the silicon carbide, and as both the metal backing on the wafer and the platinum electrode span the entire wafer, the current is focused near the border of the etched regions. Figure 2-15 demonstrates this effect on a wafer of devices that had been etched for 20 minutes at 6 mA.

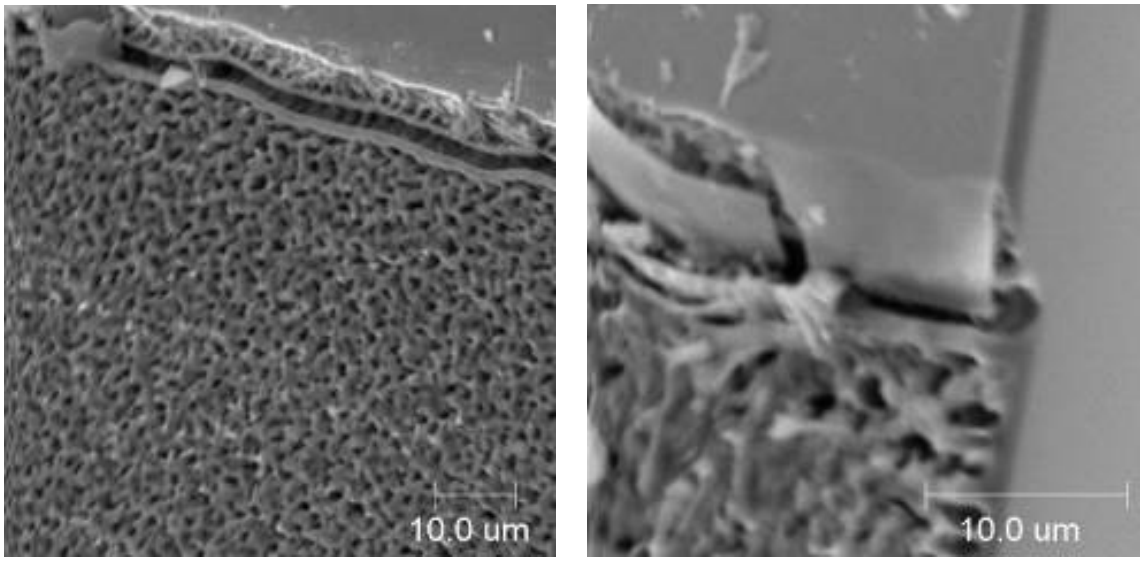

Figure 2-15: Examples of the trenching phenomenon at the border between porous silicon and a silicon carbide masking layer.

Although this effect does not present a problem with current fabrication designs, it is addressed as it could limit the scale of future devices. Because the degree of trenching increases as the size of the PS regions on the wafer decreases, the trenching effect can be amplified as devices become smaller. This limitation results because in addition to the sensing region, an area which will account for the trenching effect must be built into the design of the sensors to provide for the electrical contact between the porous silicon and the silicon carbide which must span the trench. Additionally, the trench depth determines a minimum thickness for the required metal layer to produce a successful electrical contact to the device. Since the trench depth is proportional to the length of the etch and the pore depth, devices produced with pore depths much greater than those produced here may require a thicker metal layer for electrical contact.

There are several ways to eliminate the trenching phenomenon. The most obvious of these is to produce a conformal electrode to replace the Pt sheet. One possible way to do this would be to produce a separate wafer with Pt electrodes on the regions to

be etched. Because the Pt electrodes would be facing the wafer to be etched, the mask to produce these electrodes would be a mirror image of the mask that produces the porous silicon definition in the silicon carbide layer. Additionally, the mask would need to be connected, so that all of its regions are maintained at the same potential.

A second potential method for eliminating trenching would be to use a less impervious material in place of the silicon carbide layer. During the etch, the material would be slowly (~1 micron per minute) dissolved away at the border, widening the porous silicon region. This would in turn minimize the depth of the trench by causing it to occur over a constantly changing region. An ideal material for this would be one that is non-reactive chemically, but reacts at the necessary rate during the electrochemical formation of the pores.

Pore Depth Analysis

One parameter of the porous silicon gas sensors that has not yet been tuned is the depth of the porous silicon pores. As the response time is determined by the rate of diffusion of gas into the bottom of the pores, a shorter pore depth could indicate a faster response. However, longer pores could result in a response of greater total magnitude, as a larger area of PS provides a greater change in the impedance through which a measurement could be taken. The sensitivity of the response, which is proportional to the slope of the change in resistance over time, is a function of both the response time and the magnitude of the response. In addition to these factors, longer pores can effect the flow of gas over the surface of the sensor. Evidence for this has been found during sensor testing. If a sensor is placed directly in the path of a flow of gas, and as close as possible to the flow (see Figure 2-16), there exists a flow rate which, when exceeded, leads to an

extremely noisy response. This noise is believed to originate from differences in flow patterns disturbing the sensitive surface inside the PS. The turbulent flow penetrates farther into the pores when the flow of air across its surface is greater, causing the noisy signal. This flow, while it might increase the speed of a response, could potentially hide the sensor response by producing increased noise levels.

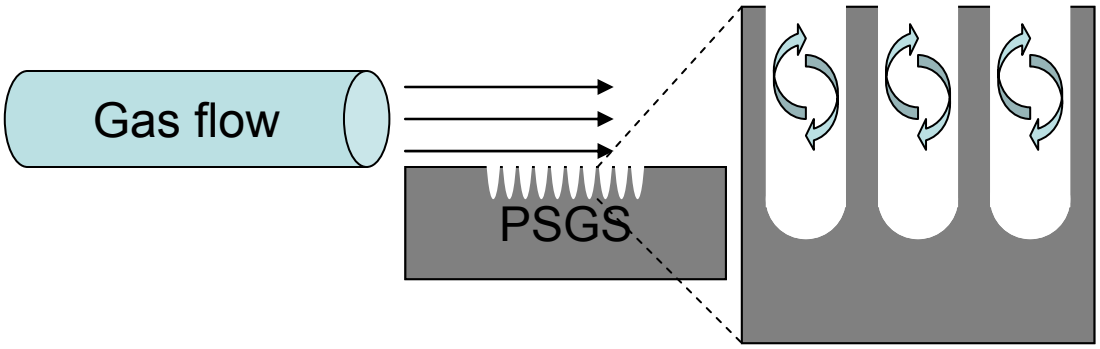

Figure 2-16: The flow of gas over the porous silicon surface causes a noisy response as the flow penetrates to some depth within the micropores. If this flow is too great, the device will be non functional.

Gas Sensor Design

Many factors need to be looked at when considering the design of a gas sensor. Most obvious of these are the metal contact region and the sensitive PS layer. Both factors must be addressed within the context of the application in which the sensor is applied. The method of making contact to the devices has the greatest impact on their subsequent design. The various methods of contact will be discussed in more depth in Chapter 3, however, the main distinction between contact methods is made between temporary and permanent electrical contact. For testing and sensor evaluation purposes, a temporary contact method is utilized which allows for the rapid removal and re-insertion of sensors. For the evaluation of practical sensor performance in real-world environments, a contact should be designed that provides for the best simulation of that

particular environment. For example, some applications may require large feature sizes for the repeated application and removal of contacts, while others may require the contact to be designed for permanent one-time contact formation.

Design Methodology

In order to individually test (and coat) the gas sensors, a relatively large, 2mm by 5mm sensor (see Figure 2-17) was designed in order that the devices could be both simple to fabricate and simple to handle. Devices of this scale were constructed so as to allow ready electrical contact connection without the need for a microscope-assisted probe station. In addition to the rapid and repeatable creation of electrical contact to the sensors, the large size of these devices also allows the sensors to be diced by hand, thus removing the necessity to use a dicing saw. Because a dicing saw uses considerable quantities of water while cutting the sensors from the wafer, its use is harmful to sensor performance.

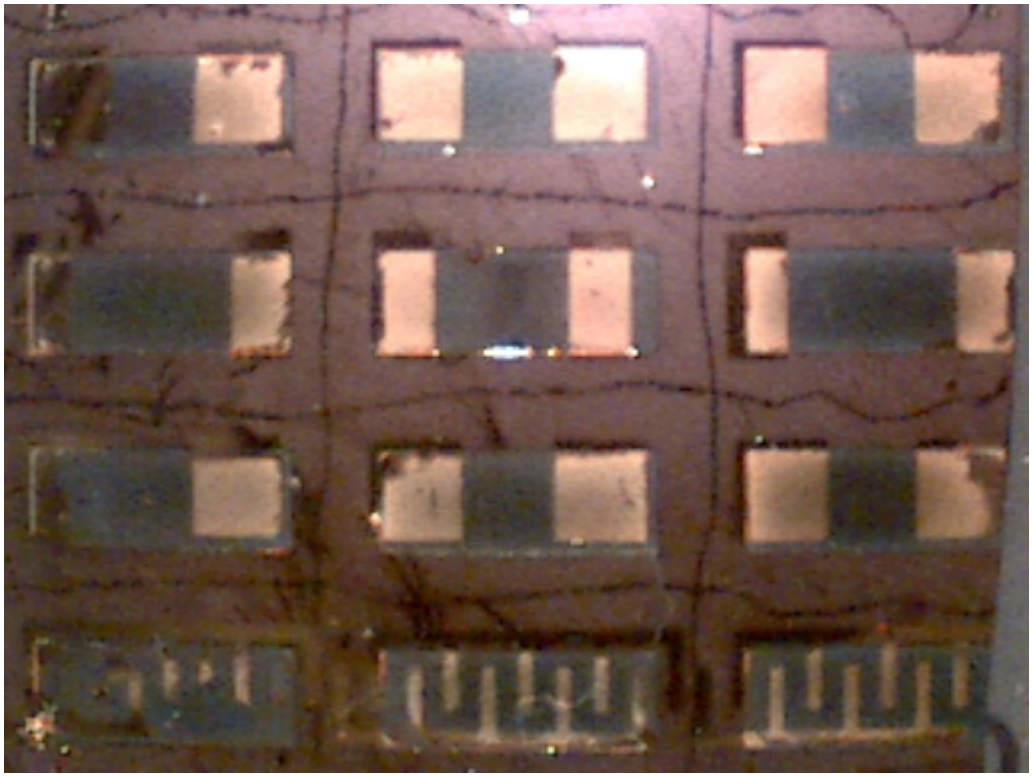

Figure 2-17: An image of the typical 2mm by 5mm gas sensors used in testing before they are diced. This figure corresponds wafer run D2, representing the last set of devices fabricated before the implementation of shadowmasking. The residual photoresist (lighter purple regions) can also be seen.

Some unsuccessful designs have also been considered. Initially, the fabrication micron-scale sensors was investigated. One of these devices, depicted in Figure 2-18, is discussed in more detail in the masters thesis of John DeBoer[15]. These approaches were abandoned for several reasons. First, the inability to consistently wire bond to these devices made testing difficult. The small scale of the gold electrodes also lead to their detachment from the wafer's surface during removal of the photoresist. Further, the small scale of the devices which made the use of a dicing saw necessary, depositing large quantities of water on the device surface.

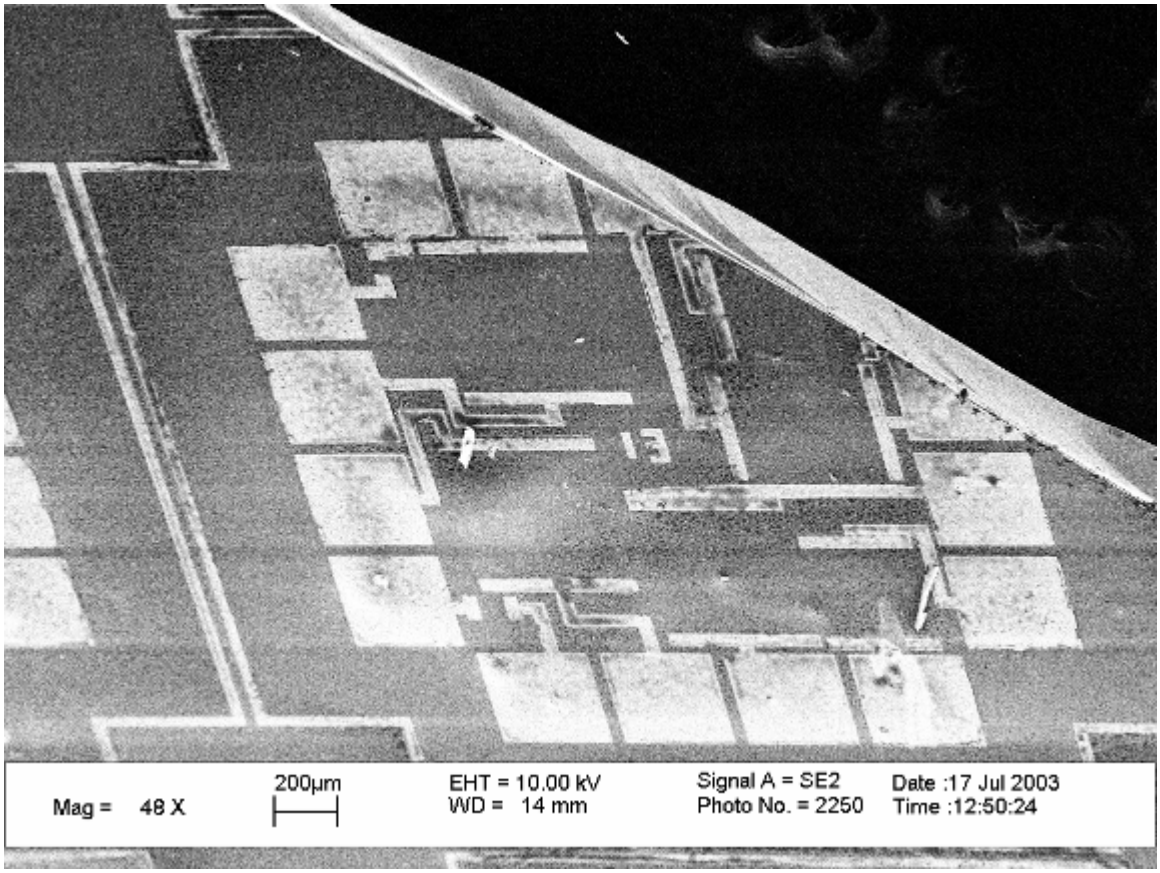

Figure 2-18: A cleaved mems-scale gas sensor is shown under magnification. Each chip measured under half a centimeter square.

Masks Used in Fabrication

The masks used to make the majority of sensors considered in this thesis are shown in Figure 2-19 and Figure 2-20. These masks were based upon Lenward Seals' initial research into gas sensors, although the fabrication methods now used for each mask are notably different from that originally used[2]. Upon the development of the fabrication step which uses the shadowmask, the second photomask (Figure 2-20) has been replaced with the shadowmask shown in Figure 2-21.

These photomasks, which are four inches square in total area, provide for the fabrication of twelve devices from a single 2" wafer. Mask 1 (Figure 2-19) defines the area of the porous silicon region of the sensors with dimensions 5mm by 2mm. The

numbering of the twelve devices for testing, as described for each of the possible masks used in step 8 of the fabrication (Figure 2-20 and Figure 2-21), allowed the tracking of device performance with regard to the region of the wafer from which the device originated. The photomask, used initially in step 8 of fabrication procedure and shown in Figure 2-20, allowed the formation of nine simple resistive devices and three interdigitated devices. The interdigitated electrodes were designed by Lenward Seals in an effort to determine how an increased metal-PS interface would influence sensitivity[3]. The shadowmask, which was later used in step 8 of the fabrication procedure, allowed the formation of nine resistive devices and three four-point devices. The four point devices were used to determine the contact resistance and barrier height of a sensor.

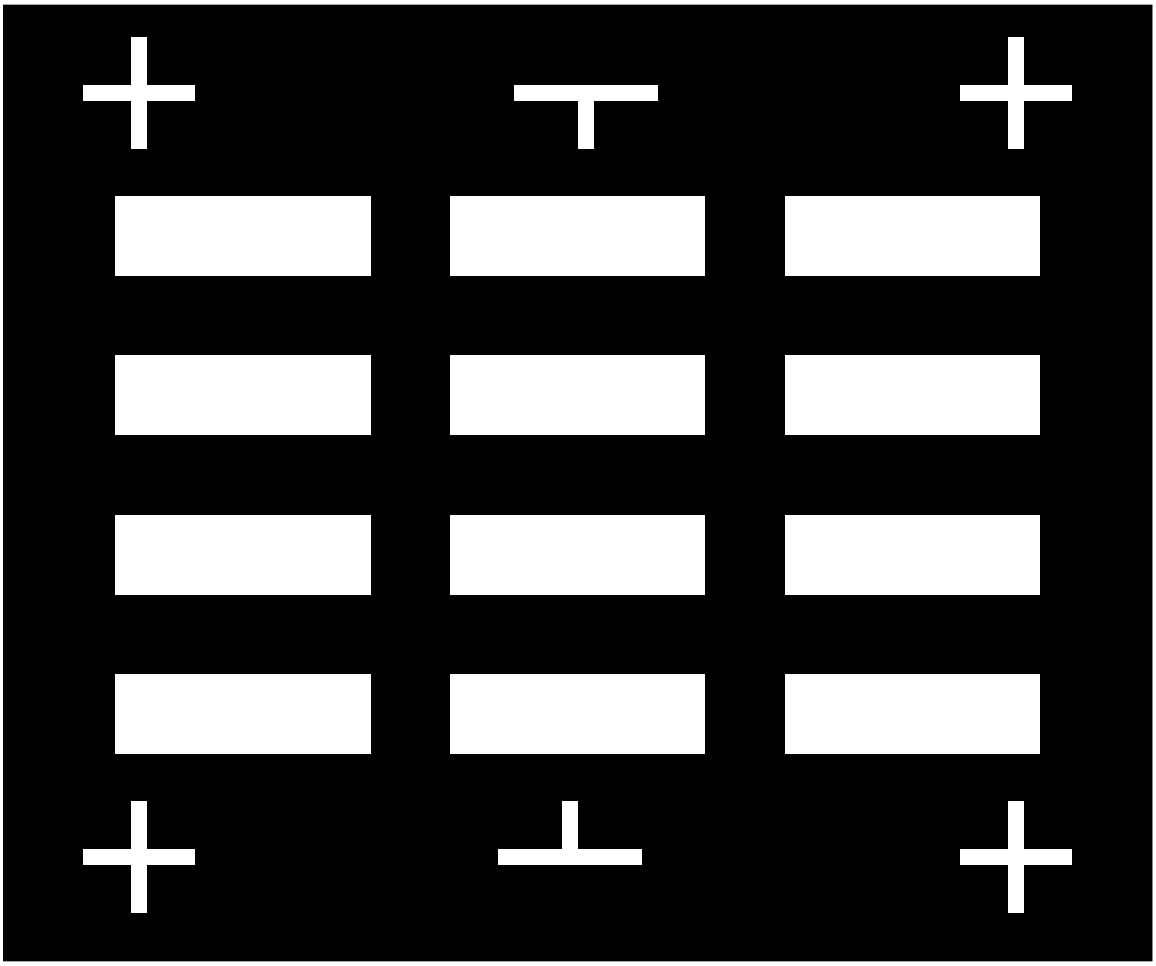

Figure 2-19: An image of the mask used to produce the silicon carbide defined regions of porous silicon for the 2mm by 5mm gas sensors. The transparent rectangles depict the locations where porous silicon will be etched, while the crosshairs provide for the alignment of a second mask later in the fabrication process.

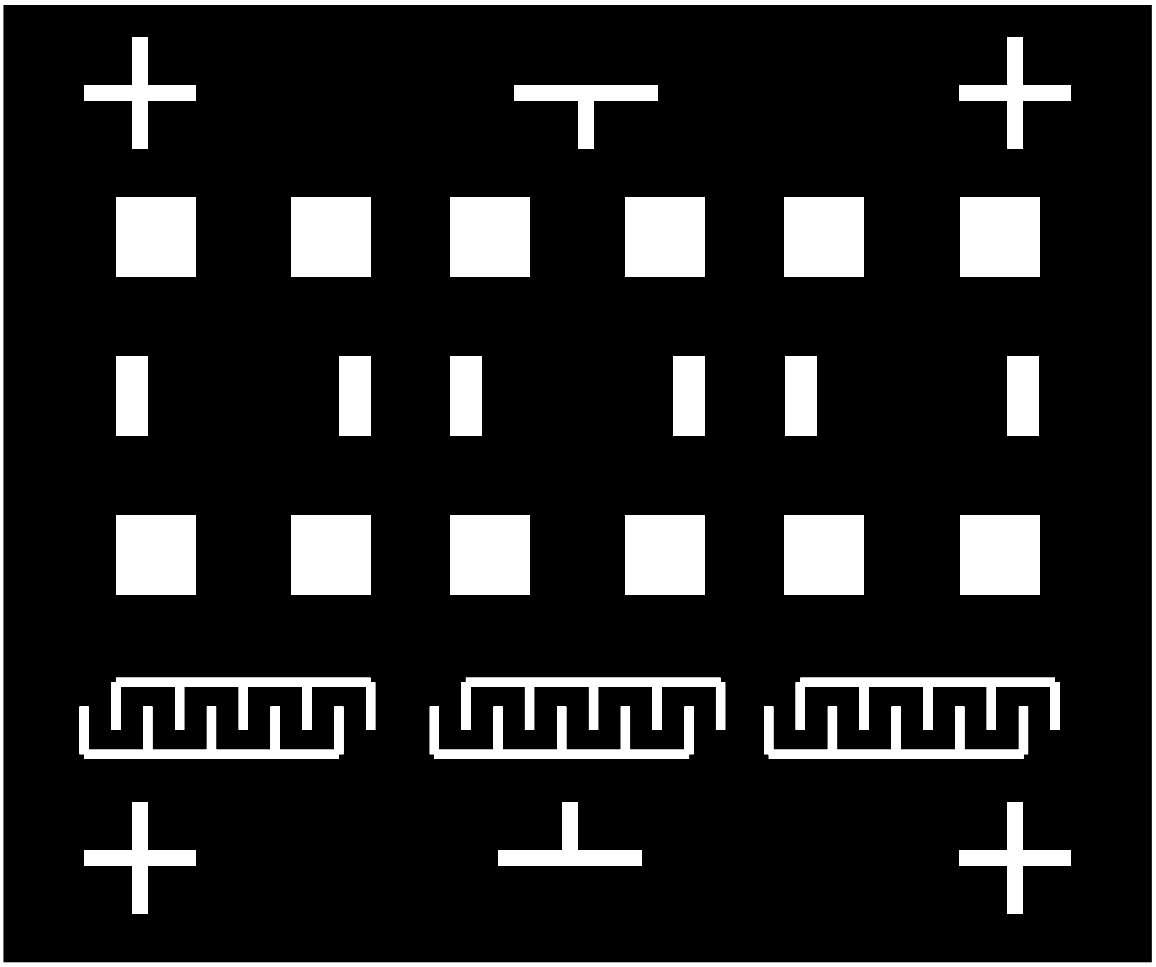

Figure 2-20: An image of the mask used to produce the metal contact regions for the 2mm by 5mm gas sensors. The same crosshairs of the first mask are present for alignment. The first nine sensors are simple resistive devices with contact pads of 1.3mm square (devices 1-3 and 7-9) and 1.3mm by 0.6mm (devices 4-6) in area. The last three devices (10-12) have interdigitated electrode contacts. Numbering is left-to-right.

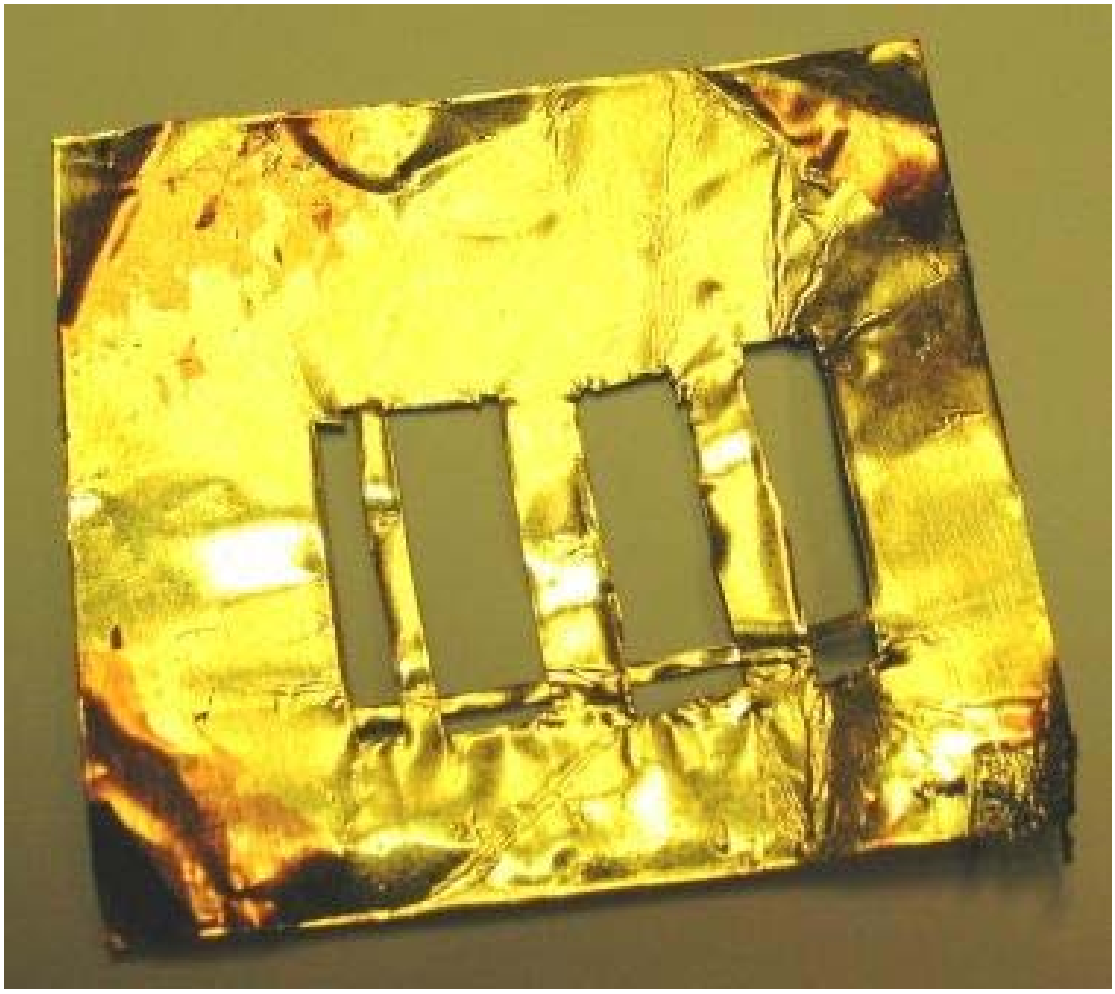

Figure 2-21: An image of the shadowmask used to deposit metal contacts on the PS sensors. The first nine sensors (1-3 in row one, 4-6 in row two, 7-9 in row 3) were simple resistive devices. The last three sensors (sensors 10-12) were four-point devices. The contact regions of separate sensors were connected on the mask and separated upon dicing of the wafer.

The most recent designs for gas sensors considered in this thesis provide the means for testing arrayed devices. These arrays are made to be tested in specially made testing apparatuses to allow the rapid removal of entire arrays of devices. In addition, the sensors on the array are designed to be both far enough apart to be individually coated, yet close enough together to fit on a single chip. There are six array designs presented in Figure 2-22 including two four point sensors, four resistive sensors (three separate designs), eight resistive sensors, and twelve resistive sensors. Figure 2-23 and Figure 2-24 show the masks used to produce these arrayed devices. These integrated, arrayed sensors are discussed in more detail in Chapter 7.

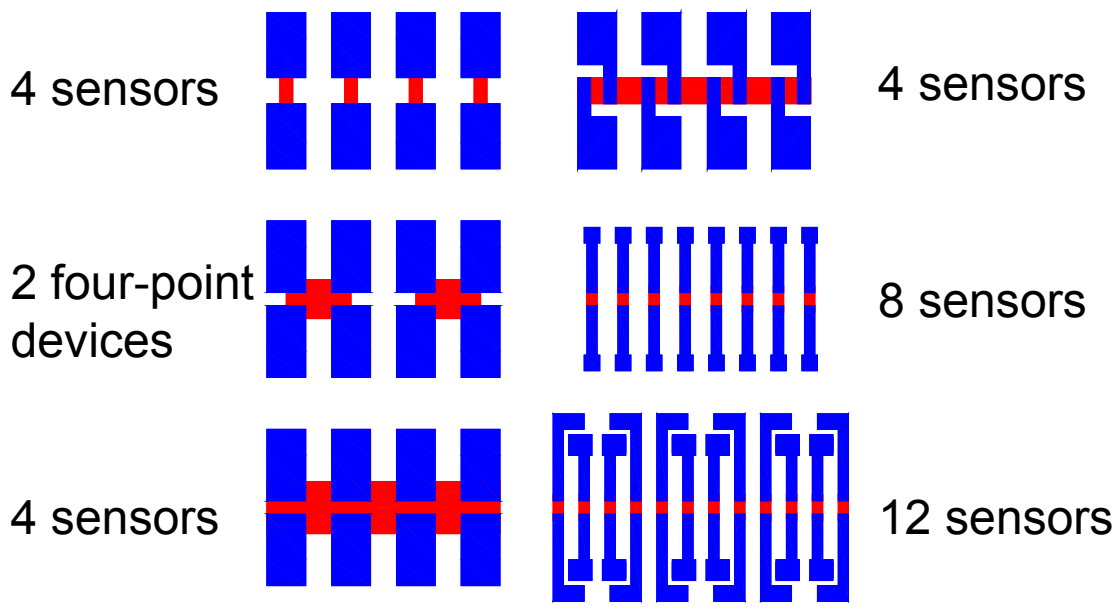

Figure 2-22: The six designs of arrays include a wide range of devices with both mm and sub mm scale contacts for both present and next-generation devices. The red areas indicate PS regions; the blue areas indicate metal contact regions

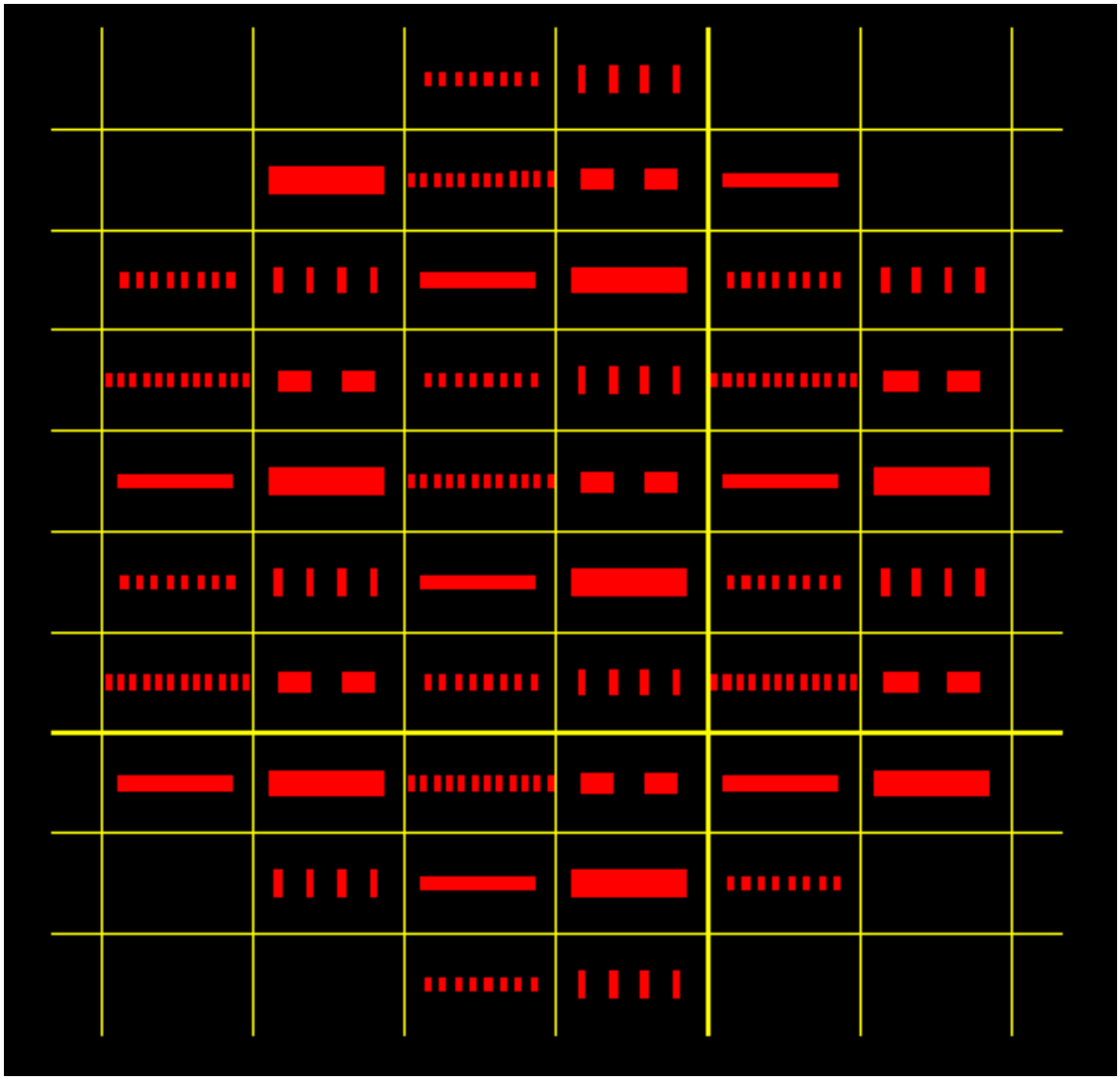

Figure 2-23: A design of the mask used to build the porous silicon area of the arrayed gas sensors. Red regions are translated into the transparent "windows" of the mask. Yellow regions are also transparent, providing for alignment. Each array of sensors (also defined by the yellow grid) is one of six possible array designs.

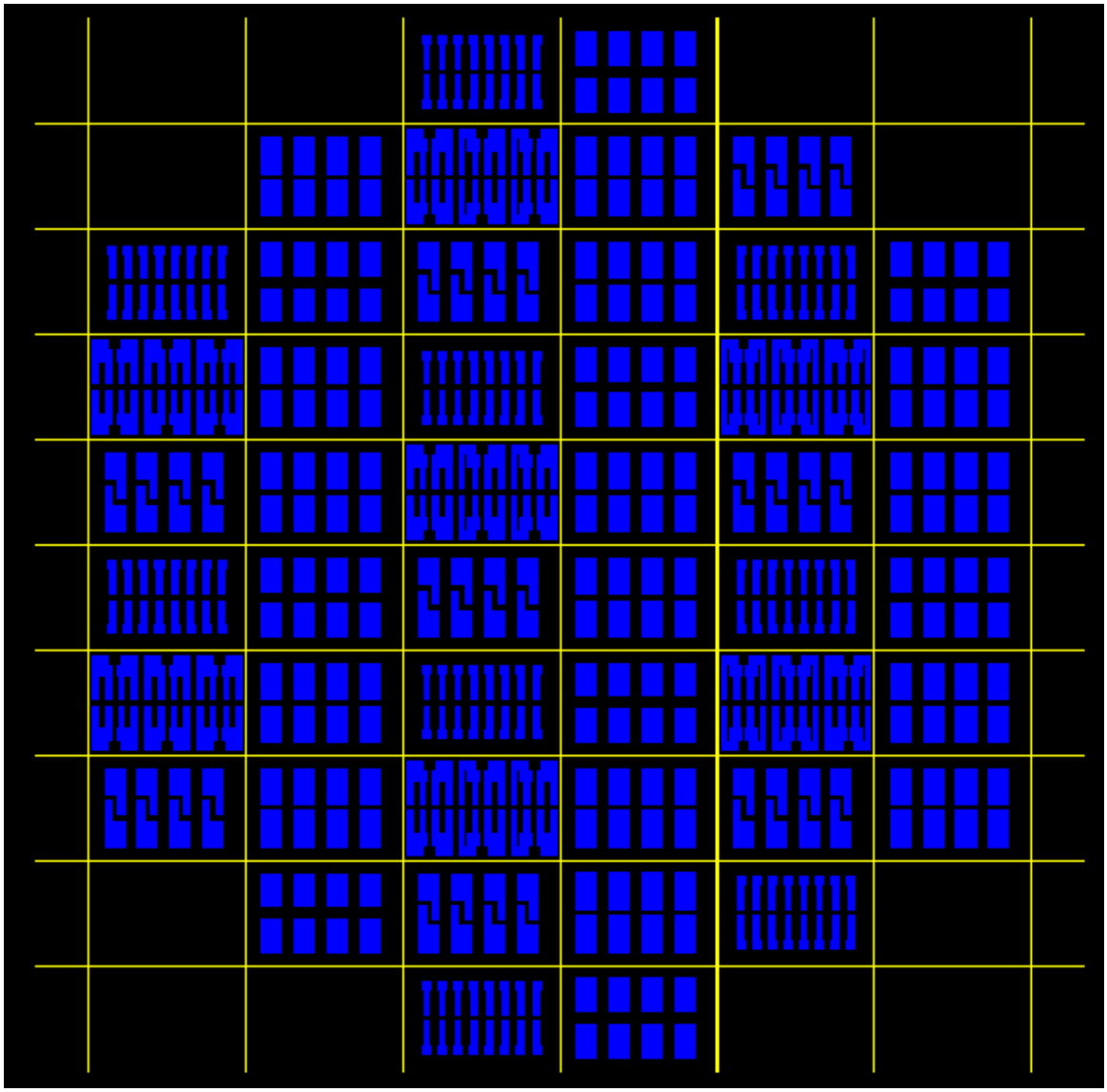

Figure 2-24: A design of the mask used to build the metal contact region of the arrayed gas sensors. The blue regions of this mask translate into the windows of the shadowmask for step 8 of fabrication which indicates where the evaporated metal will reach the sensor.

References

[1] Ben-Chorin, M., Kux, A., Schechter, I., "Adsorbate effects on photoluminescence and electrical conductivity of porous silicon", Applied Physics Letters, v 64, n 4, 24 Jan. 1994, p 481-3.

[2] L. Seals, L. A. Tse, P. J. Hesketh and J. L. Gole, "Rapid, reversible, sensitive porous silicon gas sensor," J. Applied Physics, 91, 2519-2523 (2002).

[3] L. Seals, "The Application of Porous Silicon Surface and Photo- and Electrochemical Properties to Sensor Development," thesis, Georgia Institute of Technology, July 2001.

[4] Paper(s) on other kinds of PS

[5] Bard, A. J., Faulkner, L. R., "Electrochemical Methods," Wiley, 2000.

[6] Dudel, F., Grantier, D.R., Gole, J.L., and Dixon, D.A. "On the origin of porous silicon photoluminescence-evidence for an oxyhydride-like emitter," Physical Review; Part B, 56, 2137 (1997).

[7] Gole, J.L. and Dixon, D.A. "A suggested correlation between the visible photoluminescence and the Fourier transform infrared spectrum of a porous silicon surface," Journal of Physical Chemistry, 101, 8096 (1997)

[8] Gole, J.L. and Dixon, D.A. "On the transformation, green to orange-red of a porous silicon photoluminescent surface," Journal of Physical Chemistry: Part B, 102, 33 (1998)

[9] Gole, J.L., DeVincentis, J.A., and Seals III, L.T. "Optical pumping of dye complexed and sensitized porous silicon to increase photoluminescence emission rates," Journal of Physical Chemistry: Part B, 103, 979 (1999).

[10] Gole, J.L., Seals III, L.T., DeVincentis, J.A., Lillehei, P.T., Prokes, S.M., and Dixon, D.A "Chloride salt enhancement and stabilization of the photoluminescence for a porous silicon surface," Physical Review: Part B, 61, 5615 (2000).

[11] "Photoluminescence Induced Metallization for Low Resistance Contacts", in Technology Advances, Invited, MRS Bulletin 28, 263 (2003).

[12] Gole, J.L., Seals III, L.T., and Lillehei, P.T. "Patterned metallization of porous silicon from electroless solution for direct electrical contact," J. Electrochem. Soc. 147, 3785 (2000).

[13] Cleanroom Services, (June 2005) http://grover.mirc.gatech.edu.

[14] Communications with Peter Hesketh.

[15] DeBoer, J. R., "Evaluation Methods for Porous Silicon Gas Sensors", thesis, Georgia Institute of Technology, August 2004.

[16] Lewis, S. E., DeBoer, J. R., Gole, J. L., Hesketh, P. J., "Sensitive, selective, and analytical improvements to a porous silicon gas sensor", Sensors and Actuators B, 110, 54-65 (2005).

[17] Karl Suss MJB-3 Mask Aligners, (June 2005) http://grover.mirc.gatech.edu/equipment/textInstructions.php?id=10.

CHAPTER 3

TESTING

Testing schemes for the porous silicon gas sensors have evolved parallel to improvements in fabrication methods and resulting improvements in performance of the gas sensors themselves. Some of the modes of testing for the PSGS were developed to characterize the older and noisier devices. As fabrication methods were improved, creating better, higher sensitivity, and lower noise devices, new modes of testing were developed. These new modes trended towards a more rapid, fully automated test scheme. Improvements were also made to test devices in an environment similar to the real-world environments envisioned for many of the applications of the PSGS. Paramount to this goal is the inclusion of a rapid testing scheme, the ability to test sensors and sensor arrays with multiple gases, and the ability to test sensors under repeatable conditions.

The initial test method for the gas sensor employed during Dr. Seals' research involved pumping the sensor to vacuum, subsequently exposing it to a calibrated concentration of gas and observing a change in impedance as measured by a Solartron 1260A impedance analyzer[1]. Typical tests compared the impedance of sensors exposed to concentrations of 100ppm NH_3, HCl, and NO_x in argon to the response of sensors exposed to pure argon. Figure 3-1 illustrates the data taken in these tests and reveals that although a response is collected, due to the lengthy time scale for the gas to reach the sensors, the accurate investigation of the sensitivity and response time of these sensors would require a more sophisticated system to test the sensors.

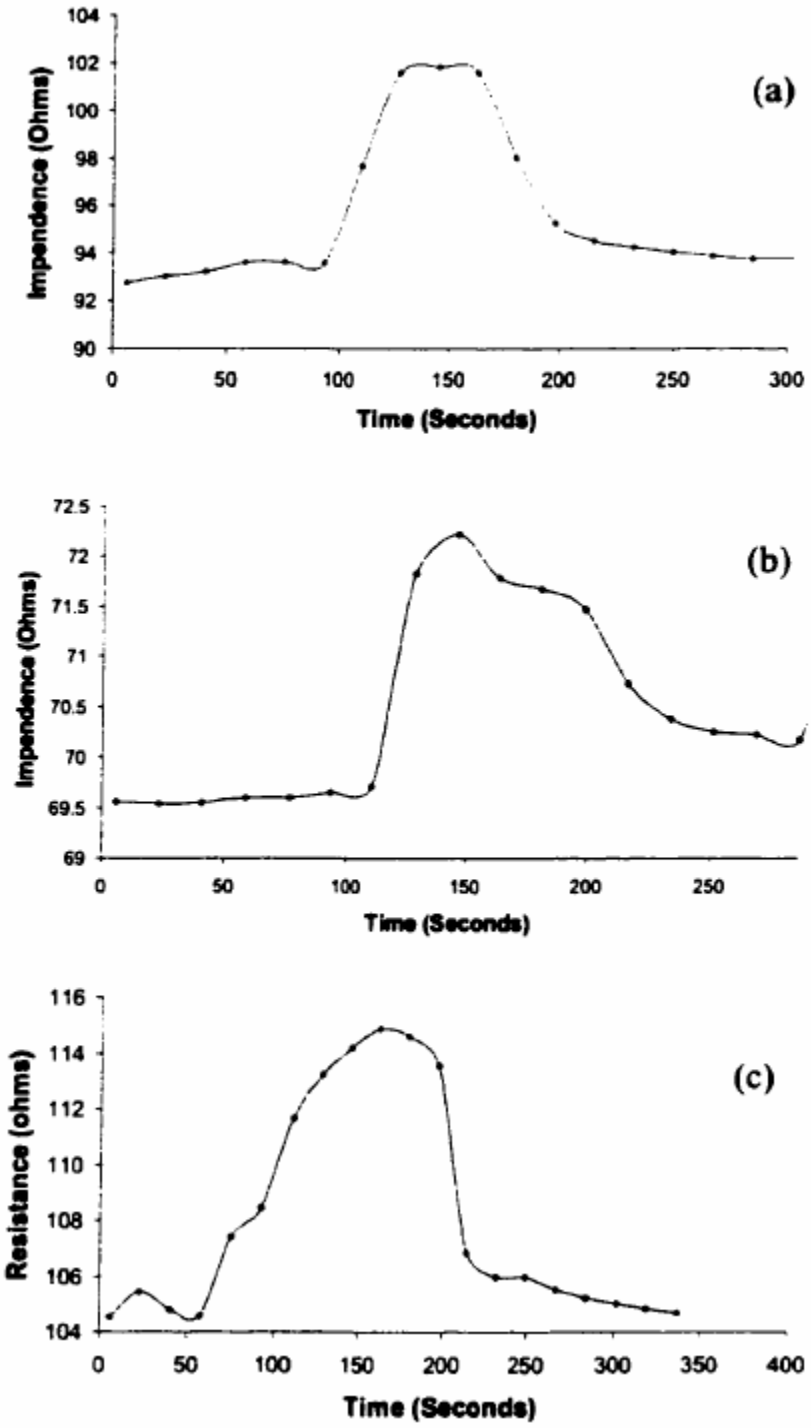

Figure 3-1: Sensor resistance measured through impedance spectroscopy at 1kHz, 10mV RMS with 1s integration time at room temperature. Sensor response: (a) response to 100 ppm HCl in argon, (b) response to 100 ppm NH_3 in argon, and (c) response to 100ppm NO in argon.

The creation and operation of this first testing system was the primary research of John DeBoer during the completion of his Masters Degree in Mechanical Engineering at Georgia Tech[2]. The system which was built met the most vital criteria for the testing, as it enabled the rapid testing of devices in a repeated fashion for multiple analyte gases. From this initial test configuration, modifications were made to provide the system with additional capabilities including a reduction in error and noise associated with the test apparatus, the ability to test arrays of sensors, and the computer controlled testing of devices.

Experimental Apparatus

The system used to test porous silicon gas sensors can be factored into three main components: 1) a gas sample creation component, 2) an interface where the gas is delivered to the sensor, and 3) a component used to measure the sensor's response. Throughout testing, each of these three components were modified to improve the accuracy and speed of testing gas sensors.

Gas Sample Creation

The control of the gas sample was made possible through the use of calibrated cylinders of gas purchased from AirGas. The gases from these cylinders were then mixed using calibrated mass flow controllers. In a detailed analysis, Koll highlights the advantages of such a system, including simplicity and cost, versus common alternatives[3]. Disadvantages can include a limited operating range as well as an incompatibility of the mass flow controllers with certain volatile organic compounds.

The first of the two cylinders contained research grade nitrogen which served as the control gas. The control gas is used to provide the sensor with a flat baseline "normal" condition onto which all responses to the test gas are compared. Nitrogen was chosen as this "normal" gas because it is the primary constituent of the Earth's atmosphere, where most envisioned applications for the developed sensors would occur. Research grade nitrogen was chosen as the entrainment gas since the next lower grade of nitrogen contains a possible CO impurity near the 1ppm level, comparable to the levels of CO that have been evaluated. With the large quantity of nitrogen being used for all testing, several cylinders of this gas were purchased, with a backup cylinder always available to replace the cylinder in use. The nitrogen cylinders were replaced upon reaching roughly 10% of their full capacity. Near this level a sensor demonstrates a noticeable increase in baseline noise, apparently caused by increased levels of impurities in the nitrogen from contaminants inside the cylinder.

The second cylinder contained a pre-calibrated concentration of the gas to be tested. This gas consisted of either ammonia (NH_3), nitric oxide (NO), carbon monoxide (CO), hydrogen sulfide (H_2S), sulfur dioxide (SO_2), hydrogen (H_2), or hydrogen chloride (HCl). In addition, tests to establish an approximate sensitivity to ozone (O_3) were done. The source of this gas was an ozone generator (Welsbach Ozonizer) and a cylinder of medical grade oxygen rather than a calibrated cylinder of ozone. The ozone concentration in the oxygen was measured using a separate ozone sensor present in the line just downstream of the generator preceding the point at which the ozone and background oxygen was delivered to the sensor.

The concentration of gas delivered to the sensor was controlled through the careful mixing of the nitrogen and test gases in a controlled fashion. This was accomplished through the use of calibrated mass flow controllers. MKS type 1179A flow controllers were used for virtually all of the experiments. The mass flow controller (MFC) that was connected to the nitrogen cylinder had an adjustable flow rate ranging from 0-100 sccm with an error of 1% of full scale, or a 1 sccm error. The nitrogen flow was run at a constant rate during each test, typically 100 sccm. The test-gas flow was varied between zero and the maximum flow rate for the mass flow controller that was connected to a particular test gas. As certain gases, particularly SO_2 and H_2S, react with and contaminate the steel gas lines and MFC's when used, separate mass flow controllers were needed for some of these test gases. The MFC's for the test gas had flow rates which ranged from either 0 to 1 sccm or 0 to 10 sccm. These controllers each had an error of 2% of full scale.

Gas was flowed from the cylinders, through ¼" stainless tubing, to and through the MFC's, then entering ⅛" lines (see Figure 3-2). This shift in tube diameter served to increase the velocity of the gas being delivered and decreased the time between activating the MFC and observing a response in the sensor. The gases from the ⅛" lines were mixed in a junction prior to reaching the sensor. The gas flowed to the sensor from the junction via ⅛" tubing. This length of tubing also served to ensure that the gases were well mixed upon reaching the sensor. Stainless steel was used exclusively for the gas handling system, including the tubing, the junction, and the material from which the MFC's were constructed. This is because stainless steel is non-reactive to most of the gases used in this study at the low concentrations being tested.

The MFC's were operated through the use of MKS type 246C single-channel and type 247D four-channel power supplies/readouts. Typically, the test gas flow was modified through the type 246C unit as it provided easily accessible front-side flow control knobs in contrast to the type 247D. The 246C unit also proved easier to integrate with a LabView-based control program. The unchanging, 100 sccm flow of the nitrogen gas was controlled by the four channel power supply, as was any MFC delivering a required constant background gas concentration. The MFC's connected to test gas cylinders which were not in use were also connected to this power supply, as the "off" state of the MFC's is only ensured when connected to a power supply. As such, to ensure an extra level of safety, the power supply/readouts were continuously powered even when experiments were not running. This ensured a flow rate of zero was maintained in the event one of the cylinders was left on accidentally.

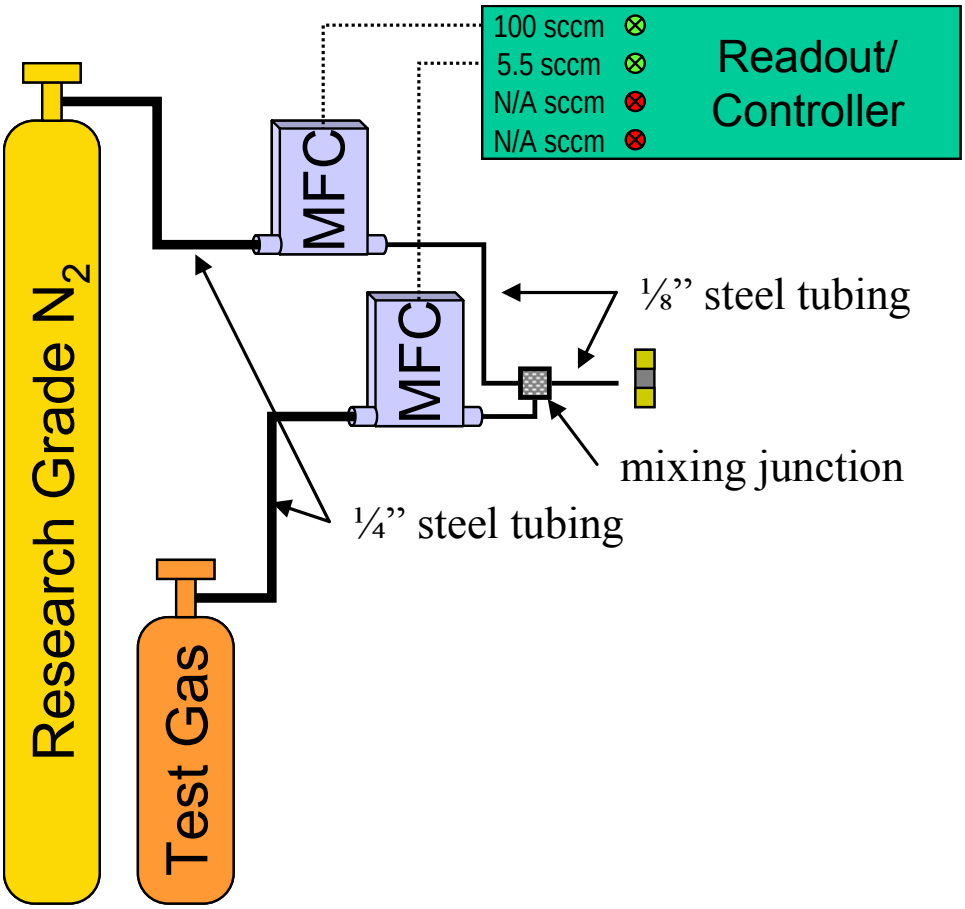

Figure 3-2: A schematic of the design for the gas flow control of the gas sensor test apparatus. The mixing junction is shown in more detail in Figure 3-3 and Figure 3-10.

The concentration of gases delivered to the sensor is calculated using both the flow rates and the concentrations of the gases entering the mixture junction. The equation for concentrations of gas species x_i at flow rates v_i being mixed from sources 'a' and 'b' to produce a gas mixture 'c' is given by Equation 3-1 and Equation 3-2. The subscript 'i' in these equations denotes the chemical (NH_3, NO_x, et al.) present in the test gas that is being mixed.

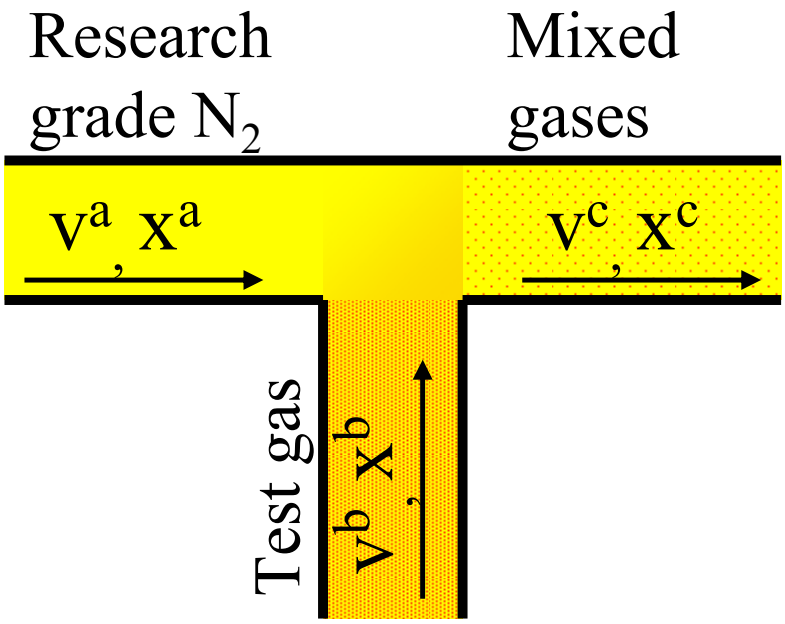

Figure 3-3: A diagram of the mixing junction where a test gas (b) is mixed into an entrainment gas (a, typically research grade nitrogen) and then exits as a mixture (c). The junction is oriented as shown in Figure 3-2.

Equation 3-1 is arrived at from the conservation of mass, which indicates that the flux of material into the junction is equal to the flux of material out of the junction. We next assume that each of the three gases have the same equation of state. This assumption is valid because each of the three regions of the junction is filled with between 99.9% and 100% nitrogen in our experiment.

Given that the gases are represented by virtually the same equation of state, and are not undergoing any change in pressure or temperature during the mixing process, the

volume of gas ‘a’ added to the volume of gas ‘b’ is very nearly equal to the volume of gas ‘c’. Considering the additive property of the volumes, and dividing by a fixed amount of time, it follows that the flow rate of the (assumed to be incompressible) gases are also additive. We can assume these gases to be incompressible each’s composition is >99% nitrogen in practice. This is represented by Equation 3-1 which typically has units of sccm: standard cubic centimeters per minute.

$$v^c = v^a + v^b$$

Equation 3-1: The flow rate of gas exiting the junction is the sum of the flow rates entering the junction by the conservation of mass.

The controlled mixture of the gases is necessary to produce a variable concentration of the resulting gas mixture for delivery to the gas sensor. The accurate calculation of this resultant concentration is possible from knowing the concentrations of the gases entering the junction and the flow rates of the gases in the junction[3]. By the conservation of mass, the number of the molecules present in a volume ‘c’ leaving the junction is equal to the number of molecules entering the junction due to the summed volumes ‘a’ and ‘b’. The partial volume of material ‘i’ entering the junction is the concentration of gas species ‘i’ multiplied by the volume entering the junction. Using this conservation of mass argument, we arrive at Equation 3-2 for the partial volume of material ‘i’ leaving the junction.

$$x_i^c \times v^c = x_i^a \times v^a + x_i^b \times v^b$$

Equation 3-2: The concentration of gas exiting the junction times the rate at which it enters is the sum of each concentration entering times its respective flow rate entering.

In operation, since one of the gases is research grade nitrogen, the concentration of the gas being mixed in this line is zero. Rewriting Equation 3-2 to express the concentration of gas exiting the junction, we arrive at Equation 3-3.

$$x^{out} = x^{test} \times \frac{v^{test}}{v^{N_2} + v^{test}}$$

Equation 3-3: The concentration of the gas over the sensor is a function of the concentration of the test gas cylinder and the flow rates.

The nitrogen line flow rate of 100 sccm allows two quick abbreviations to be made to the calculation of flow rate and the concentration of gas being delivered to the sensor. These abbreviations serve to allow the faster documentation of tests. First, since the 100 sccm flow rate is much higher than the flow rate of gases entering the chamber, the gas sensor is said to be operating under a near constant flow of 100 sccm nitrogen. Several tests were conducted to determine that the sensor did not respond to the changing of the flow rates. In these tests, research grade nitrogen was connected to both a 100 sccm MFC and a 10 sccm MFC. The response of the sensor was monitored as the 100 sccm MFC remained on, and the 10 sccm MFC was varied between 0 and 10 sccm. The gases were mixed and delivered to the sensor, however no response was observed from the variation in flow rate over the sensor between 100 and 110 sccm. As all experiments were conducted within this range of flow rates, only the flow rate of the nitrogen MFC (100 sccm) was recorded as the flow rate of the test gas MFC can be recalculated from the value of the concentration being delivered to the sensor.

A second abbreviation was made to allow the calculation of the concentration of gas being delivered to the sensor without the need for a calculator. This abbreviation was needed for record keeping purposes so that experiments could be performed in as fast a

manner as possible when sensors were available for test. In this approximation, the concentration of gas being tested was recorded as the concentration of the gas in the test gas cylinder multiplied by the ratio of the flow rates of the test gas and the nitrogen. Since the flow rate of nitrogen was typically 100, and the concentration of test gas in the test gas cylinder was typically 1000 ppm, the concentration of test gas being delivered (in ppm) was the mass flow rate of the test gas MFC (in sccm) multiplied by 10.

To exemplify a typical experiment, we consider a test recorded at 100 sccm for a concentration of 5 ppm ammonia from a source of 1000 ppm ammonia. This test is actually done at 100.5 sccm in that the nitrogen flow rate was 100 sccm and the flow rate of the ammonia MFC was set to 0.5 sccm. The actual concentration for the test gas in this example would be 4.975 ppm ammonia in nitrogen. However, as will be shown later, this correction is overshadowed by the 1 to 2 percent error associated with the MFC's.

As was mentioned earlier, the MFC's were initially controlled through the switches on the type 246C and type 247D power supplies. However, it became advantageous to develop a LabView controlled system to operate the MFC's. This system, which used a NI DAQPad-6015 was needed for the simultaneous measurement of multiple gas sensors in an array format[4]. The computer controlled system operates functionally in the same manner as the physical switching of the MFC power supplies described above. Because it was developed to facilitate the use of arrayed gas sensors, this program will be described in detail in Chapter 7.

Gas Delivery to Sensor

The next important component required for the testing of the gas sensor corresponds to the delivery of the gas sample to the sensor. This element of the experiment is critical as it accurately represents the end use of the sensor. In past experiments, the gas delivery to the sensor was un-realistic as it involved the pumping of the sensor to vacuum between exposures to test gas[1]. This mode of testing is impractical for a portable and low-power gas sensor and was necessarily abandoned. For the applications being considered, a system was designed to deliver gas pulses employing a real-time method under atmospheric pressure. This allowed both the sensor response to the test gas to be determined while, at the same time, correcting for simultaneous interference from outside effects such as pressure and temperature. These undesirable effects could then be analyzed, leading to a significant enhancement of the quality of the sensors. Important improvements include the development of the shadowmask lithography step (discussed in Chapter 2) and the pulsing method for testing devices which will be discussed in this chapter.

The most important aspect of the design of the interface between the gas flow and the sensor is that it mimics the eventual sensor operation. The mode of operation depicted in Figure 3-4 was used to test the majority of gas sensors which we will consider. After mixing at the junction, the gas exits the section of ⅛" stainless steel tubing and flows over the gas sensor in an open-air environment. The sensor is situated approximately one centimeter away from the tube exit and just below the tube so that the flow is directly over the reactive region of the sensor. The entire apparatus was located in a fumehood so as to mimic the "open-air" environment while protecting the laboratory

from the deleterious gases being tested. This fumehood operated drawing 100 linear ft/minute of air from the outside environment when fully open, causing the pressure inside the hood to be slightly lower than atmospheric pressure.

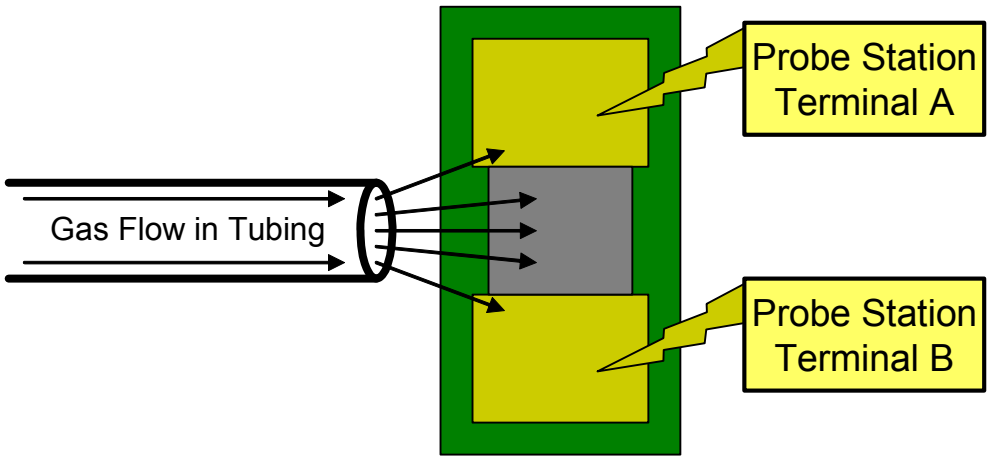

Figure 3-4: The relationship of the gas sensor, the gas flow, and the probe tips is shown.

The sensor was placed a distance of one centimeter away from the end of the tubing so as to be as close as possible to the exiting gas stream while reducing the noise caused by the airflow. Sensors which were placed closer than one centimeter experienced a dramatic increase in the random noise in the signal resulting primarily from the high flow rate. This effect was verified by placing a sensor close to the exit of the ⅛" tube and varying the flow rate of the research grade nitrogen between 50 and 100 sccm. The same sensor, when placed an adequate distance away from the tubing, exhibited no changes in noise level as the flow rate was varied.

A second way to avoid the noise associated with high flow rates over the sensor would be to reduce the overall mass flow rate of gas being delivered to the sensor. To accomplish this would require 1) the purchasing of additional MFC's capable of operating at lower flow rates, or 2) the insertion of additional tubing to shunt excess gas flow away from the sensor. Neither of these options were pursued as the sensor

responded to the lowest concentrations deliverable using the described configuration without these modifications. In addition, the extra MFC's would have cost several thousand dollars, which is an unjustifiable expense given that the existing MFC performed as needed.

A picture of the system as it was used is shown in Figure 3-5. This system shows the junction where gases mix, the tubing where the gas exits onto the sensor, two probes making electrical contact, and two additional electrical contacts (black alligator clips) to a resistive heater located below the sensor for temperature testing. The gas sensor and heater are both located inside a foam boat for insulation. The entire apparatus is located inside a fume hood for safety during the testing of hazardous gases.

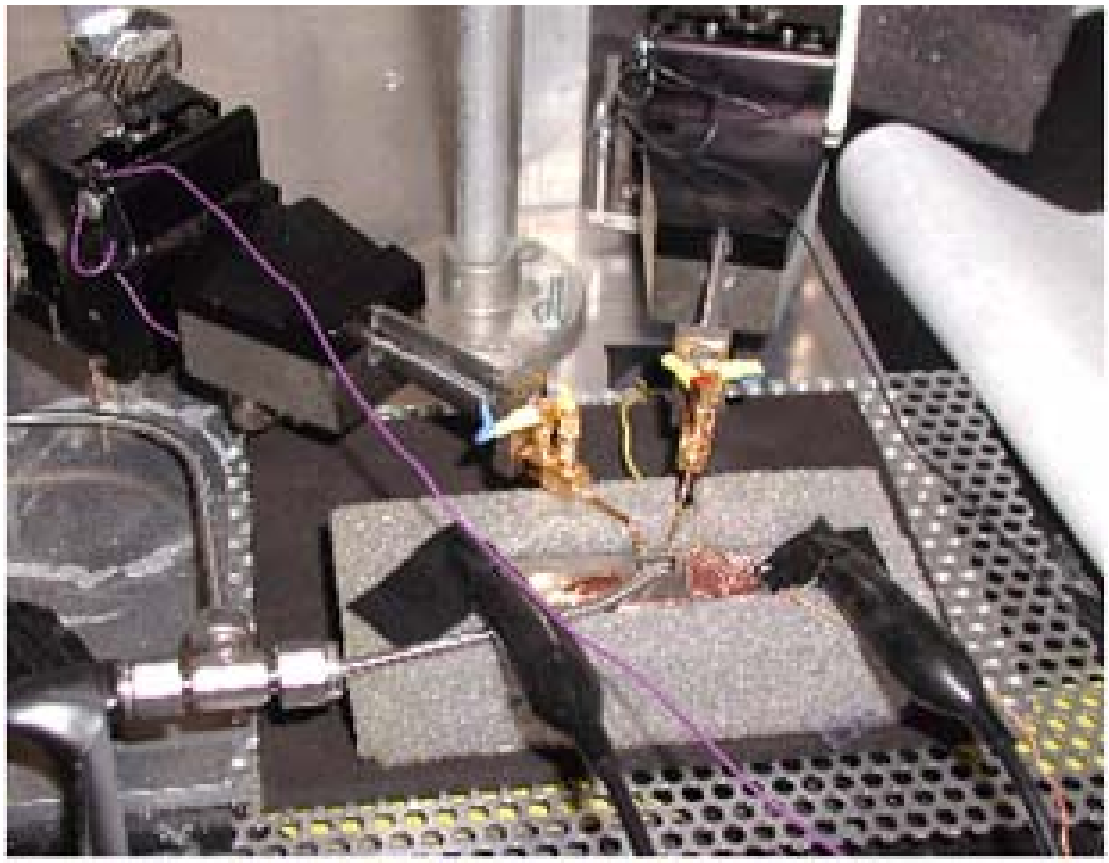

Figure 3-5: The sensor with electrical contacts made by two precision microprobes, the ⅛" tubing where the gas exits onto the sensor, and electrodes for heating the sensor.

Sensor Measurement

Measurements were initially taken with a computer-controlled Solartron 1260A impedance analyzer. This device was configured to measure the impedance of a single sensor in real time. The impedance analyzer does this by connecting four coaxial measurement lines to the sensor (Figure 3-6). The grounds of the lines are grounded to each other. The terminals which supply an AC current source are connected to either side of the sensor, which allows current to flow through the device. Voltage terminals are similarly connected to each side of the sensor, which measure the voltage drop across the sensor caused by the impedance of the device when current is passing through it. For these resistive sensors each side of the sensor was connected to one probe station. Each probe station was then connected to a voltage measurement terminal and a current source terminal of the 1260A. The 1260A reports both the real and imaginary parts of the impedance of the device being tested through a comparison of the amplitudes and phase difference between the AC current and the AC voltage. The real part of the impedance, which is the resistance, was tracked to determine the response of each sensor[2].

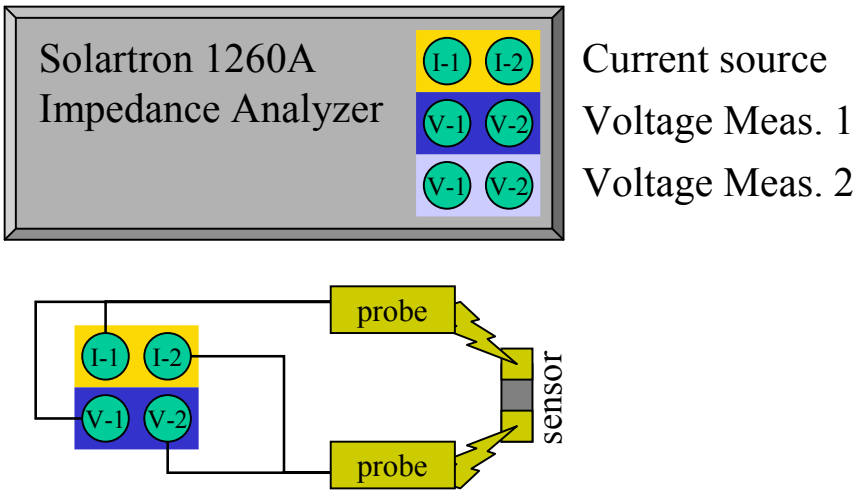

Figure 3-6: A schematic depicting how the gas sensor was connected to the Solartron impedance analyzer.

The Solartron has a maximum data collection rate of 1Hz which was utilized for all experiments. To measure sensor response, the Solartron was operated in its constant voltage-over-time mode, where the current delivered was modulated to maintain a constant AC voltage across the device. A 100mV, 1kHz signal was typically used to measure the sensor. This combination was chosen after assessing several different amplitudes and frequencies as it provided the best signal with the least noise[2]. The computer program which controlled the impedance analyzer was called ZPlot, while the program that allowed viewing of the data was called ZView. These programs are shown in Figure 3-7 and Figure 3-8.

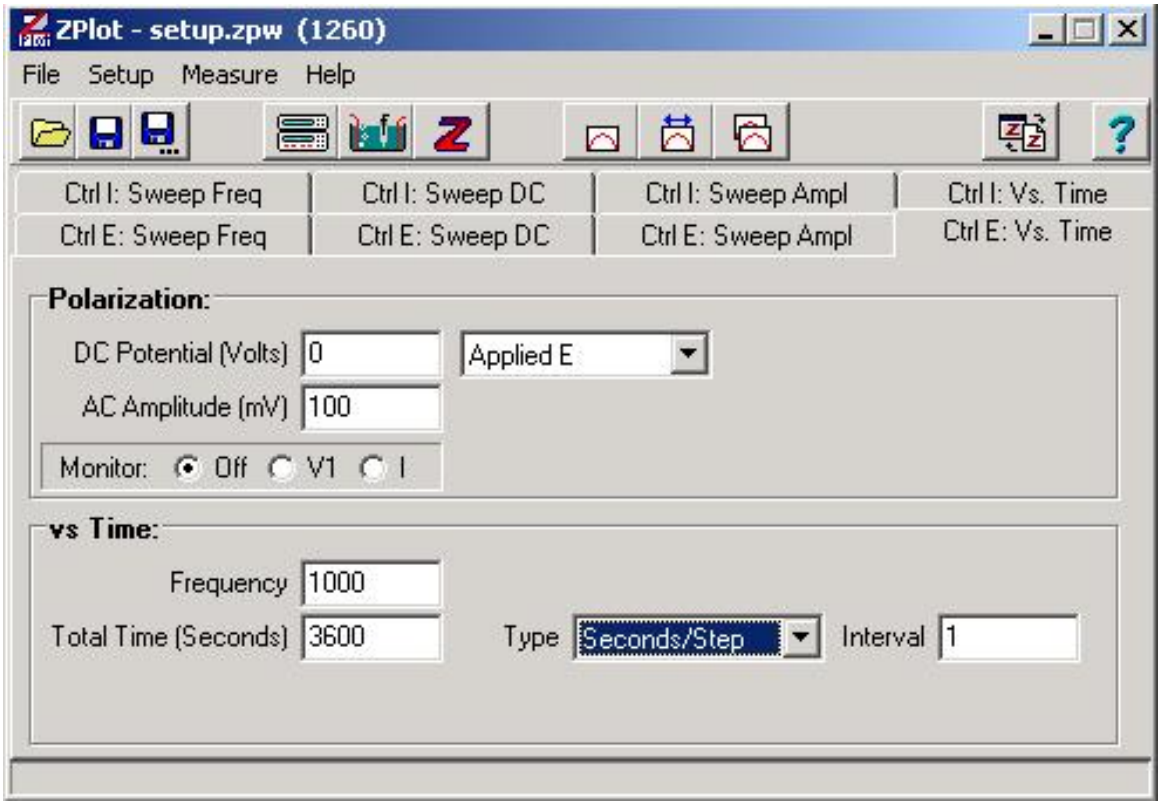

Figure 3-7: An image of the program ZPlot as it appears prior to running an experiment. This instance, ZPlot is configured to take measurements once a second, for 1 hour, by maintaining a 100mV amplitude,1kHz frequency signal through the device.

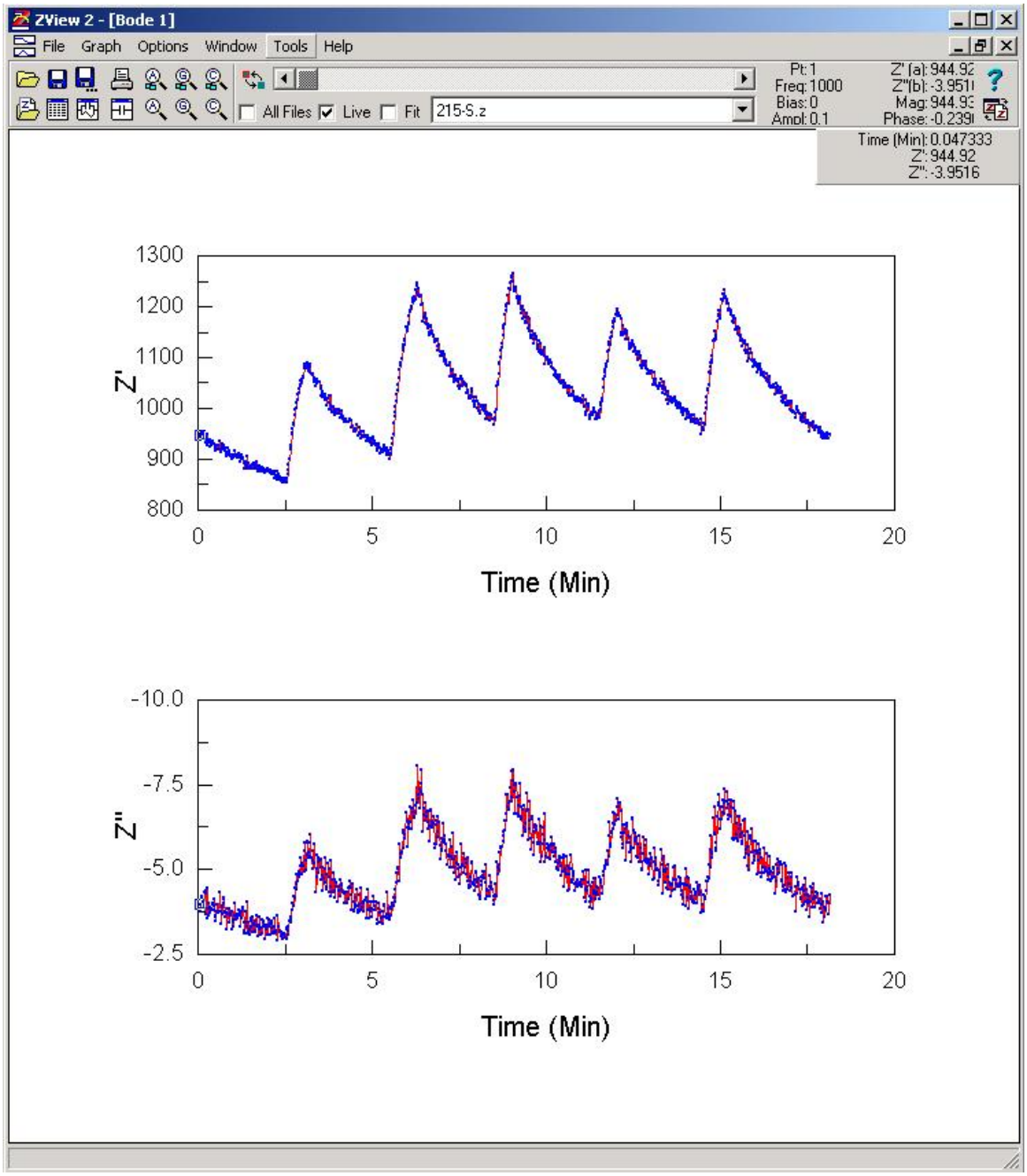

Figure 3-8: An image of the program ZView, showing the data collected after an experiment was done. Both the real part of the impedance, or resistance, (top) and the imaginary part of the impedance (bottom) are reported while ZPlot is running in real time.

Error Analysis

The following estimates of error illustrate the level of relative certainty of the PSGS performance in responding to the levels of test gas indicated in this thesis.

Gas Concentration Error

The error for both the gas concentration and the gas flow rate must be calculated to determine their contribution for later comparison to the measured sensor response. The error of the MKS MFC's, as stated by MKS, is 2.0% of full scale for the MFC used with the 1000 ppm test gas cylinders and 1.0% of full scale for the MFC for nitrogen. Finally, the 1000 ppm test gas cylinders had a 2% possible error in concentration. The error was propagated using Equation 3-3 for the 1 sccm MFC, the results of which are shown in Figure 3-9[5]. This figure illustrates that error propagation results in a 4% error at 0.5 ppm for a 1 sccm test mass flow controller. The error in the delivered concentration increases precipitously for levels below 0.5 ppm, which we define as the lowest reliable testing limit of the MFC.

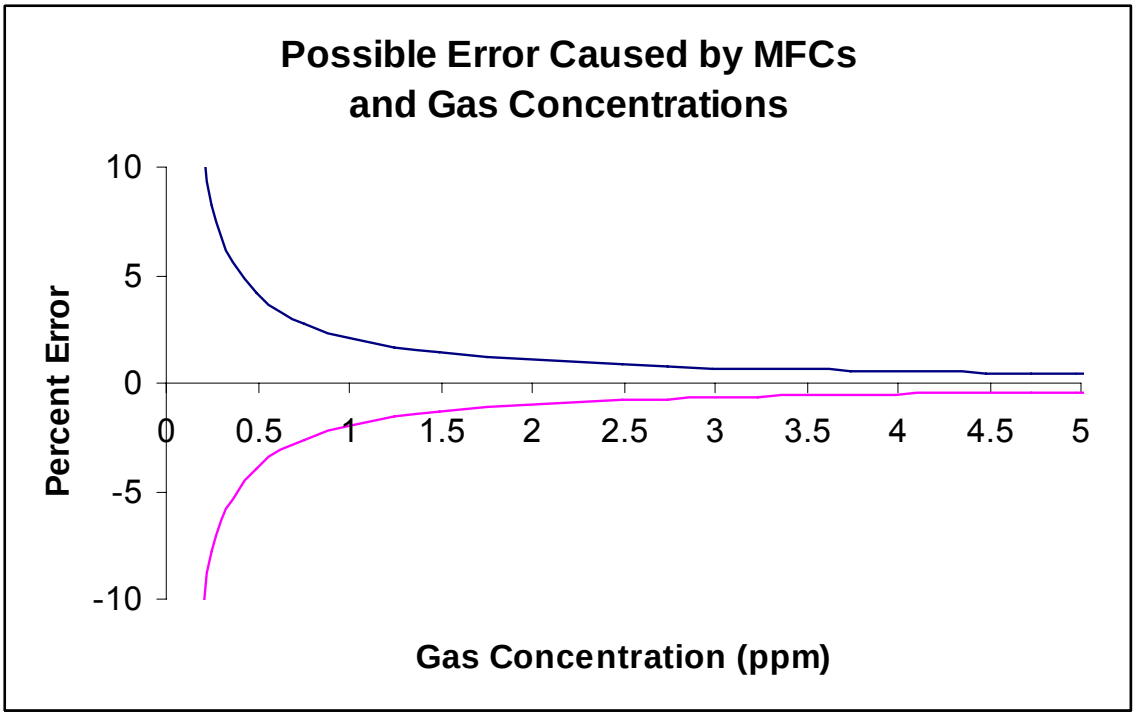

Figure 3-9: The error (maximum and minimum) for a 1 sccm MFC controlling the test gas is calculated for various expected concentrations of gas.

Gas Packet Dilution Within the Mixture Junction

The packets of gas delivered through the test gas MFC to the sensor take a finite time to traverse the length of pipe from the MFC to the junction and from the junction to the sensor. This length is critical because when the MFC is off, some amount of gas still remaining in the tubing before the junction will diffuse into the junction and across the sensor. This deleterious effect is depicted in Figure 3-10.

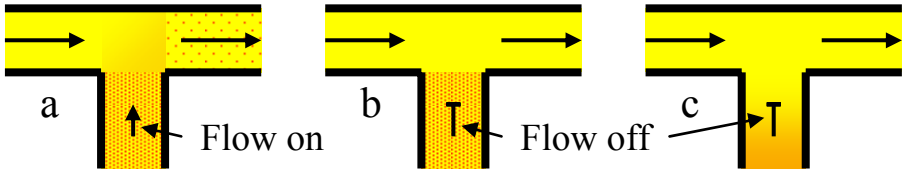

Figure 3-10: The diffusion of test gas into the nitrogen flow is depicted in three stages: a) the test gas is initially flowing into the nitrogen at the mixing junction at a constant rate, b) immediately after the flow of the test gas is turned off, the test gas remains within the tubing, but later, c) some of the test gas has diffused into the nitrogen line. The junction is oriented as shown in Figure 3-2.

This effect results in a delay in the response of the sensor when the test gas MFC is again flowing test gas into the junction because some portion of this line will be filled with diffused research grade nitrogen. To minimize the amount of test gas that diffuses into the flow of nitrogen, the pipe length, and the diameter of the pipe between the MFC and the junction was made as small as possible. Because of the diffusion into the junction, some error can arise from the residual gas trapped in the tubing between the test-gas MFC and the junction. The other lengths of tubing between the MFC's and the sensor are less significant. At 100 sccm, the time for gas to traverse the tubing between the junction and the sensor is about 75 ms. Because 75 ms is much smaller than the sampling period of the impedance analyzer, this time is not considered significant. The length and size of the tubing between the nitrogen MFC and the junction is also not considered significant because this line is constantly flowing nitrogen at 100 sccm.

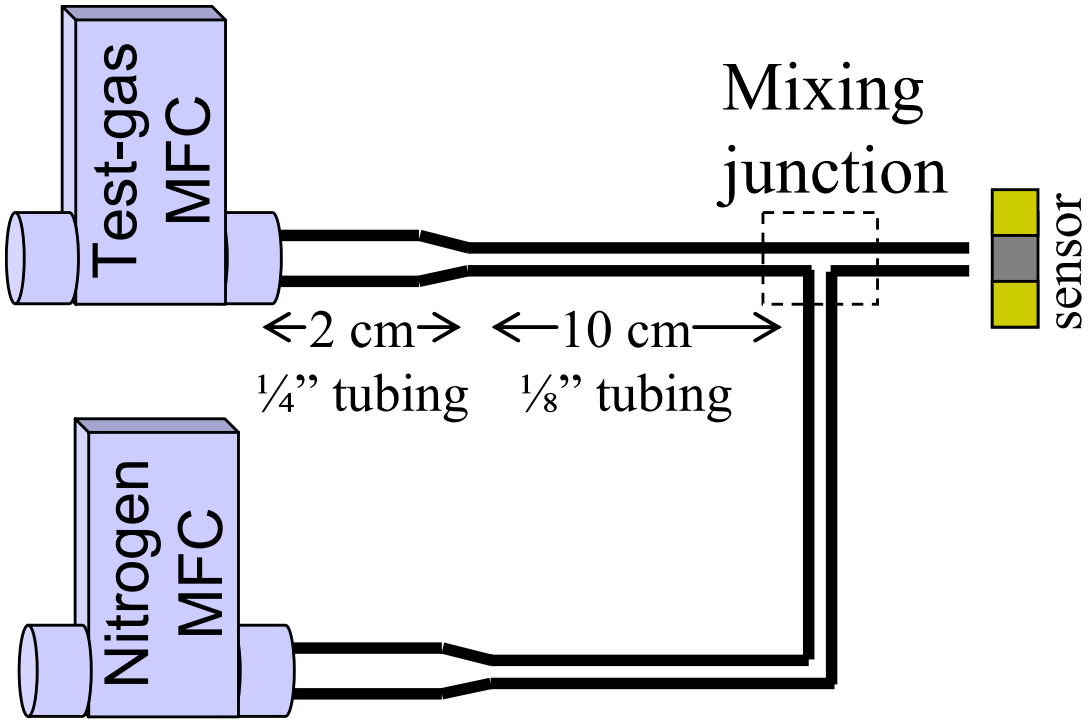

Figure 3-11: The most significant aspects of the gas-mixing apparatus are depicted, including the length of tubing between the test gas MFC and the mixing junction.

In the final construction of the sensor's test apparatus, approximately 2 cm of ¼" tubing and 10 cm of ⅛" tubing was used between the test-gas MFC and the junction (Figure 3-11). Taking the tubing wall thickness, 0.028", into account, the flow velocity of one sccm of test gas is 1.0 mm/s and 6.9 mm/s for the ¼" and ⅛" tubing respectively. For 0.1 sccm of test gas, the lowest rate of test gas commonly used, the above speeds of gas through the tubing can be divided by 10. For our system, this equates to a maximum time for the test gas to reach the sensor from the MFC of 60 seconds for 1 sccm of test gas, and 10 minutes for 0.1 sccm of test gas. However, the gas present in this 10 cm of ⅛" tubing is still close to pure test gas, with only some loss due to diffusion through this line.

An approximate value of the dilution of the test gas due to the nitrogen flow through the ⅛" tubing can be calculated. Using ammonia, which has a diffusion constant of 0.230×10^{-4} m^2/s in nitrogen as an example, we treat the flow in the tubing as a one-dimensional diffusion problem. This problem is depicted in Figure 3-12. The solution has the general form of the error function and is expressible as Equation 3-4[6].

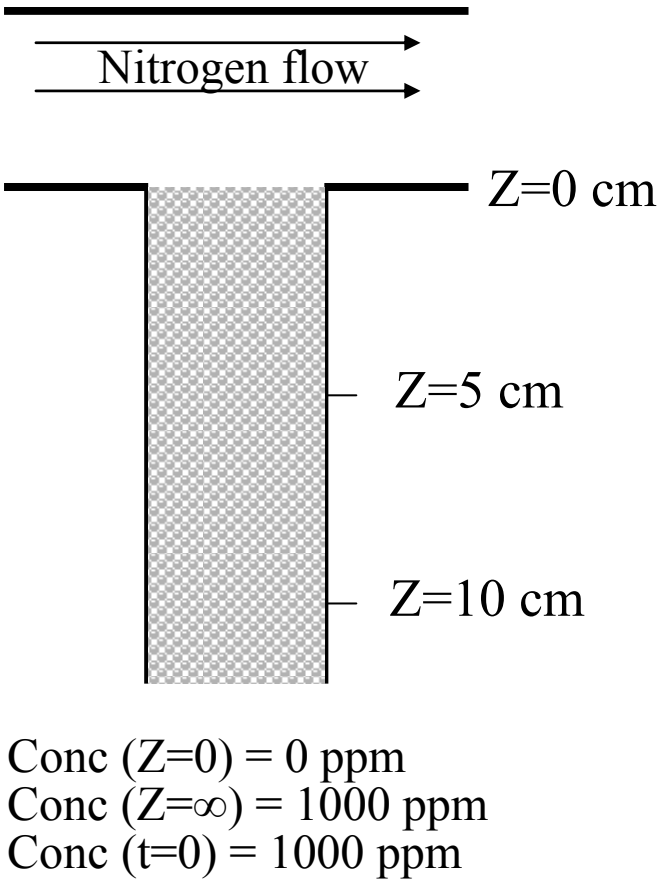

Figure 3-12: A blown-up view of the mixture junction depicting how the one-dimensional diffusion problem is setup. The concentration as a function of z (distance from the junction) and t (time from the flow being turned off) is solved for within the shaded region by Equation 3-4.

$$Conc(z,t) = 1000\,ppm \times erf\left(\frac{Z}{\sqrt{4D_{AB}t}}\right)$$

Equation 3-4: The concentration within the shaded region of Figure 3-12 is expressed by the error function and is a function of the diffusion constant of ammonia in nitrogen (D_{AB}) which is 0.230 cm^2/s.

Analyzing the diffusion into the junction from the ⅛" tubing, we determine that after 1 minute in the absence of gas flow, the concentration of ammonia 5 cm from the junction drops approximately 85%. 10 cm inside the line, the gas is over 99% that of the test gas cylinder. So, in the worst case scenario, where we test for the lowest concentrations of gas, it takes 60 seconds before 85% of the desired concentration is

delivered to the device. This error is significant and can effect the outcome of an experiment, particularly when low concentrations (< 1 ppm) of a test gas are being mixed and delivered to the sensor for a short (<30 seconds) duration.

For a typical experiment, however, the time for the test gas to reach the sensor is about 2 seconds. The time for gas to reach the sensor could be improved by 1) replacing the ⅛" tubing with an even smaller diameter of tubing to increase the flow rate, or 2) by custom building an MFC to eliminate the distance between the valve within the MFC and the mixture junction.

A final source of error pertaining to the dilution of test gas occurs when experiments are first run after not being run for a time period of several (12+) hours. This situation typically only occurs during the first experiment being performed each day. During this time, the gas present between the test-gas MFC and the test-gas cylinder will diffuse through the MFC, reducing its concentration significantly. Before running experiments each day, it is necessary to fill this length of tubing with the test gas to ensure that the MFC is delivering packets of "pure" test gas. Leaving the test gas MFC on at full capacity for ten minutes is sufficient to replenish the test gas within the tubing and will ensure that the first test of the day is accurate.

Noise Sources

Noise in this experimental system can be divided into external sources and internal sources. While some noise can be reduced or eliminated altogether through improvements in the fabrication and testing schemes, other noise sources can only be accounted for.

External Noise

External noise, or noise present due to factors "outside" of the experiment, can be the result of temperature, pressure, or humidity fluctuations within the environment of the test apparatus.

Experiments done by John DeBoer show that pressure effects leading to a drifting signal can potentially be significant and must be tracked[2]. Testing of the gas sensor in the fumehood caused the gas sensors to be exposed to an unanticipated periodic fluctuation in pressure which occurred on a timescale closely following that of the testing cycle. This pressure fluctuation was later found to be caused by a faulty controller for the fumehood flow regulator. A device's response to this pressure fluctuation only is shown in Figure 3-13. The pressure fluctuations occurred over a period of about 7 minutes. These pressure waves produced many false positive responses during the initial testing of devices and subsequently lead to the incorporation of the gas-pulsing method of device testing. An alternative method to eliminate the deleterious effects of these pressure fluctuations would be to calibrate the effects of pressure on the sensor and track the pressure of the environment with a pressure transducer located adjacent to the sensor. This would allow the low frequency pressure noise from the signal to be removed.

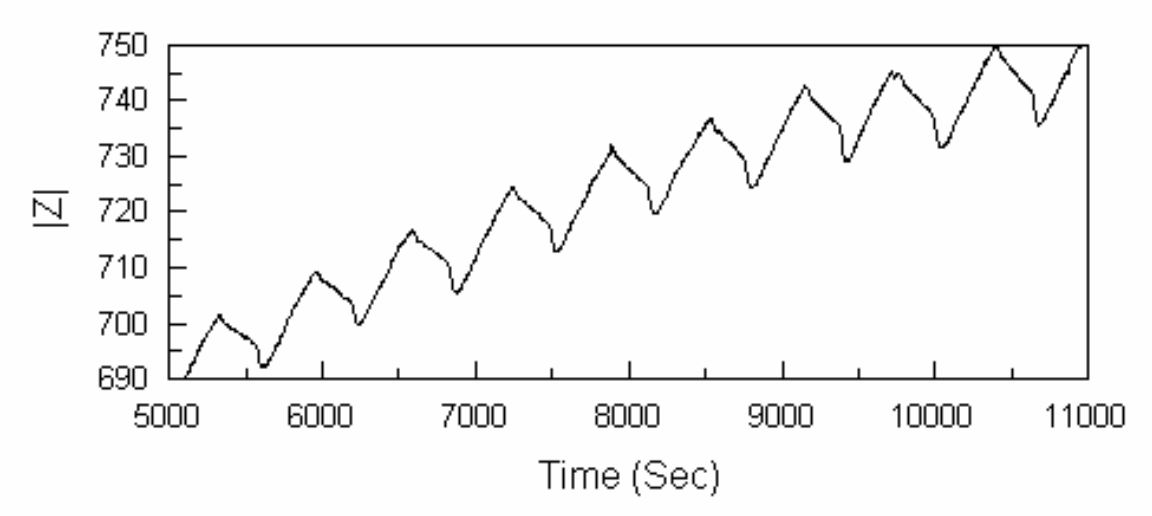

Figure 3-13: Picture of periodic pressure waves (frequency of 1.50 mHz)

In addition to the effects of slow drifting pressures, an extreme and rapid change of pressure such as that produced by a vacuum evacuation of the sensors, can cause a failure of the electrical contact to the sensor. This was found to be particularly true of wire-bonded sensors. Vacuum evacuation has been shown to irreversibly change the baseline resistance of such devices as we depict in Figure 3-14. The device monitored to produce the effects in Figure 3-14 also demonstrated a dramatic increase in noise after vacuum evacuation which reduced the performance of the sensor[2].

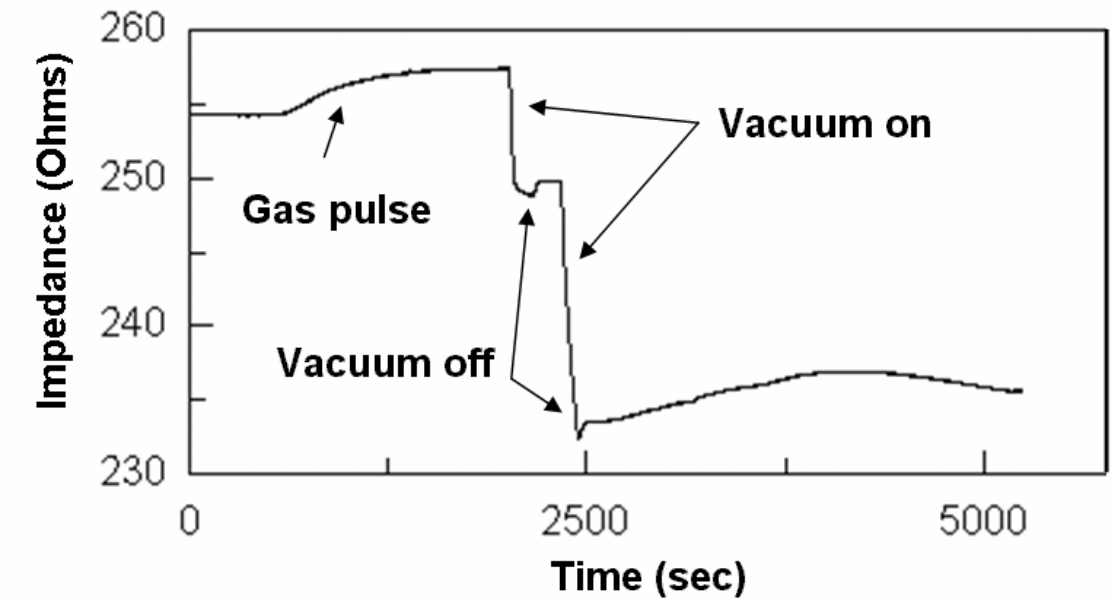

Figure 3-14: The effects of a vacuum applied to a device can produce dramatic changes in the baseline impedance. In this experiment, a gas pulse was first delivered to the sensor at about 600 seconds. The sensor was then pulled down to vacuum and returned to atmospheric pressure twice.

The temperature response of the PSGS is similarly significant. The temperature response was modulated at a period of 4 minutes by physically switching the power to a heater located beneath the sensor. After this process was performed over a period corresponding to about 15 pulses, the increase and decrease in temperature over the 4 minute period stabilized, as depicted in Figure 3-15, resulting in a periodic temperature signal with little drift in average temperature. The response of the sensor to this temperature fluctuation was monitored while the sensor was exposed to pure nitrogen. This temperature fluctuation was maintained and again used to test a device to 60 second pulses of 10 ppm ammonia in nitrogen. The results of both of these tests are shown in Figure 3-15. The tests are discussed further in the gas pulsing section of this chapter.

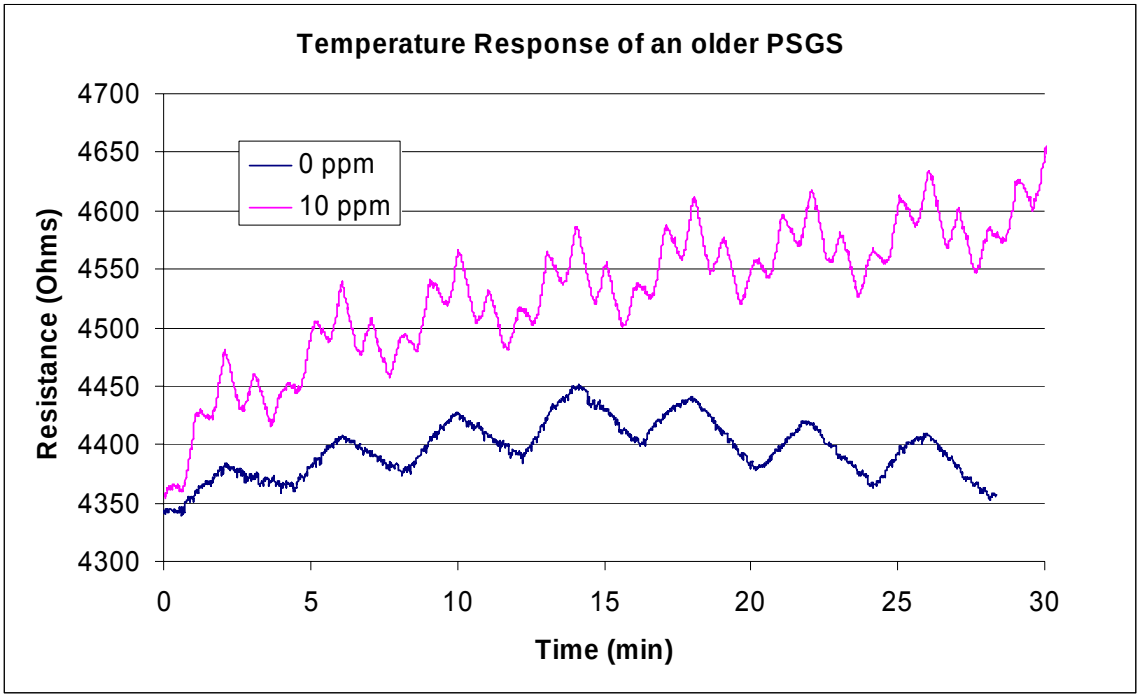

Figure 3-15: The response a PSGS (5.2.2-6) is shown for controlled oscillations in temperature between about 30 and 35 °C. This data shows how the response of a device to pulses of 10ppm ammonia once per minute (see Testing Methods below) would need to be scaled with a device in parallel (no ammonia exposure) to account for temperature fluctuations. The plot for 0ppm is scaled by a factor of 6 to be near the other device.

For a diversity of sensors, the increase of sensor temperature was studied as a possible means to improve sensitivity. However, for all such tests, the sensitivity was found to degrade dramatically and irreversibly at around 80°C. This hysteretic behavior is shown in Figure 3-16. The irreversible effects of heating the PSGS are outlined in more detail in the thesis of Mr. DeBoer[2].

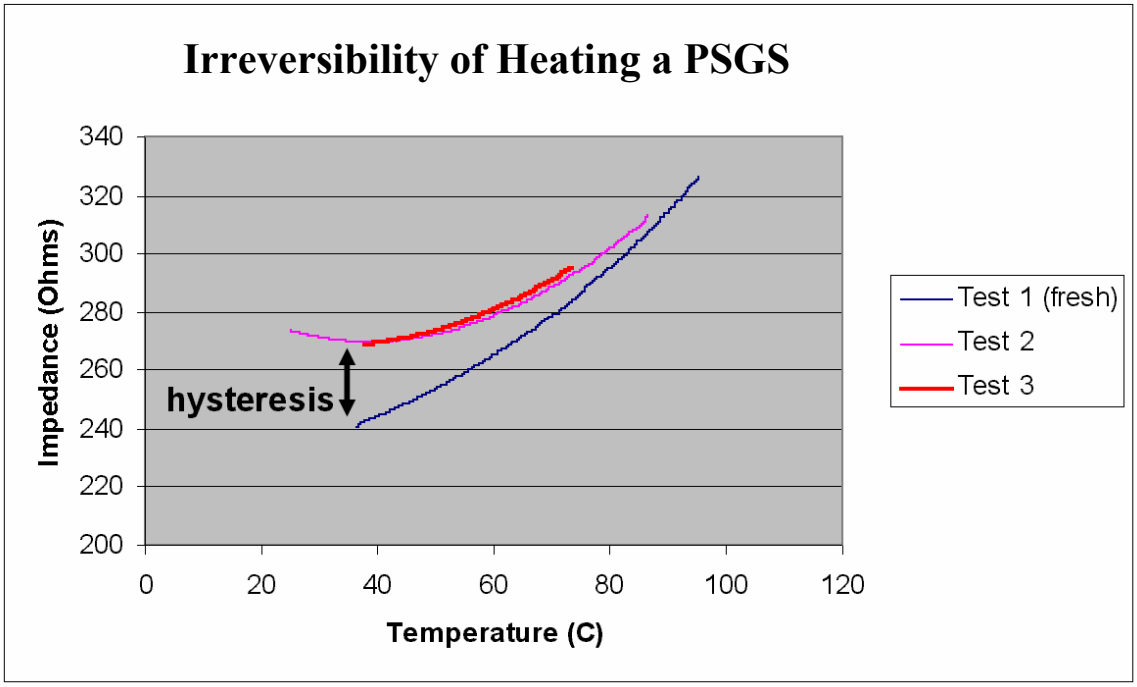

Figure 3-16: During sequential heating experiments of a PSGS, a non-reversible increase in room-temperature resistance (as well as an increase in device noise) occurs. The baseline impedance of 240Ω present in the first experiment (Test 1) can not be recovered.

The PSGS responds well to humidity changes, as was also studied by Mr. DeBoer. The effect of nitrogen, passed through a bubbler, compared to dry research grade nitrogen is shown in Figure 3-17. This response is dramatic, and demonstrates that in a practical application, the ambient humidity must be tracked to ensure against false positives.

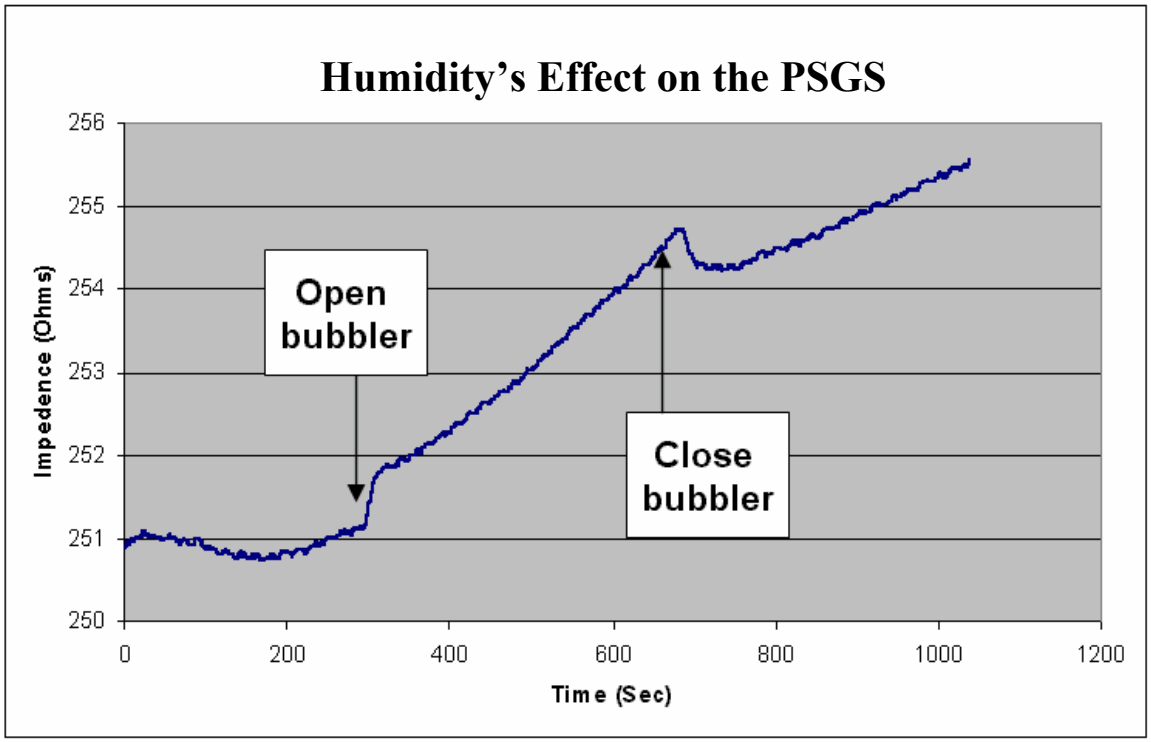

Figure 3-17: Exposing the PSGS to humidity produces a significant response.

Internal Noise

The most significant potential source of internal noise for the sensor is the variation in mass flow rate of gas over the surface of the device. This flow rate, while typically between 100 and 101 sccm, presents a possible cause of error in sensor testing. We must ask whether the sensor is responding to the concentration of test gas or to the effects of a 1% increase in flow rate over the sensor. To address this effect, the flow rate of research grade nitrogen to the device was varied in a test similar to the gas pulsing test, which will be described later in this chapter. The entraining nitrogen was varied, at a period of once per minute, between 80 sccm and 100 sccm. These quantities were chosen to represent the greatest possible spectrum of flow rates envisioned at the time (Spring 2003) which have since been only slightly exceeded. Each flow rate of nitrogen was

maintained for 30 seconds (half) of each period, for a total of 30 periods. A frequency transform of the resulting signal is shown in Figure 3-18.

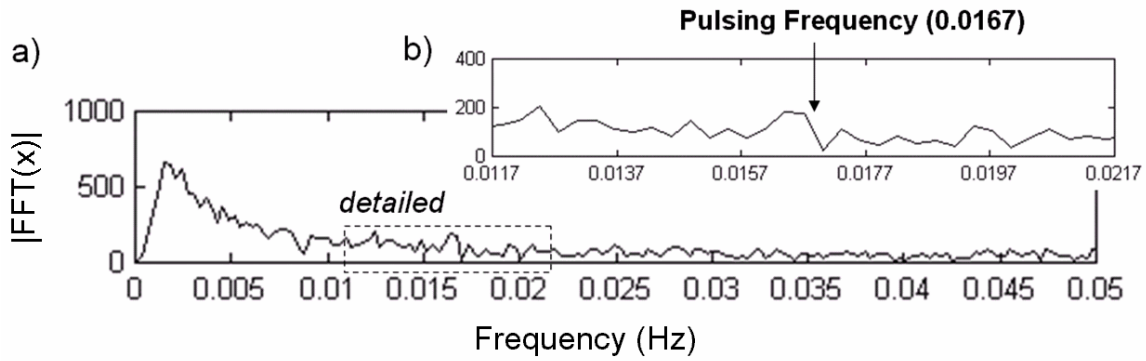

Figure 3-18: The effect of flow rate over a sensor is shown as the flow varies periodically from 80 to 100.4 sccm of research grade nitrogen. No significant signal is visible in this figure at the pulsing frequency.

The internal noise of the more recently produced devices exhibits fluctuations (the standard deviation of the response) which are less than 1% of the total resistance of the device. However, as shown in Figure 3-19, the level of relative internal noise increases when the device is exposed to a given concentration of test gas. However, this increase does not significantly effect the potential to detect low levels of test gas, since the noise levels are still extremely low. For example, the device shown in Figure 3-19 responds linearly with a change of 6000Ω per 5ppm of ammonia. This sensitivity produces a response of 1.2Ω per ppb of ammonia, so with a noise level of 15Ω, this device could theoretically respond with two standard deviations (95%) confidence to as low as 25 ppb of ammonia. 25 ppb of ammonia, with a response of 1.2Ω per ppb, is the point at which the concentration is produces a response of 30Ω, twice the noise level. We can therefore largely ignore the internal noise of the sensors, because the error of the test setup is 500 ppb, much larger than 25 ppb.

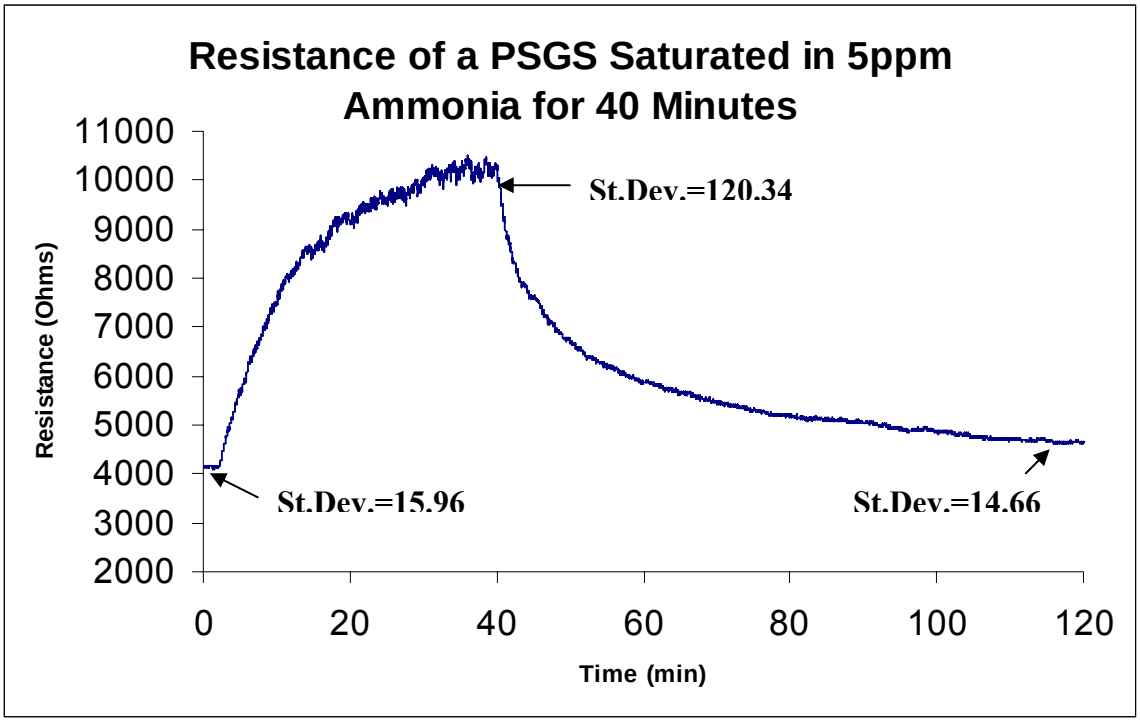

Figure 3-19: The standard deviation of the resistance of a device increases dramatically as the device increases in resistance due to exposure to a concentration of ammonia.

Testing Methods

During the characterization of the gas sensor response to various gases, three primary modes of testing were developed. These are, in order of increasing complexity, the saturation test, the lower exposure limit (LEL) test, and the gas pulsing test. Each of these methods of testing provides different information about a gas sensor's response to a particular gas concentration.

Prior to any of the above tests, it must be ascertained that a sensor is in a normal, baseline state. This is achieved by running only research grade nitrogen over the sensor and recording the sensor's resistance over a period of time. This period of time will depend upon whether the sensor is recovering from a previous test, but a time period of 5 minutes with no change in resistance with time is sufficient to indicate that the sensor is

ready for testing. This flat response can be observed during the first 5 minutes of the data presented in Figure 3-19. At the tail end of this figure (after 100 minutes) the sensor is again approaching a baseline condition. The time it takes to reach a stable condition is directly related to the length and concentration of the previous exposure of the device to a given gas. However, as is discussed in Chapter 5, an accurate understanding of the nature of the response mechanism allows a measurement to be recorded without the need to return to a baseline condition. As a rule of thumb, the wait time between tests should be about twice the time of the previous exposure to a given gas. This time is needed for the device to return to a baseline "normal" state and be ready for a subsequent test. To speed up the testing process, when the sensor is not in use during the day, the nitrogen flow is maintained over the sensor. However, to conserve nitrogen, the flow is curtailed after each day of testing.

Device Saturation Method

The simplest test that can be performed for the PSGS is the saturation test. This method of testing is the most commonly observed testing method for gas sensors. These tests are typically characterized by time scales on the order of several minutes or more. They allow the device to reach a point close to the infinite-time response (see Figure 1-14 or Figure 1-17 for examples) and are used to calculate the response of a device if it were left in the presence of a single concentration of analyte for infinite time. This infinite time response is called the total response of the sensor. As a sensor can not be tested for infinite time, the total response is calculated when the response is seen to be plateauing.

Figure 3-19 depicts the response of a device being saturated with 5 ppm ammonia for 40 minutes. This device is not saturated to the point of a stable response, which is

evident as the slope of the resistance is still greater than zero at the point which the ammonia is removed from the sensor. However, from the analysis of the transduction mechanism presented in Chapter 5, we can show that this limited data is sufficient to determine what the total response would have been were the experiment continued for infinite time. This model is based on the diffusion limited adsorption of analyte onto the PSGS surface. The response of the PSGS over time (usually around 30 minutes of exposure) is fitted against the model, which projects the response forward in time to acquire the infinite-time response.

The saturation test is useful for determining the linearity of the total response as a function of concentration, the noise of a sensor, and the reversibility of a response. Figure 1-14 and Figure 1-16 demonstrate this kind of saturation testing as it is applied to other sensor technologies. However, for the applications being considered for the present gas sensors, which include a necessary fast response time, it is more important to evaluate the sensors using the faster mode of operation provided by the LEL test.

Lower Exposure Limit Method

The lower exposure limit (LEL) method was designed to determine the LEL of a sensor in the most efficient manner possible. This mode of testing delivers packets of varying concentrations of test gas to the sensor, separated by periods of no exposure, which allow the sensor to return to a baseline condition, as shown in Figure 3-20. These packets typically range from 10 to 60 seconds in length. The response of the sensor is measured for each pulse of gas. The response is then plotted as a function of the concentration of the pulse of test gas, thus providing a means to calculate the sensitivity

and LEL of the sensor for that test gas. A detailed example for the PSGS follows the example given below.

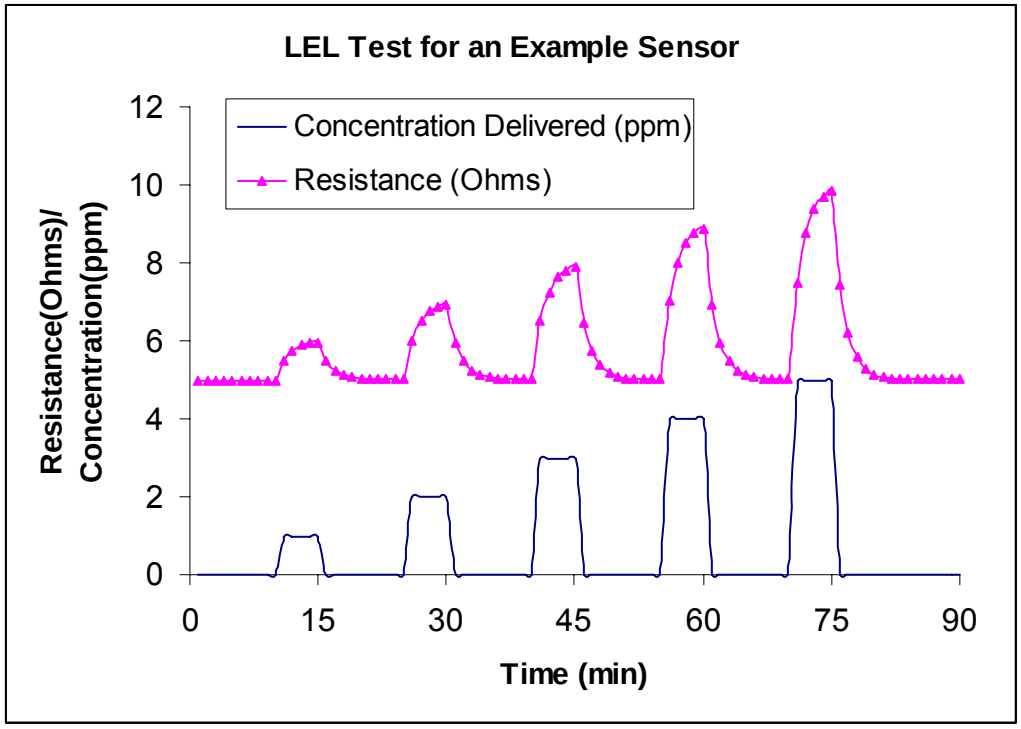

Figure 3-20: An example of an LEL test for an ideal sensor. The concentration is varied between {1,2,3,4,5} ppm and 0 ppm. The response is measured for each pulse, in this case the total resistance change.

The rapid response of the PSGS allows its sensitivity to be defined according to the rate of response, rather than with respect to the total response. This provides for a much more rapid calculation of concentration. In a typical experiment to determine the LEL and sensitivity of the sensor whose response is shown in Figure 3-21, a device is exposed to increasing concentrations of NH_3. Each packet of test gas delivered was one minute in length, followed by a two minute relaxation time. Five packets were delivered, in each of two experiments, varying in test gas concentration from one to five ppm of NH_3 in a background of N_2.

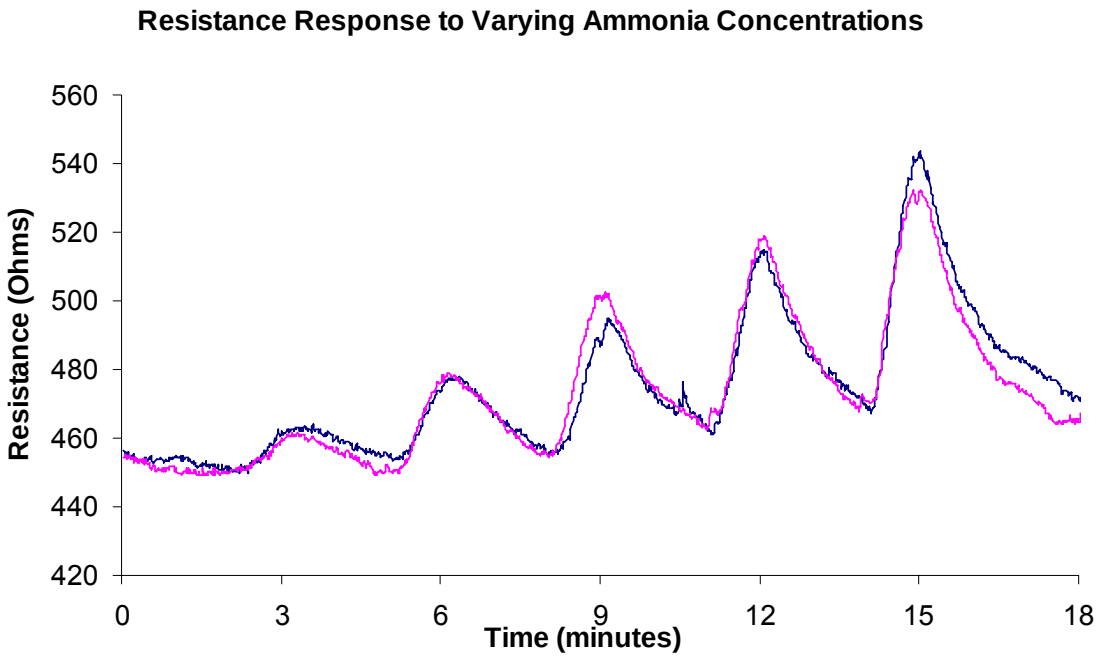

Figure 3-21: Resistance of a sensor in time exposed to one minute pulses ranging from 1-5 ppm NH_3 in N_2 with two minutes of relaxation time between each pulse. A repeat experiment is also shown.

The slopes of the responses, divided by the baseline resistance (~450 Ω) were calculated and are shown in Table 3-1.

Table 3-1: The slopes of responses for repeat tests of a PSGS response to NH_3 as shown in Figure 3-21.

NH_3 Conc. (ppm)	Slope for test 1 (mHz)	Slope for test 2 (mHz)
1	0.525118	0.430756
2	1.008102	1.261944
3	1.635515	2.052863
4	2.242355	2.252774
5	3.235923	2.640844

A plot of the data in Table 3-1 (see Figure 3-22) shows that the slope response is apparently a linear function of the concentration. It will later be demonstrated, as we present an analysis of the transduction mechanism (Chapter 5), that the slope of the sensor response (as well as the total response) is a linear function of the natural log of the

concentration. The linear profile we observe in Figure 3-22 corresponds to the low concentration limit of this logarithmic function..

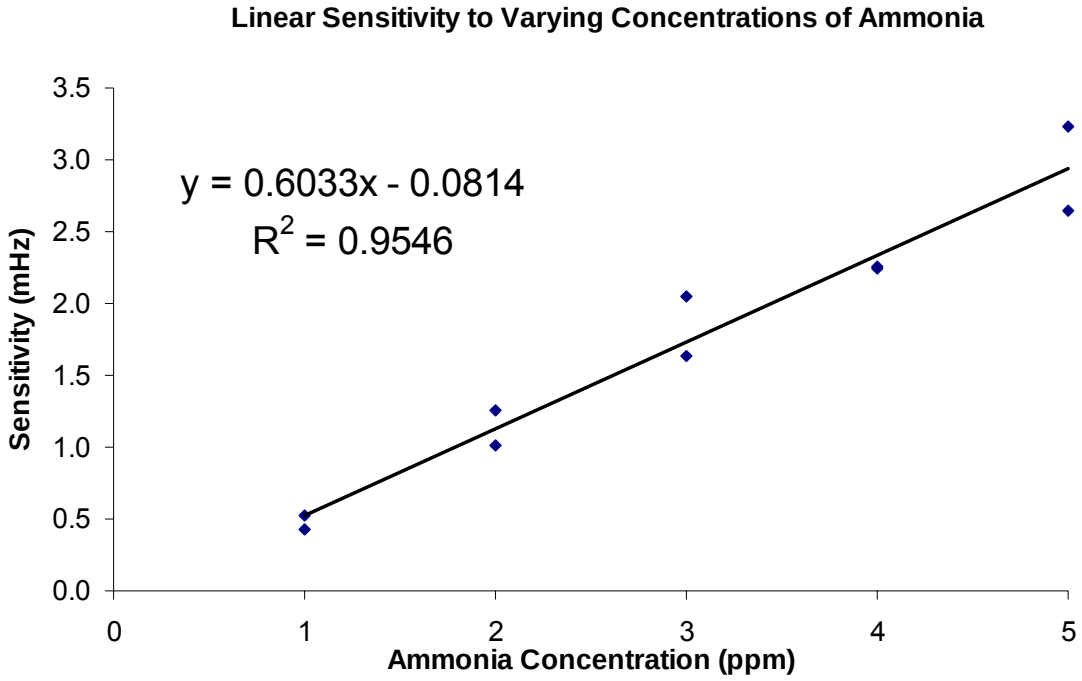

Figure 3-22: The sensitivity of the PSGS to ammonia matches well with a linear function.

The sensitivity of the PSGS as a function of concentration is described by Equation 3-5. The sensitivity indicated in Figure 3-22 (0.6033 mHz/ppm) is represented as the product of a coefficient specific to the analyte being tested and its concentration. The slope of the response divided by the baseline resistance, allows the calculation of the response in Hertz. We divide the slope by the resistance because this most accurately represents the speed of the response for devices with different baseline resistances, as is shown in Figure 3-23. The response for several gas sensor exposures to different concentrations is then used to calculate the sensitivity of the sensor.

$$S(x) = \left.\frac{d\Omega}{dt}\right|_{t>t_R} \Big/ \Omega_0 = A + B \times \ln(x+1) \cong A + B \times x$$

Equation 3-5: The sensitivity of a linearly responding device is defined as the rate of change of the resistance of the sensor divided by the baseline resistance (Ω_0) of the sensor.

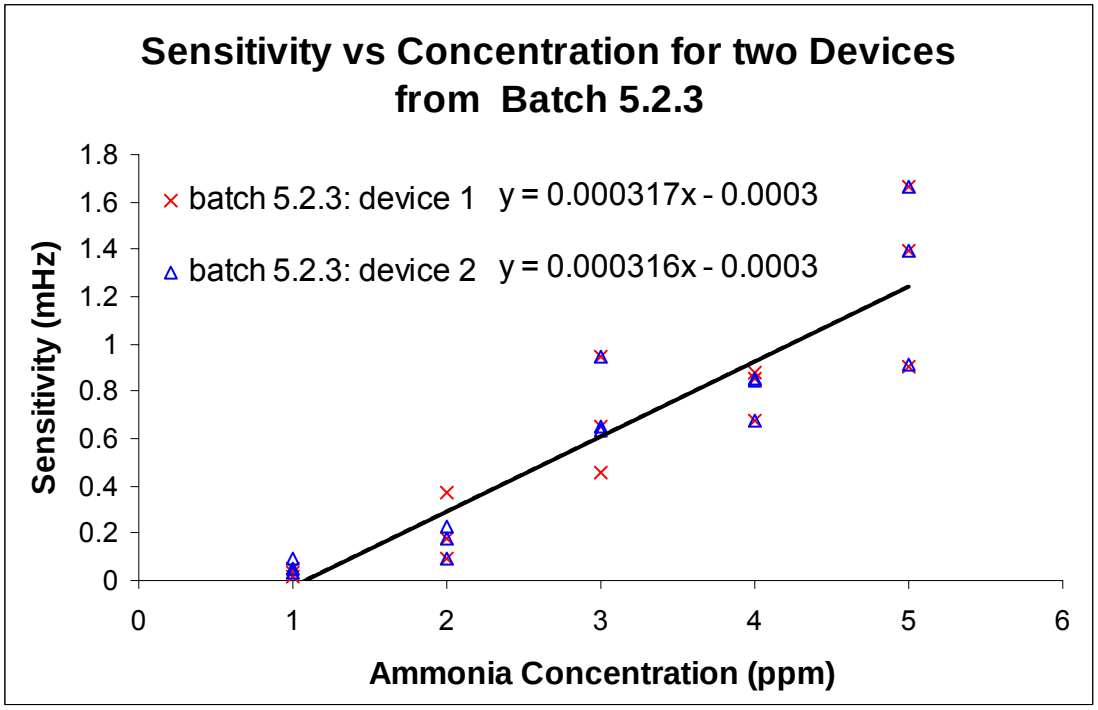

Figure 3-23: The sensitivity of two devices from a wafer batch (5.2.3) is demonstrated to be nearly the same (slope fit). The sensors tested (devices 1 and 2) had 5kΩ and 2kΩ baseline resistances respectively.

We can also calculate the LEL for this sensor using the same information. Using the method described above, we find that the deviation of the data collected for the average value of the slope given by the equation in Figure 3-22 is 0.196 mHz. Putting twice this value into the equation for the slope then provides an LEL (95% confidence of detection) of 785 ppb for this sensor.

Table 3-2: The calculation for the LEL of the gas sensor from the data depicted in Figure 3-22 is shown.

Conc.(ppm)	Response(mHz)	Expected Response (mHz)	Response Difference^2
1	0.525	0.522	0.000
2	1.008	1.125	0.014
3	1.636	1.729	0.009
4	2.242	2.332	0.008
5	3.236	2.935	0.090
1	0.431	0.522	0.008
2	1.262	1.125	0.019
3	2.053	1.729	0.105
4	2.253	2.332	0.006
5	2.641	2.935	0.087

sigma = sqrt (sum of differences / (n-1)) = 0.19604783

LEL = (2*sigma+0.0814)/0.6033 = 0.78484281

Gas Pulsing Method

The gas pulsing method was developed to assess a sensor response when the signal produced by the sensor was obscured by noise. This mode of testing relies on delivering packets of gas to the sensor at a predetermined and fixed frequency. The frequency transform of the response of the sensor, if the device is sensitive, will show a signal peak at the pulsing frequency. This mode of testing will be discussed only briefly in this thesis, as it is thoroughly analyzed in the thesis of Mr. DeBoer[2]. The design-of-experiment analysis provided in Chapter 6 provides some additional analysis that describes the choice of testing parameters for this mode of evaluation.

To minimize human error in the application of the gas pulsing method, related to the switching of the test gas MFC, a device was developed to control the gas pulsing in a periodic manner. This device, shown in Figure 3-24, was constructed from a standard computer power supply and a type UK157 fixed periodic cyclic timer[7]. The twelve volt source of the power supply powered the circuit, while the five volt source of the power supply was modulated via the timer circuit. This five volt supply controlled the on/off state of the MFC. The flow rate of the MFC was controlled through the knob on the front of the MFC, and set prior to each experiment.

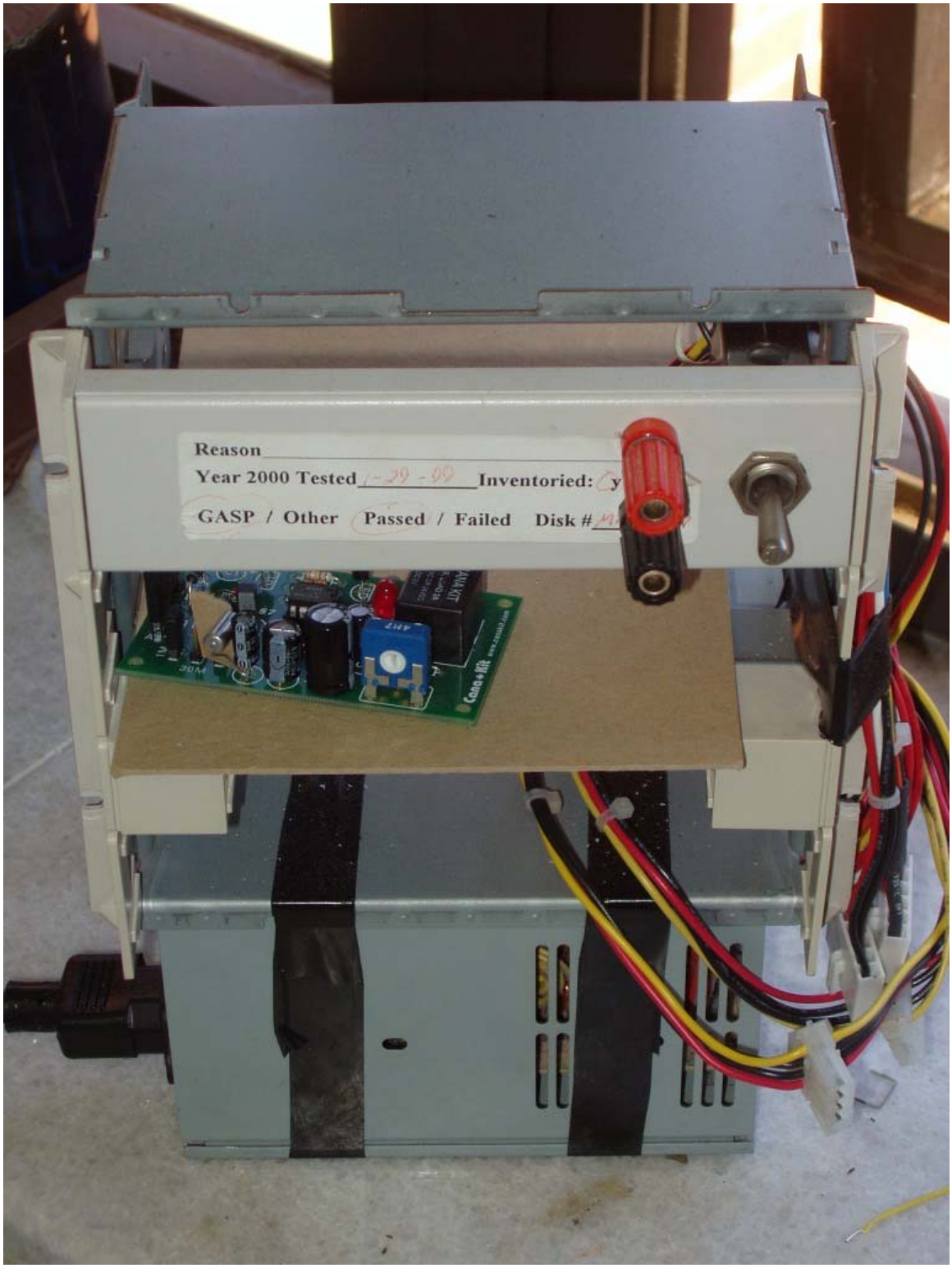

Figure 3-24: The timer circuit and power supply provided an oscillating 0,5V at a period of once per minute and a duty cycle of 50%.

For the gas pulsing method to be successful, a pulsing frequency must be chosen carefully. The pulsing frequency should be picked outside of the range of any known noise sources, while remaining in the range of mechanical/chemical practicality for the device being tested. Of important concern when designing the gas pulsing of the PSGS are the pressure wave fluctuations from the fumehood, the mechanical timing limit of the flow meters, the desire to test sensors as quickly as possible, and any limitations inherent to the sensors themselves. Figure 3-25 illustrates the known noise sources and the manner in which a frequency was chosen. From the figure it is apparent that a frequency corresponding to once per minute (0.0167 Hz) is available. Verification of the FFT of a baseline sensor response validated that this was a good pulsing frequency as there was little signal at 0.0167 Hz.

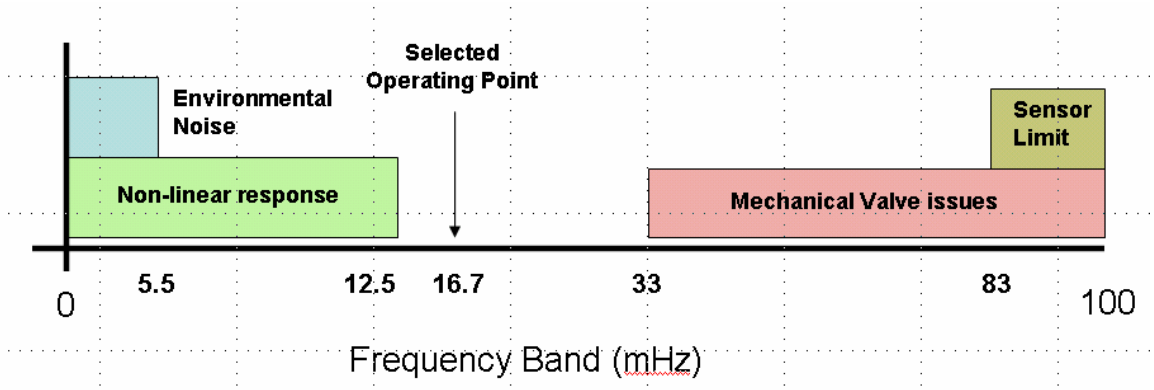

Figure 3-25: The available spectrum for the gas pulsing of the PSGS.

In most experiments, the gas sensors were pulsed once per minute at a duty cycle of 50%, or 30 seconds of test gas entrained in nitrogen and 30 seconds of just nitrogen for each pulse. Typically, the first half of the duty cycle was the "on" portion of the pulse, and the second half was the "off" portion. 30 pulses, taking a total of 30 minutes, were

needed to produce a response profile long enough in time to perform a detailed Fourier analysis of the signal.

As an example of this mode of testing, consider the temperature pulsing example shown in Figure 3-15. The temperature oscillations artificially created in the lab simulate an outside environmental factor which cannot be controlled. The pulsing method provides a means to eliminate this environmental factor without knowing its nature or cause. As long as the pulsing frequency is chosen outside of the frequency of the external noise, the signal due to the gas response can be separated from the temperature fluctuation by the FFT analysis method[2,8]. The results of this analysis as applied to the pulsing example of Figure 3-15 are shown in Figure 3-26. This method also provides for a more accurate response calculated as the average of the responses to each of the pulses of test gas.

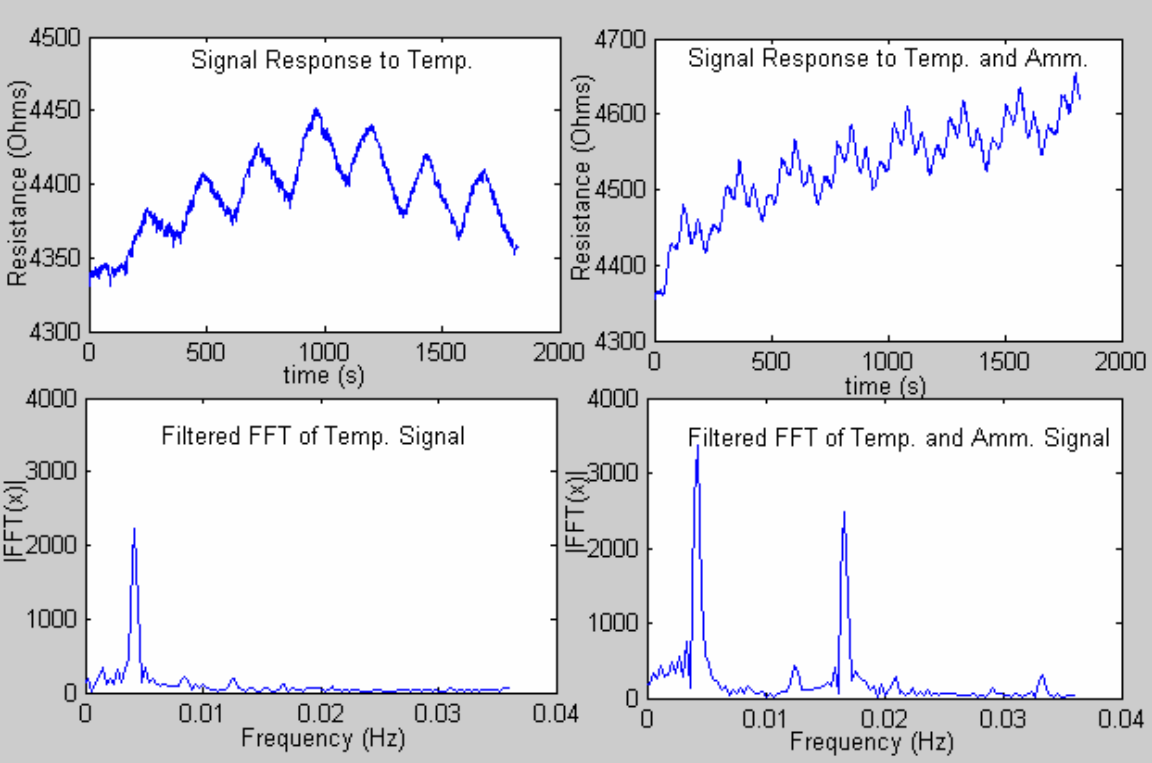

Figure 3-26: The FFT analysis of the gas pulsing experiment performed on a sensor (right) is compared to the signal of a device responding to the same external noise, but no gas pulsing (left).

The raw signal of each sensor is shown (top) as well as the filtered FFT of the sensor (bottom). Separate peaks are generated at the pulsing frequency (0.0167 Hz) and the heating frequency (0.0042 Hz).

Practical advantages of incorporating the gas pulsing method of testing include the addition of a provision for a lower LEL through the signal averaging of multiple pulses. Also, the method allows for the systematic identification and quantification of regular outside noise sources as well as a means to compare responses to noise sources between devices. The drawback to the application of this method corresponds to an increased evaluation time. In a real-world application, this pulsing method could correspond to the pulsing of the gas between the air and some control gas located within the sensor apparatus. The application of the FFT would follow upon the initial detection of a gas provided through the more rapid sensor testing mode described previously. The multifarious benefits of the gas pulsing method are discussed in much greater detail within the discussion of the optimization of the experimental configuration for the gas pulsing method (Chapter 6).

References

[1] Seals, L. T., "The Application of Porous Silicon Surface and Photo- and Electrochemical Properties to Sensor Development", thesis, Georgia Institute of Technology, July 2001.

[2] DeBoer, J. R., "Evaluation Methods for Porous Silicon Gas Sensors", thesis, Georgia Institute of Technology, August 2004.

[3] CMOS Capacitive Chemical Microsystems for Volatile Organic Compounds, A thesis of Andreas Koll, Swiss Federal Institute of Technology Zurich, 1999 DISS ETH No. 13460.

[4] "NI DAQPad-6015", (May 2005) http://sine.ni.com/nips/cds/view/p/lang/en/nid/14040.

[5] Simanek, D. E., "Error Analysis (Non-Calculus)", (June 2005) http://www.lhup.edu/~dsimanek/errors.htm.

[6] Hines, A. L., Maddox, R. N., "Mass Transfer", Prentice-Hall, Inc. 1985.

[7] Electronic Kits, UK157 - Fixed Period Cyclic Timer (Assembled) (June 2003) http://www.canakit.com/Contents/Items/UK157.asp.

[8] J. DeBoer, S. Lewis, P. J. Hesketh, J. L. Gole, "Method for signal extraction from chemical sensor response," Invention disclosure Georgia Institute of Technology, February, 2004.

CHAPTER 4

SELECTIVITY

The selectivity of a gas sensor system determines its ability to discern the concentration of an individual gas present within a gas mixture. Selectivity can be provided with the inclusion of filters, pre-concentrators, chemical coatings, or other means that distinguish between different gas species. These different methods increase the response to one gas present in the mixture relative to another. This relative change in the response can then be analyzed to determine the original concentration of gases to which the sensor system was exposed.

In the case of filters and pre-concentrators, a sensor's response is modified through the collection of select species present within the mixture. Both the modified and unmodified samples are then sent to the sensor (not necessarily simultaneously) and the signal from each is measured. Knowing the properties of the filter [pre-concentrator], for example, the fraction of each species adsorbed, one can compare the two responses of the sensor and thereby calculate the composition of the gas mixture. In practice, the fraction of species adsorbed will never be 0% or 100%. Some amount of each species in the mixture will be affected by the filtering process. This process utilizes a wide array of materials which usually exhibit catalytic properties and have a high surface area[1,2]. Examples of both a filter and a pre-concentrator are given in Figure 4-1.

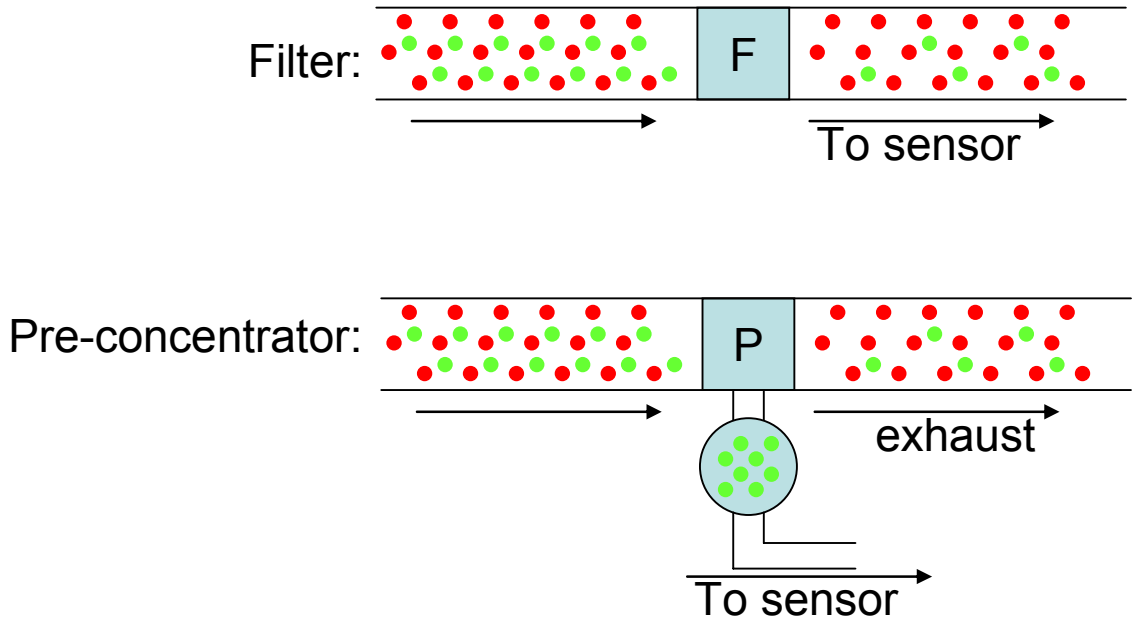

Figure 4-1: Examples of a filter 'F' and a pre-concentrator 'P' are given. The filter extracts a known fraction of the green analyte from the green and red analyte mixture. The pre-concentrator extracts the green analyte and holds it until enough is gathered to be delivered to the sensor for a response to occur.

In an example of how a filter provides the ability to discern the component gases in a mixture, consider a simple two-gas case. In this example, the sensor being used produces a pre-determined signal of 2mV per each ppm of ammonia and a signal of 5 mV per ppm of oxygen. The sensor also has a discretionary filtering mechanism that can reduce the oxygen in the stream of test gases by 50%. This filter modifies the gas sample before it reaches the gas sensor when turned on and has no effect when off. The signal is then measured from the device both with and without the filtering mechanism activated. The data from this test and resulting concentrations are shown in Table 4-1.

Table 4-1: Example of how a filter can provide selectivity.

Response with Filter on:	26 mV
Response with Filter off:	46 mV
Calculated Conc. Of O_2	8 ppm
Calculated Conc. Of NH_3	3 ppm

Since the known signal for oxygen is 5mV per ppm, the signal reduction by 20 mV upon the activation of the filter indicates that 4 ppm of oxygen was removed by the filter. Thus, 8 ppm of oxygen was in the original sample of gas. Knowing the concentration of oxygen to be 8 ppm, the concentration of ammonia is calculated to be 3 ppm.

Chemical Selectivity of the Porous Silicon Gas Sensor

Selectivity is introduced to the porous silicon gas sensor with metal and metal oxide coatings in a patented method developed specifically for this application. In general, chemical coatings can provide selectivity by changing the relative response of a sensor to gases present within a mixture through the chemical properties of the coating. For example, a coating of palladium is predicted to catalyze the reaction governing the adsorption of hydrogen[3]. A series of coatings then allows the operation of gas sensors in an arrayed format, with a multitude of differently coated sensors responding in a correlated manner in order to distinguish the component gases in a mixture. Selectivity provided by chemical coatings can also be combined with filters and pre-concentrators to enhance the selectivity provided by each individual method.

Several attempts were made to provide selectivity to the PSGS prior to the creation of coatings from electroless sources. These unsuccessful attempts included the metallization of the surface of the porous silicon sensor from the evaporation of solutions containing dissolved metallic salts and the electroplating of metal coatings[4]. Both of

these methods caused irreversible damage to the devices being coated. The evaporation of metal-salt solutions, tin (II) chloride in particular, produced a visible salt residue on the surface of the sensor. This method also increased the resistance of the device by several orders of magnitude and rendered the devices non-responsive to concentrations as high as 10 ppm of ammonia. The electroplating of gold from a gold-cyanide bath produced similar results and was also abandoned due to the damage it caused to the gas sensors.

From these initial tests, it was determined that the primary concern when considering deposition of coatings to the PSGS is the fragility of the sensitive layer. Future efforts focused on metal deposition solutions which would be much less physically and chemically harmful to the sensors' porous silicon surface.

Preparation for Electroless Metallization of Gas Sensors

The next attempts to provide selectivity to the gas sensors were based upon a successful electroless metallization to reduce the contact resistance to the porous silicon surface[5]. Electroless metallization solutions deposit metal on a surface through a spontaneous chemical process[4]. This differs from the prior coating techniques which used a deposition current in the case of electrochemical deposition and evaporative heating in the case of the deposition from ionic solutions.

Electroless depositions differ from electroplating in that they require no power to drive the reaction[4]. The energy needed to form a metal coating on the surface is present within the electroless solution in the form of an "electron donor" species. This species is chemically stable, except in the presence of a prepared surface which catalyzes the deposition reaction. At surface sites, an electron from the donor species is transferred to the metal ion (positively charged) species, causing it to become a neutral metal atom. As

this reaction is only possible at catalytic reaction sites (where electroless deposition is designed to occur), the metal atom created has sufficient proximity to the surface to be bound to it[4].

It was theorized that this process could be utilized to coat sensors with a thin layer of metal to act as a catalyst. Catalyst is defined here as a material enhancing one or more chemical reactions, providing new routes for interaction, or amplifying existing chemical reactions. The "catalyst" layer would then, depending on the metal used, serve to promote the adsorption of some gases relative to others. Because the electroless deposition method operates as an undriven, spontaneous reaction, it deposits metal coatings at a much slower rate than does the electroplating or evaporation of metal. While an electroless process that deposits metal can be made to proceed at a faster rate with an increase in temperature or with an electroplating current, these methods were not used to form coatings on the PSGS as the first goal of this experiment was to preserve the integrity of the gas sensor in a potential plating reaction.

The deposition of metal from electroless metallization sources can be enhanced by the presence of actively photoluminescing sites on the porous silicon surface[5,6]. Prior to being coated, the sensors are typically immersed in a 1:5 solution of 44% hydrochloric acid in methanol. This solution visibly enhances the photoluminescence from the PS region. This HCl treatment also provides the sensor with an enhanced sensitivity to the gases it can already detect. Figure 4-2 depicts this increase in sensitivity for a device that was tested with pulses of 10 ppm ammonia. The increase in the signal amplitude of the device is apparent.

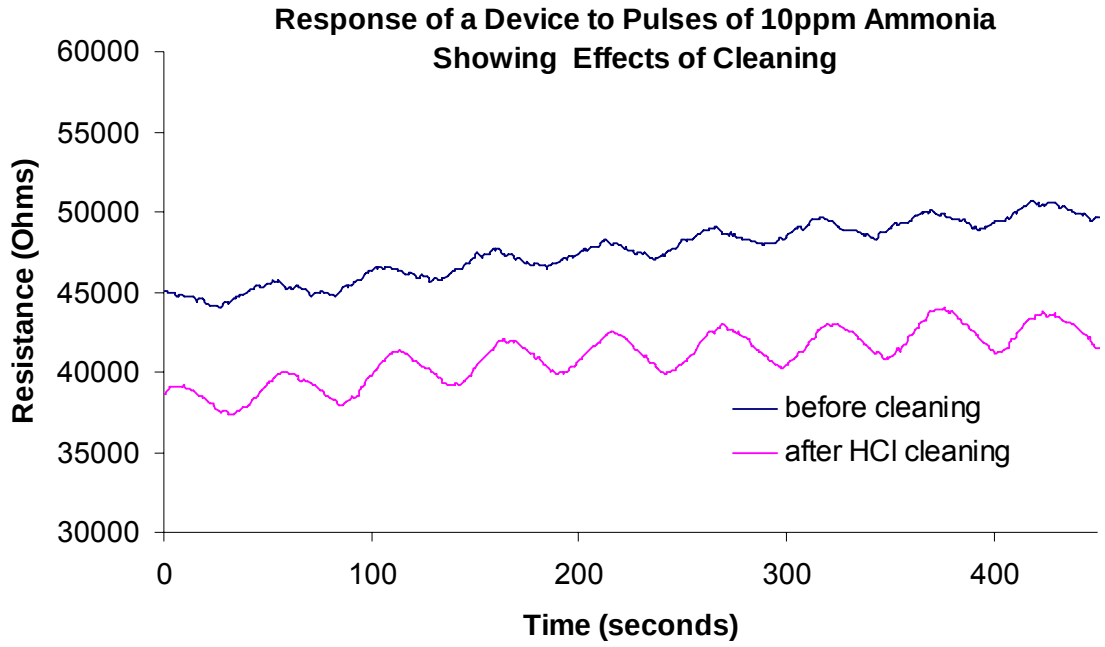

Figure 4-2: Response of a porous silicon gas sensor before and after a 4-hour cleaning in an HCl/methanol solution.

Electroless Gold Selective Coating Process

In an effort to enhance the sensitivity and selectivity of the sensor surface without damaging the sensitive nature of the sensor, a short exposure electroless metallization procedure was developed and tested. A short immersion process was first tested to determine if 1) the process would damage the sensor, and 2) if the electroless process had any effects on sensitivity. The short exposure is designed to deposit a minimal amount of metal on the sensor surface, theoretically at the most chemically active sites within the pores of the porous silicon where the sensing process is believed to occur. Two different electroless metallization solutions were tested in this manner.

The first metallization of a sensor was conducted with a commercially available (Transene) electroless gold metallization solution[4]. This experiment was preceded by a 4-hour treatment of a functioning gas sensor with the HCl/methanol solution and a

subsequent rinse in methanol for 30 seconds. The sensor was then allowed to dry overnight. The sensor was immersed in the electroless gold solution for 30 seconds, then immediately rinsed by brief (3 to 5 second) immersion in de-ionized (DI) water followed by a 30 second rinse in methanol. Following this procedure, the sensor was again allowed to dry.

The baseline impedance of the gold-coated sensor was found to decrease slightly which is likely from the deposition of additional gold conduction paths throughout the nanoporous regions of the sensor. This device produced a noticeably improved sensitivity to NH_3. This increased ability to detect ammonia was expected as it is known that a gold-silicon interface provides a means for detecting ammonia[7]. The detection mechanism associated with this form of device is generally associated with a modification of a Schottky barrier height by the adsorption of ammonia at the interface. In addition to the improved detection of ammonia, the gold coated sensor also showed a noticeable enhancement in the ability of the PSGS to detect SO_2, and a decrease in the ability of the PSGS to detect NO_x. Data from LEL tests of a sensor both before and after an electroless gold coating are shown in Figure 4-3. The sensitivity increase for ammonia appeared to be notably greater than that for SO_2.

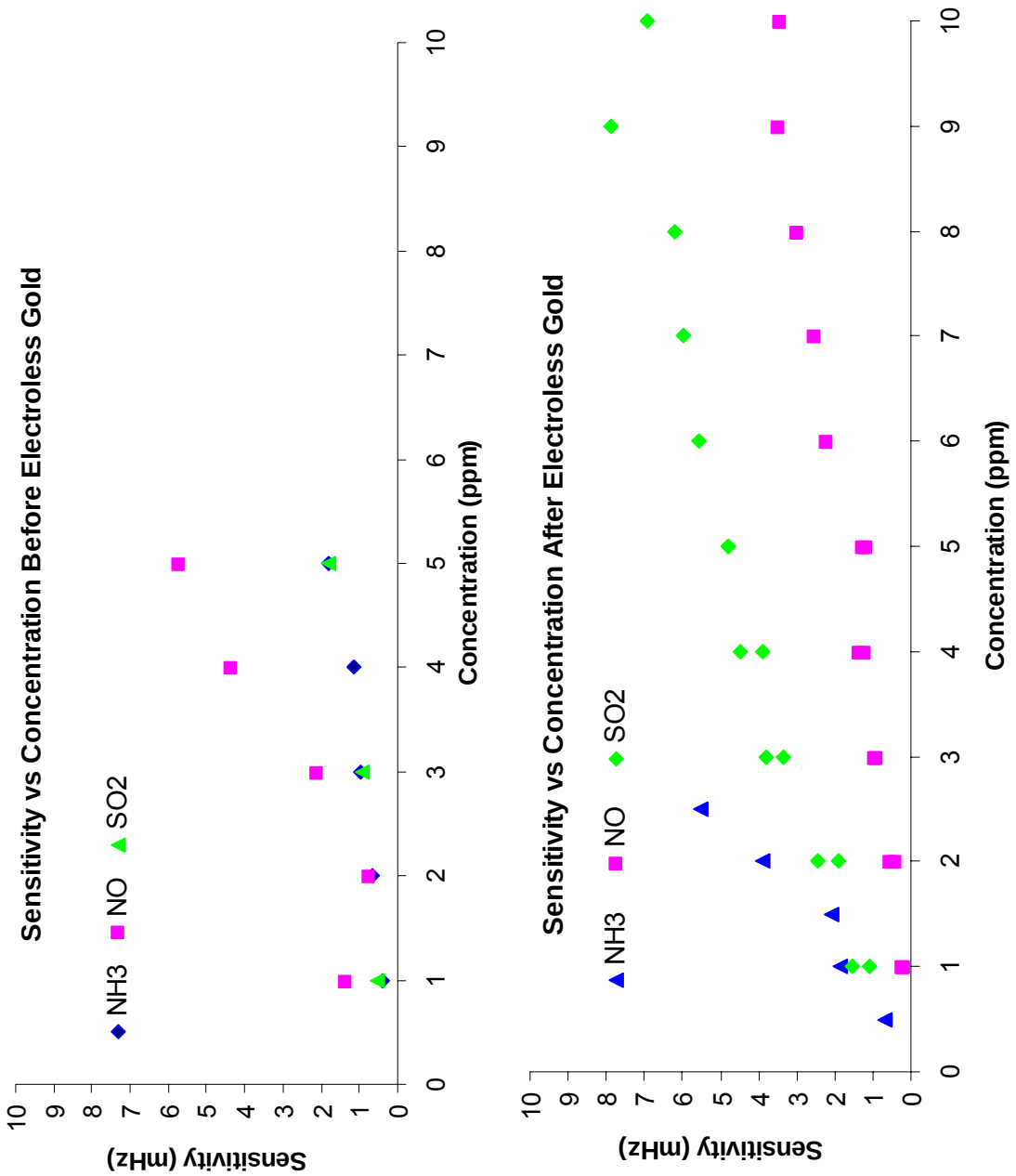

Figure 4-3: LEL tests for a sensor both before and after a coating of electroless gold was applied. Concentrations vary from 1 to 10 ppm of NH_3, NO_x, and SO_2.

After verifying the repeatability of this electroless gold coating technique, we attempted to determine the amount of gold deposited onto the sensor. One of the successfully coated devices was diced into several pieces, and then was interrogated with the energy dispersive spectrometer (EDS) capable SEM in order to analyze the elemental composition of the surface of the porous structure[8]. No gold atoms or clusters were observed from these SEM images or from the EDS analysis of the surface. These results indicate that a nanoscopic quantity of gold is being deposited onto the porous silicon surface. The conclusion that an extremely small amount of gold is being deposited is supported by the relatively small change in baseline resistance of the device. The gold coating in this case appears to be serving as only a catalyst for the gas-sensing reactions as is indicated in Figure 4-3.

Electroless Tin Selective Coating Process

An electroless solution was also used to deposit a tin coating. Tin was chosen as the second metal for electroless deposition due to an interest in detecting carbon monoxide to which uncoated and gold coated PS sensors are insensitive and the knowledge that the deposited tin would quickly be oxidized to tin oxide. Tin oxide gas sensors are a very common form of CO detector, though they normally operate at 300-500ºC[9]. These high temperature gas sensors operate through the modification of the resistance within the bulk of the tin oxide[10,11].

The electroless tin solution was made from solutions of 62.57 g/L (0.33M) $SnCl_2$, 97.05 g/L (0.33M) Sodium Citrate, and 77 g/L (3.85M) NaOH. In order to prepare this solution, 6.257g of $SnCl_2$ and 7.7g of NaOH were each dissolved separate containers of

100mL DI and heated to 70°C. These two solutions were combined with magnetic stirring as 9.705g of sodium citrate was slowly added to the solution which was maintained at 70°C. In order to prevent the electroless tin solution from collapsing (precipitating out of solution) we found it necessary to use an NaOH concentration half of that suggested in the literature[12].

The process which deposits tin onto the porous silicon surface occurs in a similar fashion to the electroless gold deposition process. An HCl-treated PSGS was immersed in the electroless tin solution for 20 seconds. After a brief rinse in water and a 30 second immersion in methanol, the sensor was allowed to dry. During this electroless metallization process and subsequent drying, the tin underwent an oxidation process to form tin oxide (see following). The PSGS was tested at concentrations of various gases both before and after receiving a tin coating. The results of several tests on this sensor are depicted in Figure 4-4.

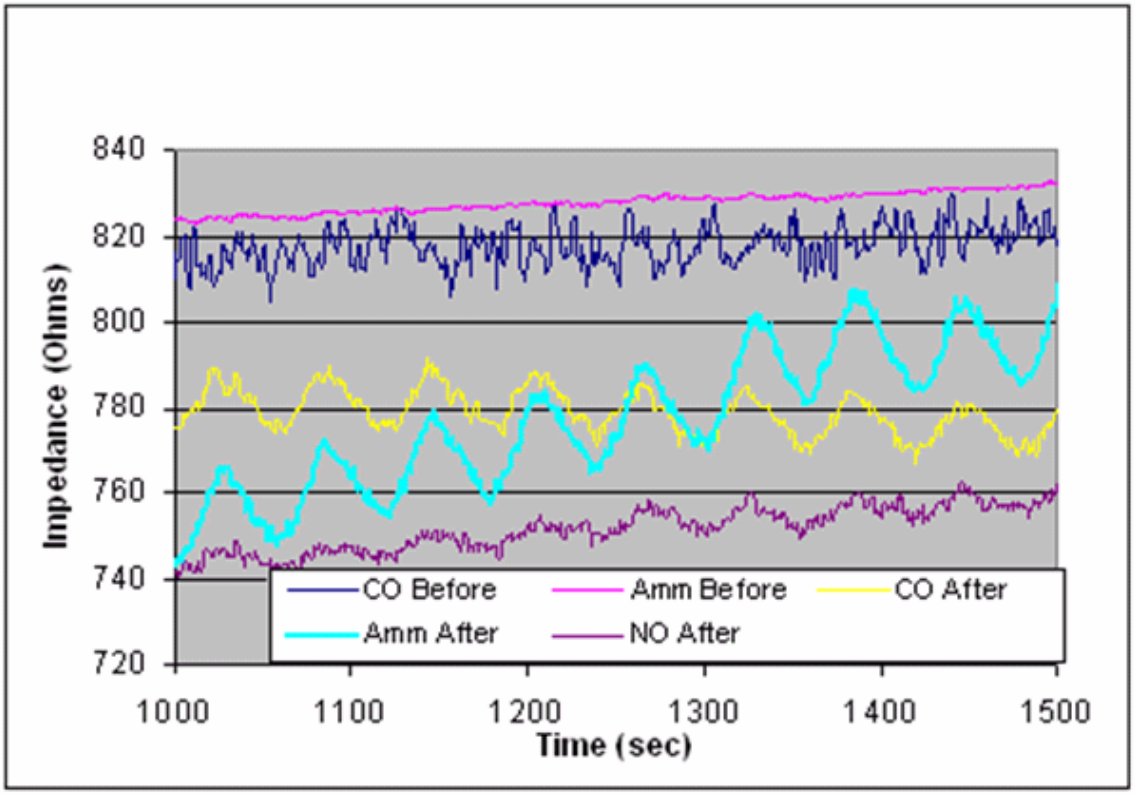

Figure 4-4: Response plots for an electroless tin coated device both before and after coating. The device was tested using the gas pulsing technique with the concentration of each gas being varied between 0 and 10 ppm for a period of one minute.

Several unique properties can be associated with the tin coated gas sensor which are not characteristic of the gold coated device. First, the tin coated PSGS has a considerable sensitivity to CO, which was nonexistent before treatment. The new sensitivity of the sensor to 10 ppm CO (which has since been lowered to < 5 ppm) strongly suggests that the tin has been oxidized to form tin oxide. This is because tin oxide is one of the few materials capable of sensing CO and the only one of these materials possibly present on the sensor. The results outlined here mark the first demonstration of a room temperature tin-oxide based CO sensor. Other PS gas sensors have demonstrated sensitivity to ppm levels of NH_3 and NO_x, but no sensitivity up to 0.5% (5000 ppm) of CO[13].

After this test was repeated, the tin oxide coated gas sensor was also evaluated using an EDS capable SEM. The imaging of the sensor also indicated no tin or tin oxide presence on the porous silicon pore walls. Again, the electroless coating method seems to deposit a nanoscopic [and purely catalytic] layer on the surface within the nanopore-coated porous silicon micropores.

Generalization of the Selective Coating Process

Through the two initial coating experiments which we have described, we have established a general approach for providing selectivity to the porous silicon gas sensors in an arrayed format. Presently, three differently coated gas sensors (gold, tin, and uncoated) are available, however the wide range of electroless solutions for the chemical deposition of metals allows a broad range of coatings to be applied to the PSGS. Each of these coatings is capable of providing an additional degree of selectivity for the gas sensor. This format enables the arrayed gas sensor to attain an increased functionality, to determine the concentrations present in a gas mixture, for each additional coated sensor inserted into the array.

Research into creating additional selective coatings was begun with the investigation of electroless platinum[4]. A platinum coated sensor would likely demonstrate a significant sensitivity to CO, which would provide a second means to detect this gas. We attempted to create a platinum-based electroless solution for coating in the same fashion as the gold and tin coatings, with the recipe for the electroless platinum solution taken from the same reference[4]. However, during the coating process the gas sensor was damaged through a dramatic and irreversible increase in sensor noise. Subsequent coating attempts yielded similar results. Presently, several additional

coatings, including nickel, palladium, silver, copper, carbon black, and visible light adsorbing nanoparticle titanium oxy-nitrides are under investigation[14]. These additional selective coatings, when used on individual sensors in an arrayed format, will provide for more robust gas sensor arrays able to distinguish between multiple constituent gases. A more complete list of potential metal and metal oxide coatings and the gases which they are able to detect is provided in Appendix A.

Analysis of Selectivity

The development of selective metal and metal oxide coatings has provided several insights into the behavior of the porous silicon gas sensor. Among these, we include potential response mechanisms as well as the sensor response to additional gases. Also, with the data collected from selectively coated devices, we can demonstrate a limited ability to predict the sensitivity of untested devices.

Prediction of Sensor Response

The accurate prediction of device performance as a function of the fabrication parameters allows the creation of sensor arrays with predetermined sensitivities. The parameters that are most important to the fabrication process are the etch current, the etch time, the sensor HCl cleaning/preparation treatment, and the selective coating being applied.

Similar porous silicon gas sensor responses have been correlated between similarly fabricated devices. Figure 4-5 shows the responses of two devices which were fabricated simultaneously in wafer batch 5.2.3. The sensors were tested with the "Lower Exposure Limit Method" as described in Chapter 3. These devices were adjacent to each

other on the etched wafer and demonstrated similar sensitivities of about 0.3 mHz/ppm of ammonia. The ability to create sensors with comparable sensitivities across a wafer is significant because it enables the accurate calibration of untested sensors. In this manner, a wafer containing several hundred sensors and having only a few sensors tested to concentrations of gas, could allow the use of the remaining sensors with knowledge of the sensitivities of all of the sensors produced in the process. The advantage of such a mass calibration of the sensors in this fashion can lead to a dramatic reduction in the production cost of the PSGS.

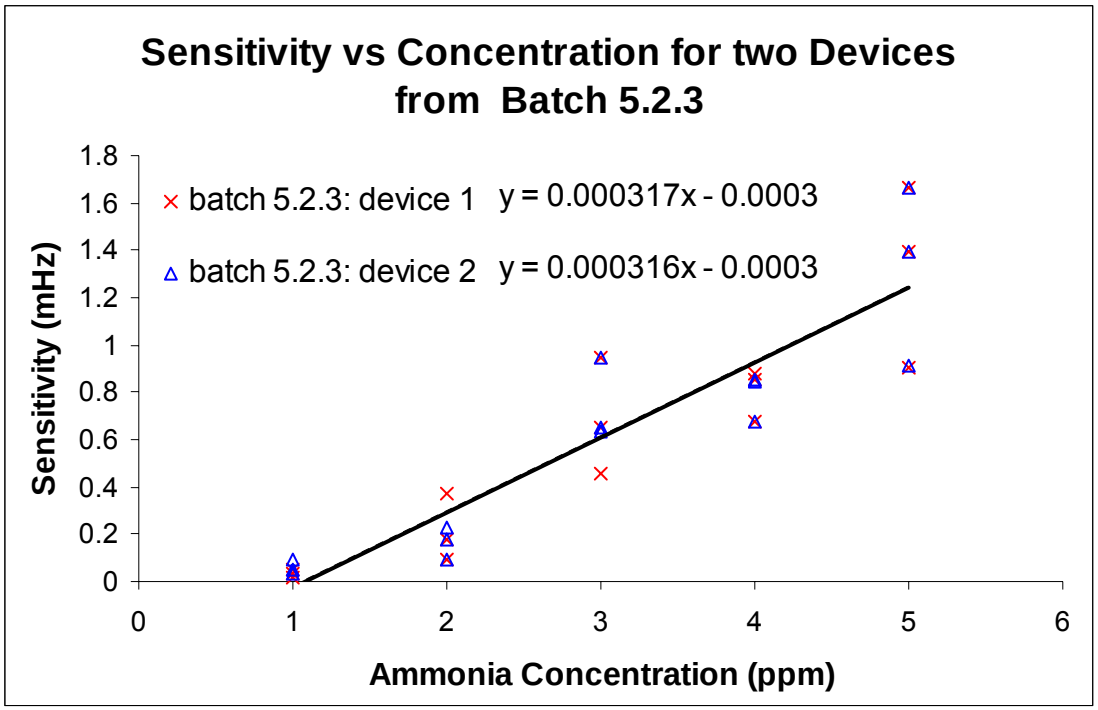

Figure 4-5: The sensitivity of two devices from a wafer batch (5.2.3) is demonstrated to be nearly the same (slope fit). The sensors tested (devices 1 and 2) had 5kΩ and 2kΩ baseline resistances respectively.

In addition to the correlation drawn between devices within a single batch, there also appears to be an ability to control the sensitivity of devices between different batches. The devices shown above in Figure 4-5 were taken from wafer batch 5.2.3, which was fabricated with an etch current of 3.3 mA for a duration of 5 minutes. These

devices demonstrated a sensitivity to ammonia of about 0.3 mHz/ppm in repeated experiments. An earlier batch of sensors, batch 5.2.2, was etched at 3.3 mA, but for 10 minutes. This increased etch duration corresponds to double the porous silicon pore depth within the sensitive PS interface. For a working device taken from wafer batch 5.2.2, the sensitivity to ammonia was about 0.6 mHz/ppm. Data from this sensor, shown in Figure 4-6, in concert with Figure 4-5, presents a possible linear relationship between the sensitivity of a device and the etch time of the porous silicon etch step in the fabrication process.

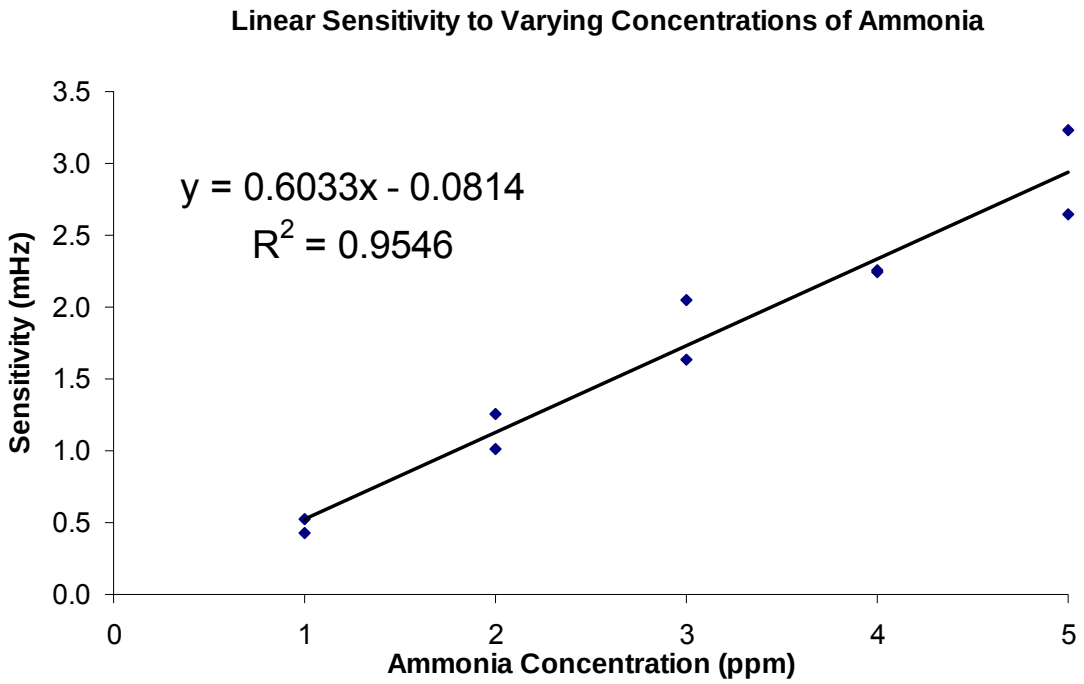

Figure 4-6: This data taken from a device in batch 5.2.2 (which had twice the etch time of batch 5.2.3) displayed a sensitivity to NH_3 approximately twice that of the devices shown in Figure 4-5.

In addition to being able to control the basic sensitivity of the PSGS, it has also been shown that the selective coating techniques for the gas sensor are reproducible. Both the electroless tin and gold coating methods have been applied to functional gas sensors with the attainment of reproducible results. In general, proportional changes in

signal due to each of the coatings can be expected to follow the data shown in Figure 4-7. This data demonstrates the average amplitude of the responses of each sensor when tested using the "Gas Pulsing Method" as described in Chapter 3. Each sensor's response was averaged over a large number of pulses of gas to 20 ppm of each gas.

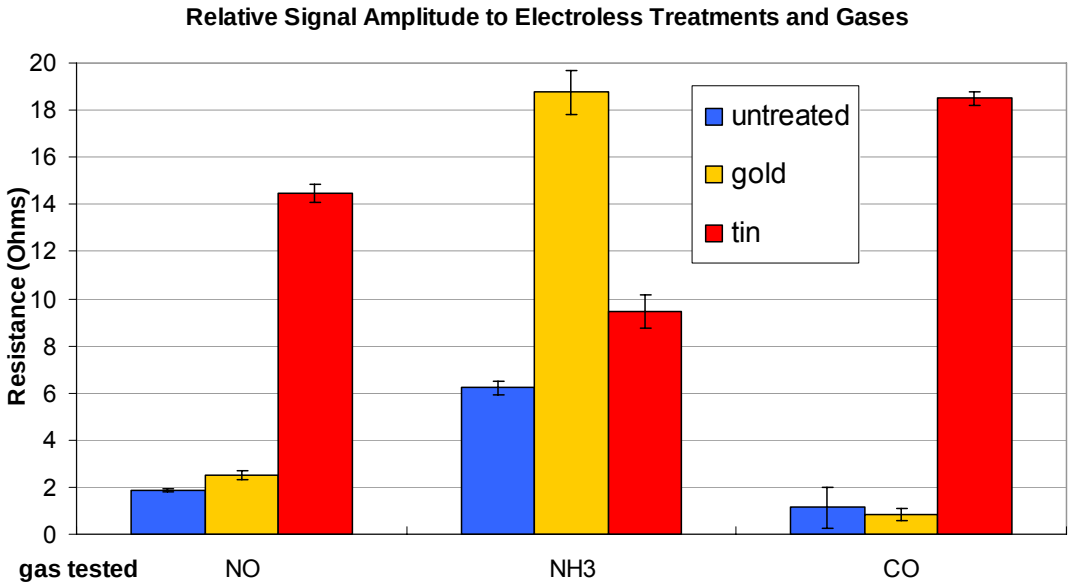

Figure 4-7: Comparison of the gas response of gas sensors that are untreated, treated with electroless gold, or treated with electroless tin. The sensors were tested with 30 repeat pulses of 20ppm NO_x, NH_3, or CO. Their average impedance change is given.

Selectively Coated Sensor Arrays

The process to create distinct and variably responding individual sensors has been addressed above. From the combination of these sensors, we wish to produce an array of sensors that can analyze the component gases within a mixture. The arrays which have been created will be discussed in detail in Chapter 7. However, the design criteria for creating arrays composed of selectively coated sensors will now be discussed.

An array of gas sensors is needed to detect individual gases in a mixture because each gas sensor responds to the combination of all gases present in the mixture. The selective coatings provide a means to identify the individual constituent gases. This is

facilitated by the necessary linear independence of the sensitivities of each gas sensor in the array. To this end, for each possible gas present in a mixture, a gas sensor with a *linearly independent response* is needed. An example of an arrayed gas sensing system will be discussed in detail to demonstrate how such a system would be created.

In this example, we consider the simplest arrayed gas sensor possible. This array would consist of an array of two gas sensors, each operating simultaneously on the same sample of test gas. The gas adsorbed by each sensor is assumed to be sufficiently small so as to not affect the overall concentration of the gases present within the gas stream. This assumption is valid for the present test configuration because the volume of gas flowing over the sensors is much larger than the amount of gas being absorbed by the sensors themselves. Therefore, each sensor does not change the concentration of gas being delivered to the entire array.

To construct this first arrayed gas sensor, we will use the data collected from a characterized porous silicon gas sensor. The sensitivities of this sensor to various gases are given in Table 4-2. In this table, the sensor's response to four gases is listed both when the sensor was uncoated, and after it was coated in gold. The arrayed sensor could not be fabricated from sensor 5.2.3-5, as the uncoated device no longer exists. However, as the end goal would be to fabricate a multitude of arrayed devices from sensors fabricated in the same way as sensor 5.2.3-5, the information presented here suffices to demonstrate how such a device would be created. The formation of similar sensitivities between similarly fabricated devices, as is demonstrated in Figure 4-5, is critical to this goal because without the ability to produce similarly responding devices, the cost of calibrating each sensor in each arrayed device would be a significant limitation.

Table 4-2: The sensitivities measured from device 5.2.3-5 for representing the basis for building a two-sensor array.

Sensitivity of Device 5.2.3-5 (mHz/ppm)

	NH_3	NO_x	CO	SO_2
No Coating	0.332	1.23	~0	0.322
Gold Coating	2.35	0.389	~0	0.684

Fundamental to this construction of an arrayed sensor is the additive property of the gas sensor's response. This property, shown in Equation 4-1, represents how a gas sensor would respond in a mixture of gases, and is based upon the observed ammonia response of a gas sensor in the presence of a strong NO_x background[15].

$$R^1 = S_1^1 \cdot x_1 + S_2^1 \cdot x_2 + \ldots$$

Equation 4-1: Evidence suggests that the response of a gas sensor to a mixture of gases is equal to the sum of its responses to each individual gas present in the mixture. 'S' represents the sensitivity or "response per concentration" of a sensor to a concentration 'x'.

With two sensors, the array being created can only distinguish between the presence of two constituent gases. This can be seen in Equation 4-2, which represents the response of the sensors in the array as the matrix product of the sensitivities and the concentrations of the gases. The matrix of sensitivities corresponds to Table 4-2. In this example, three of the four gas responses to each sensor are linearly independent, with CO being undetectable. Any variation in the CO concentration therefore will not affect the response of the sensors. The three remaining gases, NH_3, NO_x, and SO_2, are linearly independent between the two sensors because the ratio of each gas's response are not equal.

$$\begin{bmatrix} R^1 \\ R^2 \end{bmatrix} = \begin{bmatrix} S_1^1 & S_2^1 & S_3^1 & S_4^1 \\ S_1^2 & S_2^2 & S_3^2 & S_4^2 \end{bmatrix} \times \begin{bmatrix} x_1 \\ x_2 \\ x_3 \\ x_4 \end{bmatrix}$$

Equation 4-2: The response of each device 'R' is equal to the sum of its responses to each constituent gas, which is the sensitivity to that gas times the concentration.

Because there are two sensors in this device, if all three of the remaining gases were varying, the device would be unable to distinguish any of the concentrations of the component gases. However, if one of the three gases was constant during a test, then the device could determine the concentration of each of the other two gases.

Suppose, for example, that the environment being tested was known to have no SO_2 present. The environment does however have possible NO_x, NH_3, and CO levels. The concentrations of the component gases would be calculated as shown in Equation 4-3. Since none of the sensors are responsive to CO however, the level of CO would not be known.

$$\begin{bmatrix} x_{NH_3} \\ x_{NO_x} \end{bmatrix} = \begin{bmatrix} 0.332 & 1.23 \\ 2.35 & 0.389 \end{bmatrix}^{-1} \times \begin{bmatrix} R_{NC} \\ R_{Au} \end{bmatrix}$$
$$x_{CO} = ???$$

Equation 4-3: From the calibration data presented in Table 4-2 and Equation 4-2, we can arrive at expressions for the concentrations of NH_3, NO_x, and CO in a test given that no SO_2 is present in the system.

To detect and determine the CO level, a third sensor would be needed in the gas sensor array. The electroless tin coated gas sensor could fill this role, since this sensor is sensitive to CO, NH_3, and NO_x. Suppose that this tin coated sensor had responses to ammonia, NO_x, and CO of 0.4, 5.2, and 4.7 mHz/ppm. The tin coated sensor could then

be inserted into the array and the concentrations of gases would be as calculated by Equation 4-4.

$$\begin{bmatrix} x_{NH_3} \\ x_{NO_x} \\ x_{CO} \end{bmatrix} = \begin{bmatrix} 0.332 & 1.23 & 0.00 \\ 2.35 & 0.389 & 0.00 \\ 0.4 & 5.2 & 4.7 \end{bmatrix}^{-1} \times \begin{bmatrix} R_{NC} \\ R_{Au} \\ R_{Sn} \end{bmatrix}$$

Equation 4-4: Adding a tin oxide coated gas sensor to the array expressed in Equation 4-3 allows the calculation of all three component gases in the system.

Supposing that the tin coated sensor did not exist, this arrayed configuration for determining gases in a mixed format could still be configured to detect CO. The third sensor in the array could simply be selected from the range of commercially available CO detectors. The purchased sensor would still need to be calibrated to the same range of gases that could be exposed to the system. In its final form, the arrayed gas sensing system which we have developed (see Chapter 7) is composed primarily of selectively coated porous silicon gas sensors. However, the potential for the addition of a wide range of alternative gas sensors is necessary to ensure that the device could be configured for the broadest range of applications possible.

References

1 Siemens R&I/Gas Sensors for Pollution Control, Safety and Health, (January 2006) http://w4.siemens.de/FuI/en/archiv/zeitschrift/heft1_97/artikel05.

2 PNNL S&E - High-Performance Preconcentrator Materials (277), (January 2006) http://www.technet.pnl.gov/sensors/chemical/projects/ES4ECPreConMtls.stm.

3 F. Favier, E.C. Walter, M.P. Zach, T. Benter, R.M. Penner, "Hydrogen Sensors and Switches from Electrodeposited Palladium Mesowire Arrays," Phys. Rev. B, 1994.

4 Modern Electroplating (4th edition), M. Schlesinger and M. Paunovic (editors), Wiley, New York, 2000.

[5] J. L. Gole, L.T. Seals, and Peter T. Lillehei, "Patterned Metallization of Porous Silicon from Electroless Solution for Direct Electrical Contact," Journal of the Electro Chemical Society, 147, 3785-3789 (2000).

[6] J.L. Gole, J.A. Devincentis, L. Seals, "Chloride Sale Enhancement and Stabilization of the Photoluminescence from a Porous Silicon Surface," Physical Review B, 61, 5165-5631 (2000).

[7] DeBoer, J. R., "Evaluation Methods for Porous Silicon Gas Sensors", thesis, Georgia Institute of Technology, August 2004.

[8] Center for Nanostructure Characterization, (November 2005) http://www.mse.gatech.edu/Research/Equipment_Facilities/CNC/cnc.html.

[9] P.T. Moseley, "Solid State Gas Sensors," Review Article, Meas. Sci. Technol. 8, 223-237 (1997).

[10] Chemical Species Gas Sensors, (June 2005) http://www.grc.nasa.gov/WWW/chemsensors/.

[11] Tin Oxide Sensor Design, (June 2005) http://www.grc.nasa.gov/WWW/chemsensors/tin-oxide.htm.

[12] H. M. Van Noort, B. C. M. Meenderink, and A. J. Molanaar, "In situ Sn conversion electron Mossbauer study of the surface of tin layers as deposited by an electroless process", Electrochemical Society, 133, 263 (1986).

[13] L. Boarino, C. Baratto, F. Geobaldo, G. Amato, E. Comini, A. M. Rossi, F. Faglia, G. Lerondel, and G. Sbervoglieri, Mater. Sci. Eng., B 69–70, 210 (2000).

[14] J. L. Gole and S. Lee private communication.

[15] Lewis, S. E., DeBoer, J. R., Gole, J. L., Hesketh, P. J., "Sensitive, selective, and analytical improvements to a porous silicon gas sensor", Sensors and Actuators B, 110, 54-65 (2005).

CHAPTER 5

SENSOR TRANSDUCTION MECHANISMS

The porous silicon gas sensor (PSGS) detects the concentration of a gas through the changing of the sensor's resistance. This change in resistance occurs only after the analyte gas has diffused through the porous network to the gas-sensitive region of the sensor. A complete understanding of the details of this transduction process has not yet been established, and, as such, this chapter's intent is to provide a first approximation to the physical and chemical principles that govern the operation of the PSGS. An accurate model will allow both a greater understanding of this and other porous silicon devices as well as provide for the improvement of the operational capacity of the gas sensor that is being developed.

Figure 5-1 provides an effective schematic representation of the PSGS for the purpose of discussions in this chapter. In this figure, the porous network is represented by an array of cylindrical pores which have been etched into the surface of a silicon wafer. Two electrical contacts to the porous silicon region are made through gold pads on either end of this region. These gold pads are then connected to a power supply and voltage meter to measure the resistance of the sensor as is discussed in detail in Chapter 3. The resistance of the sensor is modulated through the adsorption and desorption of analyte gases onto the sensor. This chapter is devoted to obtaining an accurate first-order model of the precise interaction between analyte gases and the PSGS such that a response occurs and is transduced.

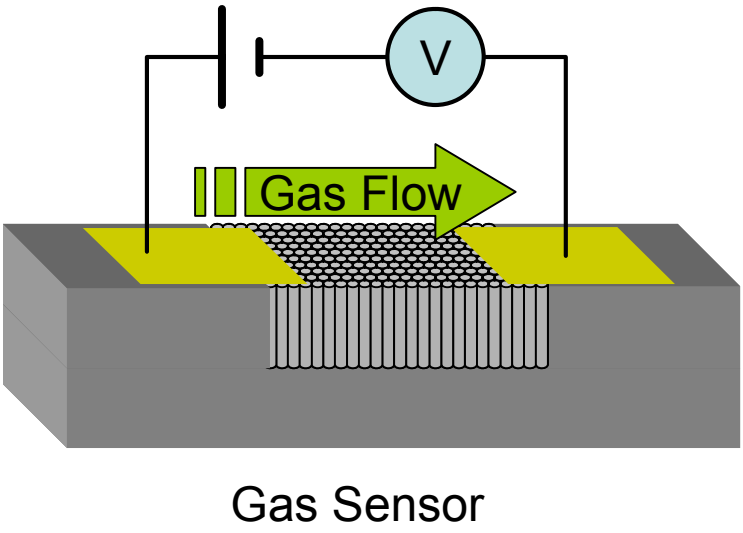

Figure 5-1: Schematic generalization of the operation of a single porous silicon gas sensor.

The sensor is functionally separated into two components for the purpose of modeling. This separation is depicted in Figure 5-2. The first of these two components corresponds to the diffusion of a steady concentration of analyte gas through the porous structure (controlled by the operator) to the second component of the gas sensor. The hybrid porous structure that the analyte gas diffuses through consists of a nanoporous structure on the surface of each micron-sized pore in the porous structure. The inter-relationship between these two porous structures and the sensing mechanism will be clarified through the analysis presented in this chapter. The second component of the gas sensor adsorbs the analyte, resulting in the transduction of the introduced gas concentration into a sensor resistance change.

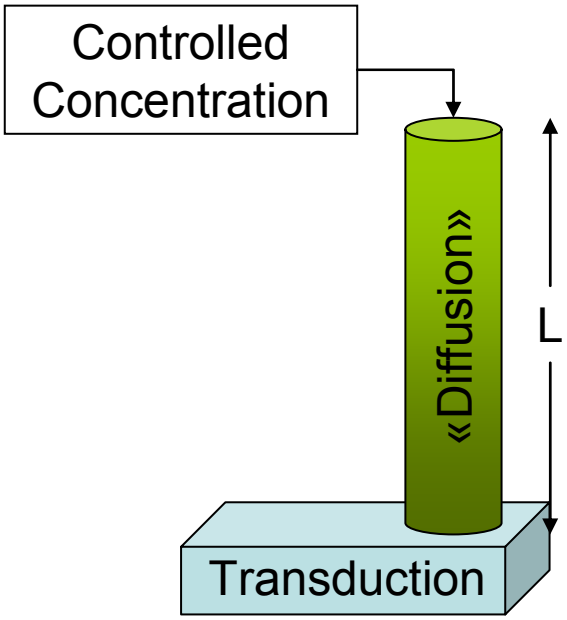

Figure 5-2: The model of the gas sensor is illustrated in this figure as a single pore into which the analyte gas concentration diffuses.

In this chapter, both the diffusion and transduction components will be described mathematically and modeled numerically. This modeling will then be compared with experimental data in order to evaluate its accuracy for future sensor design.

Model for Analyte Diffusion

In order to model the diffusion associated with the PSGS, we make two assumptions. The first assumption relates to the hybrid porous silicon structure of the gas sensor. The hybrid porous silicon structure used to create the PSGS has been identified to have two pore size scales[1,2]. These are the micron-sized pores, readily observed in SEM images of the structure, and nanometer-sized pores located on the micron-sized pore walls. The assumption made here, is that one of these porous silicon structures

dominates the rate of analyte diffusion, as opposed to a significant contribution associated with each pore dimension.

The second assumption made is that the sensor response that is seen occurs primarily at the "bottom" of the pores through which the analyte gas diffuses. Our assumption is initially validated by examining the electroless metallization experiments discussed in Chapter 4. The method of providing selective coatings utilizes a short time-scale electroless process which deposits a small amount of metal (which in most cases is quickly transformed to a metal oxide) to the surface of the sensor. The deposited metal is invisible to both SEM imaging and EDS elemental analysis detection. However, we know that a metal layer was deposited as a result of the observation of a chemical sensitivity modification. The inability to locate the deposited metal by SEM or EDS is an indication that the sensitive regions of the PSGS lie beneath the top surface of the porous structure. This observation will be used when we construct our model of the gas sensor.

From Figure 5-3, taken from the experiments of Seals, et al., we can see that the metal deposited binds to the nanoporous surface of the micropores, which indicates that sensitivity is dominated by the nano-scale structures. This experiment demonstrated that a photoluminescence induced metallization process can be utilized to provide low resistance contacts between the gas sensor and a gold pad[2]. The metal deposited spanned a high-resistance gap that exists between the gold pad and the conductive region of the porous structure. The formation of the metal at the nanoporous coating suggests that this high resistance gap is present within the nanopores, and, we assert that the lower resistance, sensitive region is the region at the bottom of the nanopores.

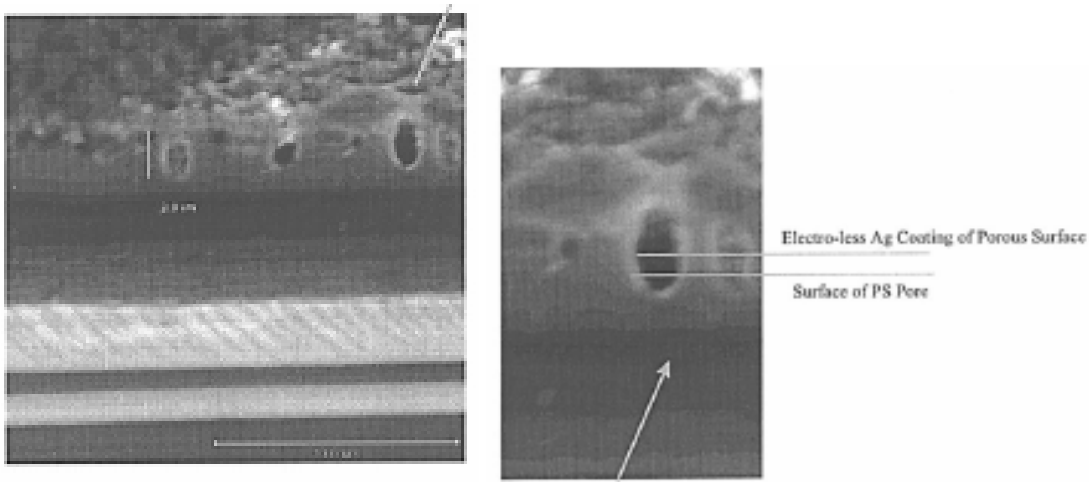

Figure 5-3: The long timescale electroless coating of silver on the PS interface demonstrates that the silver is deposited on the nanoporous coating of the micropores.

Both from the evidence discussed above, and as a result of the apparent accuracy of the model we will present, we assume that a significant majority of the sensing occurs at the termination of the porous well, as is depicted in Figure 5-4. We have also indicated that the pores that dominate the sensing mechanism are at the nano-scale. This will be reinforced through a calculation of the diffusion constant for the two size scales associated with the porous silicon pores.

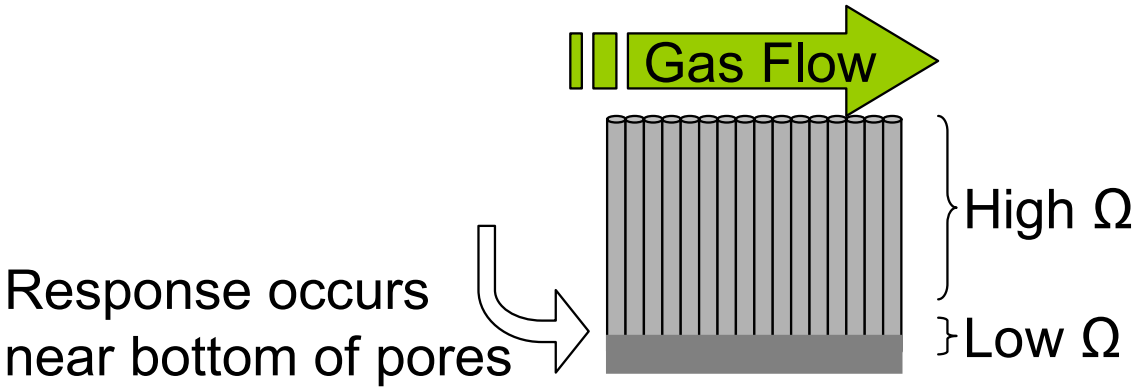

Figure 5-4: The second approximation made in the model of the PSGS assumes that the majority of the gas sensor response occurs at the bottom of the porous surface.

Given the two approximations we describe, we represent the entire porous network as a single pore, through which gas diffuses at the average rate for the entire

system of pores. This single pore is constructed with a total length 'L'. The analyte diffuses into the pore with a given diffusion constant 'D'.

The one-dimensional diffusion equation (Equation 5-1) governs the behavior of the analyte gas within this column[3,4]. The concentration of the analyte gas at one end of the well is provided as an initial condition which can be changed (programmed) between executions of the model. This concentration is given as the variable C_0 represented in Equation 5-2. A second boundary condition exists at the other end of the well (Equation 5-3) which provides for no leakage of the analyte through this region[3].

$$\frac{\partial C(x,t)}{\partial t} = D\frac{\partial^2 C(x,t)}{\partial x^2}$$

Equation 5-1: The diffusion equation models the diffusion of an analyte concentration 'C' in one dimension. This equation is valid from 0 to the pore length 'L' in 'x' and from 0 to infinity in time 't'. The diffusion constant 'D' governs the rate of diffusion.

$$C(x,t)\Big|_{x=0} = C_0(t)$$

Equation 5-2: The first boundary condition for the diffusion equation (Equation 5-1) controls the presence of analyte at the open end (top) of the pore for all times 't'.

$$\left.\frac{\partial C(x,t)}{\partial x}\right|_{x=L} = 0$$

Equation 5-3: The second boundary condition for the diffusion equation (Equation 5-1) provides for a zero flux of gas concentration 'C' through the bottom of the pore being modeled.

Finally, the initial conditions for the problem are chosen to represent an 'empty' pore, containing a zero analyte concentration. This is represented as

$$C(x,t)\Big|_{t=0} = 0$$

Equation 5-4: The initial condition for pore modeling.

Organization of the Diffusion Equation for Numerical Analysis

The first step taken to prepare the diffusion equation with the constraints for numerical analysis is to remove some dimensionality from the equations. This simplifies the analysis required and will collect the two unknown constants 'D' and 'L' into a single parameter "D/L^2". This new parameter is the only variable within the system of equations aside from the initial conditions, and effectively represents the time it takes a concentration of gas to reach the bottom of the pore. Replacing the length variable through the linear transformation provided in Equation 5-5, we arrive at three new equations which are provided in Equation 5-6.

$$y = \frac{1}{L}x \qquad \frac{d}{dy} = L\frac{d}{dx}$$

Equation 5-5: The linear transformations used to simplify the above equations expresses the length component of the pore as 'y', which varies from 0 to 1.

$$\frac{\partial C(y,t)}{\partial t} = D/L^2 \frac{\partial^2 C(y,t)}{\partial y^2}$$

$$C(y,t)\big|_{y=0} = C_0(t)$$

$$\left.\frac{\partial C(y,t)}{\partial y}\right|_{y=1} = 0$$

Equation 5-6: This representation of the diffusion equation is valid from 0 to 1 in 'y' and for all positive time 't'.

To model this set of equations, we use the built in 'ode45' function of Matlab[5]. This function solves a system of ordinary differential equations through comparison of the Runge-Kutta 4th order and Runge-Kutta 5th order solutions to ensure solution accuracy is within a tolerance to be specified[6]. In order to use this solver, it is first

necessary to represent the partial differential equation we wish to solve (the diffusion equation) as a finite series of ordinary differential equations (ODE's).

We represent this series of equations as $C_i(t)$, where the index 'i' denotes the position of the equation in 'y', as shown in Figure 5-5. The 0^{th} index marks the location of $C_0(t)$, which is not an ODE, but a boundary condition of the problem as provided in Equation 5-2. The N^{th} index marks the location of the N^{th} ODE, which determines the second boundary condition of the equation as provided in Equation 5-3.

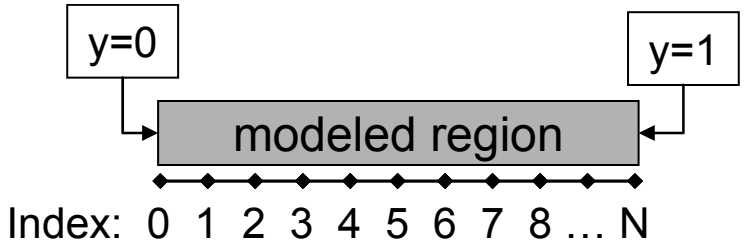

Figure 5-5: The index of the ODE $C_i(t)$ represents the position in 'y' where that differential equation is valid.

As the final step in the analysis, we expand the PDE of the diffusion equation in to an arbitrary number 'N' of ODE's represented as shown in Equation 5-7 below. In these equations, we replace the second spatial derivative in y using the explicit finite difference method[7]. This application results in the bracketed term in Equation 5-7, with the denominator of that term representing the square of the distance between equations as depicted in Figure 5-5.

$$\begin{aligned} & C_0(t) = given \\ 1 \le i \le N-1: \quad & \frac{d}{dt}C_i(t) = \frac{D}{L^2}\left[\frac{C_{i-1}(t) - 2C_i(t) + C_{i+1}(t)}{(1/N)^2}\right] \\ & C_N(t) = C_{N-1}(t) \end{aligned}$$

Equation 5-7: The representation of the diffusion equation as a set of N numerically solvable equations (not counting the initial, given equation).

Returning to the initial conditions of the problem, first given in Equation 5-4, we apply this procedure to the system of equations we have developed as shown in Equation 5-8.

$$1 \le i \le N: \quad C_i(t) = 0$$

Equation 5-8: The initial conditions for the equations governing a pore to be modeled.

Model for Analyte Transduction

For the second component of the model, the method by which a concentration of gas is able to modify the resistance of a gas sensor will be described using electrochemical principles. This format was chosen after reviewing several transduction theories used to model other sensors.

For the tin-oxide gas sensor, of which our tin-coated sensor is an analogue, the method of transduction is described within the context of changing the potential barrier height at the interface between grains of tin-oxide[8]. The effective "thickness" of the boundary layer is modified upon the sensors exposure to gas by the chemical adsorption (oxidizing gas) or depletion (reducing gas) of oxygen from the tin-oxide surface layer, thereby changing the conductance profile of the system. Some key concepts can be drawn from a consideration of this first method of transduction. First, our model needs to include the possibility for the gas response to incur either an increase or a decrease in the resistance of the PSGS. Second, we have learned that the chemical adsorption of reactants onto the active layer of the sensor provides a candidate basis for building a transduction model, as the tin oxide gas sensor responds similarly (chemically) to the tin coated PSGS.

The transduction model for an electrochemical sensor was viewed as a potential guide for the PSGS model as it demonstrates behaviors similar to the PSGS. The first of these attributes is that the response scales linearly with the natural log of the concentration of analyte, rather than linearly to the concentration itself, as is shown in Figure 5-6.

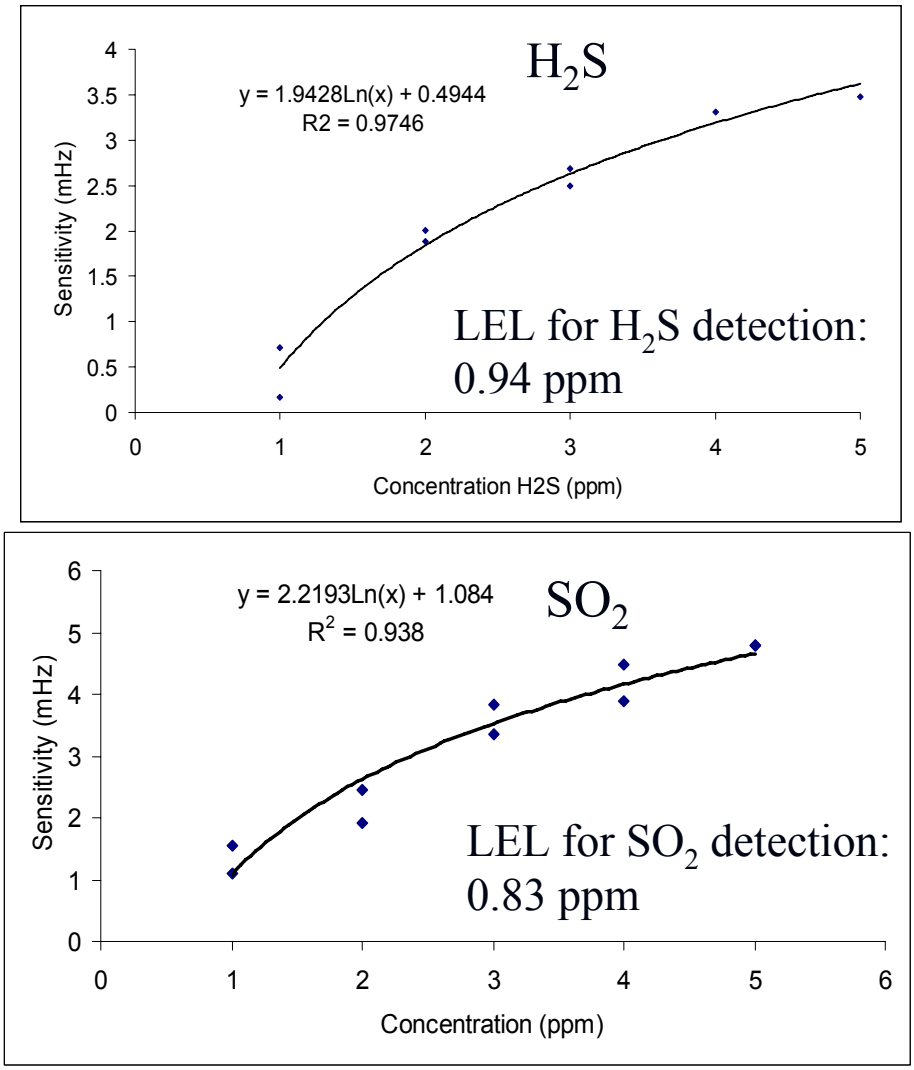

Figure 5-6: The response of the PSGS to sulfurous gases results in a response proportional to the natural log of the concentration.

This natural log scaled response occurs for the electrochemical sensor as the transduction is measured as a function of the Nernst equation. The Nernst equation,

given in Equation 5-9, indicates the half-cell potential of an electrochemical cell[9]. The Nernst equation relates the potential across a boundary to the concentrations of the oxidized and reduced forms of a chemical.

$$E = E^0 - \frac{RT}{nF} \ln\left(\frac{[ox]}{[red]}\right)$$

Equation 5-9: The Nernst equation.

While the Nernst equation does have a similar form to that desired for our model of the PSGS, it is lacking in two aspects. First, the Nernst equation breaks down for zero concentrations, causing the potential to become infinite. In electrochemical sensors, zero concentrations are never seen, as some amount of each material is considered to always be present in some concentration. However, for the gas sensor, zero concentrations of certain analytes in the atmosphere are considered possible, and, as such, the Nernst equation is inadequate to describe these analytes.

The second aspect in which the Nernst equation (Equation 5-9) is lacking is in the inclusion of a sensitivity variable to describe the activity differences between various analytes. The PSGS, for example, reacts much more strongly to 1 ppm of ammonia than to 1 ppm of nitric oxide. The Nernst equation in the form of Equation 5-9 has no parameter to describe this required feature of the PSGS. In short, a different form of the Nernst equation that is better suited to the PSGS must be chosen.

Creation of a Multi-gas Transduction Equation for the PSGS

To create an equation for the PS interface, we suppose that the interface is a reversible, chemically absorbent layer. This layer, like an electrochemical sensor, does not allow transmission of materials through it, and only reacts by changing its "potential"

relative to the semiconductor material beneath it. This change in potential, we assume, is what directly causes a change in resistance through a shift in the conduction bands of the semiconductor in a manner similar to that by which the tin oxide gas sensor transduces the presence of a gas.

A more powerful modification to the Nernst equation is the Goldman equation, Equation 5-10, which is used to describe multiple ions passing through a membrane. This equation was developed to solve for cell membrane potentials where multiple ions are passing through the membrane and the relations for their equilibration are solved. These ions are indicated by the parameters 'A' and 'M' in Equation 5-10 where A (anion) corresponds to the negative ions and M (metal) corresponds to the positive ions. This equation is more useful for describing the problem of the porous silicon gas sensor as the adsorption of multiple gases into and out of the transduction region is a similar problem and the equation also provides for an extra degree of freedom in the ion permeability variable 'P'. This variable will be utilized (parameterized) to account for the sensor selectivity for each analyte and their response to various coatings. In short, we wish to match the variables presented in Table 4-2. In the Goldman-Hogkins-Katz (GHK) equation, the I positive ionic species and J negative ionic species are summed over both the inside and the outside of the permeable layer. Each sum contains both the concentration of that particular species and the permeability of that species through the membrane.

$$E = \frac{RT}{F} \ln\left(\frac{\sum_i^I P_{M_i^+} \left[M_i^+\right]_{out} + \sum_j^J P_{A_j^-} \left[A_j^-\right]_{in}}{\sum_i^I P_{M_i^+} \left[M_i^+\right]_{in} + \sum_j^J P_{A_j^-} \left[A_j^-\right]_{out}} \right)$$

Equation 5-10: The Goldman, Goldman-Hodgkin-Katz, or GHK equation is a modification of the Nernst equation for the membrane equilibrium problem.

We modify Equation 5-10 first by analyzing the terms concerning the interior of the membrane to create an equation which represents the baseline potential accurately at zero analyte concentration. Upon examination, we assert that replacing the sums over interior gases with unity reduces Equation 5-10 to produce a correct solution for the case of zero concentration. For this case, shown in Equation 5-11, the term within the natural log results in no change to the potential.

$$\Delta E_{PS} = \frac{RT}{F} \ln\left(\frac{1 + \sum_i^+ P_{A_i^+} \left[M_i^+\right]_{out}}{1 + \sum_j^- P_{A_j^-} \left[A_j^-\right]_{out}} \right)$$

Equation 5-11: The GHK equation is modified to produce a correct solution for zero concentration of gas, the baseline condition.

Next, we assess the permeability constants 'P' initially presented in the GHK equation as well as the ion concentration terms 'A'. The permeability coefficient effectively scales the response of the sensor to each gas (either 'i' or 'j') presented. As such, this coefficient represents the sensitivity 'S' of the PSGS to the gas that is being tested. In addition to the gas 'i' that the sensor responds to, the sensors' sensitivity is also a function of the coating 'σ' present on the particular PSGS. The ion concentration terms 'A' are replaced with the standard gas sensor concentration notation 'C', with the indices for positive and negative ions replaced with oxidizing and reducing gases. This is consistent with the data that has been gathered so far. Further, only oxidizing gases

(which adsorb oxygen from the surface) have been studied and only positive changes in impedance have been observed. These changes of variables are given explicitly in Equation 5-12, and incorporated with Equation 5-11 to create Equation 5-13. For the tests carried out thus far, the summation in the denominator of Equation 5-13 can be taken as zero as no reducing gases have been tested.

$$S_i^{\sigma} = P_{A_i^+} \quad C_i^{O,R} = \left[A_i^{+,-}\right]_{out}$$

Equation 5-12: The change of parameters from permeability 'P' and ion concentration 'A' to sensitivity 'S' and gas concentration 'C' allows the direct formulation of Equation 5-13.

$$\Delta E_{PS} = \frac{RT}{F} \ln\left(\frac{1+\sum_i^O S_i^{\sigma} C_i^O}{1+\sum_j^R S_j^{\sigma} C_j^R}\right)$$

Equation 5-13: The general expression for the change in the PS interface potential considering both oxidation and reduction is further modified to incorporate the sensitivity, which is dependant on both the analyte gas and the coating present on the PSGS surface.

Using the Transduction Model to Represent Time-independent Responses

It only remains to translate the shift in potential within the PS transduction layer into a resistance change for the sensor. The simplest way to do this, while maintaining accuracy, is to assume a linear relationship between the two. The assumption of this linear relationship results in Equation 5-14.

$$R(C_i) = R_0 + R_1 \times \ln\left(\frac{1+\sum_i^O S_i^{\sigma} C_i^O}{1+\sum_j^R S_j^{\sigma} C_j^R}\right)$$

Equation 5-14: Equation 5-13 is used to calculate the resistance of the gas sensor using a linear relationship between the shift in potential and resistance.

For a single gas at low concentration, Equation 5-14 simplifies to produce Equation 5-15.

$$R(C_i) = R_0 + R_1 \times S_i^{\sigma} C_i$$

Equation 5-15: The linear response of the sensor at low concentration emerges when simplifying Equation 5-14 for a single gas.

We note that the parameter R_1 was initially included in Equation 5-14 as it is needed to make the dimensionality of the equation correct. However, the response to each gas is entirely contained within the sensitivity parameters 'S'. We are, in effect, able to choose R_1 to be whatever we want, as it is a scaling factor that affects all sensitivities 'S' linearly. Consistent with Equation 5-15, we can most easily choose the parameter R_1 to be defined as 1Ω, as this is the fundamental unit of resistance. With this choice, we define the sensitivities to be the change in resistance when a sensor is exposed to a low concentration (low enough to approximate the natural log as a linear function) of gas 'i' (measured in Ohms-per-ppm) divided by 1Ω, as shown in Equation 5-16.

$$R(C_i) = R_0 + 1\Omega \times S_i^{\sigma} C_i \qquad S_i^{\sigma} = \left(R(C_i) - R_0\right) \Big/ 1\Omega \times C_i$$

Equation 5-16: Selecting R_1 to be 1Ω allows for precise definition of the sensitivity to be created.

We rewrite Equation 5-14 one final time to incorporate the new value for R_1. From this expression, it is more apparent that the proportionality 'S' for each gas 'i' indicates a scaling factor that gauges the sensitivity of a PSGS to a particular gas. Again, this sensitivity is a number dependant on both the gas being delivered and the sensor coating 'σ'. R_0 represents the baseline resistance of the gas sensor. The concentration is deemed low enough if, for measurements of the sensor taken in the range of this

concentration, a linear relationship between the response and concentration of gas is apparent. This equation completes the transduction model. The inclusion of this model with the diffusion model for the porous silicon pores will incorporate the necessary time-dependant behavior of the PSGS in the following section.

$$R(C_i) = R_0 + 1\Omega \times \ln\left(\frac{1+\sum_{i}^{O} S_i^{\sigma} C_i^{O}}{1+\sum_{j}^{R} S_j^{\sigma} C_j^{R}}\right)$$

Equation 5-17: Equation 5-14 is rewritten to include the value of R_1 explicitly.

Incorporation of the Theories into a Numerical Simulation

The two theories which have been developed for the diffusion of gas through a PS pore and for the response/transduction mechanism of the porous silicon layer now will be incorporated into a single, functional simulation. First, the transduction equation will be used to determine the resistance of the sensor in the presence of analyte at the transduction layer at the bottom of the pores. This will be matched to the time-independent data from sensors tested with the Device Saturation Method as described in Chapter 3. Finally, the numerical model will be adapted to this result so that the time-dependant responses can be compared to the model.

Creation of a Numerical Model

The numerical simulation for the PSGS model was created in Matlab. Several different program files comprise the simulation, all of which are included in Appendix B.

The file "Diffusion_Model.m" simulates diffusion through the porous region of the gas sensor as described in *Model for Analyte Diffusion* above. This program has two

inputs, the first being an array of length equal to the time in seconds of the simulation which describes the concentration at the open end (top) of the pore for each second. The second input variable represents the diffusion constant divided by the square of the length of the pore. These two parameters fully describe the problem as defined by Equation 5-7.

The function as defined by Equation 5-7 calculates the concentration of gas at the bottom of the pore using calls to ode45 (a built-in Runge-Kutta ODE solutions package) and "Diffusion_Eq". The function "Diffusion_Eq" is defined within "Diffusion_Model.m" and represents the partial differential equation of the diffusion equation as a variable number of ODE's; for the present study, 100 ODE's are used. The number of ODE's was chosen through trial and error. We selected a fit with 100 ODE's as the results obtained using this degree of precision were indistinguishable from more precise simulations. The function returns the concentration of gas at the bottom of the well and the times corresponding to each of the intermediate concentrations in two arrays.

The file "Generate_C0_of_t.m" creates the input variable for the previously described function "Diffusion_Model" that describes the concentration of gas at the top of the well. This is a helper-function, written to make the simulations easier to construct. The input to this function is in two arrays that describe the gas being delivered to the sensor in a user-friendly fashion. The first array corresponds to the concentrations of gas being delivered, while the second indicates the duration (in minutes) of exposure to each concentration of gas. In other words, the number in the duration array at a given index 'i' corresponds to the number of minutes that the concentration (given at index 'i' in the first array) will be delivered. An example of the inputs to this function is also given in the

script file in Appendix B. The output is an array of concentrations suitable for the diffusion simulation function.

The file "Calculate_Response.m" transforms the concentrations given by "Diffusion_Model" into a gas sensor resistance. This function is capable of processing a sensor's response while being exposed to multiple different gases simultaneously as is described by Equation 5-15. The inputs to the function are arrays of (with each element corresponding to an individual gas) the concentrations output by the "Diffusion_Model", the times output by the "Diffusion_Model", and the sensitivities (S_i) in Ohms per ppm for each gas as described by Equation 5-15 and measured empirically. A final input represents the baseline response of the sensor. This function outputs arrays representing resistance and time for a single sensor. These arrays can then be plotted for comparison to experimental data.

The final file, "Diffusion_Model_Script.m", is an executable Matlab script that runs all of the aforementioned functions with sample data and plots the output. From running several trials of this function, the values of the variables were chosen to approximate the performance of a functioning PSGS. The output of this script is shown in Figure 5-7.

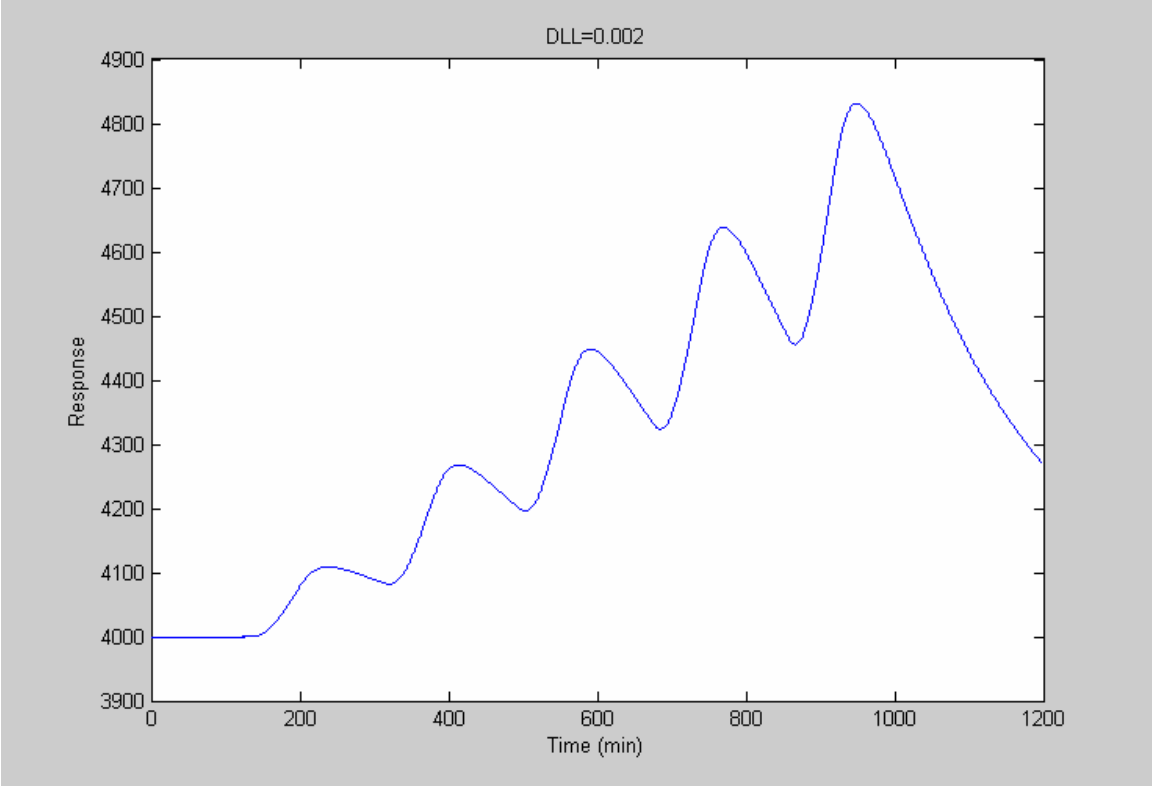

Figure 5-7: The plot generated by executing Diffusion_Model_Script.m is a simulation of a sensor being tested using the gas pulse method to concentrations between 1 and 5 ppm of gas.

Comparison of Theory with Experiment

Determination of Diffusion Constant and Pore Length

To acquire an estimation of the parameter D/L^2, which determines the rate of a sensor's response using our model, we compare the output of the model to several various selections of D/L^2. For this test, we compare the model to the experimental data for a PSGS that has a baseline resistance around 4150Ω and a saturation point of 10500Ω when exposed to 10ppm of ammonia. The comparison is shown for five different values of D/L^2 in Figure 5-8.

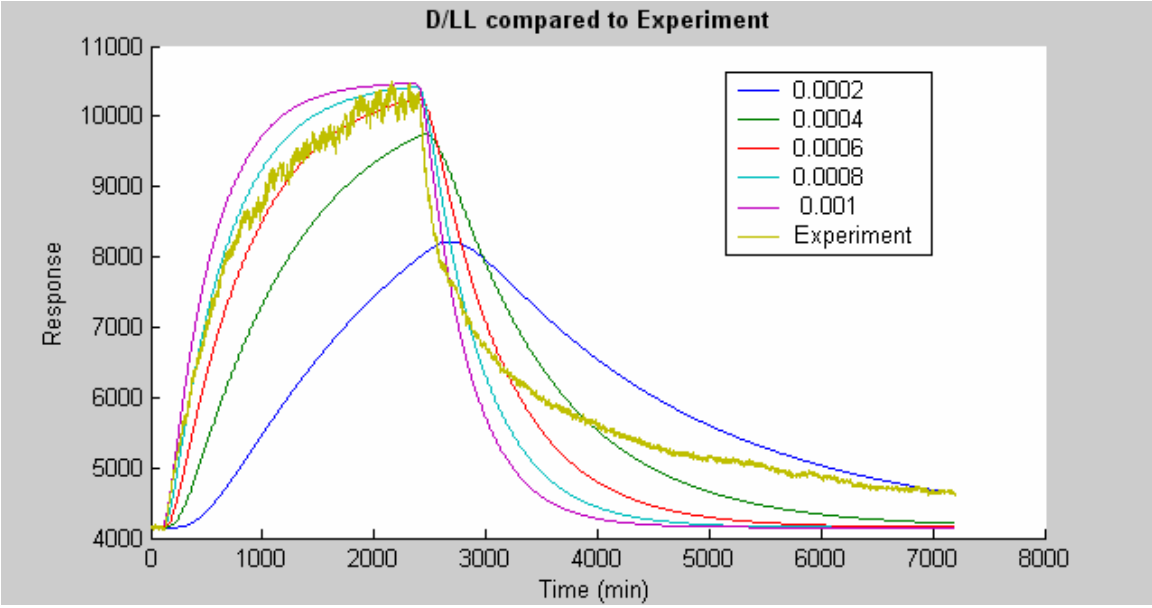

Figure 5-8: The time dependent response of a porous silicon gas sensor closely matches the simulated response with D/L^2 selected between 6 and 8 $\times 10^{-4}$ s^{-1}.

From this comparison, the range of values that D/L^2 must span for the model to match with experiment is clearly indicated. More to the point, we can now compare the evaluated value with a known diffusion constant to determine which mode of diffusion (microporous or nanoporous) is dominant within the porous silicon sensor. For the case of microporous diffusion, we know the value of the diffusion constant to be 0.230×10^{-4} m^2/s.[4] This would indicate that if microporous diffusion dominates the reaction time, the required pore depth would be approximately 30 meters. Clearly, microporous diffusion does not correspond to the rate limiting process determining the response of the PSGS.

For the case of nanopore-limited diffusion, both the pore depth and the diffusion constants are unknown. The diffusion within a nanoporous network, where pore size is on the order of the molecular size of the analyte, is characterized my much smaller diffusion constants, well below 10^{-10} m^2/s.[4] We can calculate an upper bound to the pore depth for the case of nanoporous diffusion by analyzing micrographs obtained for the porous silicon. From Figure 5-9, for example, we can see that a nanopore could be at

most 0.5 $\times 10^{-6}$ meters in depth, given an apparent maximum pore wall thickness of about 1 micron and assuming the nanopore extended almost entirely to the core of each pore wall. We find that for these values of D/L^2 and L, we arrive at a predicted value of 0.112×10^{-15} m^2/s for the nanoporous diffusion constant of ammonia at room temperature.

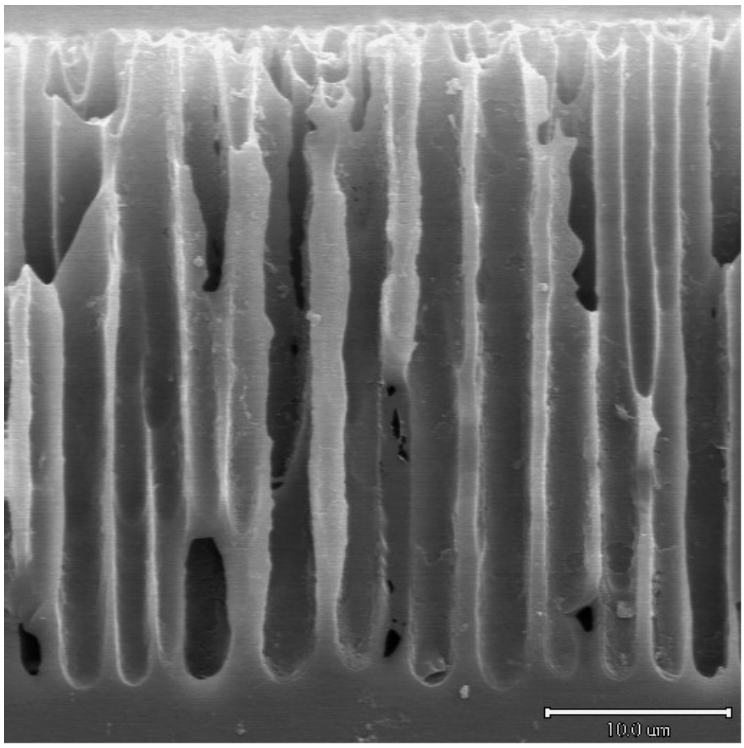

Figure 5-9: A SEM image of the cross-section of a porous silicon gas sensor.

Further Considerations

The program which we have developed may have significant use beyond the prediction of the diffusion constant for a PSGS. It is also capable of simulating the real-world operation of devices. Features such as noise, drift, and poisoning can also be incorporated into the model to improve its ability to mimic actual devices.

In the following chapter, we will use this model to calculate different modes of device operation. The model will be further modified to better mimic "actual" device operation, including a simulation of both the high frequency noise and low frequency

drift characteristics of the PSGS. Optimization of the sensors' signal-to-noise ratio as a function of multiple parameters is demonstrated for the case of the gas sensor as it is operated in a pulsed format. The value of the modeling is that the data to perform the necessary calculations in Chapter 6 can be gathered without the need for the time-consuming fabrication, testing, and validation of actual porous silicon gas sensors.

References

[1] L. Seals, L. A. Tse, P. J. Hesketh and J. L. Gole, "Rapid, reversible, sensitive porous silicon gas sensor," J. Applied Physics, 91, 2519-2523 (2002).

[2] Gole, J.L., Seals III, L.T., and Lillehei, P.T. "Patterned metallization of porous silicon from electroless solution for direct electrical contact," J. Electrochem. Soc. 147, 3785 (2000).

[3] Diffusion Equation – Wikipedia (January 2006) http://en.wikipedia.org/wiki/Diffusion_equation.

[4] Hines, A. L., Maddox, R. N., "Mass Transfer", Prentice-Hall, Inc. 1985.

[5] ode45, ode23, ode113, ode15s, ode23s, ode23t, ode23tb (MATLAB Functions), (January 2006) http://www.mathworks.com/access/helpdesk/help/techdoc/ref/ode45.html.

[6] Runge-Kutta methods – Wikipedia, (January 2006) http://en.wikipedia.org/wiki/Runge-Kutta_methods.

[7] Finite difference – Wikipedia, (January 2006) http://en.wikipedia.org/wiki/Finite_difference.

[8] Keith J. Albert, Nathan S. Lewis, Caroline L. Schauer, Gregory A. Sotzing, Shannon E. Stitzel, Thomas P. Vaid, and David R. Walt, "Cross Reactive Chemical Sensor Arrays", Chemical Reviews, Vol. 100, 7 (2000).

[9] Nernst equation – Wikipedia, (January 2006) http://en.wikipedia.org/wiki/Nernst_equation.

CHAPTER 6

PARAMETRIC ANALYSIS OF THE GAS PULSING EXPERIMENT

In characterizing and evaluating the feasibility of porous silicon gas sensors, a new method of testing and analysis has been developed[1,2]. This method was designed to meet the challenges associated with the characterization of a large number of widely ranging (in sensitivity, selectivity, and noise level) sensors in a systematic and significant fashion. A system has been implemented to meet this need which can discard or accept devices with a high level of confidence so that successive batches of sensors can be designed, fabricated, and retested efficiently.

Through the introduction of gas pulsing techniques combined with FFT analysis, the linear low pressure gas response of the PS sensor can be separated from the effects of pressure, temperature, and humidity, and acquired, and filtered on a drifting baseline, further increasing sensitivity. The introduction of the FFT technique provides the ability to operate at concentrations well below saturation and provides a means for eliminating false positives within the laboratory environment. While the concept of pulsing gas onto a surface in order to control saturation is not unique, this study focuses on the integration of gas pulsing, signal analysis, and specific criteria associated with a gas sensor for the purpose of measuring small amplitude signals. With these collective attributes, a technique for uniform characterization of devices can be presented. The specific advantages of this general approach include more accurate and statistically significant measurements, although these will always depend on the particular system to which the method is applied. The technique can also provide for the characterization of devices that

(without the application of this method) previously have been found to display an unperceivable signal.

We have also extended the application of this method to provide for the characterization of a wide range of sensors and devices. With the growing demand from scientific and industrial sectors, the need for efficient and innovative testing methods for devices and experimental systems is ever increasing, providing motivation for the development of this system beyond the confines of the porous silicon gas sensor.

Description of Method

The pulsed system frequency analysis (PSFA) method we have created for sensor characterization is broadly applicable to a diversity of devices for which we desire to know the response to some controllable parameter. The specific advantages include the potential for more accurate and statistically significant measurements, depending on the particular system to which this method is applied. The technique can also provide for the characterization of devices which (without the application of this method) have been deemed nonfunctioning due to an unperceivable signal. We apply the PSFA method in three phases, 1) Generation of a Periodic Signal, 2) Acquisition of a Frequency Spectrum, and 3) Calculation of the Response. They are briefly described in general terms below; detailed examples follow.

Generation of a Periodic Signal

Once a device/experiment is chosen, it must be configured such that the parameter which affects the output can be set to a periodic mode of operation. The periodic switching of a parameter that affects the device's state is referred to as device pulsing.

The period of the pulsing as well as the magnitude of its "on" and "off" state can be changed for separate tests, but remains constant within each test. The pulsing period is selected to lie between the minimum response time and the full response time of the device. Finally, the number of pulses delivered to the device before the output is fully realized depends on the noise present in the signal as well as the parameters of the device itself. After delivering several pulses, the response generated is expected to be periodic in time. This mode of operation allows a device to be exposed many times per test to identical stimuli at a known frequency.

The period and number of pulses delivered determines the total time for a given test. The careful selection of these parameters, given the remaining constraints of the system being tested, enables the exchange of the quality of response with the speed of the measurement in a known way. These parameters and their selection will be considered in more detail using the first example. The data sampling rate also must be considered, as it determines the resolution of the transform into the frequency domain.

Acquisition of a Frequency Spectrum

Upon acquiring a response, the frequency spectrum of the filtered response is calculated, with an expected peak at the pulsing frequency. This data can be carefully filtered to remove peaks at frequencies not associated with the pulsing frequency, since these frequencies are necessarily associated with undesirable or systematic noise sources emanating from either the device itself or the testing environment. The magnitudes and frequencies of these noise sources provide information which not only allow their determination, but also their possible elimination from the system.

Calculation of Response

After the signal is filtered and transformed into the frequency domain, it becomes possible to arrive at a value which characterizes device performance. This parameter represents the mean response to all of the pulses delivered during the test. Among the typically useful performance-quantifying numbers is the signal-to-noise ratio (SNR), a measure of the recordable output of the device in question. However, the peak of the signal in the frequency domain as well as the noise itself can also be examined to determine the intrinsic noise which compared between associated tests. Analysis of the signal can also be done to yield the standard deviation of the response. As the results of the PSFA method represent an average of many pulses, statistically significant data can be taken in a systematic and rapid fashion.

Application to a Theoretical Device

As the PSFA method was initially developed during the evaluation of enhancements to modified porous silicon gas sensors[2], we have designed a model for testing the method that mimics the performance of an "ideal" similar gas sensor. This numerical model of the gas sensor, which is presented fully in Chapter 5, is representative not only because it accurately mimics the performance of a porous silicon gas sensor, but also because it can be readily tuned to characterize the performance of the evaluation method we consider. The model will be used to demonstrate how the method is applied to a particular system as well as how the method can be used to parameterize the system quickly for the design of experiments. Six parameters are initially defined as inputs for this example, as we use the SNR of the response to characterize the output. We vary the

inputs to the modeled gas sensor, in conjunction with the PSFA method, to assist in the design of the experiment for the testing of gas sensors in an optimal fashion.

Description of Modeled Device

The model used to simulate the gas sensor is discussed in depth in Chapter 5. For the purpose of this chapter, the response (measured in Ohms) was chosen to be 1000 Ω per ppm of the concentration of gas at the bottom of the well, with a baseline resistance of 1000 Ω. Noise was also introduced to the output of the model so as to better simulate devices. This included low frequency noise to model slowly drifting external parameters, and high frequency "random" noise which represents rapidly changing (faster than the rate of measurement) internal sensor fluctuations. In this model, the signal is generated at a rate of 1 Hz. These values were chosen to accurately mimic the observed behavior of an average porous silicon gas sensor.

To operate the device for use with the algorithm that has been developed, it is pulsed between two states, exemplified in Figure 6-1. The gas present at the surface of the device is switched between 0 and 1 ppm of test gas every thirty seconds for 30 minutes. The low frequency drift present is displayed in Figure 6-1a, which has a period of near 45 minutes. It is also observed that the signal oscillates about 1500 Ω, the response to the midpoint of 0ppm and 1ppm of test gas.

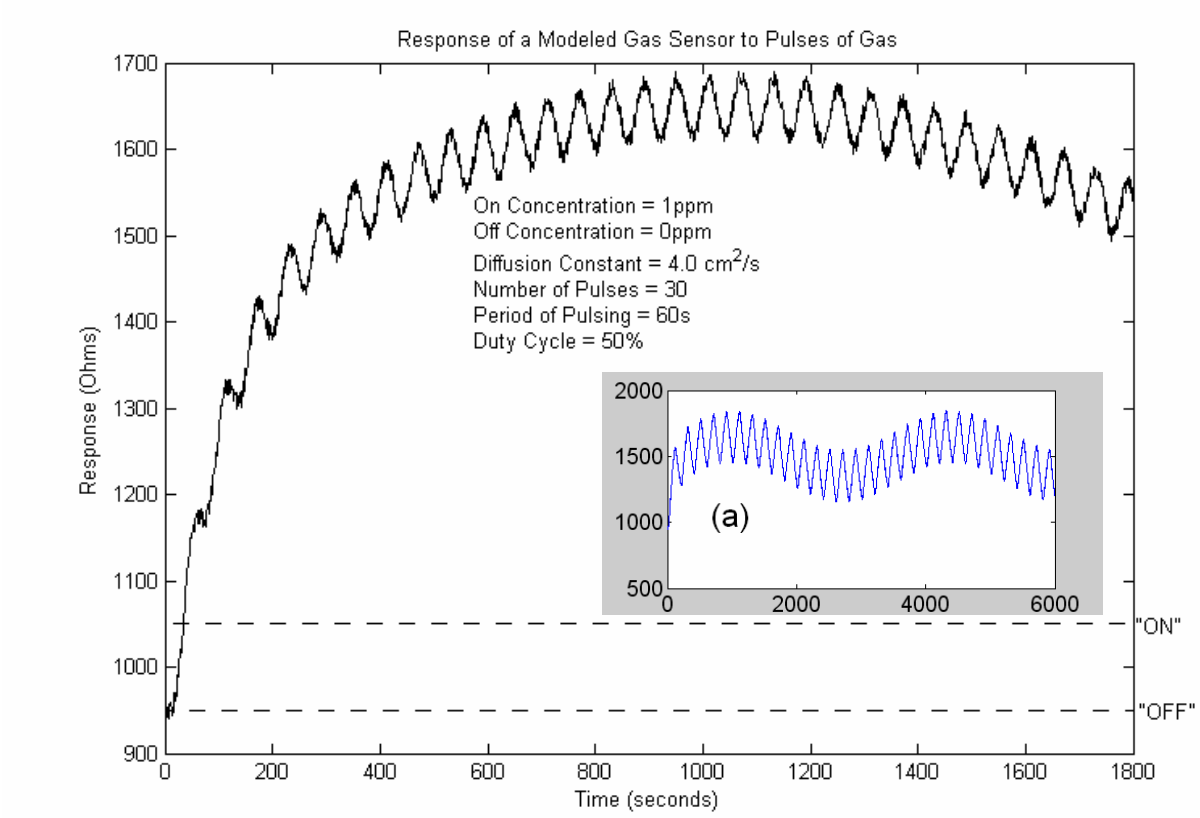

Figure 6-1: The response of a device is shown with input parameters indicated. This represents a 'typical' result obtained in testing a porous silicon gas sensor. The second response (a) with a longer period of pulsing makes clear the low frequency drift embedded in the model.

The response is measured in time and then transformed using a FFT algorithm. The algorithm also implements both a low frequency filter, and a filter which approximates the mean-resistance's drift to 1500 Ω over time as an error function. This fit was chosen as the error function corresponds to the solution to 1-D steady state diffusion. The resulting frequency transform of the data presented in Figure 6-1 is shown in Figure 6-2. The peak at 16.6 mHz corresponds to one pulse every minute. This frequency spectrum provides two measured data points. The signal of the response is the value of the transform at the pulsing frequency, and the SNR is the signal divided by a measure of the noise in the region of the signal. In this example, the signal would be approximately 4750 Ohms, and the SNR would be 19, which is 4750 Ohms divided by an

estimate of 250 Ohms for the noise. As a validation of the method, the concentration of test gas was varied between 0.05 and 50ppm. As expected, since concentration determines the amplitude between pulses, the signal is linear with the concentration of test gas as shown in Figure 6-3.

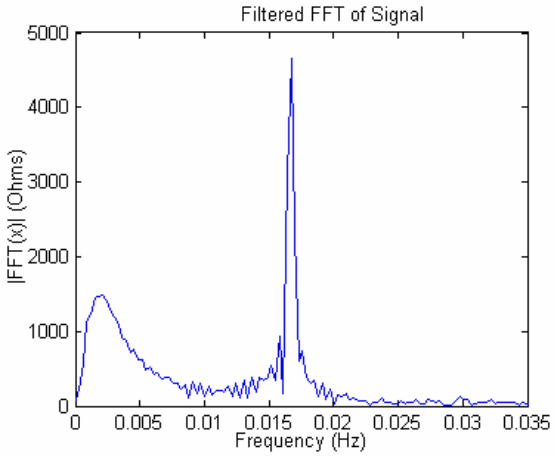

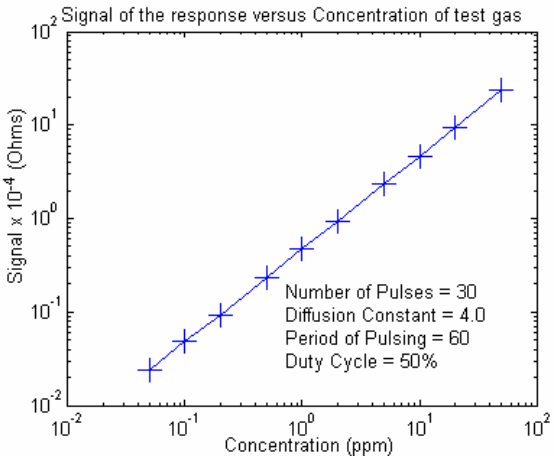

Figure 6-2 (left): The frequency transform of the response shown in Figure 6-1.

Figure 6-3 (right): The value of the frequency transform at the pulsing frequency is shown to have a linear relationship to the concentration of the test gas.

Selection of Testing Parameters & Trade-offs

Six parameters were initially chosen to optimize the performance of the algorithm. The first of these parameters is the **diffusion constant** (units of cm^2/s) which controls the rate at which gas diffuses within the model. During a given test, the gas is pulsed between the **background gas concentration** and the **test gas concentration**, the second and third parameters, in a periodic manner. The background gas concentration is held at 0 throughout this analysis. The time for one period of pulsing is the **pulse duration**, and the ratio between the time for the test gas pulse and the total pulse duration is the **duty cycle**. Finally, the total **number of pulses** represents the final parameter.

The **SNR** has been used to characterize the performance of the algorithm for each variation of the parameters.

The significance of this method is illustrated with an analysis of the effects that the duty cycle and the test gas concentration have on the SNR. This relationship, which is nonlinear in nature, can be explained empirically using Figure 6-4. We observe that, at lower concentrations of gas, the SNR is a parabolic function of the duty cycle, with a maximum at 50%. At higher concentrations, the SNR remains constant when the duty cycle is less than 50%. At low duty cycles, the response to lower concentrations of gas [A] is much weaker than to high gas concentrations [B]. As both 1) the rise of the impedance when the gas is turned on and 2) its fall when the gas is turned off contribute to the harmonic response, less signal is received when the device is recovering from a rise in resistance that is not given sufficient time to be fully realized. This behavior occurs because, at lower concentrations, the response cannot be fully realized with such a small period of exposure. A duty cycle of 50% produces the optimal SNR for low concentrations [C], and for high concentrations, the SNR at point [D] is about the same as that at [B], which indicates that a duty cycle of 50% is always optimal. Duty cycles greater than 50% are always detrimental to performance for this range of testing [E].

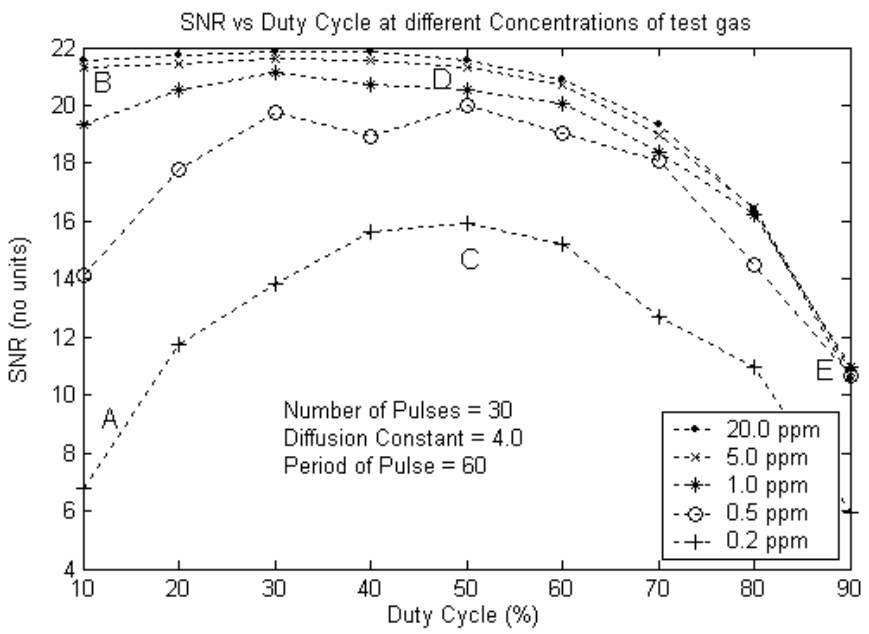

Figure 6-4: The SNR is plotted as a function of the duty cycle under various concentrations of gas. A smaller duty cycle is preferred for larger concentrations; however, as the concentration becomes difficult to detect, a duty cycle of 50% becomes optimal.

To perform a similar analysis for the four remaining parameters would be an arduous process, and detrimental to the goal of achieving a rapid understanding of the PSGS devices. Through the model's parameterization and the single output of the PSFA method, an alternative solution is feasible. Towards this end, an analysis of the experiment was conducted with the MINITAB software package. To validate the impact of the testing parameters against the SNR, a 4-parameter, 2-level full-factorial statistically designed experiment was created. Three replicate samples were taken per each run for detection of any noise-driven random effects. First and second order effects were validated for statistical significance through a t-test measured against random variation. A standard alpha level of 0.05 (the probability level for our evidence to be an unreasonable estimate), was used as the criteria for statistical significance. In Figure 6-5, the Pareto Chart demonstrates the results of the calculations[3]. With the exception of 'AC', all other parameters showed a statistical significance within the model, indicating

their effects are strongly correlated to the value of the SNR. The values of each significant term as well as their relative contribution to the SNR are also given.

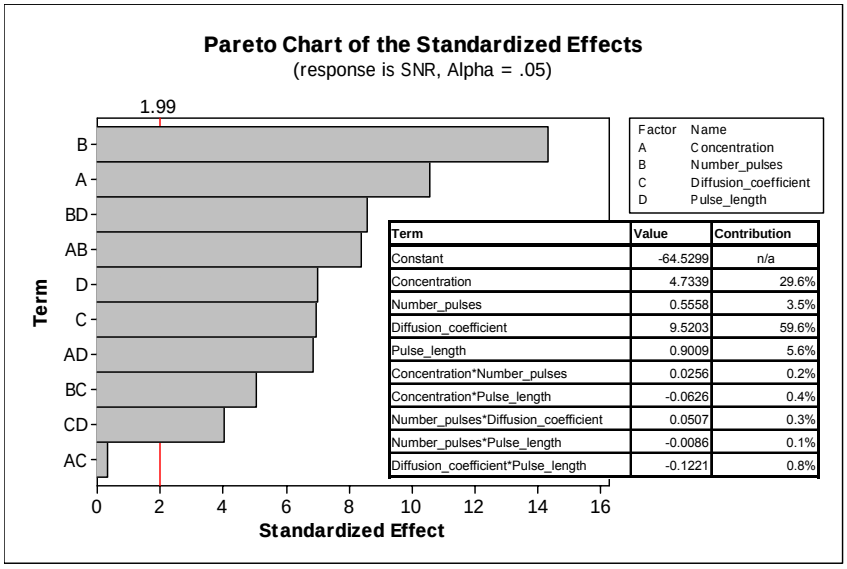

Figure 6-5: The Pareto chart of the relative effects of the four-factor model of the gas sensor demonstrates that all but one of the second order terms is statistically significant. The weights of each factor are also given, allowing the parameterization of the model's behavior.

Using a standard regression method, this model has described 91.55% of the observed behavior. Although statistically significant, all but one of the second order effects provides less than a 0.5% contribution to the SNR. As a result, the SNR can be effectively modeled by Equation 6-1.

$$SNR = -64.53 + 4.734 \times A + 0.556 \times B + 9.52 \times C + 0.9 \times D - 0.12 \times C \times D$$

Equation 6-1: The parameterized SNR of the tested sensor as a function of significant variables explains 91.55% of the sensor's behavior.

We have now achieved a parameterization of the gas sensor system that relates all of the input parameters of the pulsing technique to the SNR output. Depending on the test conducted, some of the input parameters, such as the concentration of test gas and the diffusion constant, may be inflexible. This rough linearization provides the selection of the number of pulses and pulse length so that a SNR can be measured. We also have established a model for the lower detection limit of this sensor. For a particular diffusion

coefficient and measurement time, the lowest concentration of gas that can be measured can be found at the point where the SNR approaches unity, as this point is where the signal is completely masked by the noise.

The PSFA of the gas sensor model has been used to allow testing parameters to be chosen for an experimental system. While the model constructed here made this analysis easier, the analysis could also have been conducted on the device itself, as the statistical analysis uses two to the number of [exponent] input parameters to be evaluated. This parametric mode of analysis can be generalized to any similarly reversible device or system.

Application to a Porous Silicon Gas Sensor

Implementation

The results obtained from applying the PSFA of the gas sensor model have developed better testing methods for the PSGS. The test system was first modified designed and modified to provide for a more accurate and rapid comparison of performance between devices. These metrics were needed not only to test a large number of devices that were evaluated, but also to verify the operation of these devices in sometimes noisy environments. These environments have been detailed in Chapter 3. While the behavior of the porous silicon gas sensor is described in much greater detail elsewhere[2], an overview of some key benefits to the implementation of the PSFA technique on this device follows.

The porous silicon gas sensor was tested in the gas pulsing mode of operation as is discussed in Chapter 3. The flow of the experiment and data analysis as performed is

shown in Figure 6-6. The gas pulsing experiment was conducted with various parameters. Typically, 30 minute tests over 30 pulses of gas (50% duty cycle) were used to characterize a sensor for a given concentration of gas. The background concentration is 0 ppm, and the test concentration has been varied between 0.5 and 20 ppm of test gas. Tests with ammonia, carbon monoxide, and nitric oxide were conducted using this analysis. After a test was run, the frequency spectrum was obtained and filtered. Following this evaluation, the time delay was calculated, indicating the time between the initiation of pulsing and the onset of a response. The delay corresponds to a combination of the response time of the device and the time a packet of gas takes to reach the device. The signal from the device is then calculated and this value is recorded as a measure of the sensitivity of the device for a particular concentration of gas.

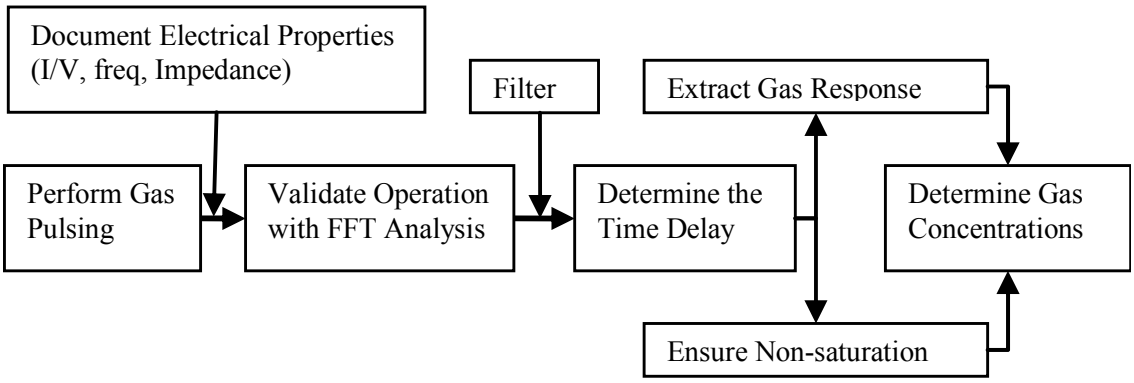

Figure 6-6: Flow chart of signal processing.

Benefits of Technique

Benefits from the implementation of the PSFA are multifarious. Immediately after the initial construction of the outlined test configuration, day-long tests were used to characterize the noise and stability of the system. These tests resolved the external perturbation of a cyclic oscillation of pressure and temperature in the laboratory which resulted from a faulty indoor environmental controller as is shown in Figure 6-7.

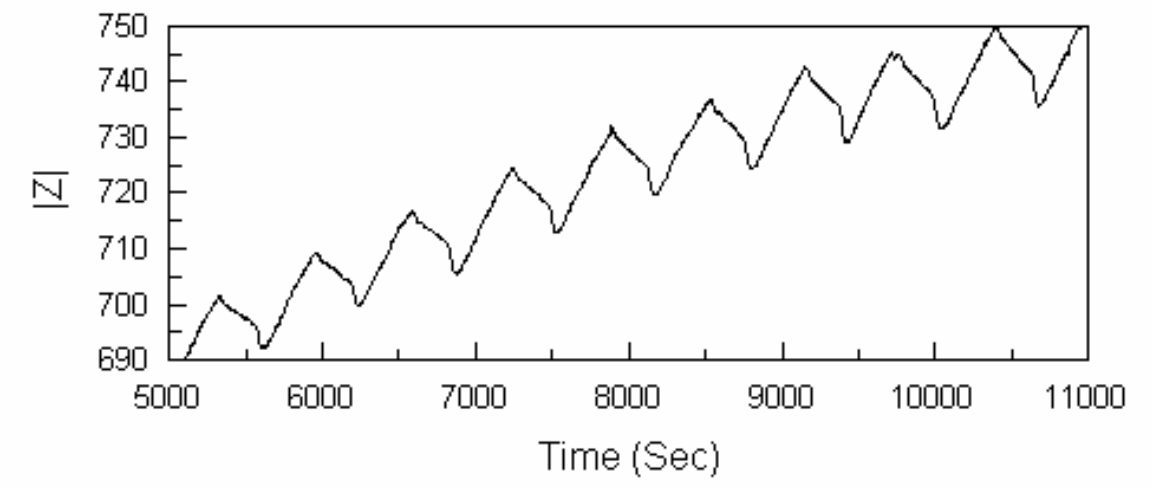

Figure 6-7: An image showing the cyclic oscillation of the sensor due to laboratory environmental factors such as pressure and temperature. This oscillation occurs at a frequency of 1.5 mHz.

The most significant benefit of the PSFA technique is its ability to compare a large number of devices in a systematic and rapid fashion, allowing non-functional devices to be easily discarded, and the specific attributes of working devices to be compared. Figure 4-7 exemplifies this benefit, demonstrating the relative effect of various surface coatings on the sensitivity of a porous silicon gas sensor.

Figure 6-8 depicts results for a device that was characterized using the PSFA method in both high and low noise environments. Before implementation, little could be learned from the results shown in Figure 6-8a. However, applying the analysis technique to both devices shows that a decrease in noise and an increase in signal and sensitivity are achieved as the measurement conditions vary from a 10mV bias voltage to a 150mV RMS voltage. The smaller peak in Figure 6-8b at 0.033Hz represents a higher harmonic of the pulsing frequency.

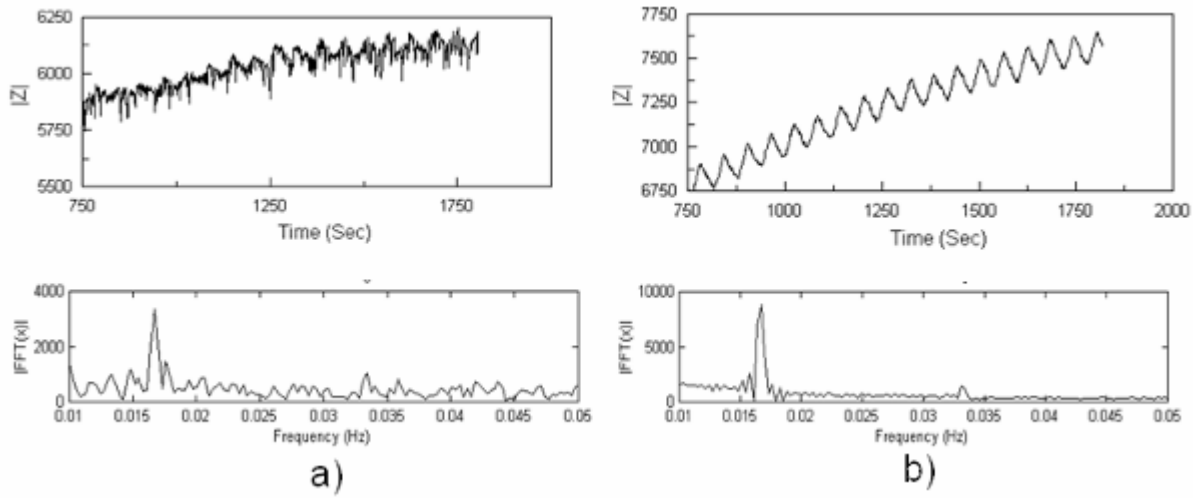

Figure 6-8: Signal and frequency transform for a device demonstrating a) high noise when measured at a 10 mV bias and b) low noise when measured with a 150 mV RMS voltage. The signal is visible at 0.0167 Hz in both tests.

Applications of the PSFA System

With the growing demand from scientific and industrial sectors, the need for more efficient and innovative testing methods for devices and experimental systems is ever increasing. To this end, patent protection for the PSFA technique has been pursued as a component of a broader patent application filed in 2005[4].

Conclusion

A novel parametric method has been developed for the analysis of the gas response of porous silicon sensors based upon periodic device pulsing and frequency analysis. A computational model of a gas sensor serves to characterize several aspects of the implementation of this analysis technique. A designed-experiment analysis of the parameters present within both a modeled gas sensor and those parameters associated with a gas-pulsing procedure demonstrates the impact that the parameters have on the SNR and thus, how they might be chosen. Operational porous silicon gas sensors were used to demonstrate the benefits of using the method for device characterization. The

method of testing and analysis outlined here is not limited to sensor applications. Any device or system which exhibits reversible and repeatable behavior could be adapted to the PSFA technique to allow a better characterization.

References

[1] L. Seals, L.A. Tse, P.J. Hesketh, J.L. Gole, "Rapid, reversible, sensitive porous silicon gas sensor", J. Appl. Phys. 91 (2002) 2519–2523.

[2] S.E. Lewis, J.R. DeBoer, J.L. Gole, and P.J. Hesketh, "Sensitive, Selective, and Analytical Improvements to a Porous Silicon Gas Sensor," Sensors and Actuators, B110 (2005) 54-65.

[3] D. C. Montgomery, G. C. Runger, N. F. Hubele, "Engineering Statistics", 2003.

[4] "Porous Gas Sensors and Method of Preparation Thereof", United States Patent Application #20050193800, September 8, 2005.

CHAPTER 7

INTEGRATED GAS SENSOR ARRAYS

The development of a prototype array-based sensor configuration is closely tied to the fact that the porous silicon gas sensor represents a platform technology, or a technology that has the potential to be easily customizable for many different specific applications. Specifications pertaining to the detection capabilities required for a given array device dictate its limitations in terms of power, size, and weight. We exemplify these considerations by outlining a sensor array which might be used for clandestine methamphetamine laboratory detection. The task of integrating the porous silicon gas sensor into an integrated system was conducted in parallel to the forming of a new company PSiSense.

A methamphetamine lab gas sensor, or meth sensor, is needed by police nationwide to both limit the production of the drug through police intervention and to provide means for an officer to safely enter such a laboratory. Jesse Hambrick of the Douglas County Sheriff's Office, a recognized nation-wide expert in the area of methamphetamine use and detection[1] has served as a primary consultant to assess the requirements for an array-based meth lab sensor. Based on his consultation and an assessment of how to develop the most useful device, it was determined that the capability of a meth sensor prototype would be to detect and report concentrations of methamphetamine-related gases while being carried or worn by a police officer in the field. The objective of this study is to evaluate those gases which, if detected simultaneously and selectively, would provide a prototype meth sensor under actual operation conditions in the field.

The most important requirement of the prototype is its ability to detect the chemicals associated with meth labs. A sensor array that targets ammonia, ether, phosphine, HCl, and acetone should be capable of targeting most illegal meth labs[2]. These five chemicals represent some of the most common exhausted gases from the most common methamphetamine production processes. Their presence in the atmosphere, as well as their presence in certain relative proportions in the atmosphere, will both be analyzed with the prototype sensor as we acquire a gas signature for the methamphetamine lab. The evaluation of the signature of these gases will provide a confidence level that the lab is likely present, thus alerting the user to this danger.

Several other aspects of a prototype system are also critical to its success. The system needs to be capable of recording information for analysis at a later time. Also, the entire system needs to be portable and as passive as possible so as to not interfere with user's normal functions. The solution to this problem is a wearable or easily carried device which would be battery operated. A measurement will be taken either continuously, or as a signal pulse is given to the device. Finally, when operated, the system needs to be as simple as possible and to operate with minimal user assessment so as to indicate, possibly with a simple light signal, when a meth-related hazard is sensed. An unacceptable system, would be one that reported the concentrations of multiple components of gas to the user, forcing the user to evaluate the readout and then make a decision on the threat level. The ease-of-use of the system is important because if it is not simple enough to operate, the prototype will be unusable by any police force. A preliminary schematic of the prototype sensor system is shown in Figure 7-1.

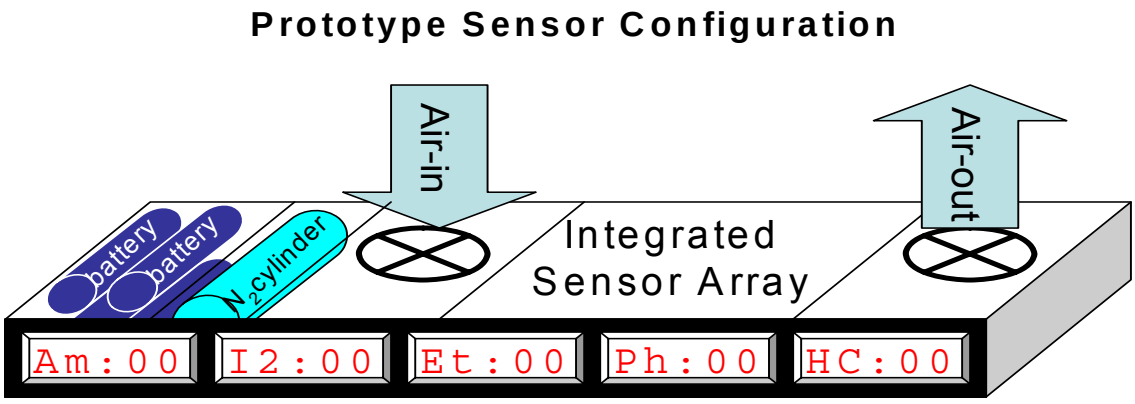

Figure 7-1: The prototype sensor contains many other components in addition to the sensor array component.

Gas Sensor Array Component

The most critical element of the methamphetamine lab sensor prototype is the gas sensor array module. This component is responsible for holding the sensor array, controlling the gas flow over the sensor array, and making electrical contact to the sensor array. This component was designed to test arrays of four sensors made with the upper left sensor array design as indicated in Figure 2-22. Additionally the sensor array component is designed to allow the rapid replacement of sensor arrays during system testing. Finally, multiple sensor array components can be placed within a single gas sensor prototype device, depending on the degree of selectivity required. Initially, the prototype has only one four-sensor array within it, however, multiple gas sensor array components are feasible with a minimal increase in system complexity.

The sensor component of the prototype device is depicted in Figure 7-2 and Figure 7-3 . There are three integral parts to the array configuration. The bulk of the sensor array system is composed using stereolithography (SLA). The SLA device represents an extension of devices which have been used with the PSGS in past

projects[34]. The circuit elements control the electricity powering the sensor array so that voltage measurements can be made to transduce the gas responses. Finally, the gas sensor array itself is housed within an SLA generated system and is subsequently connected to a measurement circuit. This measurement circuit is formed on a printed circuit board (PCB).

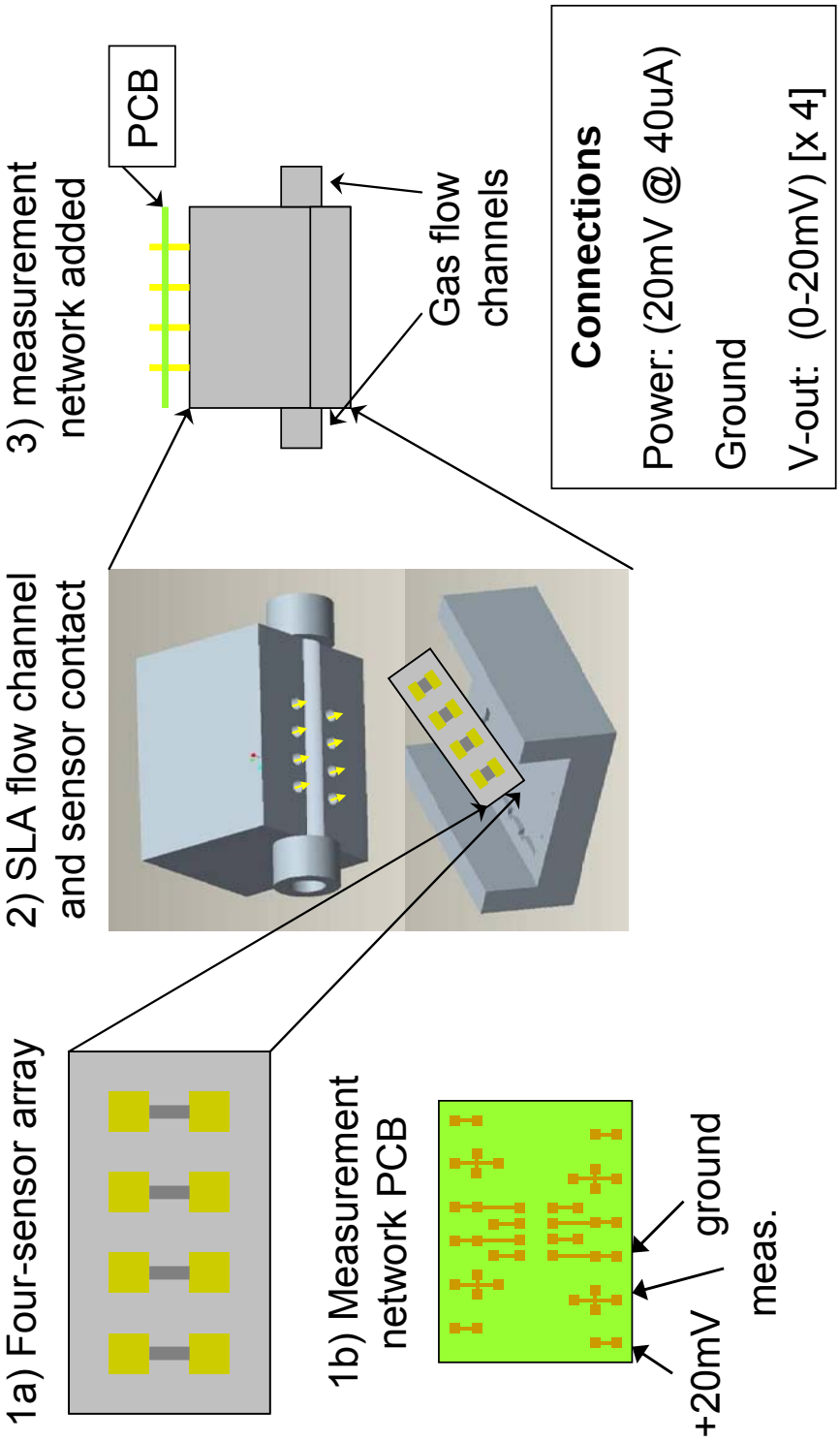

Figure 7-2: The sensor array component of a prototype device consists of several components and is assembled as shown above.

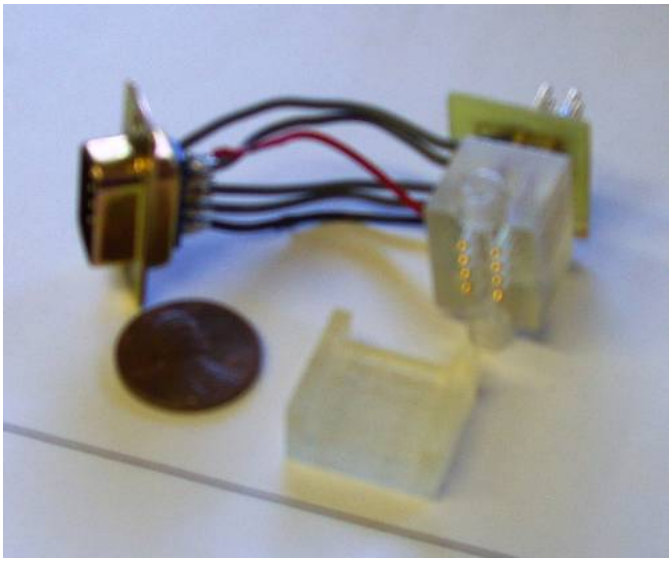

Figure 7-3: Picture of a gas sensor array component as-assembled before being integrated with the prototype system.

SLA Housing

The SLA housing serves primarily to hold the gas sensor array in position for both the delivery of gas and the establishment of a stable electrical contact. It was designed using the Pro/ENGINEER design program. The housing is created as two interlocking pieces of material. The dimensions of the two pieces are such that when put together, internal stress can hold the assembly together. As a further method to ensure that the two components remain fixed upon one another, implements such as a rubber band may be tied around the housing. The SLA housing which we describe here was created with the assistance of Prof. Rosen and Angela Tse in the Rapid Prototyping and Manufacturing Institute[5].

The lower portion of the SLA housing is shown in Figure 7-4. The dimensions of this component are close to half an inch in width and length, and a quarter inch in height. A slight rectangular inset is positioned on the inside surface of this section to allow for the gas sensor array point of rest. The inset was created to match the depth of the wafer

on which the sensor array was fabricated which is about 0.3mm. Several notches are also placed on the border of the rectangular inset for alignment purposes. These notches mark the coordinates for the electrical contacts to the sensor array, and are affixed to the upper SLA component.

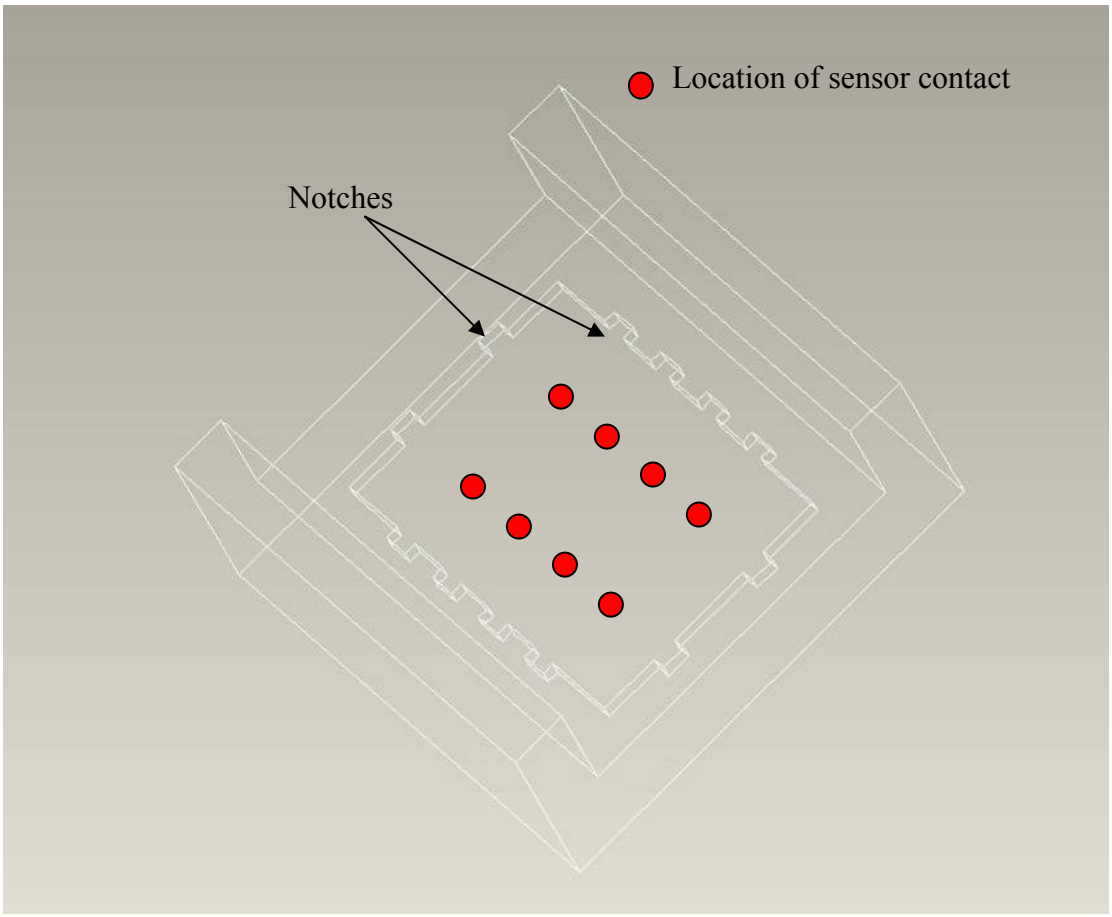

Figure 7-4: A wire-frame image of the lower SLA component.

The upper component of the SLA housing is more complex than is the lower section. In addition to being made to interconnect with the lower SLA section, this component also controls gas flow over the sensor and holds the electrical probes in contact with the sensor. The gas flow consists of a rectangular channel over the center of the gas sensor array. This channel extends the length of the SLA component combination and incorporates cylindrical connections for ⅛" stainless steel tubing on either end.

There are also eight cylindrical holes extending perpendicular from the sensor surface through to the top of the gas sensor region. These holes are designed to each hold a single spring-loaded electrical probe[6]. These probes are slightly larger than the hole diameter, and are permanently inserted after heating and slight expansion of the probe orifice, melting somewhat the SLA polymer on the walls of these holes. The probes are inserted so that only a millimeter of probe extends to the sensor. This length will be compressed onto a gold contact pad when assembled with the lower SLA section and sensor array.

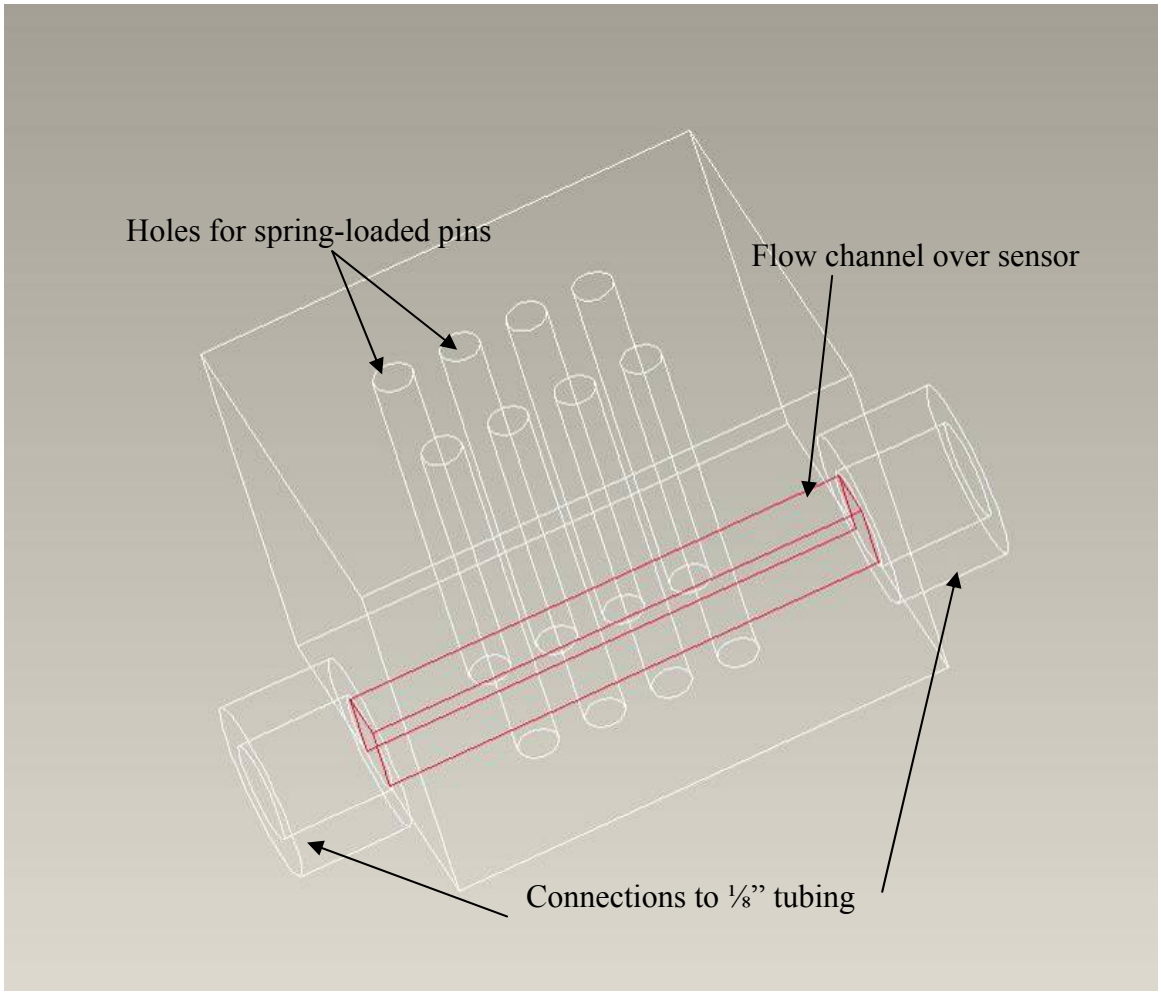

Figure 7-5: A wire-frame image of the upper SLA component. The flow channel that allows gas to pass over the sensor is highlighted in red.

Due to the nature of the SLA process, which incorporates a polymer resin, it is necessary to chemically treat the material with an inert coating before using it in any sensitive gas sensor experiments. A coat of parylene several microns in thickness was deposited in the vapor phase to stabilize the surface of the SLA components and prevent the out-gassing of residual resin solvent onto the gas sensors. While the detrimental effect of an un-coated SLA has not been documented, it is apparent that its out-gassing would be detrimental to the delivery of an unwanted analyte to the sensor. The parylene coating was performed with the assistance of Rajesh Luharuka of Prof. Hesketh's laboratory in Mechanical Engineering.

Measurement Circuitry

The sensor array in the prototype system is operated through a simple voltage measurement scheme. This circuit diagram used to test this concept and measure a single sensor is shown below in Figure 7-6. The sensor in this circuit, contacted through spring-loaded pins (not shown), has a resistance 'R_S', which is the value to be transduced. Due to a high electrical capacity of the gas sensor, a high resistance element 'R_P' is placed in parallel with the gas sensor to reduce this capacitive effect. This resistor is typically over 1000 times the resistance of the gas sensor, and thus has little effect on the measurement of the sensor's resistance. The voltage drop across the sensor is compared to the voltage drop across the entire circuit, which has a second resistor R_1 placed in series with the gas sensor. The resistance of the sensor can be calculated using the formulas shown in Equation 7-1.

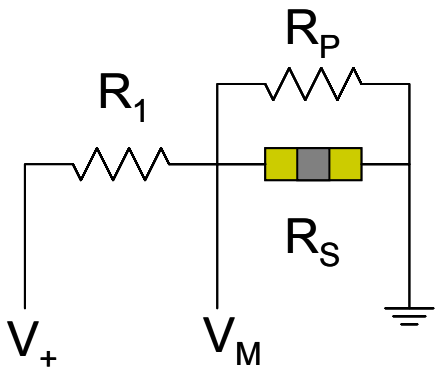

Figure 7-6: A sensor's resistance is measured through the use of the above circuit. The calculation of the resistance is shown in Equation 7-1.

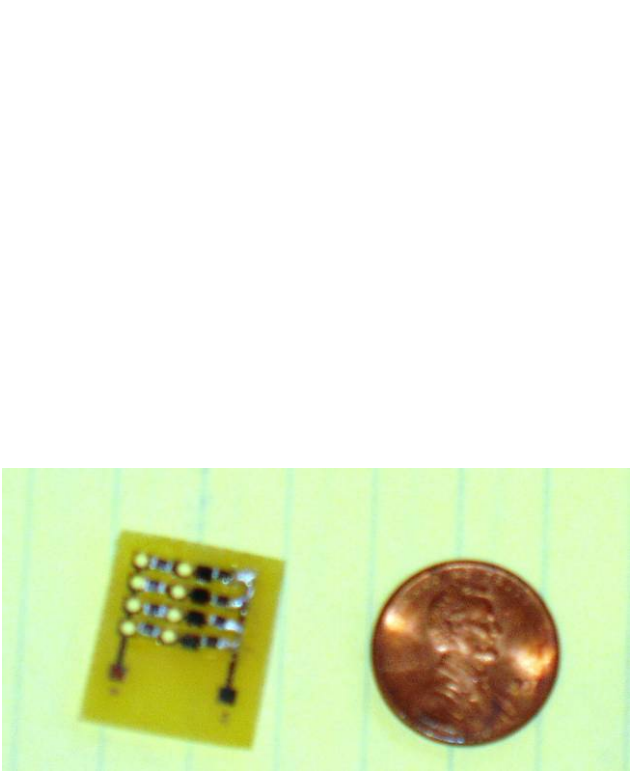

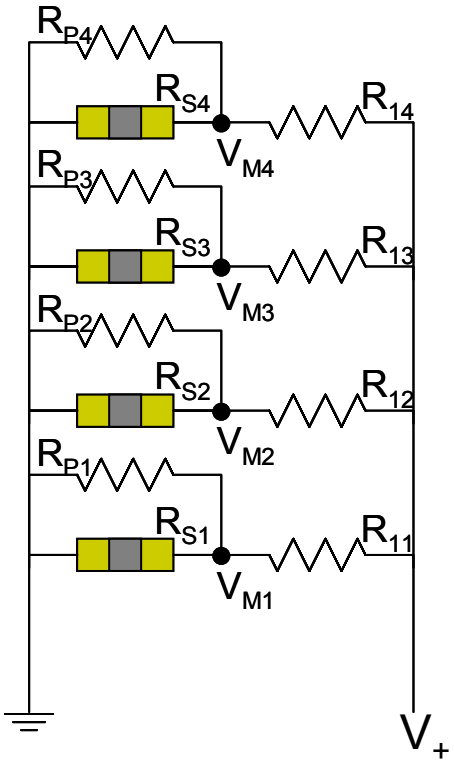

Figure 7-7: The circuit for testing an array of sensors is shown (left) along with the equivalent circuit diagram (right). The holes in the chip indicate where the PCB is soldered to the spring-loaded pins. The resistors between the holes 'R_{px}' correspond to 100kΩ, while the resistors to the right 'R_{1x}' are set at 1kΩ.

$$R_S' = \left(R_S^{-1} + R_P^{-1}\right)^{-1} \cong R_S$$
$$I = \frac{V_+}{\left(R_S' + R_1\right)} = \frac{V_M}{R_S'}$$

Equation 7-1: The above equations representing Kirchoff's Law are used to calculate the resistance of the gas sensor R_S.

The power delivered to the circuit has a significant effect on the performance of the sensor. This effect can most readily be seen in an analysis of the high frequency noise present in the system when it is powered at different voltages. Experiments were conducted to determine the best method for powering the PSGS. In the first mode of operation, the sensor is constantly powered with a continuous voltage V_+ applied across the sensor. In the second mode of operation, the sensor is powered only for the time that is required to make a measurement, approximately 10 ms with the outlined testing configuration.

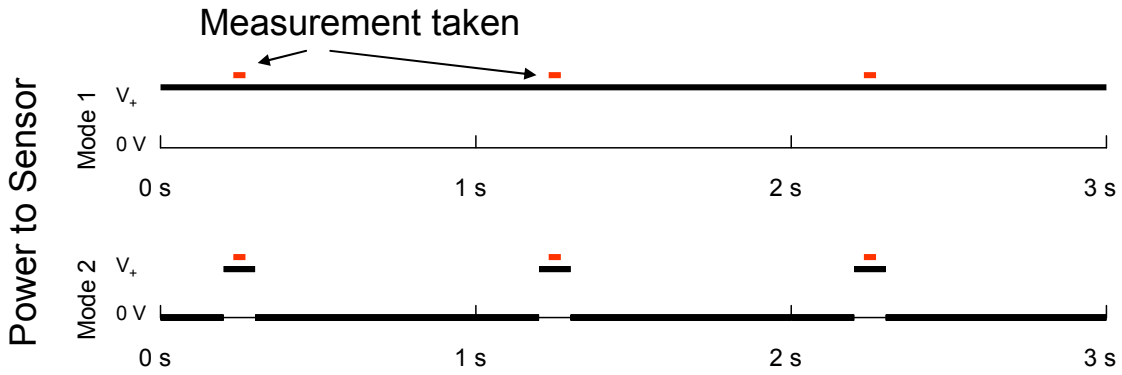

Figure 7-8: Two different modes of operating the gas sensors are demonstrated. The second mode only powers the sensor during the time a measurement is to be taken.

In the following outlined experiment, a gas sensor was tested using the circuit described in Figure 7-6. The resistance of the sensor was measured with the combination of a resistor in parallel R_P=100kΩ and a resistor in series of R_1=980Ω. For various voltages applied to the circuit, V_+, ranging from 0.1V to 3.0V, the average resistance of

the sensor and the deviation of the resistance measurements were evaluated. The measurements were taken at a frequency of 1 Hz, with 10 samples being averaged for each voltage point V_+. Four experiments were conducted with this configuration on a sensor with a LEL below 250 ppb of ammonia. Within the four experiments, both the mode of operation as described in Figure 7-8 and the concentration of ammonia being delivered to the sensor were varied. The sensor was allowed to saturate for each concentration of ammonia before a given experiment was run.

The data from this experiment is provided in Figure 7-9. From the top figure, it can be seen that the measured resistance drops with the voltage applied to the circuit. This can be explained as resulting from a reduction in the resistance of the Schottky barrier present at the gold-silicon interface at higher voltages. The bottom figure shows the relative error associated with each measurement as a function circuit voltage. This error is the deviation in the ten data points taken divided by the average resistance of the sensor and represents the high frequency noise of the system. From these figures, it is apparent that, above a voltage of approximately 1V, there is a diminishing value to powering the gas sensor circuit with an enhanced voltage. Also, mode 2 of operating the gas sensor does not diminish the quality of the sensor measurements.

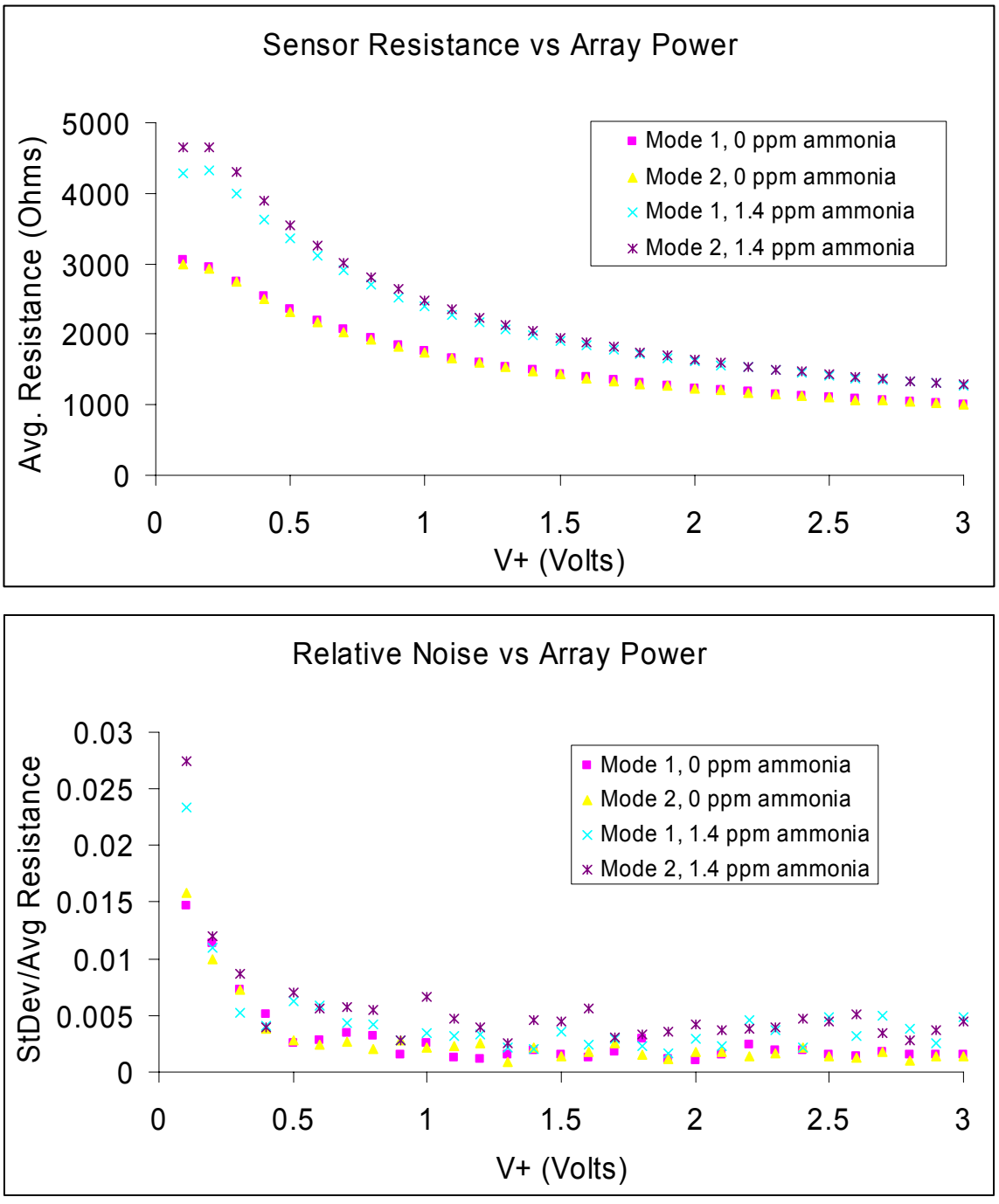

Figure 7-9: The sensor resistance and relative noise level as a function of the power delivered to the sensor are illustrated.

The most efficient method of powering the gas sensor would therefore appear to be Mode 2, since this mode consumes significantly less energy. However, to ensure a higher quality overall measurement, several measurements might be averaged within the window of power being delivered to the sensor. This mode of operation is what was used to test the most recent arrayed gas sensors. In order to integrate the gas sensors, a separate PCB board was designed and used for the final prototype device.

Other Prototype Components

In addition to the sensor array components of the system, several other components are necessary to build the PSGS prototype. Most significant of these additional components is the communications system, which allows the measured readings to be transmitted to a base system. This is a required feature of the prototype, but not necessarily of a final meth-lab sensor product, because it will be necessary that the prototype log all data taken as a part of the rigorous testing it will undergo both in the lab and in the field. The communications component of the PSGS prototype will be discussed in much greater detail later in this section.

Many other required components, however, will not be discussed in detail as they are merely incorporated around the sensor array and communications components. These components do not require development, and are, for the most part, commercially available parts. They are depicted in Figure 7-1, and include a power source, a nitrogen cylinder (for gas pulsing experiments), an air intake and exhaust system, a display component, and the body of the prototype system itself.

Communications Component

The communications component of the prototype system is built around a ZigBee architecture provided by Cirronet for the rapid prototyping of remote platform technologies[7]. The network being constructed is built around a 2.4 GHz wireless chip that is capable of transmitting sensor information to a second chip upto 40 m away. These units can also be used to form a mesh networking architecture for more complex applications. The ZMN2400HP chip we are using, shown in Figure 7-10, is roughly an inch long and one half inch wide.

Figure 7-10: The ZMN2400HP wireless chip is used for sensor communications over short distances.

The ZigBee chip is built into a prototyping board, shown in Figure 7-11, provided by Cirronet for rapid construction of prototype systems. This board is roughly 4" by 2" in area and can be powered with an AC adapter (not shown) or a 9V battery. The majority of the area of the connectors on the board is used to make easy connections to the ZMN2400HP chip. Also present is a device to provide both 5 and 3V to the chip, and a device for communicating between the chip and a USB connection. An antenna must also be attached to this board (not shown) for communications to be relayed to a second board in a network configuration.

Figure 7-11: The prototype board contains the Cirronet-Zigbee chip, a DC voltage regulator circuit providing 3V and 5V, and a serial communications circuit for USB connection. The remainder of the components are connections for easy prototype development.

Two of the prototype boards shown in Figure 7-11 are used in the prototype gas sensor system. The first board is located within the portable gas sensor unit, with the gas sensor array, and various other components needed to operate the system for the purpose of measurement. The second board is connected to a computer which operates the system and records the data. The computer also is capable of processing the collected data in real-time and alerting a wearer portable unit when a "hazardous" situation arises via an alarm mechanism located on the portable unit itself. The operation of this remote program will be discussed later in the chapter. The general layout of the network is shown in Figure 7-12.

Figure 7-12: The network of the prototype sensor system for methamphetamine lab detection is described.

The board located within the portable gas sensor is responsible for transducing measurements from the sensor array, communicating with the board located at the computer, and, in general, for the operation of the entire portable unit. The board has three ADC connections for signal measurement, which operate in the range of 0V to 3.3V. Therefore, the simplest way to configure the system would be to power the sensor array with the 3V supply provided by the board, as the ADC's on the board transduce the signal from the sensors. As there are 4 sensors in a sensor array, with multiple potential arrays in a gas sensor system, the Digital IO lines are configured to select a sensor for transduction via the ADC.

In the single array version of the prototype device, the first two sensors are transduced by one ADC channel, while the second two sensors are transduced by a second ADC channel. The third ADC channel remains unused. The sensor which is presently being transduced is configured via a single digital IO line which signals either 0V or 3.3V (0 or 1) as controlled by the program located in the computer connected to the control board. A second digital IO line is also configured to control the power being delivered to the gas sensors so that the array can be operated using mode 2 as shown in Figure 7-8. An additional digital IO line can be used to re-double the sensor capacity of the system. A third ADC channel is also unused. The channel can be implemented to further increase the sensor capacity by 50%.

Integration of Prototype Components

The integration of prototype components begins with the merger of the Cirronet board and the gas sensor array components. The outlined requirements for the board for this application required development of a circuit to merge the sensor array with the

board. This circuit utilizes five HEF4066 switches and one HCF4069 logical inverter to provide the functionality described above. The capability of the 4066 "switch" IC is to control the resistance of a pathway between two pins of the circuit with an external control voltage[8]. The resistance can be set to be either ~200Ω or 2.2MΩ. The logical inverter, or "not" gate, inverts the input signal between a logical 1 or 0[9]. For this circuit, a 0 is defined as 0V, and a 1 is defined as 3.3V. These binary signals are provided by the GPIO connections on the Cirronet board and control both the 4066 and 4069 integrated circuits. Both of these chips are powered by 3.3V from the Cirronet board.

The functional circuit diagram is shown in Figure 7-13. The voltage flows from the left to the right in this diagram. The functionality of the first switch (on the left) is to throttle the power to the entire circuit "off and on" through GPIO4, thereby powering down the sensors and conserving energy. The remaining four switches are placed in series with the gas sensors themselves. These switches allow the effective removal of one of the two sensors assigned to an ADC from the circuit, thereby isolating the other sensor for an accurate measurement. These switches are controlled by GPIO3. A logical "not" gate placed prior to switches 1 and 3 causes sensors 1 and 3 to be active while 2 and 4 are inactive and vice-versa. The PCB schematic implementing the circuit diagram in Figure 7-13 is shown in Figure 7-14. This circuit was verified to operate correctly through assembly on a breadboard prior to the creation of the system.

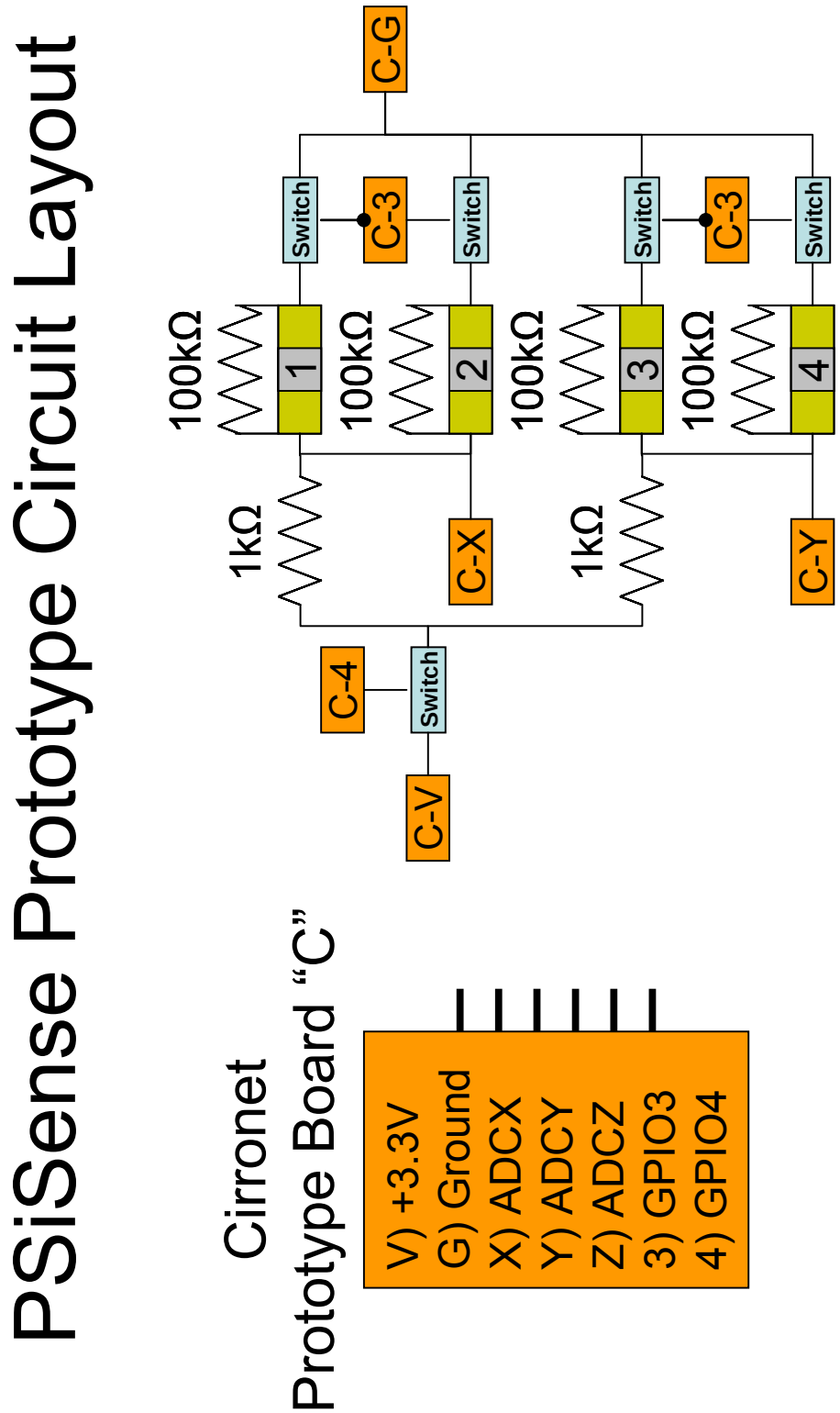

Figure 7-13: The circuit layout for the prototype array is depicted above. The indicators labeled "C-#" represent a connection to the Cirronet prototyping board.

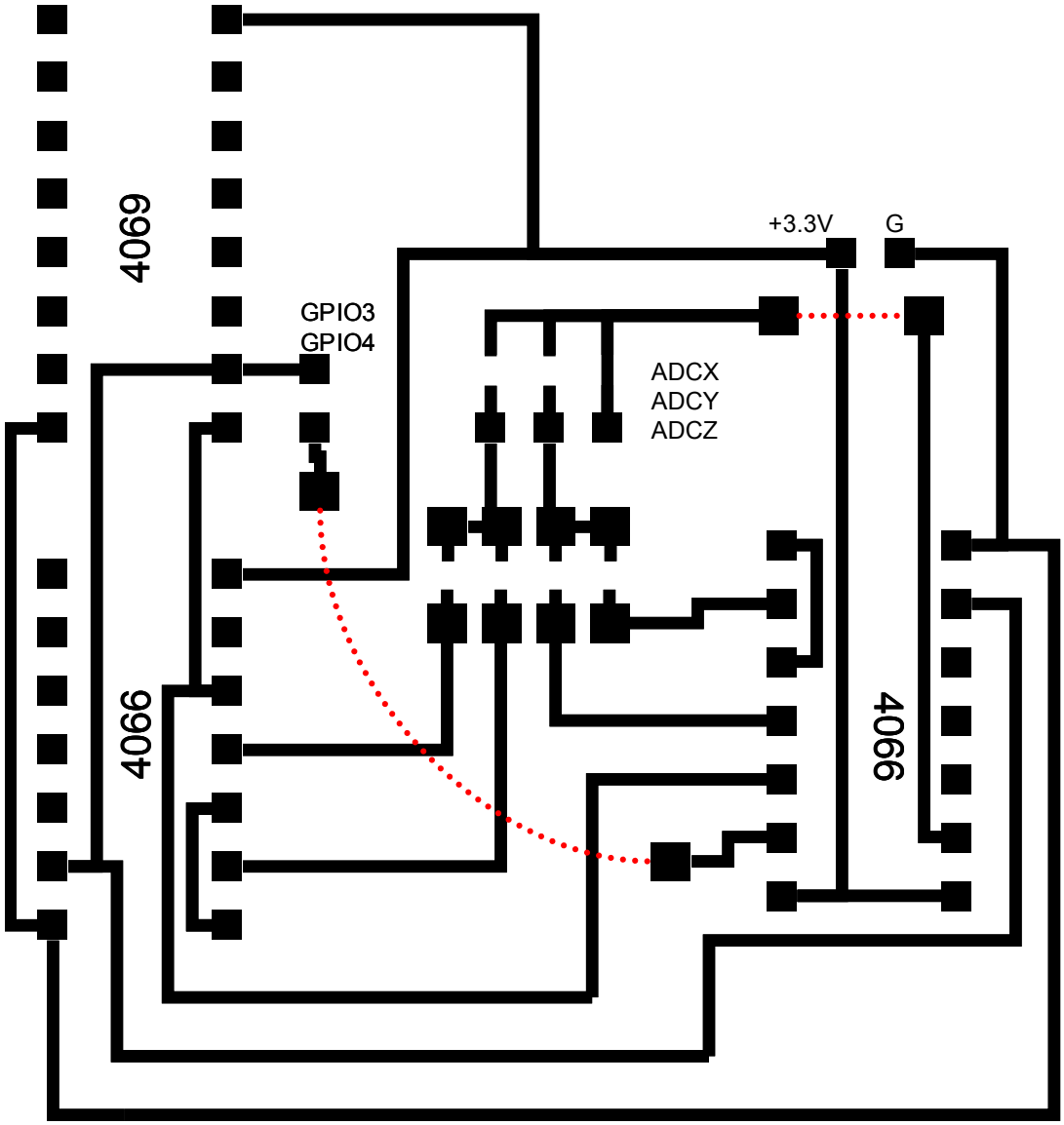

Figure 7-14: The PCB schematic corresponding to the circuit diagram in Figure 7-13. This circuit is designed to replace the PCB shown in Figure 7-7, with the sensor array pins fitting through the eight central pads. Three integrated circuits are used for the switches and the "not" gate.

The merger of the communications and sensor components required the development of a computer program to read from the Cirronet communications card. This program, shown in Figure 7-15, allows the real-time, remote operation of the sensor array. To implement the switching circuitry of Figure 7-14, a breadboard was used. An experiment was conducted to demonstrate a proof-of-concept with the remote-monitoring and operation of the sensor prototype system, and to demonstrate the feasibility of such a system.

Research is now ongoing towards the development of this prototype system. The additional components are being identified and assembled to create the prototype as the breadboard circuitry is being replaced by a more permanent PCB to be affixed to the Cirronet board and sensor array component.

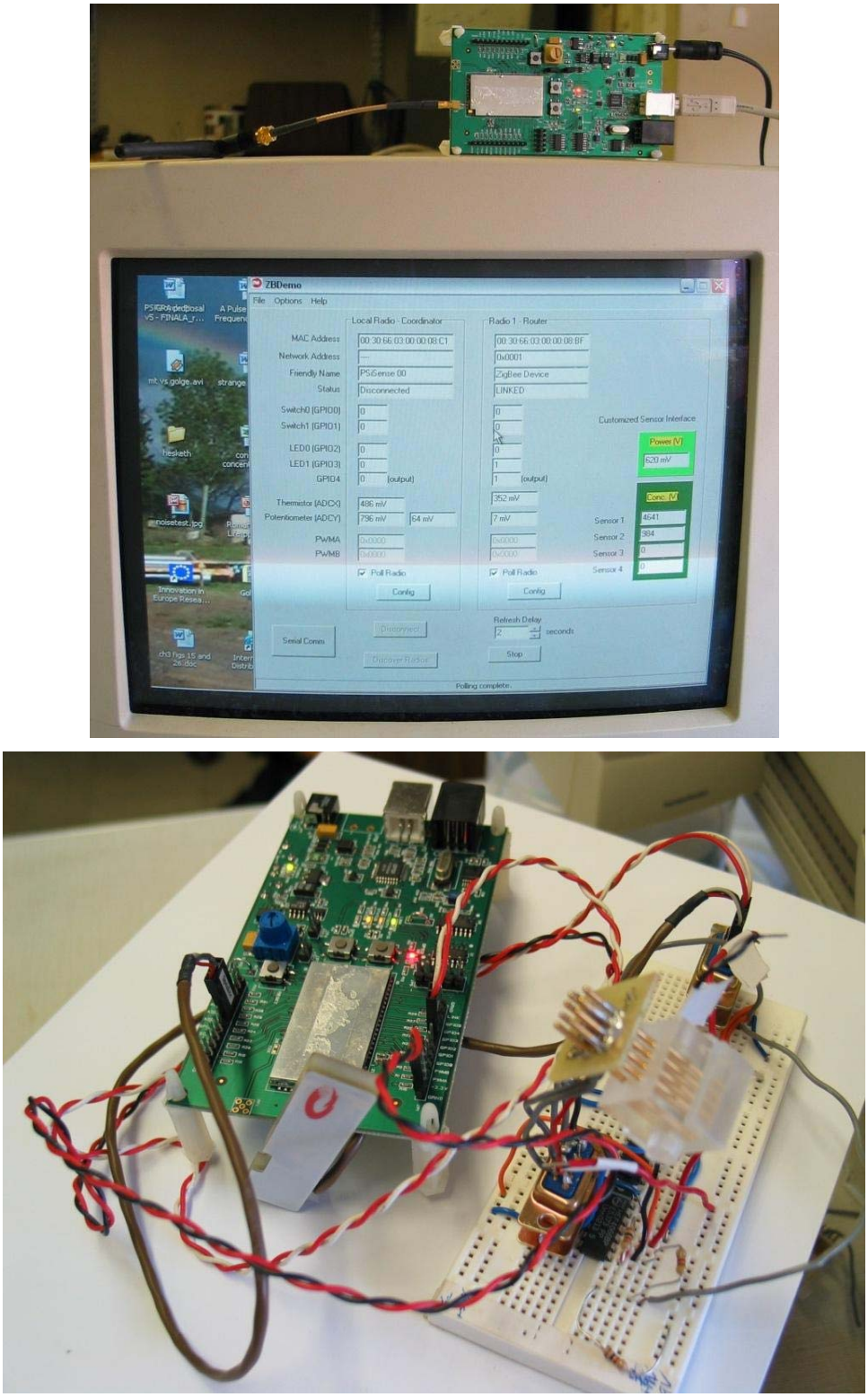

Figure 7-15: The prototype communications and sensor array components were integrated with breadboard circuitry to allow testing of the system. The remote unit (bottom) communicates in real time with the base unit (on top of monitor) which displays and logs the sensor resistances.

Markets for the Porous Silicon Gas Sensor

While the prototype methamphetamine sensor is presently the only application of the PSGS under development, PSiSense[Error! Bookmark not defined.] has not limited its market strategy to this singular device. Several additional markets for this platform technology are continuing to be investigated. Among these markets are cabin air-quality sensors and asthma detection devices. These additional devices will be based upon the methamphetamine sensor prototype, but with a customized array to detect the required analytes for each application.

The market for cabin air-quality sensors is very dispersed. These devices can appear in vehicles of all kinds, from personal cars to military aircraft. In all applications, however, the cabin air-quality sensor is needed to respond to the presence of hazardous contaminants ranging from small molecules like carbon monoxide to larger complex hydrocarbons in real-time. Speed of response is most critical, since levels of the contaminants would be concentrated within the confines of the cabin. Cost of the device is also an important aspect, especially for commercial applications. Presently, PSiSense has submitted a single SBIR for funding from the Department of Defense – Air Force to develop a cabin air quality sensor for leak detection inside the aircraft of the US military[10].

Personal health monitors are another potential market for the porous silicon gas sensors. The most viable portion of this market presently is in the area of personal asthma monitors. These devices would be carried by a person suffering from asthma, and provide an early-warning capability so that the wearer would be warned of potential exposure to allergens or atmospheric pollutants including ozone, formaldehyde, NO_2, and

sulfurous gases. Research towards this goal is presently underway in a collaborative effort with GTRI in a research contract sponsored by HUD[11]. Future SBIR and STTR proposals are planned for PSiSense to both NIH and the EPA to produce sensors that will be affective for health exposure monitoring.

Other markets are not as immediately amenable to incorporation of the PSiSense prototype device. This results from a need for increased detection levels beyond the present capabilities of the PSGS and the difficulty of detecting the required constituent gases. Explosives detection is one such market, with required detection levels in the low ppb range including also gases which are notoriously difficult to detect. These markets would not be entered until the later stages of development of the PSGS prototype device.

The PSGS has been demonstrated as a viable platform for several gas sensor applications. From the results of research presented within this dissertation, it has been shown how single gas sensors can be fabricated into arrays of working sensors, and then incorporated into a functional sensor device. Additionally, the analysis of the gas sensor has provided insight into the mechanism of how porous silicon operates as a transduction medium. From this deeper understanding of porous silicon and the gas sensors it is used to produce, we have created more sophisticated measurement schemes to better operate both this, and other gas sensor technologies.

References

1 Prisoners of Meth: About the Book's Author, (December 2005) http://www.prisonersofmeth.com/Bio.htm.

2 Development of Clandestine Methamphetamine Laboratory Detection Sensor Array, Research Proposal submitted to U.S. Dept of Housing and Urban Development, 2005.

[3] Jacobs, P. F. (1996). Stereolithography and other RP&M Technologies: from Rapid Prototyping to Rapid Tooling, Society of Manufacturing Engineers.

[4] A. L. Tse, P. J. Hesketh, J. L. Gole, and D. W. Rosen, "Rapid prototyping of chemical sensor packages with stereolithography," Microsystems Technology, Vol. 9, pp. 319-323 (2003).

[5] Rapid Prototyping and Manufacturing Institute, (October 2005) http://rpmi.marc.gatech.edu/.

[6] ECT products, (November 2005) http://www.ectinfo.com/files/product/frame_pogo.html.

[7] Cirronet, Inc., (November 2005) http://www.cirronet.com/.

[8] CD4066BC Quad Bilateral Switch, (December 2005) http://www.fairchildsemi.com/ds/CD/CD4066BC.pdf.

[9] CD4069UBC Inverter Circuits, (December 2005) http://www.fairchildsemi.com/ds/CD%2FCD4069UBC.pdf.

[10] PSiSense proposal to DOD AF06-023, "Advanced Sensor to Identify and Quantify Contaminants in Cockpit Air", proprietary, (January 2006).

[11] Research Proposal to HUD, GALHH0124-04, "Personal Exposure Monitoring Vest Development", (September 2004).

APPENDIX A

CHEMICAL SENSITIVITIES

The three tables appearing below are reproduced with permission from Prof. Jiri Janata as they appear in "Chemical Sensors for Portable, Handheld Field Instruments", an article appearing in *IEEE Sensors Journal* (2001) by Denise Michele Wilson, Member, IEEE, Sean Hoyt, Jiri Janata, Karl Booksh, and Louis Obando.

These tables indicate the chemical sensitivities of several chemical compounds as used in various devices. These materials are candidates for a porous silicon gas sensor coating to produce a device selective for the gases listed here. While these tables do not represent all possible selective coatings, they do offer a sizable and likely list of candidates that could be investigated in the future.

TABLE II
METAL–OXIDE SENSING FILMS AND THEIR COMPATIBILITY WITH PORTABLE INSTRUMENT DESIGN

Film Type	Vapors	Reference	Compatibility:
Chromium Titanium Oxide $Cr_{2-y}Ti_yO_{3+x}$	H_2S	[6]	High stability: from 250-500°C) Poor compatibility with standard IC fabrication. Moderate fabrication complexity. Moderate temperatures of operation (250-420°C).
Gallium Oxide (Ga_2O_3)	O_2, CO	[7][8][9]	High stability at high temperatures. High compatibility with standard IC fabrication. Low fabrication complexity. High temperature of operation (600-950°C). Increased sensitivity over other metal-oxide films.
Indium Oxide (In_2O_3)	Ozone (O_3)	[10][11]	Moderate stability. Moderate compatibility with standard IC fabrication. Low fabrication complexity. Moderate temperature of operation (150-350°C).
Molybdenum Oxide (MoO_3)	NH_3, NO_2	[12][13]	Moderate stability. Moderate compatibility with standard IC fabrication. Moderate fabrication complexity. Moderate temperature of operation (200-450°C).
Tin-oxide (SnO_2)	Nitrous oxides; ammonia, VOCs, hydrocarbons, and many other reducing gases.	[14]	Excellent stability. Moderate compatibility with standard IC fabrication. Moderate fabrication complexity. Moderate temperature of operation (350°C).
Tin Oxide (SnO_2) Deposited using spray pyrolis methods (SPM)	H_2, CH_4, C_3H_8, CO	[15][16][17]	Excellent stability. Moderate compatibility with standard IC fabrication. Low fabrication complexity. Moderate temperature of operation (500°C).
Tungsten Oxide (WO_3) Titanium Tungsten Oxide (Ti-WO_3)	NO_2	[18][19]	Excellent stability. Low compatibility with standard IC fabrication (high temperature of oxidation required to make WO_3) Moderate fabrication complexity. Moderate temperature of operation (200-500°C).
Tungsten Oxide: Doped $WO_3(Bi_2O_3)$	NO	[20]	Excellent stability. Low compatibility with standard IC fabrication. Moderate fabrication complexity. Moderate temperature of operation (250-350°C). High selectivity to NO (at 300°C)
Zinc Oxide ZnO	hydrocarbons; oxygen	[21][22][23] [24][25][26] [27] [28][29]	Excellent stability Moderate compatibility with standard IC fabrication. Low fabrication complexity Moderate temperature of operation (300°C). High sensitivity

TABLE III
METHODS OF MODIFYING SELECTIVITY AND SENSITIVITY IN METAL–OXIDE FILMS

Film	Tuning Parameter	Tuning Method	Ref
Al_2O_3	Selectivity to H_2, methane; Linear response over concentration	Doped with metal-oxide additives	[31]
Ga_2O_3	Sensitivity: two orders of magnitude	Doping: with SnO_2	[9]
Ga_2O_3	Sensitivity and Selectivity to CO	Doping: gold (Au) clusters	[32]
In_2O_3	Sensitivity	Doping: Ga_2O_3 to increase porosity of In_2O_3 lattice	[33]
SnO_2	Selectivity to H_2 and H_2S	Doping with 4-6 nm silver clusters	[34]
SnO_2	Selectivity to CO	Addition of 50 A^O Pd and Pt layers	[35]
SnO_2	Selectivity to CO in the presence of methane; additive response properties in the presence of multiple gases.	Fabricated using sol-gel materials to generate high surface area films; Pt and Pd catalysts used to enhance additive properties of response	[36]
SnO_2	Selectivity	Mode of operation: switched to monitoring steady-state response at various temperatures	[37][38] [39][40]
SnO_2	Sensitivity to H_2	Film Structure: adjusted to nanoparticle sizes and film thickness	[41]
SnO_2	Selectivity to CO, NO, and CH_4	Mode of operation: switched to field effect	[42]
SnO_2	Selectivity to Methane, CO, NO, H_2 and butane	Mode of operation: switched to monitoring transients at various temperatures in response to 16ms pulses	[43]
SnO_2	Selectivity to trimethylamine (TMA)	Doping: thorium	[44]
SnO_2	Sensitivity	Film Structure: Grain size	[45]
SnO_2	Sensitivity	Various additives and catalysts	[46]
SnO_2	Selectivity to hydrogen (H_2)	Film Structure: misfit regions on surface using Ru, Pd and Ag to covalently attach to surface	[47]
SnO_2	Sensitivity	Doping: Mo_2N and MoO_3 on tin-oxide surface	[48]
SnO_2	Sensitivity	Film Structure: crystal growth inhibited during fabrication to create film surfaces with very small (20, 50, and 15 A^o) crystallite sizes	[49]
SnO_2	Selectivity to hydrogen or ethanol compared to CO, methane, Hydrogen sulfide and ammonia	Doping: with La_2O_3 and Pd	[50][51]
SnO_2	Selectivity to CO and NO_2	Mode of operation: temperature modulation (sine wave) and Microfabrication: enables temperatures to be modulated on same timescale as reaction kinetics	[52]
WO_3	Vapor Sensitivity and selectivity to NO_2 (sub-ppb levels)	Fabricated using photochemically active precursors	[53]
WO_3	Vapor sensitivity and selectivity to NO_2 in the presence of CO, CH_4, H_2, SO_2, H_2S and NH_3	Addition of Pd, Pt, and Au noble metal catalysts	[54]
WO_3	Sensitivity	Film Structure: Grain size	[55]
ZnO	Vapor sensitivity to CH_4 and H_2S at reduced operating temperatures (150^oc)	Doping: with Palladium (Pd) Film type: thin film Fabrication: controlled (wet) chemical deposition	[56]
ZnO/SnO_2	Vapor sensitivity to CO	Film type: sintered pellets; composite film	[57][58] [59]
ZnO, SnO_2, TiO_2, In_2O_3	Vapor Sensitivity	Variable cluster size of nanostructured films	[60]

TABLE IV
RECENT RESEARCH EFFORTS IN THE AREA OF CHEMFET DESIGN

Ref	Analyte	Sensing Structure	Comments
[98]	Ammonium	PVA/SbQ with PVC adhesion layer FE: various enzymes	Limited sensor recovery.
[99]	Ammonium	PVC treated with HMDS for adhesion	Sensitivity: 30mV/part NH_4; Both measurement and ref FET fabricated; Detection limit: $2X10^{-6}$; Repeatability limited by stability of reference FET
[100]	Cd^{2+}; Pb^{2+}	Polysiloxane FE: cyclodextrin	Sensitivity: 29mV/decade for Cd^{2+} Sensitivity: 15mV/decade for Pb^{2+} Lifetime: 3 months.
[101]	Cu^{2+}	Etched chalcogenide glass with aluminum adhesion layer.	Sensitivity: 28mV/part Cu Response time: 5 seconds Lifetime: "several weeks
[102]	Cyanide	PVP (poly-(4-vinylpyridine-co-styrene) with horseradish peroxidase as FE.	Sensitivity: 10^{-7} to 10^{-5} molar solution Reproducibility: 20% (pH dependent)
[103]	H_2PO_4	Gold with FE's: $UO2^{2+}$ Lewis acid binding sites and amide (C(O)-NH) groups	Selectivity: up to 1000 over Cl^- and NO_2
[90]	Hydrogen	Palladium and polyaniline	Stability: Hydrogen sensor was unstable. Sensitivity: 0 to 10,000 ppm (ammonia) High selectivity, fast and stable to ammonia
[104]	K+	Polysiloxane with polyHEMA adhesion layer and methacryloxymethylphenyl hemispherand as FE's.	Sensitivity: 59mV/decade K^+ concentration Lifetime: 75 days
[105]	K^+, Na^+; Cd, Pb	Polysiloxane structure with polyHEMA adhesion layer and calix(4) arene with various substitutents as the FE's.	Size: very large devices, but photopolymerization is compatible with IC processes.
[106]	NH_4	Polyvinyl chloride (PVC) structure with polyHEMA adhesion layer and nonactine with tetrakis-(4-chlorphenyl)borate) as FEs.	Lifetime: 6-7 weeks
[106]	NH_4	Siloprene with polyHEMA adhesion layer and nonactine with tetrakis-(4-chlorphenyl)borate) as FE's	Lifetime: 14 months Response time: 10 seconds
[107]	NO_2	Platinum oxide (SGET structure)	NO_2 effect is highly electro-adsorptive (response characteristics depend on electric field)
[108]	O_2	Iridium oxide (III and IV)	Ratio of Ir III to Ir IV changes with oxygen concentration and modulates work function. works for about 2^{-15} mg/liter of O_2
[109]	pH	Tin-oxide	Sensitivity: 58mV/pH Linearity: linear between 2 and 10 pH Response time: 1 second Drift: 28mV in 9 days 80mV measurement range
[110]	pH	Diamond-like carbon films	Sensitivity: 55 mV/pH Drift: to 23 μV/hour drift for high pH
[111]	pH	Tungsten trioxide (WO_3)	Sensitivity: 44mV/pH
[112]	pH	Silicon oxynitride	Sensitivity: 47mV/pH Unmodified CMOS process Lifetime: 2 months (minimum)
[113]	pH	SnO_2 with SiN_4/SiO_2 adhesion layer	Aluminum added between SnO_2 and SiO_2 layer to prevent light sensitivity but added Al causes temperature coefficient of .157 mv/° C. Sensitivity: 56mV/pH
[114]	pH	SnO_2 in EGFET structure	Light sensitivity: 3mV maximum Sensitivity: 57mV/pH

APPENDIX B

MATLAB PROGRAMS FOR NUMERICAL SIMULATIONS

See the text (Chapter 5) for a complete discussion.

File: Diffusion_Model.m

```
function [C1,T1] = Diffusion_Model(C0,DLL)

% input C0: the concentration vector, the concentration can vary at a
% maximum resolution of once per second.

ODE_NUM = 100;      % The number of ODE's that represent the equation
plotdensity = 20;   % plot 20 points per second;
Total_time = length(C0);    % seconds in total model

% initially the entire column is empty
initial_conditions = zeros(ODE_NUM+1,1);

options = odeset('RelTol',1e-10,'AbsTol',1e-10);

% the result vector, [TIME,CONC] at time zero the response is zero
result = [0,0];

for time = 1:Total_time     % for each second we run through this look (this is to save memory)

   initial_conditions(1) = C0(time);

   [T,Y] = ode45(@Diffusion_Eq,[time-1 time],initial_conditions,options,DLL,ODE_NUM);

   % timesteps that it took to finish the ode45 call
   timesteps = length(T);

   % set initial conditions to be the results of the last call to ode45
   initial_conditions = Y(timesteps,:);

   % this is the data for the bottom of each pore
   Y = Y(:,ODE_NUM+1);

   % get the result vectors the results and keep the plot window active for the next loop
   T = T(1:round(timesteps/plotdensity):end);
   Y = Y(1:round(timesteps/plotdensity):end);

   % concatenate the result, eliminating the first element, which is
   % the same as the last element of the previous result
   result = [result;[T(2:1:end),Y(2:1:end)]];

   if (mod(time,60) == 0)       [DLL, time/60]            % prints status to screen
```

```
   end
end

C1 = result(:,2);
T1 = result(:,1);

%%% this function "Diffusion_Eq" defines the diffusion equation and is
%%% called by ode45.  The PDE is represented as ODE_NUM ODE's here
function dy = Diffusion_Eq(t,y,DLL,ODE_NUM)

dy = zeros(ODE_NUM+1,1);      % an empty column vector
dy(1) = 0;                    % top Concentration unchanging
for i=2:ODE_NUM
   dy(i) = DLL*(ODE_NUM)*(ODE_NUM)*(y(i-1)+y(i+1)-2*y(i));
end

dy(ODE_NUM+1) = dy(ODE_NUM);       % bottom B.C.
```

File: Generate_C0_of_t.m

```
function Concentration = Generate_C0_of_t (C, M)
% input is an array of concentrations and an array of minutes corresponding
% to each concentration.

%output is an array od delivered concentrations each second suitible for
%Diffusion_Model

minutes = sum(M);       % total number of minutes
Concentration = zeros(1,minutes*60);    % create output array

Conc_index = 1;        % index in output data

for i = 1 : length(C)
   Concentration(Conc_index:Conc_index+M(i)*60-1)= C(i);
   Conc_index = Conc_index+M(i)*60;
end
```

File: Calculate_Response.m

```
function [T1,R] = Calculate_Response(C1s,T1s,Ss,baseline)

% input C1,T1 from Diffusion_Model
% input baseline (Ohms) and S (ohms/ppm) from empirical observation
% S is total response to 1 ppm
% output R (and T1) describing the sensor's response

R = baseline;
T1 = T1s(:,1);

for i = 1:length(Ss);
   R = R + C1s(:,i)*10^6*Ss(:,i);
end
```

File: Diffusion_Model_Script.m

```
% This script simulates a single gas being pulsed
% at concentrations between 1 and 5 ppm
% D/L^2 = 0.002 1/s

% concentrations
Concs   = [0 1 0 2 0 3 0 4 0 5 0]*1e-6;

% minutes per concentration
Times   = [2 1 2 1 2 1 2 1 2 1 5];

% the diffusion constant divided by the square of the column length
DLL = 0.002;

% baseline resistance
baseline = 4000;

% response per ppm
S1 = 500;

C0 = Generate_C0_of_t(Concs,Times);

[C1,T1] = Diffusion_Model(C0,DLL);
[R,T] = Calculate_Response([C1],[T1],[S1],baseline);
plot(T,R);
title(['DLL=', num2str(DLL)]);
xlabel('Time (min)');
ylabel('Response');
```

VITA

Stephen Lewis was born on February 4th, 1979 in Baltimore, Maryland. He came to Georgia Tech in 1997 where he was originally a student of aerospace engineering. Eventually, he settled into pursuing dual undergraduate degrees in both physics and computer science. After receiving the B.S. in Physics in 2001, he immediately entered the physics Ph.D. program to continue working for his undergraduate advisor, Dr. Gole. He utilized the generosity of the School of Physics to acquire his B.S. in Computer Science in 2002, and then took a M.S. in Physics in 2003. Stephen continued his research under Dr. Gole until 2006, when he received his Ph.D. in Physics while forming a new company to market the gas sensor technology he developed while a student at Georgia Tech.